Investigating the Molecular Regulators of Phagocytosis and Intracellular Killing to Modulate the Innate Immune System in Response to Infection

Faith Harriet Tolliday

Registration Number: 180287905

A thesis submitted in partial fulfilment of the requirements for the degree of Doctor of Philosophy

February 2023

Supervisors: Professor Stephen Renshaw & Professor Alison Condliffe

The University of Sheffield

Faculty of Medicine, Dentistry and Health

Department of Infection, Immunity and Cardiovascular Disease (IICD)

Table of Contents

Acknowledgements

I have been extremely lucky to have Professor Stephen Renshaw and Professor Alison Condliffe as my supervisors. This endeavour would not have been possible without them, they have been incredibly supportive as well as generous with their time and knowledge, encouraging me at every meeting. I would also like to thank their respective laboratory groups, whom have always been welcoming and helpful. I will always be incredibly grateful that Steve alongside Professor David Dockrell created the opportunity for me to merge a PhD with my research technician position. I am grateful of the Medical Research Council for funding this position through the SHIELD AMR research grant. I would also like to extend my thanks the SHIELD consortium members for their insight and advice.

I would like to express my gratitude to members of staff across the RNAi screening facility, zebrafish screening facility and bioinformatics core, for their advice and assistance, in particular Dr Stephen Brown and Mark Dunning. I am grateful for the technical support from the flow cytometry facility and IICD core technical staff, primarily Jon Kilby and Katie Cooke. For MDM and neutrophil isolation, I would like to thank all volunteers for their blood donations, clinicians and trained personnel for phlebotomy and members of the Prince group.

Finally, I would like to thank my family. My husband, Jake, has been unwavering in his support and patience throughout this process. My parents, in-laws and my friends have always been so encouraging and motivating and I would like to thank them for their belief in me.

Declaration

I, the author, confirm that the Thesis is my own work. I am aware of the University's Guidance on the Use of Unfair Means (www.sheffield.ac.uk/ssid/unfair-means). This work has not been previously been presented for an award at this, or any other, university.

Summary

Antibiotic resistance is on the rise due to overuse and misuse of antimicrobial treatments. Drug resistant infections are therefore increasingly difficult to treat leading to over 700,000 deaths world-wide annually with the expected rise to 10 million deaths in 2050 if no alternative treatments are developed. Phagocytosis and subsequent intracellular killing of pathogens are key functions shared by professional phagocytes including neutrophils and macrophages. Although the mechanisms of these functions are well characterised, their regulators are not.

Phenotypic variability in the phagocytic capacity of both neutrophils and macrophages has been described on numerous occasions. There has so far been very few studies to underpin the molecular signatures of these apparent sub-populations. The first aim of this project sought to determine if the phenotypes described are stochastic or inherent to the individual cell. Neutrophils and monocyte-derived macrophages (MDMs) both showed super-ingester phenotypes in which certain cells were more likely to phagocytose particulate material than others. FACS sorting and RNA sequencing allowed identification of differentially expressed genes (DEGs) between phagocytic and non-phagocytic cells. Only 18 DEGs were identified in neutrophils whilst over 1,000 DEGs were identified at two time-points in MDMs.

The second and third aims of this project focused on enhancing intracellular killing of *Streptococcus pneumoniae*, a pathogen that is the leading cause of community acquired pneumonia which has developed resistance to penicillin. One method involved the development of a compound screen to assess the treatment with clinically approved drugs on the number of intracellular bacteria. 23 compounds were identified for further investigation into repurposing for treating infections. This followed on to the final aim of the development of an siRNA screen using a library of 18,096 siRNAs to identify novel regulators of intracellular killing and phagolysosome acidification by labelling *S. pneumoniae* with GFP and pHrodo. Over 3,500 siRNAs targets were tested, which showed 114 genes altered the number of internalised GFP positive bacteria and 82 genes altering phagosomal acidification.

Considering where there is lack of knowledge, this project aims to identify and investigate molecular regulators of phagocytosis and intracellular killing as therapeutic targets to modulate the innate immune system in response to infection.

List of Figures

List of Tables

List of Abbreviations

AKT1	RAC-alpha serine/threonine-protein kinase
AP2	Assembly protein complex 2
AP2M1	AP-2 complex subunit mu
APS	Ammonium persulfate
ARG (1/2)	Arginase (I/II)
ARHGEF10L	Rho guanine nucleotide exchange factor 10 like
Arp2/3	Actin-related protein 2/3 complex subunit 3
ATP	Adenosine triphosphate
BAFF	B-cell activating factor
BMDM	Bone-marrow derived macrophages
BSA	Bovine serum albumin
CAM	Carbinoxamine maleate
CAR-T-cells	Chimeric antigen receptor T cells
CBA	Columbian Blood Agar
CC	Candesartan cilexetil
CD	Cluster of differentiation
cDNA	Complementary DNA
cFLIP	Cellular FLICE (FADD-like IL-1β-converting enzyme)-inhibitory protein
CFU	Colony forming units
CHN1	Chimerin 1
cIAP1/2	Cellular inhibitor of apoptosis protein -1/2
CLT (A/B)	Clathrin light chain (A/B)
CME	Custom module editor
COPD	Chronic obstructive pulmonary disease
COX5B	Cytochrome C Oxidase Subunit 5B
CR	Complement receptor
CXCR3	Chemokine receptor 3
Cy5	Cyanine 5
CYBA	Cytochrome B-245 Alpha Chain
CYBB	Cytochrome B-245 Beta Chain
DAPI	Diamidino-2-phenylindole
DAZ2	Deleted in Azoospermia 2

DEG	Differentially expressed gene
DF1	DharmaFECT 1
DMEM	Dulbecco's Modified Eagle Media
DMSO	Dimethyl Sulfoxide
DNA	Deoxyribonucleic acid
dsRNA	Double stranded RNA
EC50	Half maximal effective concentration
EDTA	Ethylenediaminetetraacetic acid
EEF1A1	Eukaryotic elongation factor 1 alpha 1
FACS	Fluorescence-activated single cell sorting
Fc	Fragment crystallisable
FC	Fold change
FDA	Food and drug administration
FOXA3	Forkhead Box A3
FSC	Forward scatter
GEF	Guanine exchange factor
GFP	Green fluorescent protein
GM-CSF	Granulocyte-macrophage colony-stimulating factor
GO	Gene ontology
GPCR	G-protein coupled receptor
GTP	Guanosine-5-triphosphate
HCl	Hydrochloric acid
HIFBS	Heat inactivated fetal bovine serum
HIV	Human immunodeficiency virus
HRH1	Histamine receptor H1
HTS	High-throughput screening
Hv1/VSOP	Hydrogen voltage-gated channel 1/voltage-sensor domain-only protein
IC50	Half maximal inhibitory concentration
ICAM	Intercellular adhesion molecule
IFN	Interferon
Ig	Immunoglobulin
IL	Interleukin
IL4I1	Interleukin 4 induced 1

ITAM	Immunoreceptor tyrosine-based activation motif
JHCCL	Johns Hopkins Clinical Compound Library
LFA-1	Lymphocyte function-associated antigen-1
LP3	Lipofectamine 3000
LPS	Lipopolysaccharides
LTA	Lipoteichoic acid
Mac-1	Macrophage-1 antigen
MARCO	Macrophage receptor with collagenous structure
Mcl-1	Myeloid Cell Leukemia 1
MDCK	Madin-Darby canine kidney cells
MDMs	Monocyte-derived macrophages
METTL4	Methyltransferase like 4
METTL9	Methyltransferase like 9
MHC	Major Histocompatibility Complex
MIC	Minimum inhibitory concentration
MOI	Multiplicity of infection
MPO	Myeloperoxidase
mRNA	Messenger RNA
MRSA	Methicilin resistant *Staphylococcus aureus*
NaCl	Sodium chloride
NADPH	Nicotinamide adenine dinucleotide phosphate
NaOH	Sodium hydroxide
NDUFS5	NADH:Ubiquinone Oxidoreductase Subunit S5
NE	Neutrophil elastase
NET	Neutrophil extracellular trap
NO	Nitric oxide
NOX2	NADPH oxidase 2
OD	Optical density
OGFOD2	2-Oxoglutarate And Iron Dependent Oxygenase Domain Containing 2
P2X7R	P2X purinoceptor 7
PAK1	P21-activated kinase
PAMPs	Pathogen-associated molecular patterns
PBMC	Peripheral blood mononuclear cells

PBS	Phosphate buffered saline
PCA	Principal component analysis
PI(3)P	Phosphatidylinositol 3-phosphate
PI3K	Phosphoinositide 3-kinase
PPIA	Peptidylprolyl isomerase A
PPM1D	Protein phosphatase magnesium-dependent 1
PPP	Platelet poor plasma
PRP	Platelet rich plasma
PRRs	Pattern-recognition receptors
PSGL-1	P-selectin glycoprotein ligand 1
Q-VD-OPH	Quinoline–valine–aspartic acid–difluorophenoxymethyl ketone
Rac	Rac Family Small GTPase 1
RBPMS2	RNA Binding Protein, mRNA Processing Factor 2
rcf	Relative centrifugal force
REC	Research ethics committee
REXO1	RNA Exonuclease 1 Homolog
RISC	RNA-induced silencing complex
RNA	Ribonucleic acid
RNAi	RNA interferance
RNase	Ribonuclease
ROI	Reactive oxygen intermediates
ROS	Reactive oxygen species
rpm	Revolutions per minute
RPMI	Roswell Park Memorial Institute
RT-qPCR	Real time quantitative polymerase chain reaction
scRNAseq	Single cell RNA sequencing
SDS	Sodium Dodecyl Sulphate
SDS-PAGE	SDS-Polyacrylamide Gel Electrophoresis
SFK	Src-family kinases
siRNA	Short interfering RNA
SNAP	Soluble N-ethylmaleimide-Sensitive Factor Attachment Proteins
SNARE	SNAP receptor
SodA	Manganese-dependent superoxide dismutase

SSC	Side scatter
ssDNA	Single stranded DNA
Syk	Spleen Associated Tyrosine Kinase
TAE	Tris-acetate-EDTA
TBS	Tris buffered saline
TCA	Trichloroacetic Acid
Th2	T helper
THY	Todd-Hewitt broth supplemented with 0.5% yeast extract
TLR	Toll-like receptor
TNF	Tumour necrosis factor
TNFSF13B	TNF superfamily member 13b
TUBA1B	Tubulin alpha 1b
V-ATPase	Vacuolar type adenylpyrophosphatase
VPS34	Vacuolar Protein Sorting 34 Homolog
YJEFN3	YjeF N-Terminal Domain Containing 3

1 Introduction

Infections are caused by pathogenic microbes, resulting in an estimated 13.7 million deaths in 2019 (Ikuta *et al.*, 2022). Microbes can either be transmitted from other individuals and the environment or they can exist as commensal organisms that become pathogenic under the right conditions. For example, *Streptococcus pneumoniae* is a commensal bacterium that colonises the nasal pharynx causing no harm to the host. However, if it establishes colonies within tissues it can cause diseases such as pneumonia in the lungs and meningoencephalitis in the brain, which can be fatal (Dockrell, Whyte and Mitchell, 2012). If the bacterium enters the lungs, the immune system becomes activated to clear the pathogen before it can cause disease. Immunity is generally classified into two systems: the innate immune system and the adaptive immune system. This classification is based upon non-specific innate pathogen responses and pathogen-specific adaptive responses. Recognition of pathogens triggers an inflammatory response whereby further innate immune cells will migrate to the infection site. These cells, as well as specific receptor binding, will then activate an adaptive immune response which is specific to the pathogen and which evolves to improve with time (Chaplin, 2010). If the infection persists or worsens due to the pathogens ability to adapt to the host environment or evade the immune response, then antibiotics will be needed to kill the bacteria.

1.1 The Innate Immune System in the Context of Bacterial Infection

The innate immune system encompasses physical barriers to prevent entry to the host including epithelial cell layers and mucus layers, as well as a range of white blood cells and soluble factors (Table 1.1). The immune system is able to distinguish between self and non-self; failure to do so results in autoimmune diseases. The innate immune system recognises pathogen-associated molecular patterns (PAMPs) which are highly conserved across a wide variety of microorganisms. PAMPs are diverse and range from bacterial cell wall components such as lipopolysaccharides (LPS) and lipoteichoic acid (LTA) to viral ssDNA or dsRNA. Recognition of PAMPs occurs by binding to pattern-recognition receptors (PRRs) which are expressed by cell types of the immune system. There are three classes of PRRs: secreted PRRs which opsonise microbes, endocytic PRRs which are expressed on the cell surface of

Innate immune system component	Function during infection
Basophils	Main role in initiating allergic immune response and host defence against multicellular parasites (Medzhitov, 2007; Chhiba *et al.*, 2017)
Complement proteins	Mark pathogens for uptake by phagocytes or cause osmotic lysis of pathogens by creating pores (Chaplin, 2010).
Cytokines/Chemokines	Small secretory proteins with a wide variety of effects, binding receptors to regulate the immune response or acting as chemoattractants to recruit cells to sites of injury and infection (Foster and Slonczewski, 2011).
Defensins	Small antimicrobial peptides that insert into the bacterial cytoplasmic membrane. The resulting pore disrupts the membrane potential leading to cell death (Foster and Slonczewski, 2011).
Dendritic cells	Phagocytose pathogens and present antigen to initiate adaptive immunity. They are primarily found in lymphoid tissues but are present in most tissues (Chaplin, 2010).
Eosinophils	Defence against multicellular parasites (Medzhitov, 2007)
Epithelial cells, cilia and mucus layer.	Tight epithelial cell junctions act as a barrier preventing entry of pathogens, whilst motile cilia propel a mucus layer that traps allergens and pathogens to prevent colonisation. Present in the respiratory, gastrointestinal and urogenital tracts (Chaplin, 2010).
Macrophages	Can be tissue specific/intrinsic or differentiate *in situ* from recruited peripheral blood monocytes. Their functions include phagocytosis, intracellular killing of microbes, antigen presentation and secretion of pro-/anti-inflammatory signals (Davies *et al.*, 2013).
Mast cells	Main role in initiating an allergic immune response by secreting inflammatory mediators, these cells are found mainly in mucosal layers and connective tissues rather than the circulation (Medzhitov, 2007; Chhiba *et al.*, 2017)
Monocytes	Circulating phagocyte, present antigens and can differentiate into macrophages (Chaplin, 2010).
Natural Killer (NK) cells	Recognise and kill cells infected with intracellular pathogens (Hoebe, Janssen and Beutler, 2004).
Neutrophils	Most abundant white blood cell in circulating blood, main function is to destroy microbes by phagocytosis or degranulation (Kennedy and DeLeo, 2009).

Table 1.1: ***A general overview of the components of the innate immune system and their function.***

phagocytes and cytosolic PRRs which bind intracellular PAMPs such as foreign DNA and proteins, e.g. viral envelope proteins. Endocytic and secreted PRRs are essential for phagocytosis of pathogens and will be discussed in more detail in section 1.2 (Janeway, 1989; Iwasaki and Medzhitov, 2010).

After the pathogen has been phagocytosed and killed intracellularly, fragments can be trafficked to the surface of the cell. A group of proteins called MHC (Major Histocompatibility Complex) proteins display these pathogen fragments, called antigens, on the cell surface – this is known as antigen presentation. Dendritic cells are the main antigen presenting cells, but macrophages and even neutrophils can also present antigen in a context-specific fashion (Villadangos and Schnorrer, 2007; Vono *et al.*, 2017; Tang *et al.*, 2022). The adaptive immune system, consisting principally of T and B lymphocytes, recognises specific regions of these antigen called epitopes via the T and B cell receptors, activating them to undergo clonal expansion (Foster and Slonczewski, 2011).. There are a range of T and B cell subtypes with different functions including activation of other cells, antibody production and destruction of infected host cells, all highly antigen-specific (Chaplin, 2010; Iwasaki and Medzhitov, 2010).

1.1.1 Neutrophils

Neutrophils, the most abundant white blood cell in humans, are hugely important for pathogen clearance through functions including phagocytosis, ROS production, degranulation and NETosis which are discussed in later sections. They circulate in the blood, becoming primed for activation upon detection of pathogens (through PAMP recognition) or signals of tissue injury and inflammation such as cytokines and chemokines (Kennedy and DeLeo, 2009). Chemoattractant gradients are established upon infection for the recruitment of immune cells including neutrophils. Early neutrophil recruitment is followed by dramatic amplification of the response, by a process called swarming, of both tissue-resident and early recruited cells (Lämmermann *et al.*, 2013). Multiple receptors including Fc, adhesion, cytokine and PRRs regulate polarisation and migration of neutrophils. Activation of these receptors can also enhance neutrophil functions in the context of priming whereby soluble cytokines enhance subsequent responses such as ROS generation or degranulation on exposure to pathogens, or reverse migration from the tissues back into the circulation (Guthrie *et al.*, 1984; Colom *et al.*, 2015; Vogt *et al.*, 2018).

In response to infection or injury some cell types have altered selectin (a family of C-type lectin glycoproteins) expression levels, such as increased P-selectin levels on epithelial cells. P-selectins (amongst others) promote binding of circulating neutrophils through PSGL-1 (P-selectin glycoprotein ligand 1) which mediates a process called rolling (Moore *et al.*, 1995). The neutrophil cells roll along the vessel wall until they strongly adhere and crawl along the endothelial surface via interactions with specific adhesion molecules; most importantly the interactions between neutrophil integrins CD11a/CD18 (LFA-1) and CD11b/CD18 (Mac-1) and endothelial ICAMs (Intercellular Adhesion Molecules). Adhering neutrophils then transmigrate through the endothelium into the affected tissue which is facilitated by specific cell surface proteins such as CD44 and CD47 (Khan *et al.*, 2004; Kobayashi *et al.*, 2005).

1.1.2 Macrophage Subtypes

Macrophages have both pro- and anti-inflammatory roles in immunity to maintain normal homeostasis (Davies *et al.*, 2013). This may be by the engulfment of apoptotic cells or other tissue-specific material or by the ingestion and killing of invading micro-organisms (Italiani and Boraschi, 2014). Most mammalian organs possess tissue resident macrophages. Studies involving organ transplantation have shown that most tissue resident macrophage populations are established during embryonic development and are maintained by self-renewal (Byrne *et al.*, 2020). Tissue-specific cues and stimuli may give rise to distinct macrophages with specialised features to the tissue in which they reside. For example, the lungs contain two populations of macrophages: alveolar macrophages which are the first-line of defence against inhaled microorganisms and interstitial macrophages which have a role in the activation of dendritic cells (Gong *et al.*, 1994). After recognition of a pathogen, the tissue resident macrophages drive the activation of leukocytes which migrate to the affected area. These include circulating monocytes which differentiate into macrophages upon entering the tissue (Davies *et al.*, 2013). Generally monocyte-derived macrophages (MDMs) are distinct from tissue-resident macrophages but this appears to be dependent on the affected tissue and the signals within that environment (Italiani and Boraschi, 2014). In tissues with high cell turnover such as the gut, MDMs reinforce the tissue-resident population and comprise a high proportion of resident cells throughout life (Bain *et al.*, 2015). There is evidence for monocyte-derived macrophages replacing both Kupffer cells in the liver and alveolar macrophages in the lungs post injury and infection (Roth, Strickland and Copple, 2020; Arafa *et al.*, 2022). In both

instances the MDMs have unique functions and transcriptomic profiles. For example, in a murine model, MDMs replacing alveolar macrophages post viral infection can aid recovery from further bacterial infection (Blériot, Chakarov and Ginhoux, 2020).

Wherever they are sited, macrophage phenotype and function can be regulated by a variety of mechanisms. Some T cells are able to influence macrophage functions by the production and secretion of cytokines. For example, Th1 cells produce IFN-γ resulting in activation of macrophages, originally termed M1 macrophages. Whereas Th2 cells produce different interleukins (IL) promoting the resolution of inflammation by inducing the macrophages to produce anti-inflammatory mediators, which were termed M2 macrophages. This process is called polarisation of macrophages, although it has been shown that macrophages can have mixed phenotypes between M1 and M2, suggesting the activation of different characteristics is a continuum rather than fixed (Mills *et al.*, 2000; Benoit, Desnues and Mege, 2008; Smith *et al.*, 2016). This classical M1 and M2 characterisation was originally coined following *in vitro* studies following activation with specific stimuli however, the complex tissue micro-environments and tissue-specific signals are not reflected in these laboratory settings. Activation of either phenotype can also be reversible in response to other stimuli such as cytokines and fatty acids. In addition to M1 and M2-like macrophages, further subsets have also been described including macrophages specific to atherosclerotic plaques and regulatory macrophages which limit inflammation during the immune response (Atri, Guerfali and Laouini, 2018). Single cell RNA sequencing (scRNAseq) is further demonstrating the distinct transcriptional profiles of individual macrophages leading to the identification of novel subsets such as those found in atherosclerotic plaques (Yu *et al.*, 2023).

Despite the above enhancements in macrophage characterisation, the concept of M1/M2 polarisation remains helpful and widely used. Specific cell surface markers are typically used to identify M1 and M2 macrophages. These are CD64 and CD80 for M1 macrophages and CD163 and CD206 for M2 macrophages. The expression of these markers can be altered independently of one another by different stimulating cytokines (Skytthe, Graversen and Moestrup, 2020). As well as cell surface markers, macrophage polarisation state can be determined by identification of upregulated transcription factors, production of particular cytokines and functional characteristics, such as high levels of antigen presentation by M1-like macrophages (Porcheray *et al.*, 2005; Atri, Guerfali and Laouini, 2018). Despite M1 macrophages pro-inflammatory phenotype and more efficient NO production required for

their intracellular anti-microbial activity, recent studies have shown that M2-like macrophages are capable of higher levels of phagocytosis (Schulz *et al.*, 2019; Thiriot *et al.*, 2020).

1.1.3 *Streptococcus pneumoniae*

S. pneumoniae is a Gram-positive encapsulated coccal bacterium that colonises the nasopharynx of healthy adults and more frequently healthy children, but can cause invasive and potentially fatal disease when micro-aspiration allows entry to the lungs. It is the most common cause of community acquired pneumonia and middle ear infection. More rarely, *S. pneumoniae* infection can cause meningitis and septicaemia. A modelling study suggested that *S. pneumoniae* was responsible for 829,000 deaths in 2019, was the leading bacterial cause of death in young children globally, and was the third-leading bacterial cause of death across all ages (Ikuta *et al.*, 2022).

The polysaccharide capsule is a major virulence factor, as it resists phagocytosis in the absence of antibody or complement-mediated opsonisation (and hence antibody-deficient patients are particularly susceptible). Variations of the repeated capsular subunits distinguish the many serotypes, of which 100 have been identified to date (Ganaie *et al.*, 2021). Some serotypes are better colonisers but lack the ability to cause invasive disease, with the reverse also true (Sjöström *et al.*, 2006). Multivalent polysaccharide-protein vaccines against a number of serotypes have reduced invasive pneumococcal disease when successfully deployed, but non-vaccine serotypes frequently increase in incidence in response and some serotypes (e.g. serotype 3) are still able to cause disease despite vaccination (Weinberger *et al.*, 2018; Aydin *et al.*, 2023). Challenges also include poor vaccine uptake and the fact that vaccine target groups (children and the elderly) may not make optimal or sustained antibody responses. Other virulence factors and the ability to form biofilms also contribute to impaired phagocytosis of this pathogen hence targeting the capsule alone may not be sufficient (Domenech *et al.*, 2013).

Almost all clinical isolates of *S. pneumoniae* release the pore-forming toxin pneumolysin, which can promote both colonisation and invasion (Karthikeyan *et al.*, 2013). Pneumolysin binds cholesterol in host cell membranes and forms multimers to generate a pore, allowing influx and release of ions and small molecules. Higher concentrations lead to lysis of target cells including lung epithelium, neutrophils and macrophages. However, lower concentrations

of pneumolysin triggers host cell repair processes and generates inflammatory responses such as neutrophil influx that may limit infection (Ikuta *et al.*, 2022; Pereira *et al.*, 2022).

In mouse models, depletion of neutrophils prior to pneumococcal infection resulted in increased bacterial burden in the lungs, whilst enhanced recruitment at later time points was associated with adverse outcomes (Bou Ghanem *et al.*, 2015). This apparent contradiction illustrates that neutrophils can be harmful as well as protective. Killing of *S. pneumoniae* by neutrophils *in vitro* is dependent on azurophilic granule proteases (see section 1.3) such as elastase and cathepsin G; mice lacking these proteases failed to control infection, with no defect in neutrophil lung recruitment but markedly increased mortality (Hahn *et al.*, 2011). *S. pneumoniae* produces a range of virulence factors. For example, SodA can neutralise ROS, a key component of the neutrophils antimicrobial repertoire. Therefore, the neutrophil oxidative burst is dispensable for killing this organism. Pneumolysin can kill neutrophils, leading to the release of the serine proteases and tissue damage, for example by cleaving host immune receptors (Domon and Terao, 2021). Thus, neutrophils help clear the bacterial challenge but may damage the lungs in the process.

1.2 Phagocytosis

PRRs bind to a broad range of PAMPs leading to the engulfment of the pathogen by a process called phagocytosis. Both neutrophils and macrophages are 'professional phagocytes', although other cells can ingest pathogens. In response to pro-inflammatory cytokines, some PRRs, including collectins and ficolins are secreted, which opsonise (bind and coat) the pathogen and activate the complement system (Iwasaki and Medzhitov, 2010). Other PRRs such as Toll-like receptors (TLRs), scavenger receptors and opsonic receptors are transmembrane proteins that are present on many cells of the immune system. TLR activation does not directly result in phagocytosis but can activate other non-opsonic receptors, whereas ligand binding to opsonic receptors directly facilitates phagocytosis. Phagocytosis is also important for the clearance of apoptotic cells (efferocytosis) which is essential for tissue homeostasis (Morimoto *et al.*, 2006). Efferocytosis can be performed by both professional and non-professional phagocytes (e.g. macrophages and epithelial cells, respectively) although macrophages are the most important scavengers of dead cells. The process of recognition and phagocytosis involves alternative receptors and signalling proteins depending

on the target, some mechanisms are well understood whilst others are not (Freeman and Grinstein, 2014; Rosales and Uribe-Querol, 2017).

1.2.1 Phagocytosis Mechanism

Bacteria can be opsonised by both complement proteins and antibodies which are then recognised by complement receptors (CR) or Fc receptors (FcR), respectively (May *et al.*, 2000). Described herein (and illustrated in Figure 1.1) is phagocytosis mediated by a family of opsonic receptors called FcγRs that recognise the Fc portion of IgG antibodies. Upon ligand binding, FcγRs aggregate, leading to the phosphorylation of ITAMs (immunoreceptor tyrosine-based activation motifs) present within the cytoplasmic domain of the receptor, by Src-family kinases (SFK) (Figure 1.1). This facilitates binding of Syk which leads to the recruitment and activation variety of proteins and second messenger molecules. In terms of the formation of the phagosome, Syk leads to activation of a guanine exchange factor (GEF) protein called Vav. This in turn activates a Rho GTPase, Rac, which regulates Arp2/3 (Ravetch and Bolland, 2001; Rosales and Uribe-Querol, 2017). Arp2/3 induces the polymerisation of actin which is required for pseudopod extension (May *et al.*, 2000). F-actin is depolymerised between the pseudopod extensions to create the phagocytic cup, the plasma membrane envelops the pathogen to form the phagosome (Flannagan, Heit and Heinrichs, 2015). Maturation of the phagosome to result in intracellular killing is discussed in section 1.3.1. Activation of these receptors can also result in degranulation, transcription alterations and release of inflammatory mediators (Rosales and Uribe-Querol, 2017).

1.3 Microbicidal Mechanisms

In addition to pathogen ingestion into a phagosome, neutrophils also have the ability to release antimicrobial molecules from granules and produce extracellular traps (NETs) whilst macrophages can undergo apoptosis to assist with bacterial clearance. However, both cell types share a key mechanism for the destruction of an internalised pathogen, namely maturation of the phagosome. In the neutrophil this incorporates assembly of the NADPH oxidase and fusion of the granules with the phagosome with fairly modest and transient acidification, whilst in macrophages there is more dramatic and sustained acidification of the

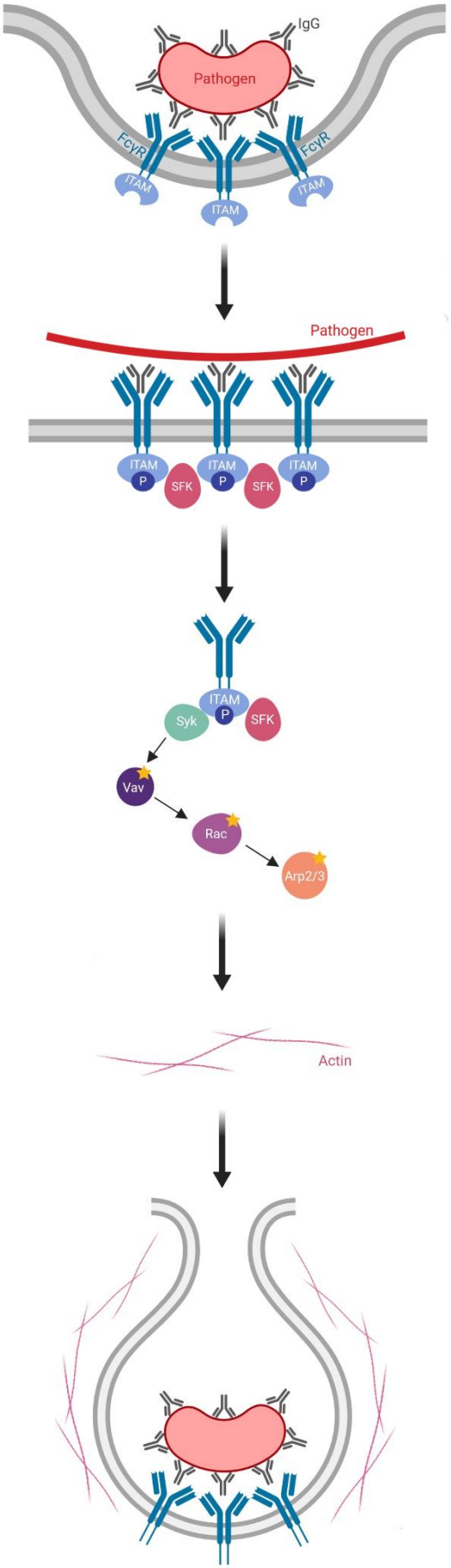

Figure 1.1 – ***Phagocytosis mechanism facilitated by Fc receptor binding.***
Pathogens opsonised by soluble factors, such as antibody (IgG) or complement proteins, are recognised by receptors on phagocytes such as macrophages and neutrophils. These receptors (FcγRs) aggregate in the plasma membrane upon binding to the Fc region of IgG. SFK is recruited which phosphorylates a receptor cytoplasmic domain, ITAM. Phosphorylation of ITAM recruits Syk which leads to the activation of Vav. Vav is now able to activate Rac, a Rho GEF which regulates Arp2/3. Arp2/3 activation induces polymerisation of actin to form the phagocytic cup. Adapted from (Rosales and Uribe-Querol, 2017). Created with Biorender.com

phagosome with prominent lysosomal fusion events (Marriott *et al.*, 2005; Yipp and Kubes, 2013). Neutrophils generate abundant ROS at the phagosomal membrane due to high levels of expression of the multi-component NADPH oxidase. *S. pneumoniae* is more resistant to ROS-mediated killing, whilst ROS are essential for the execution of some bacteria such as *Staphylococcus aureus* (Marriott *et al.*, 2008). The main mechanism of killing of this bacterium by neutrophils appears to be via the granule proteins (Standish and Weiser, 2009). Granule proteins function best at a more neutral pH, and this may explain why the neutrophil phagosomal pH is tightly controlled.

Neutrophils can release the contents of some granules into the extracellular space by exocytosis, whereby the membrane of the granules fuses with cytosolic plasma membrane; this is termed degranulation. It also results in additional membrane proteins being displayed on the surface of the neutrophil (Borregaard and Cowland, 1997). The granules are also directed to the phagosomal membrane and contribute to the killing of ingested pathogens. There are four subsets of granules with different thresholds of calcium elevation to signal their release; secretory, gelatinase (tertiary), specific (secondary) and azurophil (primary) granules (Sengeløv, Kjeldsen and Borregaard, 1993; Abdel-Latif *et al.*, 2004; Jog *et al.*, 2007). The proteins that are secreted from gelatinase and specific granules, such as lysozyme, create an environment that limits microbial growth. The resulting surface proteins allow extravasation and migration through the tissue (Johnson *et al.*, 2011; Yin and Heit, 2018). Azurophil granules contain the most potent antimicrobial proteins and therefore have the highest activation threshold to tightly regulate exocytosis, as excessive release of such mediators can result in inflammatory diseases (Johnson *et al.*, 2011). The contents of these granules include the azurosome protein complex, which consists of eight proteins including neutrophil elastase (NE) and myeloperoxidase (MPO). MPO is required for the transport and release of other proteases whilst NE is important for the degradation of bacterial virulence factors. Other proteins released from these granules can inhibit DNA, RNA and protein synthesis by blocking the uptake of essential nucleic acids and amino acids (Brogden, 2005; Soehnlein, 2009).

Azurophil degranulation is also important in NET release. This can occur in response to a variety of factors including pathogen interaction, antibodies, cytokines, chemokines, immune complexes and ROS (Vorobjeva and Chernyak, 2020). There is evidence for NET release in a situation called frustrated phagocytosis, whereby the target pathogen or particle is too large

to be phagocytosed by the neutrophil (Branzk *et al.*, 2014). Pathogens, including *S. pneumoniae,* can induce NET release. Different strains vary in their susceptible to killing by these structures, depending on the strains array of virulence factors (Storisteanu *et al.*, 2017; Martinez *et al.*, 2019). After release of the azurophil granule contents into the cytosol, serine proteases (such as NE) break down the actin cytoskeleton and translocate to the nucleus, where lamin and histones are cleaved resulting in instability of the nuclear envelope and subsequent decondensation of chromatin (Metzler *et al.*, 2014). NE also cleaves a gasdermin D protein which forms pores in the plasma membrane, allowing release of chromatin into the extracellular environment (Vorobjeva and Chernyak, 2020). Antimicrobial proteins released from aforementioned granules, bind electrostatically to the decondensed chromatin adding to the antimicrobial properties of NETs, which are capable of binding both Gram-positive and Gram-negative bacteria (Brinkmann *et al.*, 2004; Fuchs *et al.*, 2007; Yipp and Kubes, 2013).

Macrophages have two stages of intracellular killing. Early intracellular killing is attributed to the formation of a mature phagolysosome. Failure of this process may occur either due to high pathogen load or by pathogen subversion (Jubrail *et al.*, 2016; Behura *et al.*, 2021). Late phase killing is mediated by apoptotic pathways that can be induced by permeabilisation of the phagolysosome membrane. Permeabilisation occurs when lysosomal proteases of the cathepsin protein family are activated. This can lead to the cleavage of Mcl-1, an anti-apoptotic protein, via activation of caspase proteins. This mechanism is particularly important to prevent replication of intracellular pathogens as well as down-regulation of the inflammatory response (Marriott *et al.*, 2005; Bewley *et al.*, 2011).

1.3.1 Phagolysosome Acidification

The process of phagosome maturation involves intracellular vesicle fusion to provide antimicrobial molecules creating an inhospitable environment. There are similarities in this process between macrophages and neutrophils but they also differ, for example in the speed of maturation and intensity of oxidative burst (Nordenfelt and Tapper, 2011; Flannagan, Heit and Heinrichs, 2015).

In macrophages, the early phagosome characterised by the presence of Rab5, a small GTPase that promotes phagosome remodelling by activating some kinases, such as Class III phosphatidylinositol 3-kinase (PI3K) to produce the lipid PI(3)P. This process is required for phagosomal maturation (Figure 1.2) (Vieira *et al.*, 2001). The progression to late phagosome

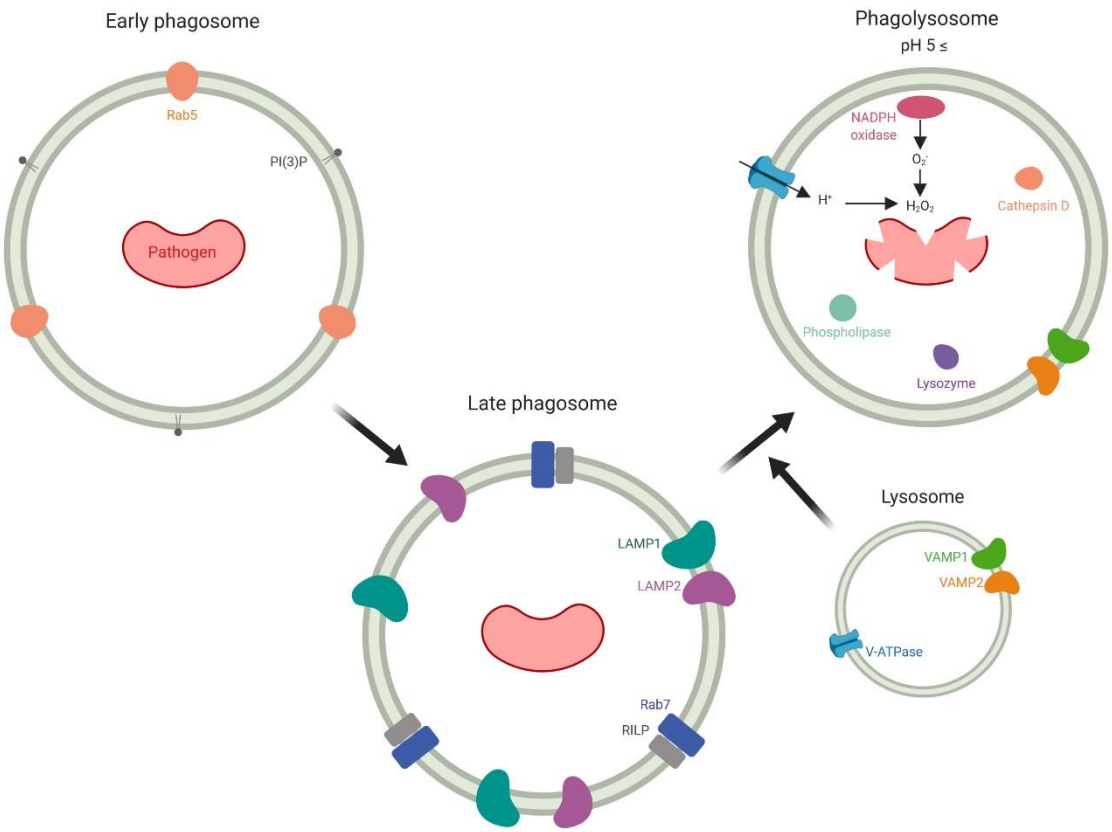

*Figure 1.2 – **Phagolysosome acidification**.* Following initial phagocytosis. The early phagosome is characterised by the presence of Rab5 which promotes the formation of PI(3)P. Progression to the late phagosome is then characterised by Rab exchange whereby Rab5 is replaced by Rab7. Rab 7 recruits RILP which is required for fusion with lysosomes. Lysosome fusion, facilitated by SNAREs and VAMPs, allows maturation and acidification through the delivery of destructive enzymes which make the environment inhospitable. Adapted from (Flannagan, Heit and Heinrichs, 2015). Created with Biorender.com

is characterised by the loss of Rab5 and the acquisition of Rab7, which is required for lysosomal fusion by recruiting Rab7-interacting protein (RILP). The late phagosome also contains lysosome-associated membrane protein (LAMP) 1 and 2 which allows trafficking of the late phagosome towards lysosomes (Harrison *et al.*, 2003; Huynh *et al.*, 2007). Fusions with these lysosomes is facilitated by SNARE proteins and vesicle-associated membrane proteins (VAMP) 7 and 8 (Wade *et al.*, 2001). Vacuolar ATPase (v-ATPase) is also required for complete phagosomal maturation as it pumps protons from the cytoplasm into the lumen of the phagosome decreasing the pH to 5 or lower (Flannagan, Heit and Heinrichs, 2015). Antimicrobial proteins within the phagosome contribute directly to the breakdown of specific pathogen components. Two proteins from the cathepsin family, cathepsin L and cathepsin D, are important for proteolytic cleavage with the latter involved in degrading secreted bacterial

toxins (Flannagan, Heit and Heinrichs, 2015). Enzymes required for the lysis of the bacterial cell include lysozyme, which is involved in the hydrolysis of peptidoglycan linkages, and phospholipases which disrupt the bacterial membrane (Miyauchi *et al.*, 1985; Flannagan, Heit and Heinrichs, 2015).

The dramatic neutrophil respiratory burst occurs when the multi-component NADPH oxidase is assembled at the phagosomal membrane, generating abundant ROS. In addition to the bactericidal effect, the resulting flux of protons partially counteracts the acidification generated by v-ATPase. In the setting of chronic granulomatous disease, there is a rapid and extensive acidification of the phagosome due to defective NADPH oxidase (Segal *et al.*, 1981). Hv1/VSOP (hydrogen voltage-gated channel 1/voltage-sensor domain-only protein) counteracts the charge imbalance induced by activation of NADPH oxidase, contributing to pH regulation; neutrophils lacking Hv1/VSOP generated phagosomes with dysregulated pH, with large population of alkaline (37%) and a smaller proportion (14%) of acidic phagosomes (El Chemaly *et al.*, 2010). Even with normal Hv1 expression and function, individual phagosomes vary, and many neutrophil phagosomes do undergo significant acidification (Nunes, Guido and Demaurex, 2015; Hesselink *et al.*, 2020). Failure of this acidification may result in impaired killing of micro-organisms and is relevant in critical illness (Hesselink *et al.*, 2020). Importantly, the complement component C5a was found to impair neutrophil phagosomal acidification and killing of *Staphylococcus aureus* (as did inhibition of the Class III PI3K VPS34, which generates PI(3)P), recapitulating events seen in neutrophils from critically ill patients (Wood *et al.*, 2020).

1.4 Antibiotic Resistance

Antibacterial resistance is caused by bacterial genetic mutations, which can be horizontally transferred, and natural selection for resistant organisms in the presence of antibiotics resulting in a global problem. Even required usage of antibiotics can select for bacteria with genetic mutations that encode resistance to antibiotics. This has been further accelerated by the misuse and overuse of antimicrobial treatments. It is estimated that antimicrobial resistance results in 700,000 deaths worldwide per year with the shocking expectation that this will rise to 10 million by 2050 if no new treatments are developed (HM Government, 2019).

Many microbes have evolved to rapidly respond to a changing environment, which also includes existing in the presence of other microbes. In order to ensure their survival they can

produce antimicrobials to kill competing strains. As a result of this many antibiotics are derived from other bacteria and fungi. Penicillin, streptomycin and chloramphenicol are all produced by fungi (Clardy, Fischbach and Currie, 2009).

B-lactam antibiotics, such as penicillin, target bacterial penicillin-binding proteins (PBPs). PBPs are essential for cell wall maintenance, therefore targeting these proteins results in the weakening of the cell wall during bacterial growth and eventual lysis (Gordon *et al.*, 2000). Penicillin resistance has been described in *S. pneumoniae*, as early as the 1970's. Resistance to penicillin occurs through PBP mutations which results in alterations of the binding site. The inability of penicillin to bind to PBPs results in treatment being ineffective against the infection (Hakenbeck *et al.*, 2012). As a result of this, *S. pneumoniae* is now listed as medium on the priority list for the development of new treatments by the World Health Organisation. Gram-negative bacteria can develop β-lactam resistance by producing β-lactamases that cleave the antibiotic rendering it ineffective. Other mechanisms of antibiotic resistance include efflux pumps that allow the removal of toxic substances, including antibiotics and protection of the binding site by other associated proteins (Munita and Arias, 2016).

1.4.1 Current immunotherapies against infectious diseases

Immunotherapies target and manipulate the immune response in order to eliminate pathogens or diseased cells. Immunotherapy is also used in the treatment of cancer. Some infectious diseases can be prevented through vaccinations. However, these are specific to certain microbes as they work by targeting the adaptive immune response. Other immunotherapies include monoclonal antibodies which can work with a variety of mechanisms (Shepard *et al.*, 2017). They can bind to cell surface receptors to induce cell death of diseased cells and can recruit immune cells through Fc region binding in a process called antibody-dependent cellular cytotoxicity. T-cell engineering in which patient T cells are genetically modified to enhance their function through the addition of a chimeric antigen receptor which will interact with a specific target. These T-cells (CAR-T-cells) are then re-introduced to the patient. Cytokine therapy can alter disease states, for example an increase in dendritic cells resulting in an enhanced immune response against *Mycobacterium tuberculosis* was observed through treatment *in vivo* with albumin-fused GM-CSF which also increased its biostability (Ramamurthy *et al.*, 2021).

A practical approach to dealing with the lack of new developments in antibiotic treatment, coupled with the gaps in knowledge of many mechanisms of pathogenesis, would be to target and enhance the host. The innate immune system offers targets for manipulation to treat resistant infections due to its broad effectiveness again microbes. A pan-caspase inhibitor has recently shown promising results for treatment of antibiotic resistant infections *in vivo*. The inhibitor, Q-VD-OPH (quinoline–valine–aspartic acid–difluorophenoxymethyl ketone), is cell permeable, with no toxicity *in vivo* and previous data revealed inhibition of apoptosis in models of injury and viral infection. Q-VD-OPH had no effect on the growth rate of any of the bacteria; MRSA (methicillin-resistant *Staphylococcus aureus*), *Streptococcus pyogenes* and *Pseudomonas aeruginosa*. 4 hours post inoculation with aforementioned bacteria, the mice were given a single dose of Q-VD-OPH. In all conditions both the bacterial burden and the abscess size decreased. Survival of mice infected with *P. aeruginosa* increased from 60% in the control groups to 100% with Q-VD-OPH treatment. Treatment also resulted in increased monocyte, macrophage and neutrophil infiltrates, with activity dependent on TNF and IL-1β (Alphonse *et al*., 2021).

1.5 Hypothesis and Aims

This project aims to understand the variability of bacterial phagocytosis and killing within cell populations, hypothesising that this will reveal therapeutically targetable regulators that can be used to enhance the immune response to bacteria as an alternative avenue to antibiotic treatment. To achieve this, I will focus on the following 3 aims:

1. Identify and validate the genetic factors regulating phagocyte phenotypic diversity in macrophages and neutrophils.
2. Develop and perform a genome-wide siRNA screen in human monocyte-derived macrophages to identify regulators of early intracellular killing of bacteria.
3. Screen macrophages challenged with GFP labelled *Streptococcus pneumoniae* using the Johns Hopkins Clinical Compound library, quantifying effects on bacterial killing.

2 Materials and methods

2.1 Ethics Statements

2.1.1 Macrophage Ethics

The South Sheffield Research Ethics Committee (REC) provided ethical approval for the collection of blood for the study of monocyte derived macrophages (REC reference 07/Q2305/7). Whole blood was collected from healthy human donors that had provided informed written consent in order to participate.

2.1.2 Neutrophil Ethics

Written informed consent was obtained before blood was taken from healthy volunteers according to the protocol approved by the National Research Ethics Committee - Yorkshire & The Humber - Sheffield (05/Q2305/4) for the isolation and study of neutrophils.

2.2 Primary Cell Isolation and Cell Line Maintenance

2.2.1 Neutrophil Isolation

After collection from a healthy donor, blood was added to 5ml 3.8% sodium citrate (Matindale Pharmaceuticals) in a 50ml tube and inverted to mix. Blood was centrifuged at 177rcf for 20 minutes at 20°C (all steps in the isolation of neutrophils are at 20°C unless stated otherwise). The upper phase (platelet rich plasma (PRP)) was transferred to a clean 50ml tube. 6ml of 6% Dextran, pre-warmed to 37°C, (3g dextran dissolved in 50ml saline and filter sterilised) (Pharmacosmos A/S) was added to the lower phase, filled to 50ml with 0.9% saline (Baxter) and inverted. Any bubbles formed were removed from both the tube and the top of the lid. Red blood cells were left to sediment for 20-30 minutes whilst the PRP was centrifuged at 493rcf for 20 minutes. After centrifugation the supernatant (platelet poor plasma (PPP)) was poured into a clean tube. The upper white layer above the sedimented red blood cells was transferred to a fresh 50ml tube and centrifuged at 123rcf for 6 minutes. To set up the Percoll (GE Healthcare) gradient, the upper phase (0.84ml 90% Percoll (9ml Percoll and 1ml saline) added to 1.16ml PPP) was overlaid onto the lower phase (1.02ml of 90% Percoll and 0.98ml of PPP). The pelleted cells were re-suspended in 2ml PPP and added to the top of the Percoll gradient. The gradient was centrifuged at 149rcf for 11 minutes generating three clear layers. A thin band of cells in the top layer containing PBMCs (peripheral blood mononuclear

cells) were removed and added to 10ml PPP. The middle layer of cells containing the granulocytes was added to another tube containing 10ml PPP. The cell suspension was made up to 40ml with 1xHBSS (Gibco) then counted using a haemocytometer. Cells were centrifuged at 277rcf for 6 minutes before re-suspending in RPMI 1640 + HEFES + L-Glutamine (Gibco) supplemented with 10% HIFBS (PAN Biotech) to give a cell density of 5 x 10^6/ml. Figure 2.1 summarises the isolation procedure.

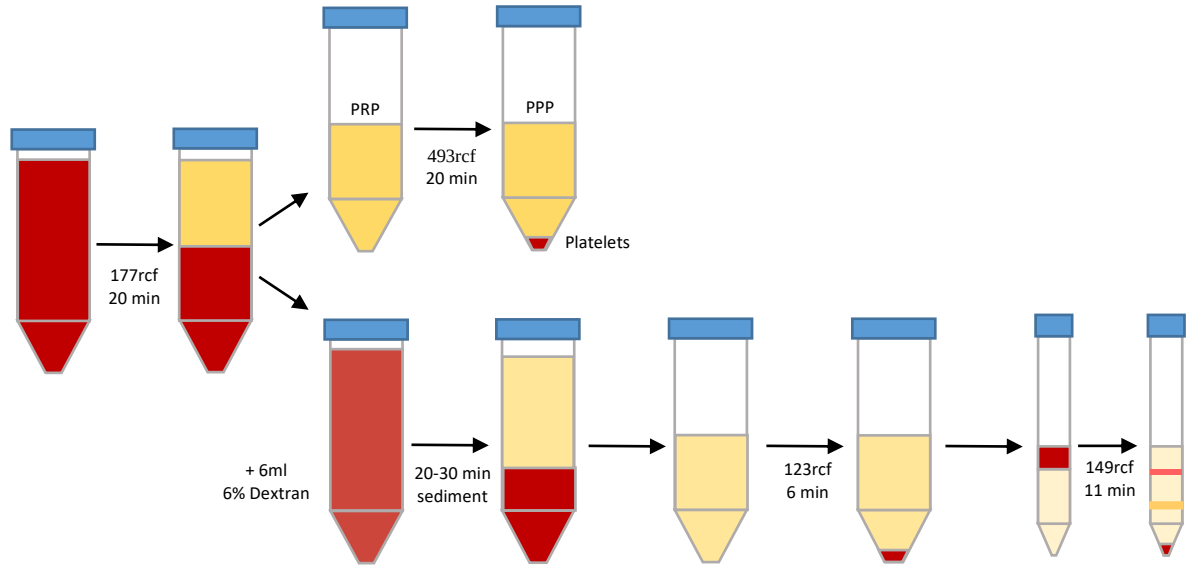

Figure 2.1: ***Neutrophil isolation method using a Percoll gradient.***

2.2.2 PBMC Isolation and Differentiation of Monocyte-derived Macrophages (MDMs)

25ml blood was transferred from a sterile collection bag and gently pipetted on top of 12.5ml of Ficoll-Paque (GE Healthcare Lifescience) in a 50ml tube leaving a clear interface. Blood was centrifuged for 277rcf for 23 minutes at 20°C. The resulting PBMC layer was transferred to a clean 50ml tube and made up to 50ml with PBS (Corning). Cells were centrifuged at 123rcf for 13 minutes at 4°C and the remaining pellet re-suspended in 2ml PBS. If the volume of blood taken required multiple tubes, all the cells were combined and centrifuged again at 123rcf for 13 minutes at 4°C. The pellet was re-suspended in 10ml pre-warmed RPMI 1640 (Lonza) + 10% New Born Calf Serum (Gibco) then counted using a haemocytometer. After counting, cells were diluted to 2x10^6/ml, assuming 10% of PBMCs seeded are monocytes. Media was changed every 3-4 days with RPMI + 10% HIFBS (PanBiotech) + 2mM L-Glutamine (Lonza). After 14 days all non-adherent cells have been washed away with the media changes leaving a monolayer of monocyte-derived macrophages (MDMs). The diagram in Figure 2.2 depicts this method of PBMC isolation.

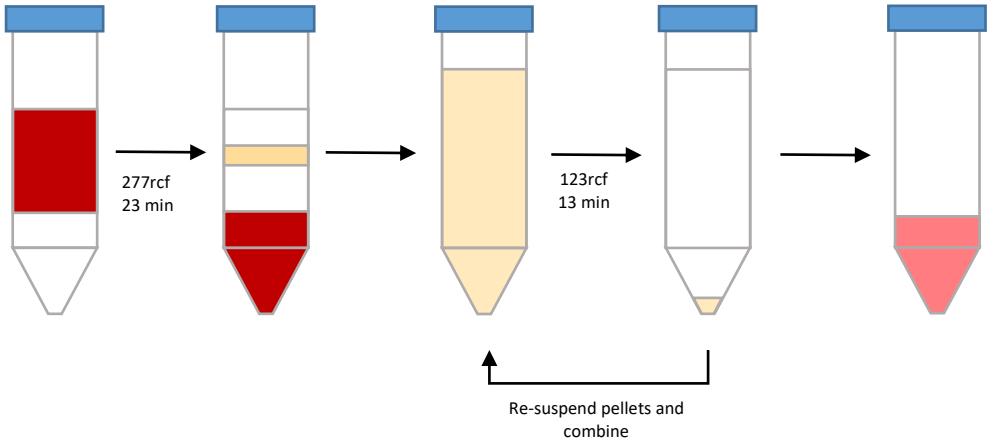

Figure 2.2: ***PBMC isolation method using Ficoll-Paque.***

2.2.3 RAW 264.7 cell line maintenance

RAW 264.7 cells were stored in cryovials in liquid nitrogen. After removing a cryovial from liquid nitrogen, it was defrosted in 37°C water bath for maximum of 2 minutes, with the lid kept above the waterline. Once defrosted the cells were transferred to 10ml pre-warmed cDMEM (complete media, Dulbecco's Modified Eagle Media (Lonza), 2mM L-Glutamine (Lonza), penicillin/streptomycin mix (Lonza) and HIFBS). The diluted cells were centrifuged at 1000rcf for 5 minutes. The supernatant was discarded and the cells were re-suspended in 15ml cDMEM, transferred to a T75 flask and incubated at 37°C / 5% CO_2. Media was removed and replaced with fresh pre-warmed media every other day. Twice weekly the cells were passaged. Media was discarded and the bottom of the flask washed with 5ml PBS. 10ml fresh media was added and a cell scraper was used to remove cells from the bottom of the flask. The cell suspension was gently pipetted up and down to ensure that the cells were not clumped together. A 1:10 dilution in PBS was carried out before counting the cells using a haemocytometer. $1x10^6$ cells were added to clean T75 flasks and made up to 15ml using cDMEM. To set up for experiments in 96 well plates, media without penicillin/streptomycin was used and 10,000 cells were added to each well ($1x10^5$ cells/ml) for use 48 hours later. Cells were used to passage 15, counting defrosted cells as passage 0.

To freeze cells, media of 3 T75 flasks containing confluent cells was replaced. The cells were scraped and the contents of the flasks were combined. A cell count was performed to calculate cell density for $1x10^6$ cells/ml. The cell suspension was centrifuged at 1000rcf for 5 minutes. The pellet was re-suspended in calculated volume of freezing media (DMEM + 5%

DMSO (Sigma)). 1ml was transferred to each cryovial. Cryovials were transferred to a Mr Frosty which was placed at -80°C for at least 24 hours before transfer to liquid nitrogen.

2.3 *Streptococcus pneumoniae* Growth and Labelling

2.3.1 THY Broth

S. pneumoniae was grown in Todd-Hewitt broth supplemented with 0.5% yeast extract (BD). 30g Todd-Hewitt broth and 5g yeast extract were dissolved in 1 litre of distilled water then autoclaved (121°C, 15 minutes) to sterilise.

2.3.2 Overnight Culture

S. pneumoniae was streaked onto Columbian Blood Agar (CBA) plates (Oxoid) and incubated for 24 hours at 37°C / 5% CO_2. Approximately 10 colonies were selected using a sterile loop and transferred to 5ml THY broth then vortexed. 10µl of bacterial suspension was transferred to another 5ml THY broth then inverted. This was repeated a further 4 times after which the tubes were incubated with loose lids for 16 hours at 37°C / 5% CO_2. The most turbid tube without sedimented bacteria was selected. 1.4ml of suspension was added to 20ml THY broth. After mixing, OD_{600nm} was measured on a spectrophotometer (Jenway). If the OD was not between 0.01 and 0.05, the culture was then adjusted accordingly with the addition of more broth or bacterial suspension. When the OD reached 0.4-0.5, 40% glycerol was added at a ratio of 1.6:1, vortexed thoroughly then frozen in 1ml Eppendorf tubes.

2.3.3 CFU Counts

To check the CFU (colony forming units) of the frozen stock, serial dilutions were carried out for each new stock. 100µl of defrosted bacterial suspension was added to 900µl PBS and vortexed. This was repeated a further 5 times until $1:10^6$ dilution was achieved. CBA plates were divided into 8 segments labelled with numbers corresponding to dilutions 10^3 - 10^6. Tubes were vortexed then a 10µl drop was added to the plate, repeating 2 more times for each tube. After allowing the droplets to dry, the plates were incubated at 37°C, 5% CO_2 overnight. The following day, the colonies were counted and the CFU/ml was calculated using the method below:

1. Viable count = number of colonies in segment/3 = average CFU/10ul
2. Multiply by 100 to give CFU/ml for that dilution
3. Multiply by $10^{'segment\ number'}$ to factor in dilution

   e.g. 14 colonies in segment 6

   Viable count = 14/3 x 100 x 10^6 = $\underline{4.7 \times 10^8\ CFU/ml}$

2.3.4 pHrodo Labelling

pHrodo labelled bacteria is used for experiments investigating phagolysosome acidification. Bacteria was defrosted and centrifuged at 9000rcf for 3 minutes. The supernatant was discarded and the pellet re-suspended in 1ml PBS. Centrifugation was repeated with the pellet re-suspended in 200µl PBS. 0.5µl of 2.55mM pHrodo (Invitrogen) was added, vortexed thoroughly then incubated at 37°C for 30 minutes on a shaker. Bacteria were centrifuged, re-suspended in 1ml Tris (Fisher Bioreagents) 150mM pH 8.4 and centrifuged again. The pellet was re-suspended in 1ml PBS before the final centrifuge step. The pellet was re-suspended in 1ml RPMI then further diluted accordingly for desired MOI (multiplicity of infection) for macrophage challenge.

2.4 Phagocytosis Assays

2.4.1 Challenging Neutrophils with Beads

For 1x10^8 beads in 1ml, 17.5µl red latex beads (Sigma-Aldrich) (from 5.7135x10^9 beads/ml stock) was added to 432.5µl RMPI + 50µl human serum (Merck) to opsonise. The bead solution was shaken for 30 minutes at 37°C after which 500µl RPMI + 10% HIFBS was added. 100µl of bead solution was added to each well for ratio of 10:1 (beads:cells), with 100µl RPMI + 10% HIFBS used as control. After isolation, neutrophils were re-suspended to a density of 1x10^7 cells/ml. 100µl of cells was added to each well containing beads or RPMI and incubated 37°C / 5% CO_2. At the desired time-point each condition was transferred to a separate Eppendorf tube and centrifuged at 400rcf for 2 minutes. The pellet was re-suspended in 200µl PBS + 2.5% BSA (made by dissolving 12.5g BSA (Melford) in 50ml PBS then filter sterilised). Centrifugation and re-suspension were repeated and samples placed on ice for analysis on the LSRII flow cytometer, recording 50,000 neutrophils each time.

2.4.2 Double-Feeding Neutrophils

To investigate if phagocytosis is a random process or not, double-feeding experiments were carried out. As previously described in 2.4.1, opsonised red beads were added to neutrophils at a ratio of 10:1. After a 30 minute incubation with red beads, the cells were transferred to an Eppendorf tube and centrifuged at 400rcf for 2 minutes. The pellet was re-suspended in 200µl PBS + 2.5% BSA. Neutrophils were centrifuged again and re-suspended in 100µl RPMI + 10% HIFBS and added to a well containing 100µl opsonised green latex beads (Sigma-Aldrich) a ratio of 10:1. After a further 30 minutes incubation at 37ºC / 5% CO_2. The wash centrifuge steps were repeated and the cells finally re-suspended in 200µl PBS + 2.5% BSA, placed on ice and analysed on the LSRII flow cytometer.

2.4.3 Challenging MDMs with Beads

Fully differentiated MDMs (achieved by day 14) were washed twice with sterile PBS. Red beads were opsonised as described in section 2.4.1 and added to MDMs at a ratio of 10:1 in 3ml RPMI + 10% HIFBS in a 6 well plate setting (Corning). After 4 hours the wells were washed 3 times with PBS. To dissociate the cells, 1.5ml Accutase (Sigma-Aldrich) was added to each well and incubated for 20 minutes at 37ºC / 5% CO_2. Cells were gently scraped using a cell scraper and each condition was transferred to separate 1.5ml Eppendorf tubes. Cells were centrifuged at 200rcf for 10 minutes then re-suspended in 500µl RPMI + 10% HIFBS and placed on ice. Samples were analysed on the LSRII flow cytometer.

2.4.4 Double-Feeding MDMs

After incubating MDMs with red beads for 2 hours at a ratio of 10:1 the cells were washed 3 times with PBS. Opsonised green beads were then added at the same ratio and incubated at 37ºC / 5% CO_2. After a further 2 hours, the cells were washed 3 times with PBS. The same cell dissociation and analysis method was used as described in section 3.4.5.

2.4.5 Flow Cytometry Analysis

Using the LSRII flow cytometer, cell populations were identified using forward and side scatter patterns. Forward scatter (FSC) voltages were 330 and 159, side scatter (SSC) voltages were 230 and 190 for neutrophils and MDMs respectively. The red beads were detected using Blue 610/20 laser and the green beads detected using Blue 530/30 laser. To overcome the

emission spectra overlap during analysis of double-feeding experiments, compensation was set up. To remove the red spill over into the green channel, neutrophils incubated with red beads only were analysed and compensated 7.3% so that the median of ingesters and non-ingesters were the same. Cells incubated with green beads only were analysed compensated 19.5% to remove spill over into the red channel. This was repeated for the MDM experiments.

2.4.6 Cell Sorting

Neutrophils and MDMs were sorted into 3 populations using either FACSAria or the FACSMelody (BD Biosciences), respectively. The populations were cells that had phagocytosed no beads, cells that had phagocytosed 1-2 beads and those that had phagocytosed 3 or more. As many cells as possible were sorted into clean FACS tubes for cytospinning.

2.4.7 Cytospinning and Staining

Cells were cytospun onto glass slides at 300rpm (Shandon Cytospin4) for 3 minutes, left to dry for 30 minutes. Slides fixed with 4% formaldehyde (Polysciences Inc) for a further 30 minutes before rinsing with water. Once dry, 1 drop of Antifade Mounting Medium with DAPI (VECTASHIELD) was placed onto the cells on the microscope slide. A coverslip was placed on top ensuring no bubbles were created then secured in place. Slides were imaged on spinning disc confocal Perkin Elmer Ultraview VoX inverted Olympus IX81.

2.4.8 Sample preparation for RNA Sequencing and subsequent analysis

Cells were sorted, as described in section 2.4.6, directly into 100µl Buffer TCL (QIAGEN) then placed on ice. 1µl 2-Mercaptoethanol was added to prevent RNA degradation by ribonucleases. Tubes were vortexed, briefly centrifuged and frozen on dry ice before transferring to -80°C. RNA purification was performed by Professor Muzlifah Haniffa's group at the University of Newcastle using a modified version of SmartSeq-2 as previously described (Villani *et al.*, 2017). RNA samples were sequenced using Illumina NextSeq500. Lanes from each sample were merged using Commandline. MultiQC was used to check the quality of the data in which average sequence length was 125bp, the average number of unique reads was 5 million and the GC content was 47% which was normally distributed showing no signs of contaminations from adapter dimers or other species. The FastQ files were subsequently analysed using R (version 4.1.1, August

2021). Reads were aligned and quantified simultaneously using the *salmon* tool to the human reference genome obtained from Ensembl (Homo_sapiens.GRCh38.104.gft.gz). The R package GOfuncR was used for gene ontology enrichment analysis which uses the gene ontology software 'FUNC'. The R script in Appendix A, provided by University of Sheffield Bioinformatics Core, was used for sequencing data analysis.

2.5 General screen optimisation

2.5.1 Infecting RAW 264.7 cells and MDMs in 96 or 384 Well Plates with *S. pneumoniae*

The strain used in these experiments was D39 ΔCPS hlpA GFP. D39 is a serotype 2 strain with chromosomal expression of GFP and its capsule encoding gene deleted. The bacteria was prepared for infection by pHrodo labelling (section 2.3.4). The volume required was calculated for desired MOI, detail is given below. The labelled bacteria was transferred to a fresh tube and diluted appropriately with RPMI + 10% HIFBS.

Cells per well x Desired MOI = CFU needed per well

CFU frozen stocks / CFU needed per well = **χ**

1000µl (frozen aliquot volume) / **χ** = volume needed in 1 well

Total volume bacteria needed = vol. for 1 well x Number of wells x 1.5 (account for error and dead volume)

Fresh RPMI needed = (100µl or 50µl (depending on well plate) x number wells x 1.5) – total volume bacteria

Wells were washed 3 times with PBS before adding the bacteria suspension (100µl per well in 96 well plates or 25µl per well in 384 well plates). The plate was then centrifuged at 150rcf for 5 minutes at room temperature then transferred to an incubator at 37°C / 5% CO_2 until a predetermined time-point. The wells were washed 3 times with PBS and RPMI containing 20µg/ml Gentamicin and 40 Units/ml Penicillin was added to each well then incubated for 30 minutes. If there were additional time-points the Pen-Strep was replaced with 0.75µg/ml of Vancomycin. The wells were then washed twice with PBS and stained following the method in 2.5.2.

2.5.2 Staining and Fixing MDM and RAW cells

0.05x CellMask in Deep Red (Invitrogen) was made by diluting 0.5µl CellMask in 10ml PBS. 25µl CellMask stain was added to each well of a 384 well plate (Greiner) containing a monolayer of MDMs and incubated in the dark for 10 minutes at 37°C. Each well was then washed twice with PBS and 4% formaldehyde was added to fix the cells. After 15 minutes in the dark, at room temperature, the cells were washed once with PBS. 25µl of 3µM DAPI (Invitrogen) was added to each well and incubated for 5 minutes. The cells were washed 3 times with PBS then 50µl PBS was added to each well for microscopy. For staining MDMs in a 96 well plate, these volumes were multiplied by 4.

2.5.3 Image Xpress

The plates were imaged on the ImageXpress Micro, high-content microscope and analysed using MetaXpress Custom Module Editor (CME). The exposure settings for both RAW 267.4 cells and MDMs are available in Table 2.1. The segmentation settings used for image analysis are detailed in Tables 2.2 and 2.3. Representative images of the segmentation are given in Figure 2.3. In brief, the 'Top Hat' tool was used on all channels to improve the signal:noise ratio. 'Find round objects' was used to identify nuclei (DAPI) and cells (CellMask / Cy5) above a set background threshold and specified sizes. 'Fill dark holes' and 'grow cells' tools were both used on the Cy5 channel to achieve better segmentation of the cells but also allows for extended membrane that may not have been captured in the z-plane. For capturing bacteria (GFP and pHrodo) 2 images were taken at each site at different z-planes. These images were be superimposed using the 'Add' function and segmented from here using the same 'find round objects' tool, specifying the size of the objects. Required measurement were set up using the cell membrane as a mask to find objects within. The number of nuclei were measured as well as the number of GFP and pHrodo positive bacteria within cells.

To analyse the data from the images, data was formatted in tab delimited text files as described by Boutros and colleagues. The published script was adapted to for both compound screen and siRNA screen data and available in Appendix C (Boutros, Hahne, & Huber, 2013).

Channel	Exposure for RAW 264.7 cells	Exposure for MDMs
DAPI	100	50
Cy5	150	150
GFP	200	200
Texas Red	n/a	300

Table 2.1: ***Exposure settings for ImageXpress microscopy.*** Exposure (given in ms) for each channel used for image acquisition for both compound and siRNA screen optimisation.

Object	Segmentation step	Settings for RAW 264.7 cells	Settings for MDMs
Cell membrane	**Top Hat** (finds small bright spots based on a filter shape and size)	Source: Cy5; Size (pixels): 170; Filter shape: Circle; Grayscale reconstruction: yes; Result: Top Hat – Membrane	Source: Cy5; Size (pixels): 170; Filter shape: Circle; Grayscale reconstruction: yes; Result: Top Hat – Membrane
	Holes (finds and, optionally, fills light or dark holes in an image and displays them as bright areas)	Source: Top Hat – Membrane; Method: FillDarkHoles; Result: Fill Holes - Membrane	Source: Top Hat – Membrane; Method: FillDarkHoles; Result: Fill Holes - Membrane
	Find round objects (identifies small, symmetrically round objects using size and intensity criteria that you specify)	Source: Fill Holes – Membrane; Approximate minimum width (µm): 3; Approximate maximum width (µm): 22; Intensity above local background: 6; Result: Find Round Objects	Source: Fill Holes – Membrane; Approximate minimum width (µm): 12; Approximate maximum width (µm): 33; Intensity above local background: 4; Result: Find Round Objects
	Grow objects without touching (expands objects by the number of pixels that you specify. Does not allow objects to touch)	Source: Find Round Objects; Grow by (pixels): 18; Ultimate: no; Result: Grow – Membrane	Source: Find Round Objects; Grow by (pixels): 20; Ultimate: no; Result: Grow – Membrane

	Remove border objects (excludes all objects that touch the edge of the image)	Source: Grow - Membrane Result: Membrane	Source: Grow - Membrane Result: Membrane
Nuclei	Top Hat	Source: DAPI; Size (pixels): 35; Filter shape: Circle; Grayscale reconstruction: yes; Result: Top Hat – Nuclei	Source: DAPI; Size (pixels): 35; Filter shape: Circle; Grayscale reconstruction: yes; Result: Top Hat – Nuclei
	Find Round Objects	Source: Top Hat – Nuclei; Approximate minimum width (µm): 5; Approximate maximum width (µm): 9; Intensity above local background: 40; Result: Find Nuclei	Source: Top Hat – Nuclei; Approximate minimum width (µm): 5; Approximate maximum width (µm): 9; Intensity above local background: 100; Result: Find Nuclei
	Remove Border Objects	Source: Find Nuclei; Result: Nuclei	Source: Find Nuclei; Result: Nuclei
GFP Bacteria	**Add** (combines the intensity values of 2 images)	Source 1: GFP; Source 2: GFP2; Constant: 0; Results: Add GFP	Source 1: GFP; Source 2: GFP2; Constant: 0; Results: Add GFP
	Top Hat	Source: Add GFP; Size (pixels): 100; Filter shape: Circle; Grayscale reconstruction: yes; Result: GFP Top Hat	Source: Add GFP; Size (pixels): 100; Filter shape: Area; Grayscale reconstruction: yes; Result: GFP Top Hat
	Find Round Objects	Source: GFP Top Hat; Approximate minimum width (µm): 0.7; Approximate maximum width (µm): 1.5; Intensity above local background: 10; Result: GFP bact	Source: GFP Top Hat; Approximate minimum width (µm): 0.6; Approximate maximum width (µm): 1.5; Intensity above local background: 40; Result: GFP bact
pHrodo Bacteria	Add		Source 1: pHrodo; Source 2: pHrodo2; Constant: 0; Results: Add pHrodo
	Top Hat		Source: Add pHrodo; Size (pixels): 100; Filter shape: Area;

			Grayscale reconstruction: yes; Result: Top Hat pHrodo
	Find Round Objects		Source: Top Hat pHrodo; Approximate minimum width (μm): 0.6; Approximate maximum width (μm): 2; Intensity above local background: 30; Result: pHrodo bact

Table 2.2: ***Segmentation tools.*** Analysis settings for image analysis of RAW 264.7 cells and MDMs challenged with GFP and pHrodo labelled un-encapsulated S. pneumoniae.

Measurement Mask	**Object**
Measurement inputs	Standard area: 1; Create Object Overlay: no
Objects to Measure	Mask of Objects: Membrane; Image to Measure: Cy5
Features within Each Object	Mask of Objects: Nuclei; Image to Measure: DAPI
Features within Each Object	Mask of Objects: GFP bact; Image to Measure: Add GFP
Features within Each Object	Mask of Objects: pHrodo bact; Image to Measure: Add pHrodo

Table 2.3: ***Measurement mask.*** Objects and features used to obtaining measurements. Aside from pHrodo settings, all apply to both RAW 264.7 and MDM image analysis.

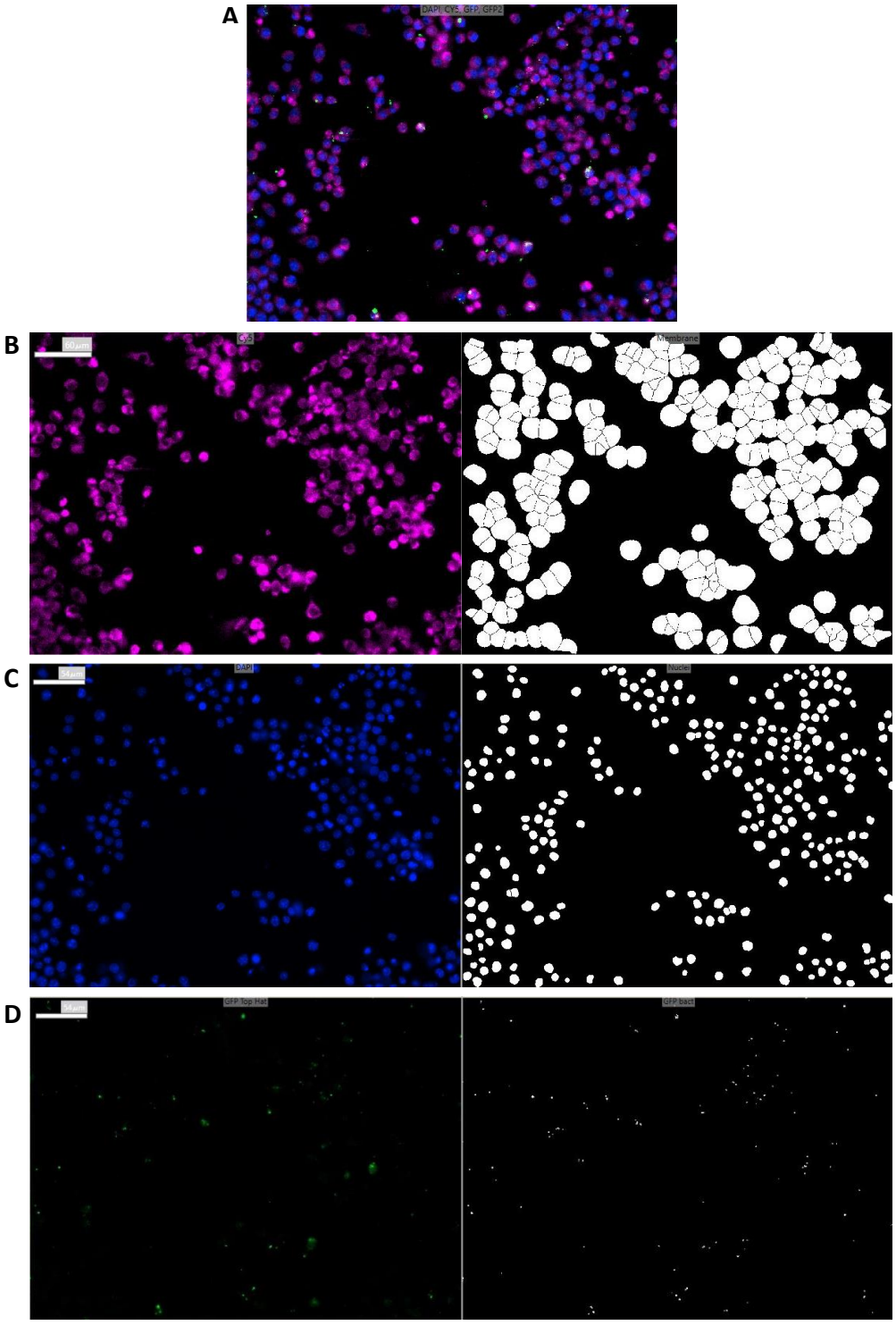

Figure 2.3: ***Representative images segmentation method in MetaXpress for image analysis.*** Illustrating the segmentation method used to determine the number of GFP positive cells within RAW 264.7 cells. The same method is used for MDMs with the addition of the Texas Red channel for pHrodo positive bacteria. (A) shows a representative imaged of RAW cells stained with CellMask Far Red and DAPI and infected with D39 ΔCPS GFP. (B) CellMask Far Red stain was used to stain the cell membrane, the segmentation acts as mask to measure number of bacteria within. (C) DAPI was used to stain nuclei to confirm an intact cell and to determine the ratio of cells to GFP bacteria. (D) GFP positive bacteria segmentation to measure number of bacteria within each cell.

2.6 Compound screen optimisation

2.6.1 Positive control optimisation reagents

Recombinant murine IFN-γ (PeproTech) was prepared as per manufacturer's instructions. IFN-γ was initially reconstituted in water to 1mg/ml, which was further diluted in PBS + 0.1% BSA to 20µg/ml for extended storage at -20ºC. IFN-γ was used at 20ng/ml (1ul/ml) unless specified.

VPS34 inhibitor was pre-prepared in DMSO at 10mM (Insight Biotechnology) and stored at -80ºC as per manufacturer's instructions.

10mg clemastine fumerate salt (Sigma), henceforth referred to as clemastine, was dissolved in 14.54ml pre-warmed DMSO. The stock solution at 20mM was stored at room temperature in the dark.

Pilot plates contained 2.5µl of compound in DMSO at 2.5mM. 3.75µl sterile RNase free water was added to each well resulting in a stock solution of 1mM. Plates were frozen at -80ºC and thoroughly defrosted before use. To account for further dilution within each well, 0.5µl of each compound was added to each well for a final concentration of 5µM, total volume 100µl.

2.6.2 Screen method

The Johns Hopkins Clinical Compound library contains 1,690 compounds. Plates 1-19 contain compounds in dissolved in DMSO, the remaining 2 plates (plates 20 and 21) contain compounds dissolved in water. All plates contain 5µl at 2.5mM. Plates were diluted to 1mM by adding 7.5µl sterile RNase free water.

RAW 264.7 cells were set up as described in section 2.2.3. After 48 hours cells were washed and challenged with *S. pneumoniae* as described in section 2.5.1 with the following modifications. To reduce the number of cells lost through wash steps, wells were washed once before challenge with *S. pneumoniae* and once before initially antibiotic treatment. After Penicillin/Gentamicin was been removed, 0.5µl of drugs were added to each well, including positive and negative controls, to give a final concentration of 5µM.

Positive control compounds were VPS34 inhibitor and clemastine which were made up to an intermediate stock of 1mM and 0.5µl was added to each well. VPS34 inhibitor was added to wells E12 and F12. Clemastine was added to wells G12 and H12.

Except for plate 21, wells A1, B1, C1, D1, G1 and H1 were left untreated. 5µl DMSO was diluted with 7.5µl sterile water to mimic test compounds and was loaded into well E1 of each library plate. 12.5µl sterile water was added to well F1 of each library plate, 0.5µl of both were added alongside test compounds.

2.7 siRNA screen optimisation

2.7.1 MDM Cell Dissociation

To detach MDMs from 6 well plates the following methods were used after the MDM monolayer was washed once with PBS.

a) A cell scraper was used to scrape once around the edge of the well then once across the middle. 1ml PBS was added to the well and pipetted up and down to dislodge any loose cells then transferred either to an Eppendorf tube or to a large tube if more than one well was scraped.
b) 1.5ml of pre-warmed (37°C) PBS was added to each well and incubated at 37°C / 5% CO_2 for 20 minutes. The cells were then scraped and transferred to an appropriate tube.
c) 1.5ml of pre-warmed Accutase (Sigma-Aldrich) was added to each well. The cells were then scraped and transferred to an appropriate tube.

After dissociating the cells were centrifuged at 200rcf for 10 minutes then re-suspended in RPMI + 10% HIFBS. 50µl of MDMs was added to 50µl 0.4% Trypan blue (Invitrogen), a cell count was performed noting both healthy and dead (blue) cells to determine the percentage viability.

2.7.2 Re-seeding Cells

After dissociating MDMs using Accutase, a cell sample was stained with 0.4% Trypan blue to check viability. The suspension was then diluted to give 5 different densities of cells: 1, 1.5, 2, 2.5 and $3x10^5$ cells/ml. 25µl of each density was then seeded into 384 well plates using a multi-drop (Thermoscientific). The following day, 25µl fresh media was added to each well and left to incubate for a further 24 hours. The cells were then washed 3 times with PBS. Cells were stained and fixed using the procedure in section 2.5.2.

2.7.3 Optimising siRNA Transfection Reagent

The transfection reagent for siRNA transfection was optimised in 96 well plates (Greiner) using siGLO Green (Dharmacon) as a simple read-out for successful transfection. Stock siGLO 20µM was diluted to 150nM by adding 4.5µl stock to 595.5µl RNase free water (QIAGEN). 7.2µl DF1 (DharmaFect 1) was added to 592.8µl RPMI only then combined with 150nM siGLO and left to complex for 30 minutes. Lipofectamine 3000 (Invitrogen) suggests 2 recommended concentrations to test. For the lower concentration (A) 3.6µl Lipofectamine (LP3) was added 120µl RPMI and for the higher concentration (B) 7.2µl was added to the same volume of RPMI. A and B were both added to an equal volume of 150nM siGLO Green and left to complex at room temperature for 15 minutes. 40µl of transfection solution was added to each well. For wells that already contained a monolayer of MDMs, 60µl fresh RPMI + 10% HIFBS was added. For reverse transfection 60µl of MDMs in RPMI + 10% HIFBS at a density of 3.33 x 10^5 cells/ml was added to each well containing transfection reagent resulting in giving 20,000 cells per well. The plate was left in the hood for 60 minutes then incubated at 37°C / 5% CO_2 for 24 hours. Media at this point could either be replaced or added. Both were carried out to compare toxicity and transfection efficiency. Wells either had 100µl media removed and replaced by 200µl fresh RPMI + 10 HIFBS, or 100µl fresh media added, diluting the transfection reagents/siGLO. The plates were then incubated for a further 24 hours at which point they were stained with CellMask, fixed and stained with DAPI as described in section 2.5.3.

2.7.4 Mcl-1 Transfection

Human Mcl-1 and non-targeting siRNAs (5nmol) were obtained from Dharmacon. 1x siRNA buffer was made by diluting 1ml 5x siRNA buffer (Dharmacon) in 4ml RNase-free water. 2ml 1x siRNA buffer was added to Mcl-1 siRNA and vortexed thoroughly to give a master stock of 2.5µM. 20µM non-targeting siRNA stock was made by adding 250µl 1x siRNA buffer.

MDMs were seeded in 6 well plates. On day 13 MDMs were washed and transfected with DF1. 150nM of Mcl-1 siRNA was made by adding 24µl of 2.5µM stock to 376µl RNase-free water. 150nM of non-targeting siRNA was made by adding 3µl 20µM stock in 397µl RNase-free water. Both were then added to 400µl RPMI containing 4.8µl DF1 and left to complex for 30 minutes. 800µl of siRNA/transfection reagent was added to designated well plus 1200µl RPMI + 10% HIFBS. For the non-transfected control 800µl RPMI only was added to the well

first. After 24 hours a further 2ml RPMI + 10% HIFBS was added then incubated for a further 24 hours before extracting RNA for qPCR or protein for Western Blotting.

2.7.5 Screen method

As described in section 2.2.2, PBMCs were isolated from heathy volunteers and maintained until MDMs were fully differentiated. On day 13, 384 well plates containing the siRNA library were defrosted and centrifuged at 1000rpm for 2 minutes to sediment the siRNA. 48µl DharmaFECT 1 (DF1) was added to 3952µl RPMI (without serum). 5µl of DF1 solution was added to each well and incubated at room temperature for 30 minutes to allow the transfection reagent and siRNA to complex. Meanwhile MDMs were dissociated from 6-well plates using Accutase and scraping as described in section 2.7.1 (c). After counting, the cell density was adjusted to 3.33x105 cells/ml. 15µl of cell suspension (5,000 cells) was added to each well. The plate was left at room temperature for approximately 30 minutes to reduce any temperature effects on the wells at the edge of the plates. The plate was then incubated at 37°C / 5% CO2 for 24 hours before adding 25µl fresh media (RPMI + 10% HIFBS + 2mM L-Glutamine) to each well. The plate was incubated for further 24 hours before challenging with *S. pneumoniae* at an MOI 20:1 as described in section 2.5.1. After centrifuging the plate at 150rcf for 5 minutes, the cells were incubated at 37°C / 5% CO_2 for 3 hours. Wells were washed twice before 20µg/ml Gentamicin and 40 Units/ml Penicillin was added for 30 minutes followed by a further 2 hours with 0.75µg/ml Vancomycin. After which the cells were washed twice with PBS and stained following the steps in section 2.5.2. Plates were imaged and analysed as described in sections 2.5.3.

2.8 Molecular biology

2.8.1 RNA Extraction

RNA was extracted using the QIAGEN RNeasy mini kit and protocol. All repeats were frozen at -80°C. The concentration of RNA extracted was determined using a nanodrop in order to calculate the volume needed for 1µg total RNA. Concentration was given in ng/µl therefore to calculate 1µg: 1000ng/concentration (ng/µl) = volume required (µl).

2.8.2 cDNA Synthesis

First strand cDNA synthesis was performed following the ThermoFisherScientic protocol using Supercript™ II Reverse transcriptase (RT). In brief, Table 2.4 details the components used in the first step, which were heated to 65°C for 5 minutes then chilled on ice before briefly centrifuging. Table 2.5 shows the remaining components added for cDNA synthesis. This was incubated for a further 2 minutes at 42°C, allowing binding of Oligo(dT). Superscript™ II RT was then added and the reaction tube was incubated at 42°C for 50 minutes followed by 15 minutes at 70°C to inactivate the enzyme. cDNA was then used as a template for PCR amplification of the target gene.

Component	Volume
Oligo(dT) (500µg/ml)	1 µl
1 µg total RNA	(x) µl (to be calculated)
dNTP Mix (10mM each)	1 µl
RNase free water	To 12 µl

Table 2.4: ***Components for Oligo(dT) annealing***

Component	Volume
5X First-Strand Buffer	4 µl
0.1 M DTT	2 µl
RNase OUT (40 units/µl)	1 µl
SuperScript™II RT	1 µl

Table 2.5: ***Components for cDNA synthesis***

2.8.3 Primer Design and PCR

cDNA sequences were obtained from Ensembl and used to design primers using ApE and Primer 3 software. Primer sequences (Table 2.6) were ran in BLAST to check that there is little to no overlap with sequences for other genes or one another. Primer sequences were then ordered from Integrated DNA Technologies, Inc. (IDT, USA).

The components in Table 2.7 were used to set up the PCR with either primer set 1 or 2 to test primer specificity. Tubes were loaded into the PCR machine (Bio-Rad C1000 Touch Thermocycler). Tables 2.8 and 2.9 detail the PCR programmes used for amplification. PCR samples were loaded into a 1% or 1.5% agarose gel depending on PCR product size (1.5%: 1.5g agarose heated and dissolved in 100ml of 1xTAE buffer). The gel was run in 1xTAE buffer (Fisher Bioreagent) at 100V for 30-45 minutes.

Gene ID	Primer set	OLIGO	tm	Sequence	Product size
MCL-1	1	Forward	58.98	GCTGCATCGAACCATTAGCA	186
MCL-1	1	Reverse	59.00	ATGCCAAACCAGCTCCTACT	186
MCL-1	2	Forward	59.32	GCCAAGGACACAAAGCCAAT	194
MCL-1	2	Reverse	58.91	CCGTCGCTGAAAACATGGAT	194
MARCO	1	Forward	58.87	TGAGTGAGACCCAACAAGCT	110
MARCO	1	Reverse	58.73	CACCACAGCTAGGGAGAAGT	110
MARCO	2	Forward	58.66	AGCGGGTAGACAACTTCACT	61
MARCO	2	Reverse	59.40	GCGCCTTGTTCACCTTTGAT	61
IL4I1	1	Forward	59.25	CATAAAGGCCATGGGTGCTG	143
IL4I1	1	Reverse	59.02	TGCATTTCTCGAAGGGGTCT	143
IL4I1	2	Forward	58.46	CAGAGGGTGATTGTGGTTGG	108
IL4I1	2	Reverse	58.95	CCCGATCCTGTTATCTGCCT	108
ARHGEF10L	1	Forward	59.25	TCACTGTCCTGGAAGCCAC	149
ARHGEF10L	1	Reverse	59.40	AGTGTGGAAGAGGCGGATG	149
ARHGEF10L	2	Forward	59.08	AAGGATGGGCTGGAGAAGAC	128
ARHGEF10L	2	Reverse	58.86	TTGATGTCCGAAACGCTGAC	128
TNFSF13B	1	Forward	58.75	AGCTTTAAAAGGGGAAGTGCC	118
TNFSF13B	1	Reverse	58.88	GTCCCATGGCGTAGGTCTTA	118
TNFSF13B	2	Forward	58.72	TGGGGATGAATTGAGTCTGGT	99
TNFSF13B	2	Reverse	58.96	AGTTTTGCAATGCCAGCTGA	99

Table 2.6: ***Primer sequences.*** Mcl-1 primers were used for confirming successful transfection. All other primers were used for validation of RNA sequencing results.

Component	Volume
FirePol DNase Polymerase	4 µl
Forward primer (10µM)	1 µl
Reverse primer (10µM)	1 µl
cDNA (1µg)	1 µl
RNase free water	13 µl

Table 2.7: ***PCR master mix reagents.***

Step	Temperature (°C)	Incubation time
1	94	2 min
2	94	20 sec
3	58	20 sec
4	72	30 sec
5	72	5 min
6	10	∞

Table 2.8: ***PCR programme for amplification of Mcl-1.***

Step	Temperature (°C)	Incubation time
1	95	2 min
2	95	30 sec
3	60	30 sec
4	72	20 sec
5	72	5 min
6	10	∞

x 34

Table 2.9: ***PCR programme for amplification of remaining genes***

2.8.4 qPCR

Melt curve analysis was assessed to determine if PCR amplification produced a specific single product. Table 2.10 details the components for each well. The main component, SYBR Green, is a fluorescent dye that binds non-specifically to double stranded DNA during polymerisation allowing quantification of the product that is synthesised. A control cDNA sample was diluted 1:10, 1:20, 1:50, 1:100, 1:200 and 1:500 and plated out in triplicate. Two reference genes were included (18s ribosomal RNA (18s) and eukaryotic elongation factor 1 alpha 1 (*EEF1A1*)) alongside *MCL-1*. 18s has previously been used in qPCR experiments to quantify mRNA silencing by siRNA in human macrophages (Folco *et al.*, 2009). *EEF1A1* was tested in case 18s primers proved inefficient, as *EEF1A1* has been shown to be relatively stable in human bone-marrow derived cells (Studer *et al.*, 2012).

Figure 2.4 shows the plate layout for melt curve analysis which was loaded into the qPCR machine (Bio-Rad CFX96 Touch Real-Time machine). The qPCR programme can be found in Table 2.11. For subsequent qPCR all cDNA samples were diluted (A) 1:20 and (B) 1:10 and plated out in triplicate as shown in Figure 2.5.

Component	Volume
SYBR Green	10 µl
Forward primer (10µM)	1 µl
Reverse primer (10µM)	1 µl
cDNA (1µg then diluted)	4 µl
RNase free water	4 µl

Table 2.10: ***Components for each well used during qPCR.***

Step	Temperature (°C)	Incubation time
1	95	7 min
2	95	15 sec
3	60	30 sec

Table 2.11: ***qPCR settings.*** Steps 2 and 3 were repeated 39 times.

A

	1	2	3	4	5	6	7	8	9	10	11	12
18s	1:10	1:10	1:10	1:20	1:20	1:20	1:50	1:50	1:50	1:100	1:100	1:100
18s	1:200	1:200	1:200	1:500	1:500	1:500	H_2O	H_2O	H_2O	No cDNA	No cDNA	No cDNA
EEF1A1	1:10	1:10	1:10	1:20	1:20	1:20	1:50	1:50	1:50	1:100	1:100	1:100
EEF1A1	1:200	1:200	1:200	1:500	1:500	1:500						
MCL-1 **Pair 1**	1:10	1:10	1:10	1:20	1:20	1:20	1:50	1:50	1:50	1:100	1:100	1:100
MCL-1 **Pair 1**	1:200	1:200	1:200	1:500	1:500	1:500						
g												
h												

B

	1	2	3	4	5	6	7	8	9	10	11	12
18s	1:10	1:10	1:10	1:20	1:20	1:20	1:50	1:50	1:50	1:100	1:100	1:100
18s	1:200	1:200	1:200	1:500	1:500	1:500	H_2O	H_2O	H_2O	No cDNA	No cDNA	No cDNA
MARCO **Pair 1**	1:10	1:10	1:10	1:20	1:20	1:20	1:50	1:50	1:50	1:100	1:100	1:100
MARCO **Pair 1**	1:200	1:200	1:200	1:500	1:500	1:500						
IL4I1 **Pair 2**	1:10	1:10	1:10	1:20	1:20	1:20	1:50	1:50	1:50	1:100	1:100	1:100
IL4I1 **Pair 2**	1:200	1:200	1:200	1:500	1:500	1:500						
TNFSF13B **Pair 1**	1:10	1:10	1:10	1:20	1:20	1:20	1:50	1:50	1:50	1:100	1:100	1:100
TNFSF13B **Pair 1**	1:200	1:200	1:200	1:500	1:500	1:500						

Figure 2.4: ***Well plate layout for melt curve analysis.*** Primers tested are listed on the left size of the well-plate layout with cDNA dilutions given in the table. Controls of H_2O and no cDNA confirm no contamination. (A) layout for testing reference genes and Mcl-1 melt curve analysis. (B) layout for melt curve analysis for RNAseq validation.

A

	1	2	3	4	5	6	7	8	9	10	11	12
18s	NT1	NT1	NT1	S1	S1	S1	M1	M1	M1	NT2	NT2	NT2
18s	S2	S2	S2	M2	M2	M2	NT3	NT3	NT3	S3	S3	S3
18s	M3	M3	M3	NT4	NT4	NT4	S4	S4	S5	M4	M4	M4
18s	NT5	NT5	NT5	S5	S5	S5	M5	M5	M5	H_2O	H_2O	H_2O
MCL-1	NT1	NT1	NT1	S1	S1	S1	M1	M1	M1	NT2	NT2	NT2
MCL-1	S2	S2	S2	M2	M2	M2	NT3	NT3	NT3	S3	S3	S3
MCL-1	M3	M3	M3	NT4	NT4	NT4	S4	S4	S5	M4	M4	M4
MCL-1	NT5	NT5	NT5	S5	S5	S5	M5	M5	M5	No cDNA	No cDNA	No cDNA

B

	1	2	3	4	5	6	7	8	9	10	11	12
18s	R1 0	R1 0	R1 0	R1 1+	R1 1+	R1 1+	R2 0	R2 0	R2 0	R2 1+	R2 1+	R2 1+
18s	R3 0	R3 0	R3 0	R3 1+	R3 1+	R3 1+	H_2O	H_2O	H_2O			
MARCO	R1 0	R1 0	R1 0	R1 1+	R1 1+	R1 1+	R2 0	R2 0	R2 0	R2 1+	R2 1+	R2 1+
MARCO	R3 0	R3 0	R3 0	R3 1+	R3 1+	R3 1+	No cDNA	No cDNA	No cDNA			
IL4I1	R1 0	R1 0	R1 0	R1 1+	R1 1+	R1 1+	R2 0	R2 0	R2 0	R2 1+	R2 1+	R2 1+
IL4I1	R3 0	R3 0	R3 0	R3 1+	R3 1+	R3 1+						
TNFSF13B	R1 0	R1 0	R1 0	R1 1+	R1 1+	R1 1+	R2 0	R2 0	R2 0	R2 1+	R2 1+	R2 1+
TNFSF13B	R3 0	R3 0	R3 0	R3 1+	R3 1+	R3 1+						

Figure 2.5: ***Well plate layout for qPCR.*** (A) NT = non-transfected. S = scrambled/non-targeting siRNA. M = Mcl-1 siRNA transfected sample. Number = biological repeat. (B) R# = biological repeat number, 0 = cDNA from population of cells that have not phagocytosed any beads, 1+ = cDNA from population of cells that phagocytosed 1 or more beads.

2.8.5 Reagents for Protein Extraction and Western Blotting

To make 10 x TBS, 97.3g sodium chloride (NaCl) (Fisher Bioreagents) was added to 100ml 1M Tris-HCl pH8 (Sigma). The mixture was made up to 1 litre with distilled H_2O. 100ml 10 x TBS was diluted in 900ml dH_2O to make 1 x TBS.

10 x TBS-Tween was made as above with the addition of 5ml Tween-20 (Sigma).

10 x running buffer was made by adding 30.3g Tris and 190g Glycine to 50ml 20% SDS solution (all Fisher Bioreagents). The solution was made up to 1 litre with dH_2O. To dilute to 1 x running buffer, 100ml of 10x running buffer was added to 900ml dH_2O.

Transfer buffer was made by dissolving 2.9g Tris and 1.45g Glycine in 100ml Methanol and 925µl 20% SDS. The solution was made up to 500ml with dH_2O.

Tris-EDTA contained the following reagents and volumes: 5ml Tris-HCl (pH7.4, 1M), 37.5ml NaCl (1M), 2.5ml EDTA (0.5M), 2.5ml EGTA (0.5M) and 202.5ml dH_2O. Tris-EDTA-SDS was made up using the same recipe with 12.5ml SDS (20%) and 180ml dH_2O.

2.8.6 Protein Extraction

Wells were washed with 1ml PBS followed by one wash with TBS-EDTA. 600µl TBS-EDTA-SDS lysis buffer containing protease inhibitor (Roche) (1:25 dilution) was added to each well. 100µl 100% TCA (Sigma) was added and the wells were swilled to precipitate the protein and aggregate the DNA. The precipitated protein was transferred to 1.5ml centrifuge tube and centrifuged for 5 minutes at 13,000rpm. The supernatant was removed and the pellet re-suspended in 1ml 2.5% TCA. The tube was then centrifuged on the same settings and the supernatant was discarded. 20µl of 3M Tris base was added and incubated at room temperature for 1 hour to dissolve the protein. An equal volume of water was then added and stored at -80°C until running the Western Blot.

2.8.7 Western Blot (SDS-PAGE)

Table 2.12 details the components used to make the 12% resolving gel which was poured between glass plates in a casting rig. Isopropanol was overlaid and the gel was left to set for 15 minutes. The isopropanol was removed and the top of the gel was rinsed with distilled water. The stacking gel components are listed in Table 2.13 were added to the top of the resolving gel, a comb was inserted and the gel was left to set for a further 15 minutes. After the comb was removed, the wells were washed with distilled water and the gel set up in vertical gel electrophoresis apparatus (BioRad) with 1 x running buffer. Equal volume of 2x loading buffer was added to each sample. Samples were heated to 100°C for two minutes and centrifuged at high speed briefly. The samples were loaded into each well with the first lane containing broad range protein standard (New England BioLabs). The gel was run 15 minutes at 100V then for a further hour at 140V. After removing the gel, the stacking gel was cut away and the resolving gel was placed in transfer buffer.

Resolving gel	12%
H_2O (ml)	6.4
40 % acrylamide (ml)	4.5
1.5 M Tris 8.8 (ml)	3.8
20% SDS (µl)	75
20% APS (µl)	150
TEMED (µl)	6

Table 2.12: ***Components of resolving gel***

Stacking gel	Volume (µl)
H_2O	2978
40 % acrylamide	622
0.5M Tris pH 6.8	1260
20% SDS	25
20% APS	50
TEMED	5

Table 2.13: ***Components of stacking gel***

2.8.8 Semi-dry Transfer

A sheet of nitrocellulose membrane and 6 sheets of filter paper were cut to the size of the gel and soaked in transfer buffer. Figure 2.6 shows the arrangement of the filter paper, membrane and gel which were gently rolled to ensure no air bubble were remaining. The gel was ran in a semi-dry blotter (BioRad) at 15V for 1 hour.

The membrane was transferred to a shallow container with ponceau S (BioRad) then rinsed several times with distilled water to confirm protein was present. The membrane was rinsed with 1xTBS-Tween before blocking with 5% non-fat milk powder in TBS-Tween (2g milk powder (Sigma) / 40ml 1 x TBS Tween) for 1 hour on an orbital shaker. The membrane was transferred to a falcon tube with 5ml of 5% non-fat milk powder in TBS-Tween containing 5µl rabbit anti-Mcl-1 antibody (clone S-19, Santa Cruz (sc-819)) and incubated at 4°C on a tube roller overnight. The following day the membrane was transferred to the shallow container and washed with 3 times with 1 x TBS-Tween on an orbital shaker for 10 minutes. The membrane was transferred to a falcon tube containing 5ml of 5% non-fat milk powder in TBS-Tween containing 2.5µl goat anti-rabbit secondary antibody (Dako (P0488)) and placed on a tube roller at room temperature for 1 hour. The same wash step with 1xTBS-Tween was repeated 3 times before washing with 1xTBS. All solution was removed before adding 1.5ml Bio-Rad Clarity ECL (containing equal volumes of Peroxide and Luminol/Enhancer reagent) to the top of the membrane and incubated for 5 minutes. Excess ECL reagent was blotted from the membrane and placed in clear plastic for imaging using the Bio-Rad ChemiDoc XRS+ imaging system.

To strip the membrane of antibody and re-probe for Tubulin (Sigma) the membrane was washed twice with distilled water for 10 minutes followed by a 15 minute wash with 0.2M

sodium hydroxide (NaOH). The membrane was washed twice again with distilled water before blocking with 5% non-fat milk powder in 1 x TBS-Tween. The same procedure for probing with anti-Mcl-1 antibody was repeated with a mouse anti-human Tubulin antibody (1:2000 dilution, Sigma (T5168)) then imaged.

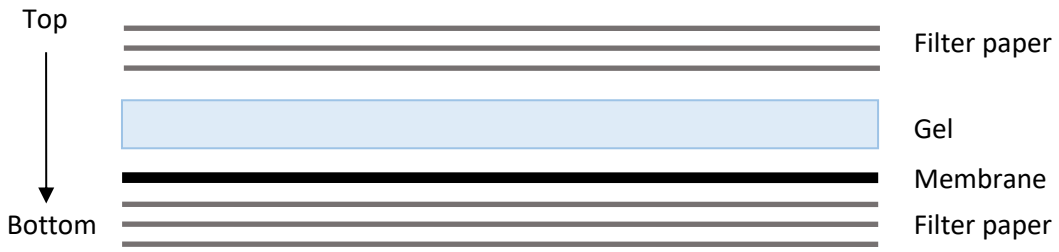

Figure 2.6 - ***Arrangement of filter paper, membrane and gel for Semi-dry transfer.***

2.9 Statistical analysis

Statistical analysis was performed using Prism version 7.03 (GraphPad) with the p-values annotated in figure legends where appropriate. Experiments using primary MDMs and neutrophils, biological replicate and n-number refer to the number of donors used. In the case of experiments using RAW 264.7 cells, n-number refers to the number of repeats performed on a different day with a different passage of cells.

R Studio software, version 4.2.0, was used for RNA sequencing data analysis and analysis of data sets from both the compound and siRNA screens.

3 Chapter 3: Differential gene expression between neutrophils and macrophages with distinct phagocytosis phenotypes

3.1 Introduction

Phagocytosis is not only vital for the clearance of pathogens, it is also important for the clearance of debris, apoptotic and infected cells. Apoptosis is required for homeostasis, as is the phagocytosis and clearance of these cells. Apoptotic cells express particular markers such as phosphatidyl serine (PS) which is recognised by multiple receptors (Nagata *et al.*, 2016). The receptors required on the phagocyte depend on the object to be phagocytosed. For example, non-opsonic receptors, such as MARCO and CD14, recognise PAMPs on the surface of bacteria. Bacteria can also be opsonised by antibodies or proteins from the complement pathway, which bind other receptors. As discussed in section 1.2.1 phagocytosis of antibody opsonised bacteria involves FcRs (Kishore *et al.*, 2020).

Professional phagocytes, such as macrophages and neutrophils, appear to have a range of phagocytic capacities. There is evidence that some phagocytose avidly whilst others appear to be inactive in this context (Hellebrekers *et al.*, 2017). This could be a stochastic phenomenon, due to chance interactions with foreign material. However, Hellebrekers and colleagues demonstrated that this is not the case by carrying out experiments in which neutrophils were challenged with 2 rounds of differently labelled *Staphylococcus aureus*. The ratios of the neutrophils with intracellular bacteria showed that if the neutrophils phagocytose in the first round (GFP *S. aureus*) they are more likely to phagocytose further in the second round (mCherry *S. aureus*) (Hellebrekers *et al.*, 2017). Whether or not this is due to expression of particular markers or these neutrophils are inherently more primed for phagocytosis remains unknown.

3.1.1 Neutrophil plasticity

McPhail and colleagues suggested neutrophils can be primed to enhance their response at their target site. For example, initial treatment with fMLP resulted in a small increase in NADPH oxidase activity (for the production of high levels of superoxide for conversion into antimicrobial compounds). When treated again with fMLP no increase in activity was noted, however when a second stimulus was added, calcimycin, a marked increase in NADPH oxidase

activity was observed. (McPhail, Clayton and Snyderman, 1984). Further work has shown neutrophils have the ability to return to basal levels of activation, which upon re-stimulation, have the capacity to be re-primed (Kitchen *et al.*, 1996). Priming agents can be produced by both the host and microorganisms, many of which result in the increased production of superoxide (Kobayashi *et al.*, 2005). Primed neutrophils differ in phenotype to unstimulated, circulating neutrophils. These basal state neutrophils exhibit a round morphology, lack adherence to the vascular wall and are less responsive to activating stimuli whilst primed neutrophils exhibit protrusions, have up-regulated adhesion molecules and enhanced responses to activation (Miralda, Uriarte and McLeish, 2017). Neutrophil heterogeneity has been increasingly studied in recent years, but it remains unclear whether identified 'subsets' represent distinct lineages or different activation states (Deniset and Kubes, 2018). Whilst single cell RNAseq of neutrophils has proved challenging due to their relatively low transcriptional activity, recent developments have confirmed that circulating and tissue-recruited neutrophils are indeed transcriptionally varied (Wang *et al.*, 2022; Wigerblad *et al.*, 2022).

3.1.2 Macrophage plasticity

Macrophages all share the fundamental characteristics of chemotaxis and phagocytosis however, the adaptability of macrophages has long been evident, from specialised tissue resident macrophages to responses to both pro and anti-inflammatory stimuli (Locati, Curtale and Mantovani, 2020). Cytokines such as interferon γ (IFNγ) can prime macrophages to increase their responsiveness to pathogens (Schulthess *et al.*, 2019). Recognition of PAMPs has been shown to induce changes in expression and therefore surface receptors such as increased expression of MARCO (macrophage receptor with collagenous structure) (Bowdish *et al.*, 2007). Little work has been carried out to determine if there are regulators intrinsic to macrophages with high phagocytic capacities. One study on carried out transcriptomic analysis after sorting of phagocytic and non-phagocytic cells from different tissues of parabiotic mice after 8 weeks. They found 634 differentially expressed genes (DEGs). Regardless of the tissue they originated from, all the phagocytic macrophages had DEGs that separated them from their non-phagocytic counterparts. They also found that in some tissue-specific populations, the scavenger receptor CD206 was upregulated and was required for phagocytosis of apoptotic bodies (A-Gonzalez et al., 2017). However, this was not examined

in terms of bacterial infection or attempting to influence the levels of phagocytosis. Moreover, as the A-Gonzalez study focuses at a late time-point, these transcriptomic signatures may be induced by the processes of phagocytosis, rather than being its cause.

3.2 Results

3.2.1 Neutrophils display phenotypic variability in phagocytosis

To investigate the characteristics of neutrophil phagocytosis of particulate material, freshly isolated human neutrophils from healthy volunteers were incubated with serum-opsonised red fluorescent latex beads (2µm diameter) at a ratio of either 5:1 or 10:1 (beads:neutrophils). At different time-points (15, 30 and 60 minutes), the samples were washed, placed on ice and analysed on the LSRII flow cytometer which allowed visualisation of populations that had phagocytosed 1 (depicted in green), 2 (blue) or 3 or more beads (purple) as shown in Figure 3.1A. These results show that approximately 15% of neutrophils phagocytosed beads at a ratio of 5:1 which is increased to 20-25% at a ratio of 10:1, although this is not significant. There is also no significant difference in uptake between the time-points studied (Figure 3.1B). The distribution of neutrophils that have phagocytosed different numbers of beads does not appear to be changed by either increased ratio or longer exposure to opsonised beads suggesting sub-populations of neutrophils may possess differing phagocytic capacities (Figure 3.1C and D).

To determine whether neutrophils that perform phagocytosis are determined by chance alone or if this is characteristic is intrinsic to the cells, a 'double feeding' experiment was performed. This experiment is similar to that previously performed by Hellebrekkers in which they incubated neutrophils with different fluorescently labelled *Staphylococcus aureus* sequentially (Hellebrekers *et al.*, 2017). After opsonising red and green fluorescent beads separately, red beads were initially incubated with neutrophils at a ratio of 5:1 for 30 minutes. The cells were then washed twice before adding green beads at the same ratio for a further 30 minutes. Figure 3.2A shows one representative experiment of 3 repeats where quadrants (Q) 1-4 show cells that have phagocytosed red beads only, red and green beads, no beads, and green beads only, respectively. The ratios of ingesters to non-ingesters were calculated based on the second feed (green beads against no green beads phagocytosed). If this were a stochastic process, the ratios of the number of beads phagocytosed in the second feed, would be the same independent of whether the neutrophils had phagocytosed in the first feed. As

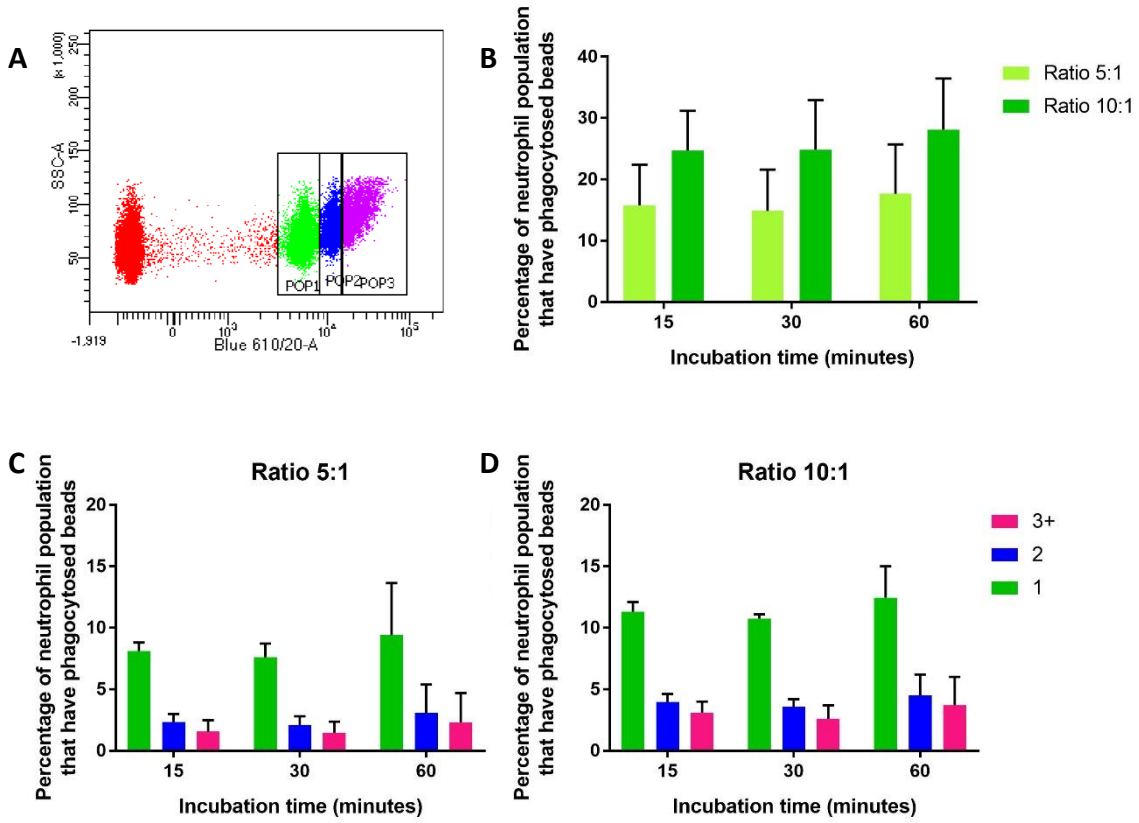

Figure 3.1 – ***Neutrophils display phenotypic variability when exposed to opsonised latex beads.*** Neutrophils were incubated with beads at the indicated time-points and ratios of beads:neutrophils. Samples were washed with 2.5% BSA in PBS before placing on ice and analysing on the LSRII flow cytometer. **A.** Depicts a representative experiment whereby neutrophils were incubated for 30 minutes with beads at a ratio of 10:1. The coloured populations within the gates represent the number of beads phagocytosed (red = 0 beads, green = 1 bead, blue = 2 beads, purple = 3 or more beads). **B.** Shows the percentage of neutrophils that have phagocytosed beads at different time-points and ratios. Data show the mean of 3 individual healthy donors ± SD. (two-way ANOVA, followed by Tukey's multiple-comparison post-test). Percentage of neutrophils separated based on the number of beads phagocytosed at ratio of 5:1 **(C)** and 10:1 **(D).**

shown in Figure 3.2B, this is not the case, suggesting that phagocytic capacity is not stochastic; these results are consistent with those presented by Hellebrekers (2017). This experiment also allowed determination of ratios dependent on the actual number of beads phagocytosed and show that a neutrophil is more likely to phagocytose material in the second feed if it has previously phagocytosed 3 or more beads in the first feed (Figure 3.2B). We have termed these neutrophils 'super-ingesters'.

Following the observation of a 'super-ingester' phenotype, neutrophils were FACS-sorted into 3 populations using the FACSAria II (BD Biocsciences) into three groups: 0 beads phagocytosed, 1-2 beads and 3 or more. To confirm that the populations were sorted correctly, the samples were cytospun onto microscope slides, stained with DAPI (nuclear stain) and imaged (Figure 3.3). Figure 3.3A shows a representative image of neutrophils that

have phagocytosed 1-2 beads whilst B and C show 3 or more beads. To investigate if there is any variation in gene expression profiles between the populations that display different phagocytosis phenotypes, 4,000 cells were sorted into lysis buffer supplemented with 1% β-mercaptoethanol. Samples were stored at -80°C until 4 biological replicates had been obtained and subsequently sent for RNA sequencing.

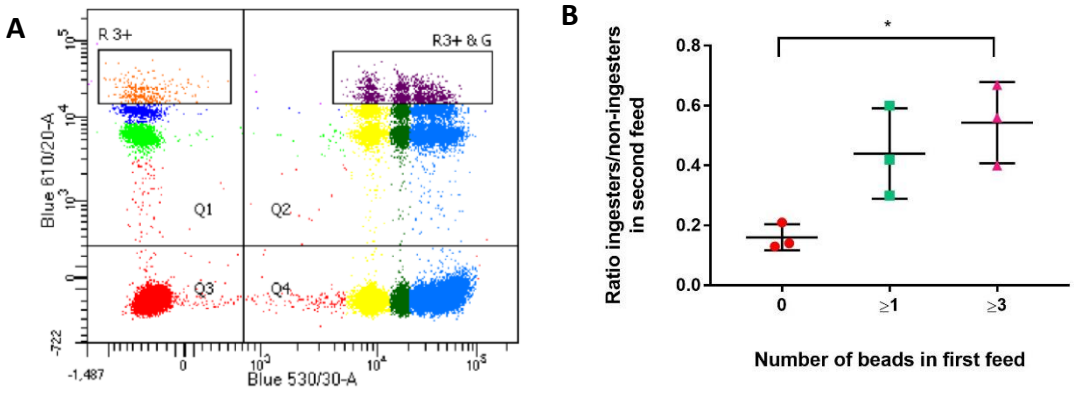

Figure 3.2 – ***A sub-population of neutrophils display a super-ingester phenotype.*** (A) A flow cytometry quadrant plot from a representative experiment (n=3), in which neutrophils were incubated firstly for 30 minutes with red beads (y-axis), ratio of 10:1, followed by a second 30 minutes with green beads (x-axis). (B) Ratio of ingesters to non-ingesters in the second round were calculated as follows. 0 beads: number of cells in Q4/Q3. 1 or more beads: Q2/Q1. 3 or more beads: Gated population in Q2 / gated population in Q1. Data show the mean of 3 individual healthy donors ± SD; *P<0.05 (one-way ANOVA, followed by Tukey's multiple-comparison post-test).

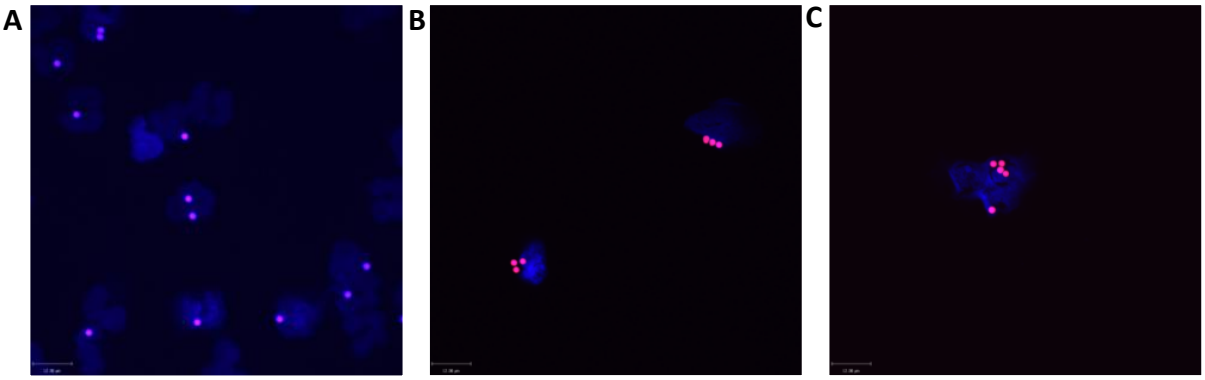

Figure 3.3 – ***Representative images of neutrophils after FACS sorting.*** Neutrophils were sorted based on the number of beads they had phagocytosed then used for cytospin slide preparation. Slides were fixed, stained with DAPI and a coverslip was mounted. Blue = DAPI stained nuclei, pink = fluorescent red beads. (A) shows a representative image of 1 to 2 beads phagocytosed whilst (B) and (C) represent 3 or more beads phagocytosed. Scale bars = 12µm.

3.2.2 Neutrophil RNA sequencing analysis

RNA sequencing was carried out at University of Newcastle and data was received in FastQ file format. Each sample was run in four lanes which required merging of the files before quality control could be carried out to ensure the sequence quality scores, sequence length and duplication levels were within normal limits. The length of reads between samples did differ considerably but the quality of these reads was good across all samples. *Salmon* was the tool used for quantifying expression of transcripts which were then used for differential expression analysis (Patro *et al.*, 2017). A flow chart of this process is depicted in Figure 3.4 and the code used for analysis in available in Appendix A.

Principal component analysis (PCA) clusters the samples based on their similarity. The axes of the plot represent principal component (PC) 1 and 2, displaying the most and second most significant source of variation between the samples. As shown in Figure 3.5 the samples in group 'one' (one and two beads phagocytosed) and group 'three' (three or more beads phagocytosed) are clustered close together, whereas group 'zero' (no beads phagocytosed) samples extend across the plot. The lack of distinct clusters indicates considerable similarity between the samples. It is therefore unlikely that there will be many genes that are differentially expressed.

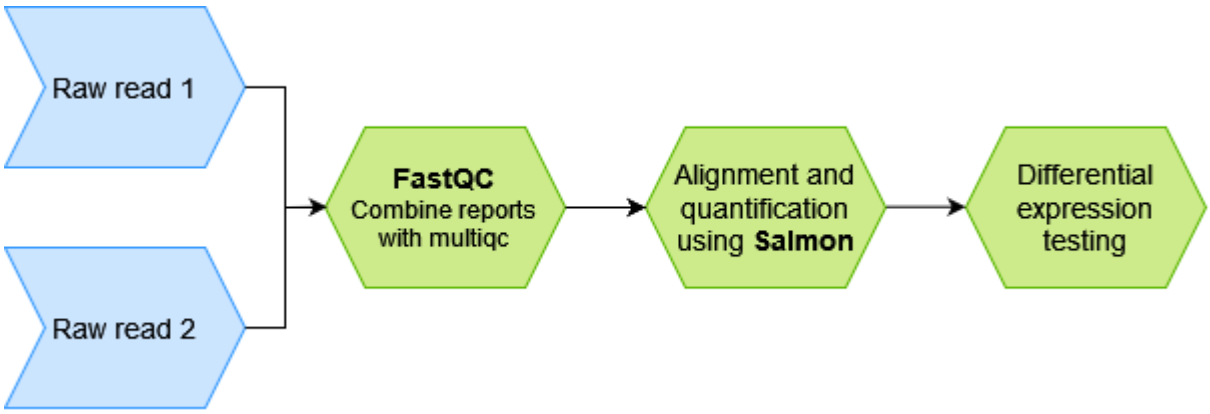

Figure 3.4 – ***Flow chart of RNA sequencing data analysis.***

3.2.3 Differentially expressed genes between phagocytic and non-phagocytic neutrophils

Genes that met the criteria of $p>0.05$ and $|\log_2 FC|>1$ were considered differentially expressed. There were just 14 differentially expressed genes (DEGs) between group 'zero' and group 'three' which are detailed in Table 3.1. Table 3.2 details the 9 DEGs between group

'zero' and group 'one' of which 5 were common to both groups, highlighted in green. All DEGs, with the exception of METTL4, were down-regulated.

PPM1D (protein phosphatase magnesium-dependent 1, Delta (also known as Wip1)) is a serine/threonine phosphatase. Upon neutrophil activation in both human and mice, expression of PPM1D is significantly downregulated by 3 hours post activation (Sun *et al.*, 2014). The data shown here combined with the data from Sun *et al*., may indicate a population of neutrophils that inherently have a lower expression of PPM1D and therefore are prepared for infection. This is further supported by the negative correlation of expression with inflammatory cytokine production and the increased clearance of *S. aureus* in KO mice (Sun *et al.*, 2014).

METTL9 catalyses the methylation of histidine of several known target proteins including S100A9, a calcium binding protein (Davydova *et al.*, 2021). S100A9 has known roles in immune responses after release from activated neutrophils and has been shown to enhance bactericidal activities by promoting phagocytosis and ROS production (Simard *et al.*, 2011). Methylation of S100A9 is not required for heterodimerisation with S100A8 but whether or not it has a role in the activating properties of S100A9 remains unknown (Daitoku *et al.*, 2021).

Due to the small number of significant differentially expressed genes between the sample groups, it is not possible to conduct any gene enrichment and pathway analysis. In light of this, we turned to macrophages which share the same phenotypic variability.

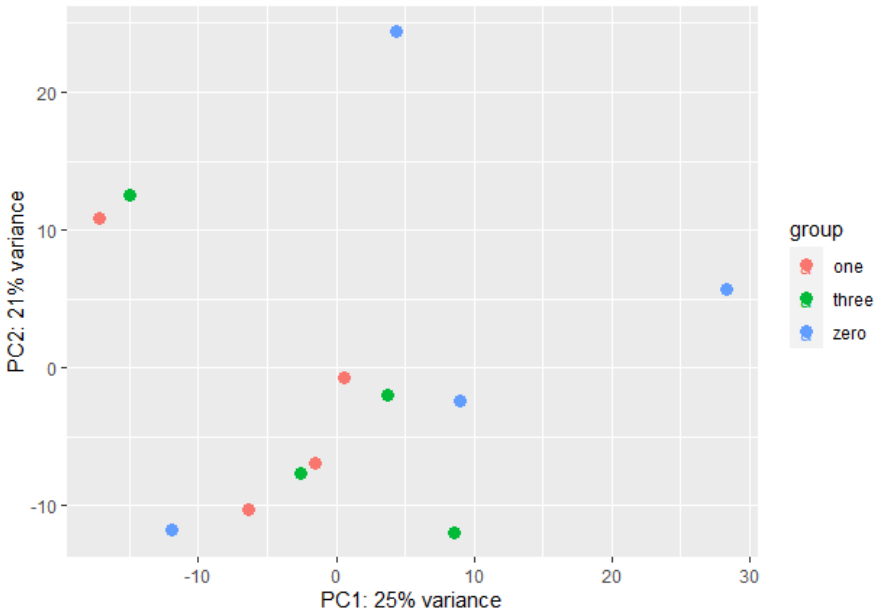

Figure 3.5 – ***Neutrophil PCA plot*** where PC1 (principal component 1) represents the most variability between samples.

Gene ID	Gene Name	Description	P-value
METTL9	methyltransferase like 9	Mediates methylation of histidine in motif His-x-His. Catalyses formation of *N*π-methylhistidine in protein S100A9, shown to be proinflammatory with antimicrobial activity (Daitoku *et al.*, 2021; Davydova *et al.*, 2021).	0.000854
CDK6	cyclin dependent kinase 6	Proposed to regulate cell cycle entry (from G_0) and is required for neutrophil NET formation (Amulic *et al.*, 2017)	0.001886
KDELR2	KDEL endoplasmic reticulum (ER) protein retention receptor 2	Role in ER quality control by recognising K-D-E-L motif to initiate retrograde transport. Up-regulation is associated with tumour progression (Tiwarekar, Fehrholz and Schneider-Schaulies, 2019; Hui *et al.*, 2020).	0.011194
XKR8	XK related 8	Once cleaved by caspases during apoptosis has a role in scrambling of phospholipids between inner and outer leaflets of the plasma membrane (Suzuki, Imanishi and Nagata, 2016).	0.013856
PRELID1	PRELI domain containing 1	Roles in regulation of mitochondrial ROS signalling and tumour progression (Gillen *et al.*, 2017).	0.016316
TMEM38B	transmembrane protein 38B	A ER cation channel. Mutations are associated with osteogenesis imperfecta (brittle bone disease) (Cabral *et al.*, 2016).	0.02197
OGFR	opioid growth factor receptor	Dysregulation of OGF-OFGr axis may have roles in autoimmune diseases such as multiple sclerosis (Zagon and McLaughlin, 2018).	0.027622
IER2	immediate early response 2	Role in cell adhesion and motility. Has been shown to be downregulated in patients with *S. aureus* infections but upregulated in neutrophils challenged with *S. aureus* (Smith *et al.*, 2016)	0.027622
HERC5	HECT and RLD domain containing E3 ubiquitin protein ligase 5	May have antiviral properties as upregulated in phagocytes, including neutrophils, and lung epithelial cells challenged with influenza A (Zhou *et al.*, 2021).	0.032017
CERS4	ceramide synthase 4	The least studied ceramide synthase. Upregulated in liver and colon cancer (Mojakgomo, Mbita and Dlamini, 2015).	0.032438
PPM1D	protein phosphatase, Mg2+/Mn2+ dependent 1D	Shown to be downregulated in neutrophils during activation. No change in phagocytosis capacity of neutrophils in KO mice but increase clearance of *S. aureus* compared with WT mice (Sun *et al.*, 2014).	0.033757

PSMD2	proteasome 26S subunit ubiquitin receptor, non-ATPase 2	Regulates expression levels of cell cycle and growth regulators. Increase cellular fatty acid and lipid synthesis to promote tumour cell proliferation (Tan *et al.*, 2019).	0.033757
CRTAP	cartilage associated protein	Associated with collagen assembly. Down-regulated in patients with Dengue virus (Afroz *et al.*, 2016).	0.041956
METTL4	methyltransferase like 4	A small nuclear RNA N-6-methyladenosine (m6A) methyltransferase which, in hypoxic conditions, results in an increase in m6A modifications (van den Homberg *et al.*, 2022).	0.044571

Table 3.1 – ***14 differentially expressed genes in neutrophil super-ingester population****.* Highlighted in green are genes common to both 1 and 3+ groups. All genes listed are down regulated, except METTL4, compared to non-ingester population.

Gene ID	Gene Name	Description	P-value
MATR3	matrin 3	A nuclear matrix protein in which mutations are associated with motor neurone disease (Caputo *et al.*, 2022).	0.000349
PPM1D	protein phosphatase, Mg2+/Mn2+ dependent 1D	See table 3.1	0.002611
METTL9	methyltransferase like 9	See table 3.1	0.020038
RAB5IF	RAB5 interacting factor	Long noncoding RNA that is upregulated in hepatocellular carcinoma (Koo *et al.*, 2019).	0.020312
TAFAZZIN	tafazzin, phospholipid-lysophospholipid transacylase	Membrane bound mitochondrial enzyme that transfers fatty acids from phospholipids to lysophosoplipids (Schlame and Xu, 2020).	0.020312
CRTAP	cartilage associated protein	See table 3.1	0.020312
AGPS	alkylglycerone phosphate synthase	An enzyme that catalyses ether ester synthesis with a role in cancer pathogenesis (Chen *et al.*, 2020).	0.021045
IER2	immediate early response 2	See table 3.1	0.021045
PRELID1	PRELI domain containing 1	See table 3.1	0.044084

Table 3.2 – ***9 differentially expressed genes in neutrophils that had phagocytosed 1 or 2 beads compared to non-phagocytic neutrophils.*** Highlighted in green are genes common to both 1 and 3+ groups. All genes listed are down regulated compared to non-ingester population.

3.2.4 Macrophages also show variability in phagocytosis phenotype

To determine if the 'super-ingester' phenotype is a shared feature of other phagocytic cells, MDMs were used as a comparator as they are also professional phagocytes. Figure 3.6A shows an example experiment in which MDMs were incubated with red beads at a ratio of 10:1 for 4 hours. MDMs are larger in size than neutrophils and as a result contain more granules, hence there is an increased distribution on the side scatter scale (y-axis, indication of granularity). The results in Figure 3.6A show the presence of distinct populations, with regard to the number of beads phagocytosed, similar to those seen in neutrophils. Like neutrophils, MDMs also show distinct variability in the number of beads phagocytosed, with around 20-30% of macrophages phagocytosing 3 or more beads compared to only 10-15% phagocytosing 1 or 2 beads (Figure 3.6B). There is similarity in the percentage of MDMs and neutrophils that phagocytose 1 or 2 beads (Figure 3.6C). However, the difference between neutrophils and MDMs that phagocytose 3 or more beads is very clear, less than 5% compared to over 20%, respectively. No statistical analysis has been performed due samples being acquired at different time-points.

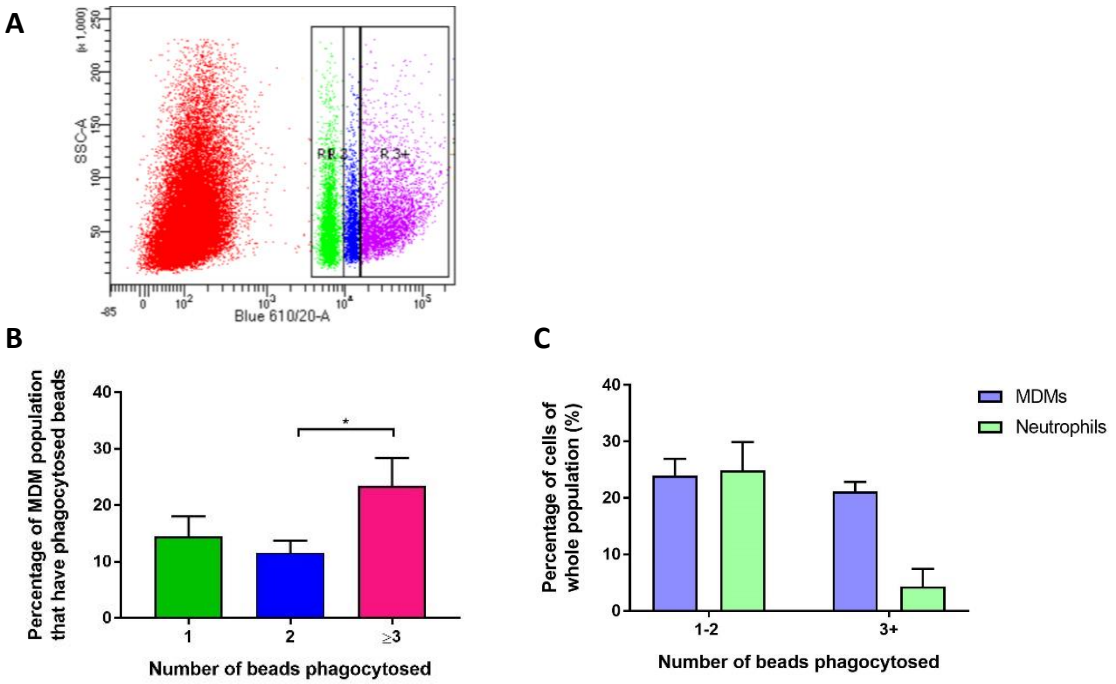

Figure 3.6 – ***MDMs also show phenotypic variability in the number of beads phagocytosed.*** **A.** representative experiment of macrophages incubated for 4 hours with red beads at a ratio of 10:1 then analysed by flow cytometry. The coloured populations represent the number of beads phagocytosed (green = 1 bead, blue = 2 beads, purple = 3 or more beads). **B.** At 4 hours significantly more macrophages phagocytose 3 or more beads compared to 1 or 2 beads. Data show the mean of 3 individual healthy donors ± SD; *P<0.02 (one-way ANOVA, followed by Tukey's multiple-comparison post-test, n=3). **C.** Shows the percentage of macrophages and neutrophils that phagocytose 1-2 beads or at least 3 beads.

The same double-feeding experiment was carried out in which the MDMs were incubated with red beads at a ratio of 10:1 for 2 hours, washed with PBS three times then incubated for a further 2 hours with green beads at the same ratio (Figure 3.7A). Analysis of this data in the same way as described for neutrophils did not show the same super-ingester phenotype, although the phenotype of moderate ingesters is dramatically different. These results show that if MDMs phagocytose 1 or 2 beads then they are more likely to phagocytose in the second feed (Figure 3.7B).

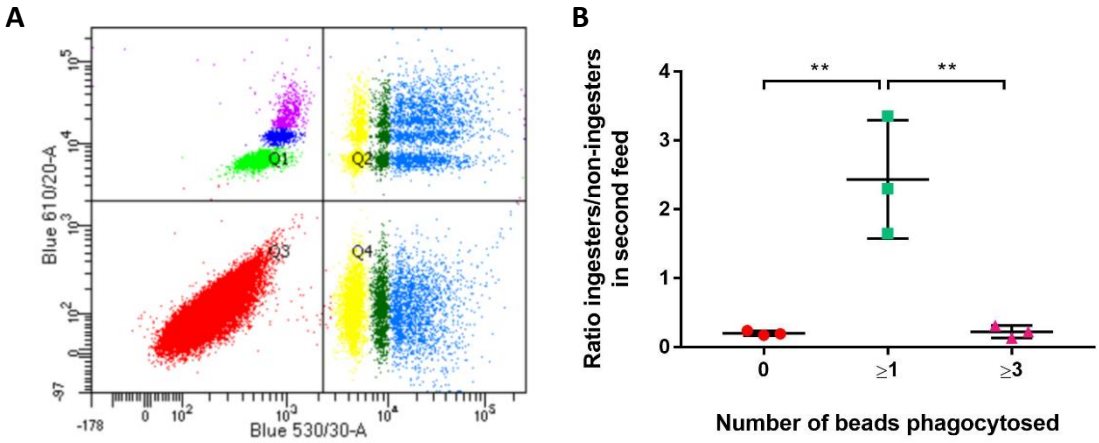

Figure 3.7 – ***The number of beads phagocytosed by MDMs is not stochastic.*** **A.** Depicts a representative double-feeding experiment (of 3 biological replicates). MDMs were incubated firstly for 2 hours with red beads (y axis), ratio of 10:1, followed by a second 2 hours with green beads (x axis). **B.** Ratios of ingesters to non-ingesters in the second round were calculated. Data show the mean of 3 individual healthy donors ± SD; **P<0.005 (one-way ANOVA, followed by Tukey's multiple-comparison post-test).

MDMs were sorted into the same populations as neutrophils using the FACSMelody (BD Bioscience): 0 beads phagocytosed, 1-2 beads and 3 or more. These were cytospun and stained with DAPI, representative images are shown in Figure 3.8. Figure 3.8A shows MDMs that have phagocytosed 1-2 beads. Figure 3.8B and C show MDMs that have phagocytosed 3 or more beads.

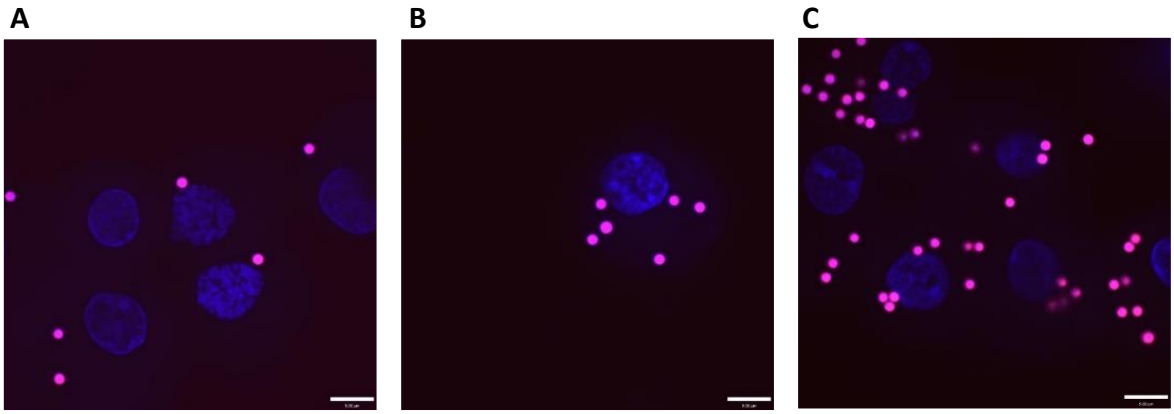

Figure 3.8 – ***Representative images of MDMs after FACS sorting.*** MDMs were sorted based on the number of beads they had phagocytosed then used for cytospin slide preparation. Slides were fixed, stained with DAPI and a coverslip was mounted. Blue = DAPI stained nuclei, pink = fluorescent red beads. **A.** shows a representative image of 1 to 2 beads phagocytosed whilst **B** and **C** represent 3 or more beads phagocytosed. Scale bar = 5µm.

3.2.5 Macrophage RNAseq principle component analysis

MDM samples were collected after incubation with opsonised beads for 2 and 4 hours. The same sample groups for neutrophils applied; 'zero', 'one' and 'three', with 4,000 cells sorted directly into lysis buffer for each sample until 4 biological replicates were obtained. Collecting samples at two different time-points enables a variety of comparisons to be made. It will be possible to observe commonly differentially expressed genes at both time-points, although as the sample for different time-points were collected from different donors, samples for each time-point will be required to be analysed separately.

Figure 3.9 shows that samples in all 3 groups generally cluster together at both time-points. The different patterns in clustering between A and B may indicate differences in differentially expressed genes between the time-points.

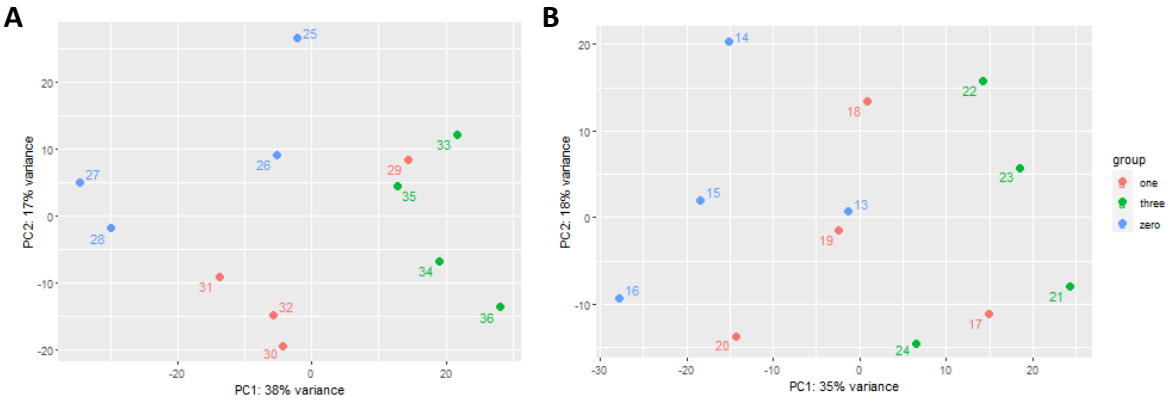

Figure 3.9 – ***PCA plots show clustering of phagocytic and non-phagocytic MDM samples.*** Representation of variability between samples at the **A.** 2 hour time-point. **B.** 4 hour time-point.

3.2.6 Pathway enrichment analysis

Gene ontology (GO) provides specific definitions for gene functions called GO terms. Figure 3.10 shows the most significant GO terms in biological processes at both time-points between group 'zero' and group 'three' in MDMs. The different GO terms displayed on each graph further indicates differential gene expression between the different time-points. At 2 hours the GO terms are all related to protein transport, transcription and translation (Figure 3.10A). This may indicate initiation of serval processes to change the phenotype or function of the macrophage. The different GO terms displayed at 4 hours may suggest the MDMs are becoming more pro-inflammatory in response to foreign material as they are all related to responses to infection (Figure 3.10B). It therefore may be most useful to look at common differentially expressed genes between the two time-points, in order to determine if there are any DEGs that are innate to the MDMs and not related to the phagocytosis response and activation.

3.2.7 Differential expression between macrophage groups

The R package *DESEQ2* was applied to the all groups at both time-points (analysed separately) to find the differentially expressed genes (DEGs) in group 'one' and 'three' compared to group 'zero'. To control for the false discovery rate, *DESEQ2* uses the Benjamini and Hochberg method to correct for multiple testing and adjust the p-value (p-adj) accordingly. In these data, genes with associated p-adj values less than 0.05 were classed as differentially expressed. At the 2 hour time-point there were 353 and 1,594 DEGs in group 'one' and group 'three', respectively. At 4 hours the number of genes differentially expressed were 69 and 1,154 in group 'one' and 'three' respectively. The number of up and down-regulated genes for each group are shown in Table 3.3. As depicted in the Venn diagram in Figure 3.11, there were 23 DEGs common for all four groups, 20 of which met the additional criteria of $|\log_2 FC| \geq 1.0$. These are available in table 3.4 with brief descriptions for each gene function and their associated, average p-adj value.

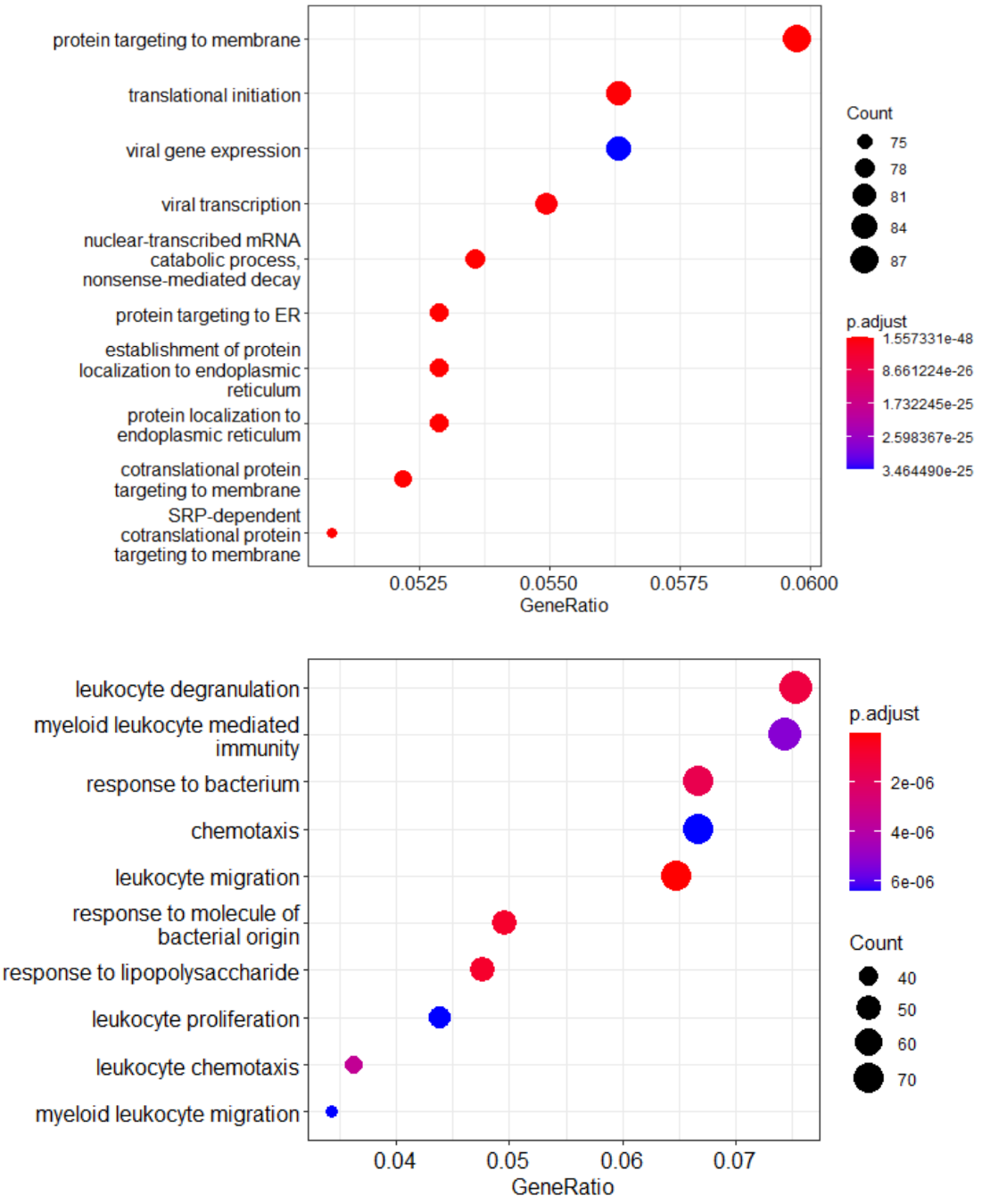

Figure 3.10 – ***Gene ontology (GO) plot at different time-points.*** **A. 2** hour time-point. **B.** 4 hour time-point. Gene ratio indicates the percentage of all differentially expressed genes, i.e. 0.05 = 5%. The number of genes enriched in each GO term (shown on the left axis) is given by the gene count.

Sample	Total DEGs	Up-regulated	Down-regulated
2 hour 'one'	353	167	186
2 hour 'three'	1,594	785	809
4 hour 'one'	69	49	20
4 hour 'three'	1,154	646	508

Table 3.3 – ***Total DEGs across all MDM samples.*** Genes were classified as differentially expressed if p-adj < 0.05.

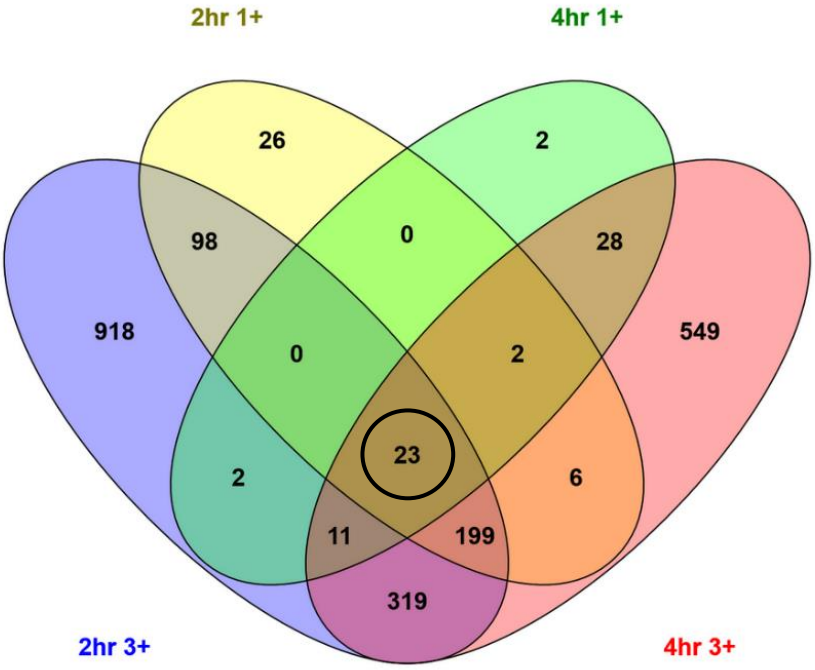

Figure 3.11 – ***Venn diagram showing the number of significantly differentially expressed genes are common between groups.*** Circled shows that there are 23 genes that are differentially expressed common to all phagocytic samples at both time-points compared to non-ingesters. Creating using Venny 2.1.0.

Gene ID	Gene Name	Description	Average p value
IL4I1	Interleukin 4 induced 1	Expressed in macrophages and dendritic cells after induction via IL-4. Inhibits T-cell activation (Molinier-Frenkel, Prévost-Blondel and Castellano, 2019).	0.00240
TIE1	Tyrosine kinase with immunoglobulin like and EGF like domains 1	Role in angiogenesis. Receptors for TIE1 are expressed on vascular endothelial cells and a certain subset of macrophages that have been associated in angiogenesis (Fagiani and Christofori, 2013).	0.00338
TMEM86A	Transmembrane protein 86A	Unknown function but shown to be upregulated in differentiating keratinocytes (Zhang *et al.*, 2021).	0.00345
ARHGEF10L	Rho guanine nucleotide exchange factor 10 like	Low expression (in monocytes) is associated with disease severity and mortality of ICU sepsis patients (Liepelt *et al.*, 2020)	0.00351
SUCNR1	succinate receptor 1	A G-protein coupled receptor, also known as GPR91, with an inflammatory role in myeloid cells. Activates MAPK pathway upon binding of succinate (Harber *et al.*, 2020).	0.00572
TCF4	transcription factor 4	A DNA binding protein with roles in multiple pathway. Role in macrophage susceptibility to HIV-1 (Aljawai *et al.*, 2014)	0.00584
DEPP1	DEPP1 autophagy regulator	Induced by progesterone. Possible role in autophagy and energy metabolism (Li *et al.*, 2018).	0.00628
C1QB	complement C1q B chain	Activated by antigen-antibody complexes which in turn activates phagocytosis by interacting with VSIG4 (Zhao *et al.*, 2021).	0.00649
TNFSF13B	TNF superfamily member 13b	Encodes BAFF. Stimulation results in expression of inflammatory mediators through MAPK and NF-kB activation (Lim *et al.*, 2017)	0.00679
ETV5	ETS variant transcription factor 5	Role in different cancers but key in the expression of ICAM-1 in infected macrophages, which promote cell-cell interactions (Cheng *et al.*, 2020)	0.00709
CARMIL1	capping protein regulator and myosin 1 linker 1	Involved in cell motility and co-localises with capping protein (CP) at the leading edge ((Zwolak *et al.*, 2013).	0.00991
NUPR1	nuclear protein 1, transcriptional regulator	Stress-induced with roles in regulation of cell-cycle, apoptosis, autophagy and DNA repair responses. Depletion in cancer cell lines favours expression of phagocytosis-related genes ((Cano *et al.*, 2012; Neira *et al.*, 2020)	0.01017

MARCO	Macrophage receptor with collagenous structure	A class A scavenger receptor. Structure and function is well described with upregulation post infection and roles in phagocytosis and modification of inflammatory responses to pathogens (Kraal *et al.*, 2000)	0.01109
RNASE2	ribonuclease A family member 2	Required by TLR8 activation in response to a variety of pathogenic stimuli (Ostendorf *et al.*, 2020)	0.01136
MDK	Midkine	Upregulated in inflammatory and hypoxic conditions. Can activate pathways regulating cell survival and migration upon binding to receptors (Aynacıoğlu, Bilir and Tuna, 2019)	0.01526
DUSP7	dual specificity phosphatase 7	Required for regulation of MAPK activation by dephosphorylation (Wu *et al.*, 2020)	0.01550
PTGIR	prostaglandin I2 receptor	Through binding of prostacyclin, has roles in vascular function and smooth muscle relaxation (Morawska-Pucinska, Szymanska and Blitek, 2014)	0.01571
MFSD4A	major facilitator superfamily domain containing 4A	Predicted to be ion and nutritional transporters (Perland *et al.*, 2017)	0.01684
PTGER2	prostaglandin E receptor 2	Suppresses phagocytosis and intracellular killing upon binding and uptake of apoptotic cells (medeiros	0.01710
SEC14L2	SEC14 like lipid binding 2	A phodphotidylinositol transfer protein, localised to the ER, involved in endosome fission (Gong *et al.*, 2021)	0.01790

Table 3.4 – ***Gene description for the 20 differentially expressed genes common to all groups with p-adj values of less than 0.05 and |log2FC| ≥ 1.0.*** Average p value is taken from all groups. Genes coloured blue are up-regulated compared to cells that did not phagocytose beads and those coloured red are down-regulated. Bold and underlined genes are those that were taken forward for validation.

Expression of *IL4I1* is upregulated in macrophages and dendritic cells upon stimulation with IL-4. It is localised to the membrane of the ER with a primary function of catalysing the oxidative deamination of L-aromatic amino acids, such as phenylalanine. During the oxidation of amino acids, keto-acids are formed alongside hydrogen peroxide (H_2O_2) and ammonia. The combination of the depletion of amino acids and the production of H_2O_2 contribute to growth inhibition of both Gram-positive and Gram-negative bacteria (Puiffe *et al.*, 2013). Despite this key antibacterial activity, other studies have shown the stimulation of IL4I1 in IL-4 treated macrophages has led to M2, anti-inflammatory phenotypes and deletion in mouse studies

have shown reduced *M. tuberculosis* burden (Yue *et al.*, 2015; Hlaka *et al.*, 2021). However, it remains unknown if IL4I1 has any role in the regulation of phagocytosis.

RNA sequencing of samples from septic ICU patients revealed that low expression of *ARHGEF10L* is associated with disease severity and mortality of these patients (Liepelt *et al.*, 2020). Further work is required to understand why the mortality of sepsis patients correlated with low expression of *ARHGEF10L*. However, this may suggest that *ARHGEF10L* is highly important for the clearance of bacteria.

TNFSF13B encodes a cytokine called B-cell activating factor (BAFF) with known roles in B cell proliferation, differentiation and antibody production (Hashiguchi *et al.*, 2018). Expression on the surface of macrophages in both human and mouse samples has been observed but its function here is understudied. Whilst having a pro-inflammatory effect, BAFF has also been shown to reduce phagocytic capacity of THP-1 cells as well as other processes requiring cytoskeleton remodelling which seems contradictory to the data shown here (Jeon *et al.*, 2010).

MARCO is a scavenger receptor with a role in non-opsonic phagocytosis (Bowdish *et al.*, 2007). IL-6 deficient mice show a reduced expression of MARCO on the cell surface of macrophages with correlated with reduced phagocytic capacity of *S. pneumoniae* and influenza A virus (IAV) (Gou *et al.*, 2020). This is supported by knockdown of *MARCO* in the zebrafish model which resulted in increased burden of *M. marinum* through reduced phagocytosis (Benard *et al.*, 2014). Increased MARCO expression in a post-influenza infection model was shown to be associated with Nrf2 and Akt related signalling. Sulforaphane and SC79 can induce activation of Nrf2 and Akt signalling pathways, respectively, both of which led to an increase in MARCO expression and phagocytosis *in vitro*. This same treatment *in vivo* resulted in improved host survival to post-influenza bacterial pneumonia, which was not observed in MARCO knockout mice (Wu *et al.*, 2017).

3.2.8 Validation of macrophage RNA sequencing data

MDMs were incubated with opsonised red beads for 4 hours after which they were sorted at 4°C using FACS Melody, as for RNA-seq samples, into PBS. As the group 'three' population only represents around 20% of the MDM population it was unlikely that it would be possible to extract enough RNA for downstream RT-qPCR therefore, cells were sorted into only two groups; phagocytic cells and non-phagocytic cells. After sorting, the cells were pelleted and

at kept at -80ºC until four biological replicates had been acquired. After RNA extraction the concentration was determined using a nanodrop which showed 3 out of 4 replicates had sufficient RNA concentrations (≥50ng/ml) for qPCR.

Two primer pairs were designed for MARCO, IL4I1, ARHGEF10L and TNFSF13B. To test the primers for specificity, a PCR was performed using RNA from non-phagocytic cells and products were ran on 1% agarose gel. Primers targeting ARHGEF10L resulted in only a weak band (A1) or did not yield a product (A2), shown in Figure 3.12. Stronger bands were observed with primer pair 1 for MARCO and TNFSF13B and primer pair 2 for IL4-I1 therefore, these were used for RT-qPCR.

In order to confirm primer efficiency, melt curve analysis revealed primer efficiency ≥99% for all primers tested as shown if Figure 3.13. Defined peaks indicate the amplification of a single product and confirms that a cDNA dilution of 1 in 10 dilution is suitable for qPCR.

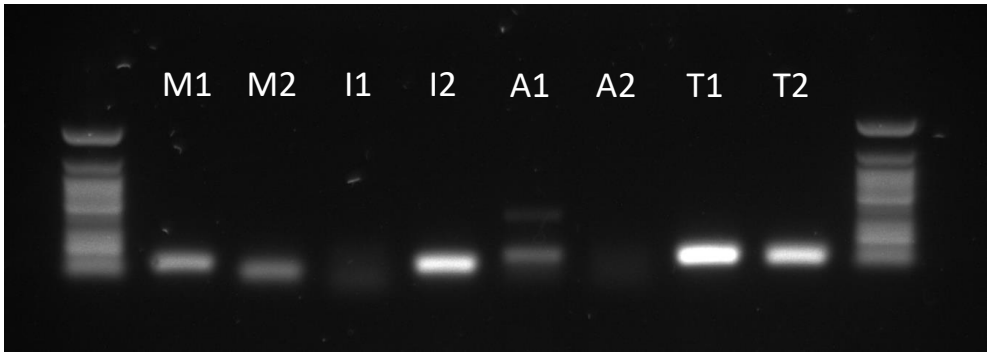

Figure 3.12 – ***Primer pairs were tested for specificity****.* Gel electrophoresis following PCR amplification of all primer pairs using 50bp ladder. M = MARCO, I = IL4I1, A = ARHGEF10L, T= TNFSF13B with numbers indicating primer pair. I1 and A2 showed no product and A1 showed 2 amplicons. All other primer pairs had one band indicating one amplicon.

Expression data following qPCR analysis, shown in Figure 3.14, shows that all three genes tested have a trend in increasing expression, although not significant. IL4I1 has the most significant trend, which correlates with the lowest average p-adj value of the 20 common DEGs. Figure 3.14A shows the relative expression given as ΔΔCt, where a decrease in this value indicates more transcript, taking less cycles for the product to be amplified. Figure 3.14B shows the fold difference compared to the transcript levels of cells that phagocytosed 0 beads. This indicates a trend for up-regulation with some samples showing a large increase in transcript levels of MARCO and TNFSF13B.

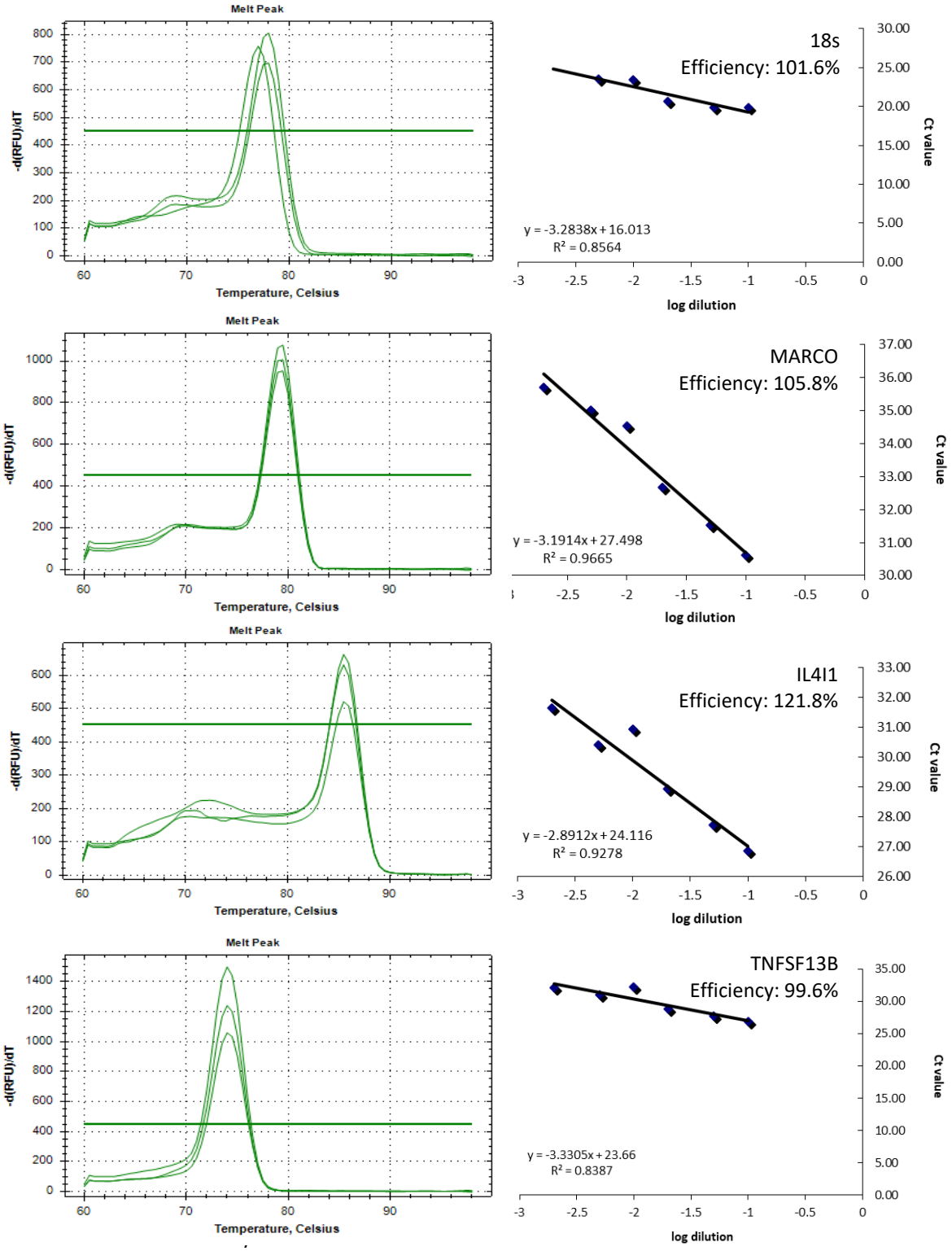

Figure 3.13 – ***Melt curve analysis showed that all primers had good efficiency and resulted in 1 amplicon***. Primers were tested on one sample of RNA from MDMs that had not phagocytosed any beads. Melt peaks show 3 technical replicates of 1 in 10 cDNA dilution. Primer efficiency graphs show log dilution plotted against average Ct value, the gradient of the slope is used to calculate the primer efficiency.

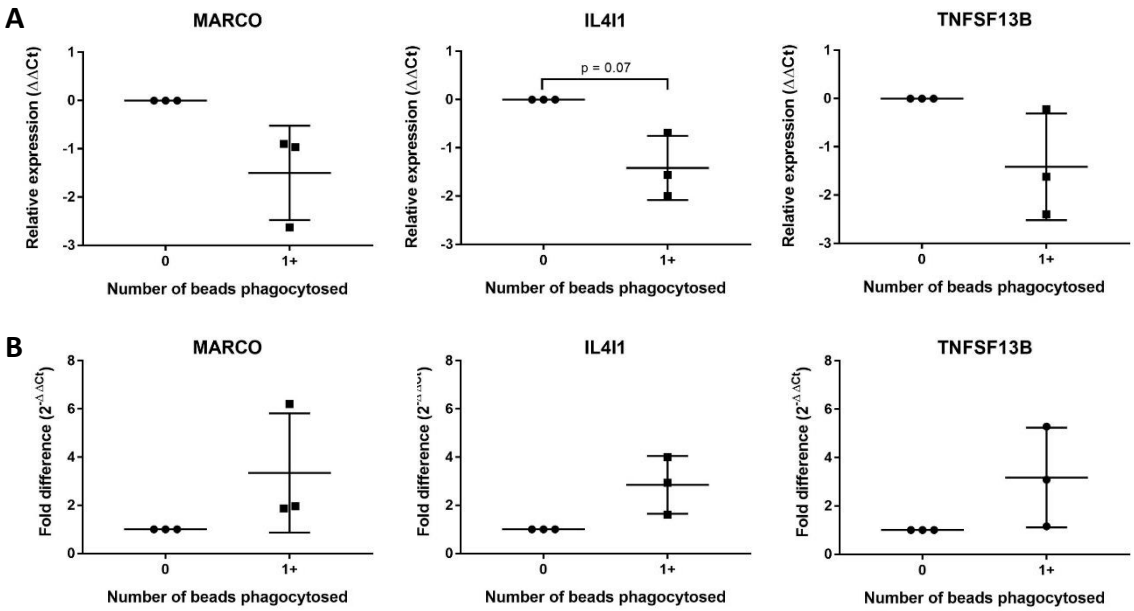

Figure 3.14 – ***qPCR validation of RNA sequencing hits showed a trend in increased expression***. Panel **A.** shows the relative expression (ΔΔCt). Data show the mean of 3 individual healthy donors ± SD (paired t-test, n=3). MARCO: p = 0.12, IL4I1: p = 0.07, TNFSF13B: p=0.16. Panel **B.** shows the fold difference ($2^{-\Delta\Delta Ct}$) compared to cells that phagocytosed 0 beads.

3.3 Discussion

Incubating both neutrophils and monocyte-derived macrophages with fluorescent latex beads and subsequent analysis via flow cytometry allowed quantification of how many cells phagocytosed beads and how many beads were phagocytosed by each cell. In order to determine if the quantity of beads phagocytosed was random or pre-programmed, a 'double-feed' experiment was performed whereby cells were initially incubated with red beads followed by green beads. This experiment revealed that neutrophils displayed a 'super-ingester' phenotype in which they were more likely to phagocytose further if they had already phagocytosed 3 or more beads. The 'super-ingester' phenotype not mirrored in the macrophages despite the fact that a higher percentage of macrophages phagocytosed a higher number of beads. However, the ratios between non-phagocytic MDMs and phagocytic MDMs also indicated that phagocytosis of a higher number of beads was not due to chance interactions. If MDMs had phagocytosed one or two beads they were more likely to phagocytose further in the second feed. Differential phagocytic capacities within phagocytes has long been described, however whether there are key molecular regulators inherent to

the cells with high phagocytic capacity that is not shared with cells that appear to not undergo phagocytosis is remains to be explored.

Despite the neutrophil 'super-ingester' phenotype, there were only 14 DEGs between non-phagocytic cells and those that had phagocytosed more than three beads in the neutrophils whereas the same comparison in macrophages revealed 1,594 and 1,154 DEGs at 2 and 4 hours, respectively. There were also no DEGs that were common to both neutrophils and macrophages, which may indicate regulators of phagocytosis are more cell specific.

Although neutrophils require RNA synthesis for many functions, their gene expression profile is lower in comparison to other cells such as macrophages (Garratt, 2021). This may contribute to the low number of DEGs in neutrophils. Although there are clear phenotypic differences in phagocytic capacity, the process of phagocytosis may induce changes without the need for transcription. This may occur through the fusion of secretory vesicles to the plasma membrane, altering the presence of adhesion receptors on the cell surface thereby enabling the neutrophil to interact with more foreign particles. In addition to this, there may be variability in age or priming status of the neutrophils that may not influence phagocytic capacity but may result in variability in gene expression between the phagocytic groups. To determine if there is any correlation between age and phagocytic capacity, neutrophils challenged with beads could be stained with anti-CD64 antibody, a marker for immature neutrophils, and analysed via flow cytometry. In sepsis patients immature $CD64^{+}$ neutrophils showed reduced phagocytic capacity (Meghraoui-Kheddar *et al.*, 2022). Although not significant, GM-CSF showed an increasing trend in the phagocytic capacity of neutrophils in a phase IIa clinical trial study compared to placebo (Pinder *et al.*, 2018). This supports the theory of immune modulation in neutrophils.

The differences between both time-points in macrophages could possibly be induced by the process of phagocytosis, phagolysosome acidification or other pro-inflammatory processes as indicated by the changes in GO. 'Protein targeting to membrane' was the most enriched pathway at 2 hours whereas all the enriched pathways at 4-hours were related to classical responses to infection. This may indicate activation at 2 hours due to the presence of foreign material to result in trafficking of more proteins involved in phagocytosis or receptors to cytokines on the cell membrane. To narrow down hits it may be best to focus on those that would be expected to yield the biggest effect therapeutically. Therefore, focusing on the common DEGs to 2 and 4 hour time-points in the group 'three' compared to group

'zero'. There were 51 common DEGs to both time-points that showed upregulation with $|\log_2 FC|>2$ and 91 DEGs that were downregulated. The common genes could next be targeted by siRNA in a 'mini-screen' system for further validation, whereby the cells could be challenged with serum-opsonised fluorescent beads after transfection. High-content fluorescence microscopy would allow determination of the effect of gene silencing. Silencing of DEGs in the upregulated group should result in decreased phagocytosis whereas silencing in the downregulated group should result in increased phagocytosis. It would also be useful to confirm if these findings were specific to Gram-positive and Gram-negative bacteria or opsonised material. There is the possibility that taking forward some of the hits may only be useful for either Gram-positive or Gram-negative bacteria. This is because sensing of these occurs via different receptors, TLR4 and TLR2, respectively, resulting in different downstream signalling pathways (Paul-Clark *et al.*, 2006). Further investigation would be required to determine if any biologically relevant genes are therapeutically targetable which would result in non-phagocytic cells altering their phenotype to aid clearance of bacteria. However, whether or not this leads to further intracellular killing remains to be elucidated. A drawback of this could be over-activation and the possibility that the non-phagocytic cells inherently have an anti-inflammatory phenotype in order to prevent host damage, which may be detectable through typical anti-inflammatory M2 marker staining.

Genetic targets, that upon manipulation, display the expected change in phagocytic phenotype could be entered into databases such as DrugBank to determine if there are any existing drugs that target our genes of interest. Further testing could be carried out *in vivo,* utilising the zebrafish model of infection. In the case of downregulated genes of interest, knockout zebrafish could be infected with *S. pnuemoniae* to determine the effect on bacterial clearance and survival.

4 Chapter 4: Screening a repurposing drug library for enhanced intracellular killing of *Streptococcus pneumoniae*.

4.1 Introduction

Drug development can begin with a hypothesis that a particular pathway or protein or phenotype, crucial to the pathology of a disease or condition, could be therapeutically targeted. Once a target has been validated, lead discovery begins by which compounds are generally screened for the desired effect in biochemical and *in vitro* assays. Alternatively, unbiased screens may be used to identify compounds that lead to a desired phenotype, such as increased bacterial killing – this approach may find unexpected candidates not flagged by hypothesis-driven approaches. There are several different methods of screening. High-throughput screening consists of large numbers of compounds run through assays. Screens can also be highly focussed, for example if the crystal structure of a known target is available, particularly the binding site, libraries of molecules that can be designed to fit said binding site either *in vitro* assays or *in silico* using computer algorithms and molecular docking approaches. Medicinal chemistry approaches may be used to design improved compounds based on the identified lead. Once one or two compounds have been shown to have the desired effect in cell-based assays and/or *in vivo* they may be moved into pre-clinical and clinical development where, if successful, will be marketed for availability to patients (Hughes *et al.*, 2011)

The process of drug discovery is long and costly with each approved drug taking an average of 12-15 years from bench to bedside with an associated estimated cost of $1-3 billion (Hughes *et al.*, 2011). Therefore, repurposing approved drugs is becoming increasingly attractive as usually the preclinical stages have been completed, hugely reducing the time and cost of development, as well as the reduced risk of failure due to drugs previously passing safety criteria. For example, zidovudine was originally marketed and tested as a cancer drug but *in vitro* screening of compound libraries found it to be effective treatment for HIV and became the first anti-HIV drug to be FDA approved (Pushpakom *et al.*, 2018). Sildenafil was originally intended as an anti-hypertensive/anti-anginal medication; although it was ineffective an unexpected effect noted during phase 1 clinical trials led to its repurposing for erectile dysfunction (Ghofrani, Osterloh and Grimminger, 2006).

As discussed in section 1.4, some bacteria have developed antibiotic resistance for example through mutations resulting in conformational changes of proteins causing antibiotics to fail to bind their target protein or by horizontal acquisition of efflux pumps to expel the drugs once inside the bacterial cell. The combination of cost and risk of emergence of resistance makes developing new antibiotics unappealing to the pharmaceutical industry. Therefore, enhancing host bactericidal mechanisms when antibiotics do not work would be a valuable alternative to aid bacterial burden. Enhancing the adaptive response (e.g. using vaccines), is limited by pathogen evolution in response to selective pressure, the limited range of strains protected by a specific response and by maturation time. Vaccine uptake and longevity of protection is also challenging. Targeting the innate immune response has received less attention but would enable more rapid engagement, and the generic nature of the innate response means its manipulation could target many pathogens, with less potential for selection of resistance. Since macrophages are key to the initial control of *S. pneumoniae* and many other respiratory infections, I undertook a phenotypic repurposing screen to identify existing drugs that might augment the intracellular killing of S. pneumoniae by macrophage-like cells, based on quantifying the signal from intracellular GFP-labelled bacteria.

4.2 Results

4.2.1 Optimisation of cell density

Murine bone-marrow derived macrophages (BMDMs) were originally used to begin optimisation for the compound screen as they have been widely used in bacterial challenge studies (Weischenfeldt and Porse, 2008). However, due to challenges in obtaining cells (particularly after the COVID-29 pandemic) and high levels of cell loss during wash steps, further experiments were carried out with RAW 264.7 cells. RAW 264.7 cells are a murine macrophage-like cell line and have also been widely used to investigate host-pathogen interactions (Wu *et al.*, 2016; Ellis *et al.*, 2019). The have similar functional characteristics to murine bone-marrow and human monocyte-derived macrophages in that they are adherent, phagocytose and kill bacteria intracellularly, including *S. pneumoniae*.

After harvesting, RAW 264.7 cells were initially seeded at 10,000 cells/well for use on day 3. It was clear the cells were over confluent and the ImageXpress software could not differentiate between overlapping cells leading to poor segmentation (Figure 4.1A). Imaging day 2 cells revealed more space between each cell which would result in better segmentation

(Figure 4.1B). To precisely determine the number of cells per well, important for ensuring that subsequent MOIs (multiplicity of infection) were accurate, day 2 RAW 264.7 cells were treated with Accutase for 20 minutes then pipetted up and down to detach all cells. Cells were then counted using a haemocytometer to calculate the number of cells per well. The average number of cells across 3 wells per repeat (n=3) was approximated to 40,000.

A

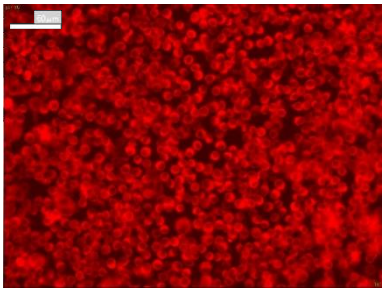

B

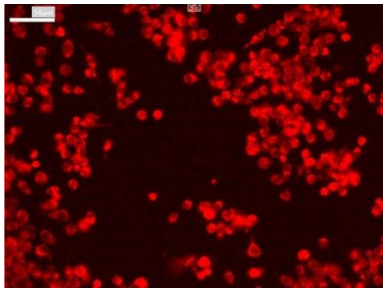

C

	Average (3 wells)
Repeat 1	43,000
Repeat 2	33,000
Repeat 3	42,000
	39,333

Figure 4.1 – ***Day 3 RAW 264.7 cells are over confluent.*** RAW 264.7 cells were seeded at 10,000 cells per well in a 96 well plate. Representative images of **(A)** day 3 and **(B)** day 2 RAW 264.7 cells, stained with CellMask Far Red. Scale bar = 60µm **(A)** and 56µm **(B)**. To determine the actual number of cells per well, day 2 cells were treated with Accutase for 20 minutes then pipetted up and down to dislodge all cells. The table **(C)** gives the average cell count across 3 random wells. Each repeat represents cells seeded on different days.

4.2.2 Optimisation of MOI

S. pneumoniae has a polysaccharide capsule with an alkaline pH that allows evasion of entrapment in mucosal surfaces and hinders phagocytosis (Paton and Trappetti, 2019). Opsonisation (by antibody or complement) would introduce a complex variable into the assay, as different biological preparations of antibody and complement may behave differently, and mouse proteins would be required to interact with the RAW 264.7 cells. Therefore, in these experiments a strain with a capsule deletion was used to allow effective phagocytosis without opsonisation. This allows for observation of intracellular killing; of note *S. pneumoniae* does not interfere with phagosomal maturation as seen with some bacteria such as *S. aureus* (Flannagan, Heit and Heinrichs, 2015; Jubrail *et al.*, 2016). The *S. pneumoniae* strain used in these experiments was D39ΔCPS hlpA GFP, a non-encapsulated strain with a chromosomal insertion of GFP (green fluorescent protein), developed by Dr Andrew Fenton. This strain has been shown to be susceptible to clearance and intracellular killing in zebrafish (Prajsnar *et al.*, 2022).

The MOI (multiplicity of infection) is the number of bacteria added in relation to cells, in this case RAW 264.7 cells. MOI requires optimisation as the assay readout is the number of

GFP positive bacteria remaining within the RAW 264.7 cells. An MOI that is too high can cause problems with the MetaXpress image analysis software being unable to distinguish between individual bacterial cells. An MOI too low could result in bacterial clearance or too few remaining within the RAW 264.7 cells resulting in poor signal-noise ratio and therefore inaccurate results.

10,000 RAW 264.7 cells were used, which as shown in section 1.2.1 results in approximately 40,000 cells/well at the end. The MOIs were calculated accordingly. Interferon γ (IFNγ) has been shown to activate macrophages and enhance intracellular killing of the Gram-positive pathogen *S. aureus* after 18-hour pre-treatment (Greenlee-Wacker and Nauseef, 2017). Therefore, in addition to optimising MOI, IFNγ treatment was used alongside to determine as proof-of-principle if we could observe enhanced intracellular killing of *S. pneumoniae* and use this as a positive control.

RAW cells were seeded at 10,000 cells/well. On day 1 (the day after seeding), media was replaced and cells were treated with and without 20ng/ml IFNγ. After 18 hours, cells were challenged with *S. pneumoniae* with an MOI of 5, 10, 15 or 20. After 3 hours wells were treated with 20µg/ml Gentamicin and 40 Units/ml Penicillin to kill the extracellular bacteria. Some wells for each condition were stained and fixed whilst the remaining wells were treated with low dose vancomycin (0.75µg/ml) for a further 2 hours. This allows the calculation of the percentage decrease in intracellular bacteria. In Figure 4.2A, a greater percentage decrease in intracellular bacteria represents a greater degree of intracellular killing. A minor trend to increased intracellular killing at higher MOI with IFNγ treatment was observed but this difference is not defined enough to be considered a suitable positive control and these higher MOIs of 15 and 20 resulted in too many intracellular bacteria making it difficult to distinguish between individual bacteria. Figure 4.2B depicts the average cell number per well to confirm that the addition of either IFNγ or bacteria did not have an adverse effect on cell number.

As no significant increase in intracellular killing was observed with the addition of 20ng/ml IFNγ, cells were pre-treated with a range of IFNγ concentrations in order to determine if an effective concentration could be identified. After 18 hours incubation with IFNγ cells were infected with *S. pneumoniae* at MOIs of 2 or 4 and images were taken as above to determine percentage decrease in intracellular bacteria. No obvious effect or dose-response was observed and results were varied indicated by the large error bars in Figure 4.2C. To check that IFNγ was not having an adverse effect on cell number resulting in inconsistency between

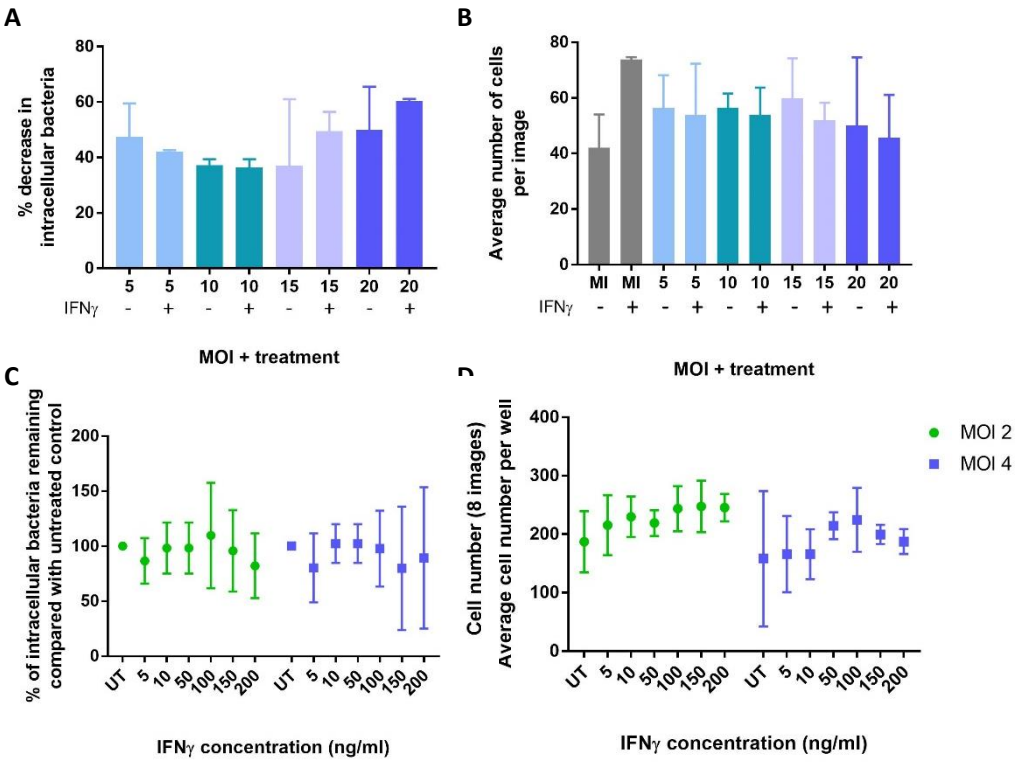

Figure 4.2 – ***18 hour pre-treatment with IFNγ does not increase intracellular killing of*** **S. pneumoniae** ***in RAW 264.7 cells.*** MI = mock infected, UT = untreated. **(A)** RAW 264.7 cells infected with *S. pneumoniae* at MOIs ranging from 5 to 20, with and without IFNγ pre-treatment (20ng/ml) for 18 hours. (n=2). **(B)** Cell numbers per image were analysed by DAPI counts to determine if pre-treatment or MOI had an adverse effect on cell number (n=2). **(C)** Cells were pre-treated with a range of IFNγ concentrations. After 18 hours cells were infected with MOI 2 and 4 and images were taken 3 and 5 hours after bacterial challenge to determine percentage decrease in intracellular bacteria. Cell numbers were determined **(D)** to ensure inconsistency between repeats was not due to IFN pre-treatment (n=3, in which each n represents an individual experiment from a different cell passage with an average from 4 replicate wells). Data show the mean ± SD (two way ANOVA, Sidak's multiple comparison test (n=3, each n represents 4 wells)).

repeats, cell counts were carried out. There was no correlation between IFNγ concentration and cell number (Figure 4.2D).

Focusing on determining the most appropriate MOI, RAW 264.7 cells were challenged with *S. pneumoniae* at MOIs ranging from 2 to 10. Eight wells were used per condition. After an initial 3 hour incubation, all wells were washed and treated with antibiotic to kill the extracellular bacteria. Four wells at this point were fixed and stained with the remaining four treated with low dose vancomycin to keep the extracellular environment sterile. These were fixed and stained after a further 2 hours in order to determine the decrease of intracellular bacteria between the two time-points. Most conditions resulted in 40-50% decrease in intracellular bacteria from 3 to 5 hours (Figure 4.3A). This will allow for further decrease if drugs enhance intracellular killing. MOI of 2 was the most consistent across the range of MOIs between experiments shown through the least variation (n=3). Cell number was assessed at

to ensure that the correlation of higher MOIs and large differences in intracellular killing was not due to cell death. Cell number slightly decreases with increasing MOI but this is not statistically significant (Figure 4.3B).

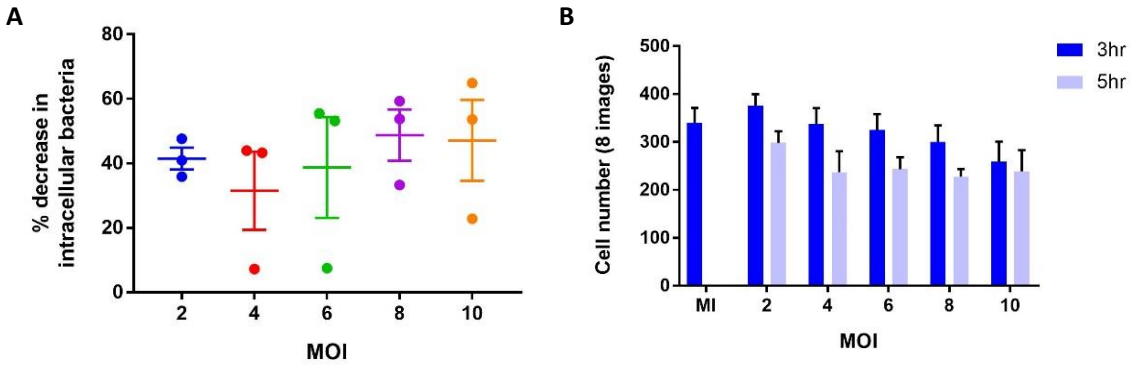

Figure 4.3 – ***The most consistent decrease in intracellular bacteria is observed when RAW 264.7 cells are challenged with an MOI of 2.*** RAW 264.7 cells were challenged with *S. pneumoniae* at MOIs ranging from 2 to 10. Wells were fixed at 3 and 5 hours post-infection after antibiotic treatment. **A.** The number of bacteria at each time point was compared to give a percentage decrease. Greater percentage decrease in intracellular bacteria represents a greater degree of intracellular killing. Data show the mean ± SD (one way ANOVA, Tukey's multiple comparison test (n=3, in which each n represents an individual experiment from a different cell passage)). **B.** To ensure that bacterial challenge does not have an adverse effect on cell viability, cell number at different MOIs and different time-points was assessed. Data show the mean ± SD (two way ANOVA, Sidak's multiple comparison test.

4.2.3 Optimisation of a suitable positive control to enhance intracellular killing

Clemastine is an anti-histamine drug with histamine H1 receptor as its main target. It also increases the sensitivity of P2X7 receptor to ATP (Nörenberg *et al.*, 2011). P2X7 is an ATP-gated ion channel that mediates many functions of both the innate and adaptive immune systems. P2X7R has been shown to be inducible in RAW 264.7 cells (Wilson *et al.*, 2004). Treatment with clemastine has been shown to enhance mycobacterium control by macrophages in zebrafish (Matty *et al.*, 2019). Unpublished data by Clark Russell at University of Edinburgh has also shown enhanced killing of *S. pneumoniae* by human monocyte derived macrophages after treatment with clemastine. This is also supported by Lees *et al,* whereby a loss of function mutation in P2X7R resulted in reduced killing of *Mycobacterium tuberculosis* and *Toxoplasma gondii* in RAW 264.7 cells and primary murine macrophages (Lees *et al.*, 2010). VPS34 is a Class III PI3 kinase with a known role in autophagy (Tao *et al.*, 2021). It has been found to be associated with phagosomes but its role is unknown (Minakami *et al.*, 2010). A colleague, Natalia Hadjamowicz, had found that inhibition of VPS34 resulted in an increase

in intracellular killing of *S. aureus* by neutrophils with no direct antibacterial effect and no effect on phagocytosis (unpublished data). These were tested at 5µM, 10µM and 30µM. 2 different time-points for addition of these compounds were tested, with the first and second antibiotic treatments; pre-treatments would not be physiologically relevant. As depicted in Figure 4.4A, RAW264.7 cells were challenged with GFP-expressing *S. pneumoniae* at MOI 2 for 3 hours. Cells were treated with gentamicin and penicillin to kill extracellular bacteria. Figure 4.4B correlates with treatment with clemastine or VPS34 inhibitor (or vehicle) at this stage, whereas Figure 4.4C correlates with treatment with vancomycin 30 min later. Both compounds were reconstituted in DMSO however, 3 plates of the compound screen included drugs reconstituted in H_2O hence requirement for H_2O and DMSO vehicle controls. There was no significant difference at both time-points of vehicle controls to untreated control meaning significant differences in intracellular bacteria upon treatment with compounds were not due to vehicle. Treatment with both VPS34 inhibitor and Clemastine at 5µM both resulted in a decrease in intracellular bacteria when added at with vancomycin, although a clear dose-response was not observed with Clemastine.

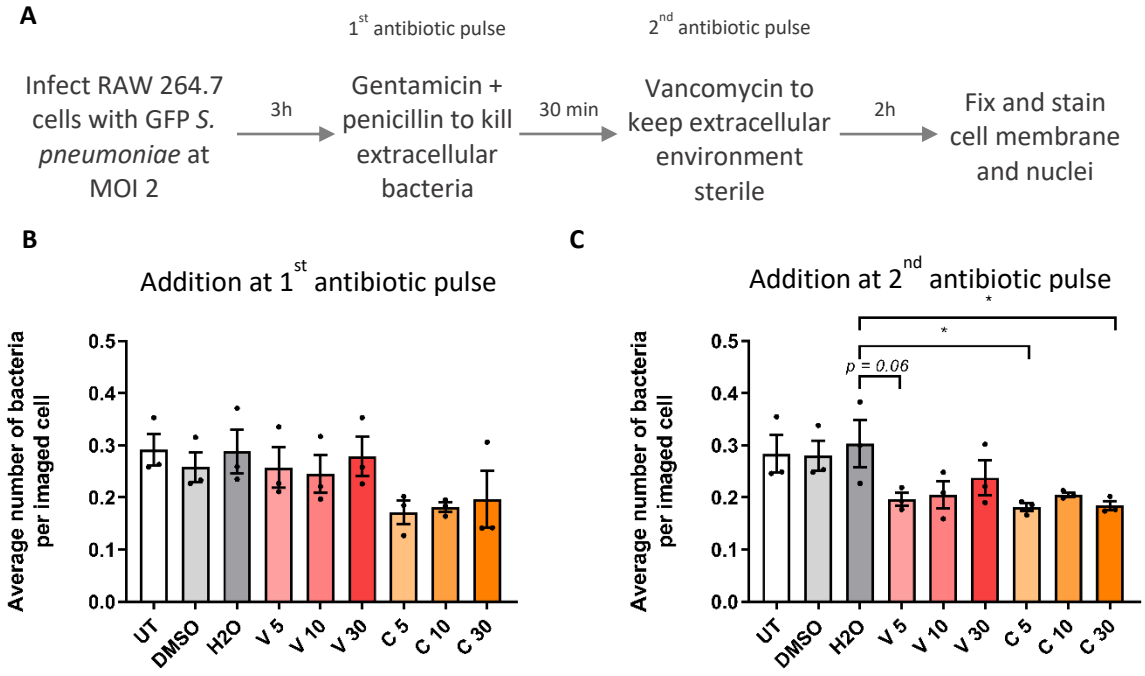

Figure 4.4 – ***VPS34 inhibitor and Clemastine are suitable positive controls for increasing intracellular killing.*** **A.** Illustration of the experimental procedure carried out to determine time-point for compound addition. RAW 264.7 cells were challenged with *S. pneumoniae* with MOI 2. VPS34 inhibitor (V) and clemastine (C) were added at different concentrations either with the first antibiotic pulse (**B**) or the second low dose antibiotic (**C**) to determine if either would be suitable for a positive control. Both treatments were imaged at 1st and 2nd antibiotic steps. The average number of remaining intracellular bacteria per cell at both time points was quantified. Data show the mean ± SD; *P<0.05, (one way ANOVA, Tukey's multiple comparison test (n=3, in which each n represents an individual experiment from a different cell passage)).

4.2.4 Pilot plate 1

RAW 264.7 cells were challenged with *S. pneumoniae* with MOI 2 as above. Plate 14 from the TOCRIS compound library was used as a pilot plate and was added at 5µM final concentration with the second antibiotic pulse. The aim of testing a pilot plate was to determine if control compounds (VPS34 inhibitor and Clemastine) were suitable and if there were any noticeable problems with automation. 2 hours after compound addition, cells were washed, stained and fixed before imaging using the ImageXpress high-content microscope. MetaXpress image analysis software was used for RAW 264.7 cell and intracellular bacteria counts. Appendix C contains the R code used for analysis, using the *cellHTS2* package (Boutros, Hahne and Huber, 2013). Figure 4.5A shows that the data points were reasonably normally distributed. However, the distinction between red and blue points along the x-axis, depicting positive and negative controls, respectively, should be either side of the mean (0). Figure 4.5B represents the mean values with the darker green representing a lower number of bacteria. There appears to be edge effects in column 1 and 12 where the controls are positioned with

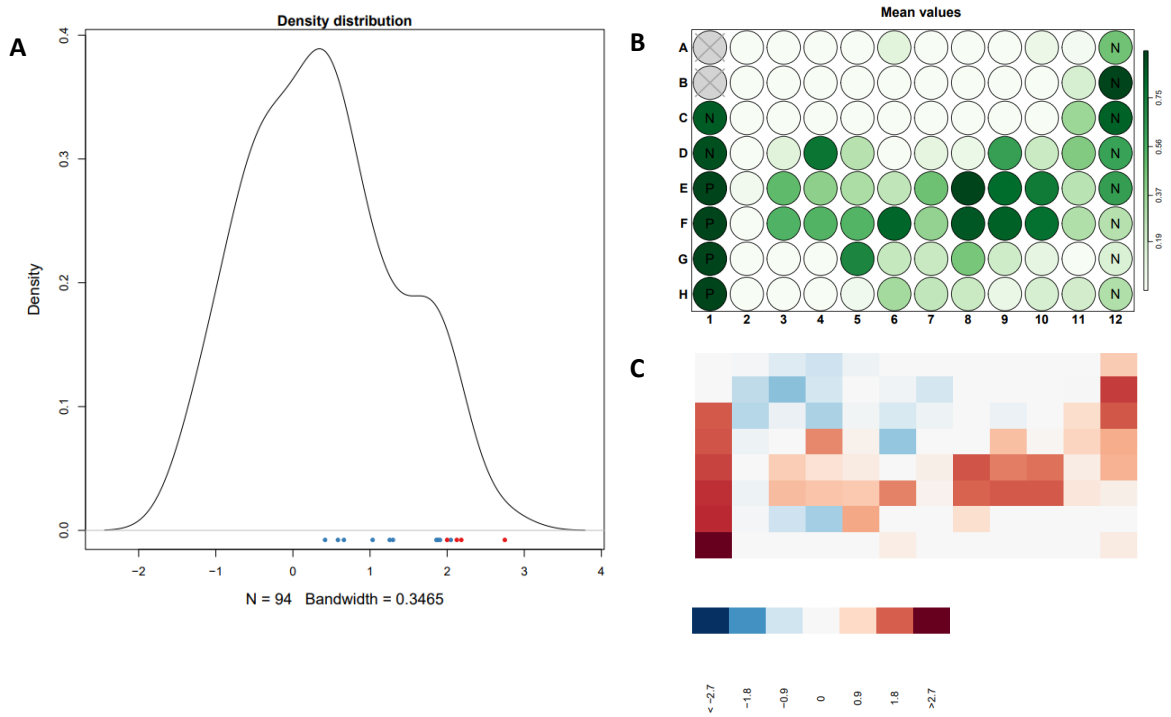

Figure 4.5 – ***Pilot plate (TOCRIS 14) showed further optimisation was required.*** RAW 264.7 cells were challenged with *S. pneumoniae*, compounds from plate 14 from the TOCRIS library (pilot plate) were added with the second antibiotic pulse. **A.** Density distribution plot with blue and red points on the x axis represent negative and positive controls, respectively. **B.** Representation of mean values with darker green signifying wells that had a lower number of intracellular bacteria. **C.** Representation of significant values with blue representing wells with a higher number of intracellular bacteria and red wells indicating increased intracellular killing through a lower number of intracellular bacteria compared to the median.

some negative controls (N) appearing to cause a decrease in intracellular bacteria. This is shown to be significant in some wells shown in Figure 4.5C in which the scale bar shows the relation of colour to z-score. A z-score of 1.96 or above (or -1.96 or below) is classed as significant. In this data a score of over 1.96 will be classified as a 'hit' compound in enhancing intracellular killing.

4.2.5 Pilot plate 2

In order to overcome the apparent edge effects displayed in Figure 4.5A and B, negative controls were positioned in column 1 and positive controls in column 12, using plate 13 from the LOPAC compound library. The top 3 wells in both columns were excluded as these wells in column 12 showed a decrease in intracellular bacteria in the TOCRIS plate. The orientation of the plates during incubation periods was checked to be the same. Figure 4.6A shows blue dots (negative controls) to the left of 0 and red dots (positive controls) to the right, with more distinction between the these controls compared to Figure 4.5A. The density distribution also shows a tighter peak which is to be expected from a single plate. A broader peak would

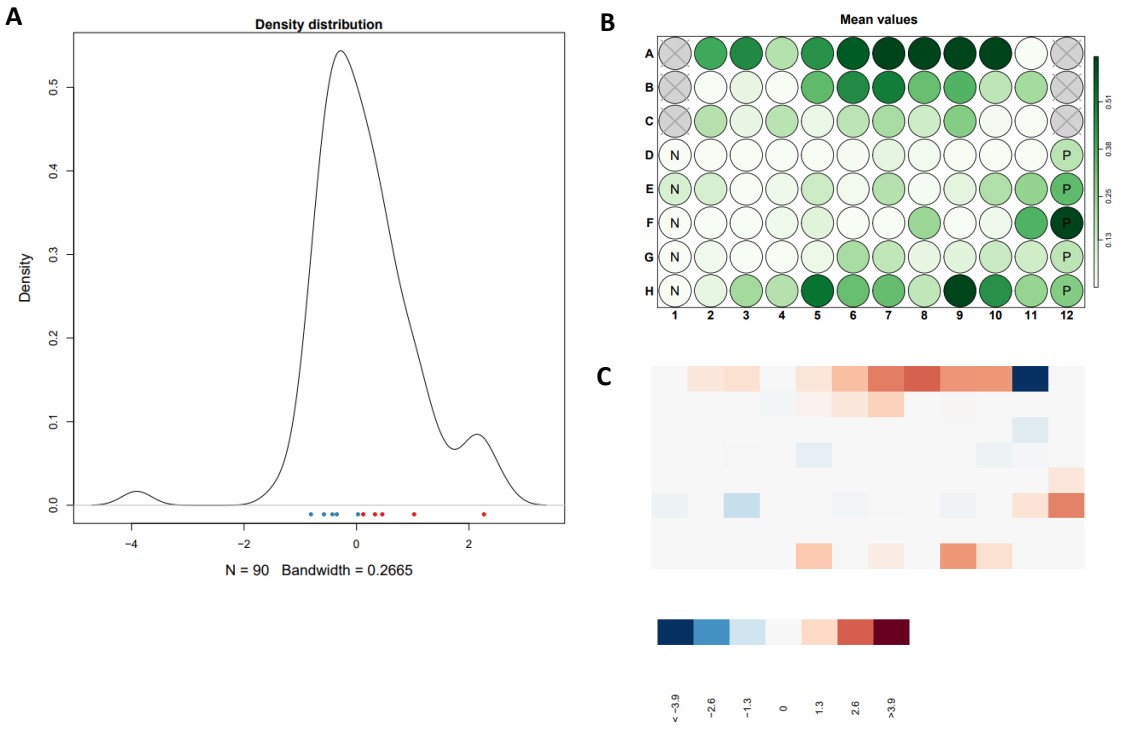

Figure 4.6 – ***Pilot plate 2 (LOPAC 13) showed reduction in edge effects.*** RAW 264.7 cells were challenged with *S. pneumoniae*, compounds from plate 13 from the LOPAC library (pilot plate). **A.** Density distribution plot with blue and red points along the x-axis representing negative and positive controls, respectively. **B.** Representation of mean values with darker green signifying wells that had a lower number of intracellular bacteria. **C.** Representation of significant values with blue representing wells with a higher number of intracellular bacteria and red wells indicating a lower number of intracellular bacteria compared to the median.

indicate more 'hits' with data points further from the mean which would be more expected from a whole screen with a range of hits. However, row A indicated a possible edge effects as shown in Figure 4.6B and C which may require further assessment and perhaps elimination when running the full compound library. The negative controls appear to be paler than in Figure 4.6B and C compared to 4.5B indicating no reduction in intracellular bacteria as expected. The positive controls show a reduction in intracellular bacteria in both Figure 4.6B and C however only 2 of these wells reached significance.

4.2.6 Johns Hopkins clinical compound library screening data

The compound library used here is the Johns Hopkins Clinical Compound Library (JHCCL) which consists of 1,524 pharmacologically active compounds across 21 x 96 well plates. These were diluted in DMSO to a 1mM working stock concentration. The first and last columns in each plate were left as blank for controls as described above.

RAW 247.6 cells were seeded at 10,000 cells per well. On day 2 they were challenged with GFP labelled, non-encapsulated *S. pneumoniae* at MOI 2. After 3 hours the cells were treated with penicillin and gentamicin for 30 minutes. Compounds and low-dose vancomycin were added for 2 hours after which cells were stained and fixed for image analysis using the ImageXpress high-content microscope and MetaXpress analysis software. The library was tested in triplicate with plates 1-10 first followed by plates 11-21 in order to ensure time-points were maintained throughout screening. An automated pipettor was also used for all addition and wash steps to maintain time-points, with the exception of compound addition due to the low volume required. The *cellHTS2* R package was used for analysis of the data produced by MetaXpress. Initially the DAPI data, for cell nuclei and therefore cell count, was analysed first to confirm that there were no plates or wells that needed removing from downstream analysis. A low cell count would yield a false positive result as a low cell count will correlate with a low number of intracellular bacteria. Figure 4.7A shows normalisation of the data to the median. The pink plot depicts the raw data and the blue plot depicts the normalised data. The raw data in the top panel shows low values for plate 5 for all replicate 2 so this was removed. Also huge disparity in cell number was observed in plate 10 both before and after normalisation. This is also shown in the plot of scored values in Figure 4.7B in which half the plate is blue, indicating a very low cell number and half the plate is red indicating a higher cell number. This plate also removed from analysis to ensure no false positives. On the

lower panel we can see the normalised values have a similar variation between all the remaining plates.

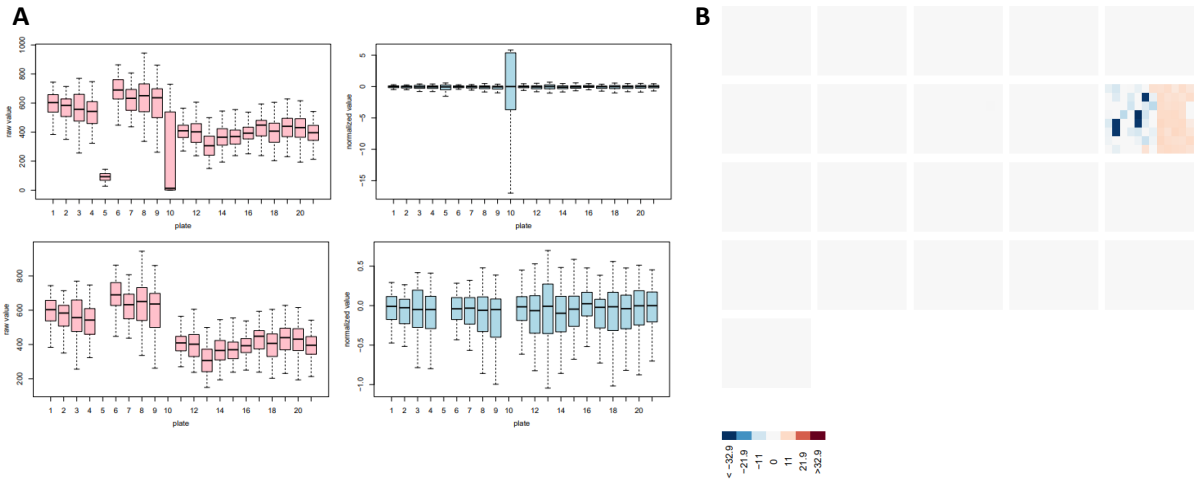

Figure 4.7 – ***DAPI analysis showed plates 5 and 10 from repeat 2 needed to be removed from analysis.*** **A.** Normalisation plots of replicate 2 before (pink) and after (blue) normalisation to the median. The top panel depicts all plates whereas the bottom panel depicts normalisation after removal of plates 5 and 10 from analysis. **B.** Scored value plot with blue points indicated low cell numbers whereas red points indicate wells with higher cell numbers.

Figure 4.8A shows the score value plot for the whole screen, which indicates a few very highly significant points suggesting a huge increase in intracellular bacterial numbers. The normal range for intracellular bacteria in this assay is around 50-100 (data not shown) whereas these wells were showing values of 1000-5000. Figure 4.8B depicts a Q-Q plot (quantile-quantile plot) which indicates whether the data is normally distributed. Points along the dotted line suggest normal distribution however tails deviating a long way from this either suggest significance or values that do not fit into the normal distribution.

After observing the raw images and the wells on the plates, these wells correspond to those with coloured compounds so it is likely that these outliers were due to optical interference with fluorescence. Keeping these wells in the data for analysis may skew the normalisation, therefore they were eliminated. Excluding these wells from also made it easier to see a range of possible hits (Figure 4.9A). There is the possibility that edge effects occurred in plates 8 and 9 as the first few columns read as having higher apparent bacteria counts (blue colours in 4.9A) and the final columns suggest lower bacteria counts (red colouration in Figure 4.91). Hits from these plates should be taken forward for further testing to ensure they are not false positives. Figure 4.9B shows improved distribution of the data following removal of outliers. Generally positive and negative controls are skewed to the right and left of the density

distribution plot, respectively (positive value representing enhanced killing with negative values representing higher bacterial number per cell). There is not the distinction between controls in the middle of the x-axis as expected however, as the data are not normalised to either set of controls this should have no effect on the results.

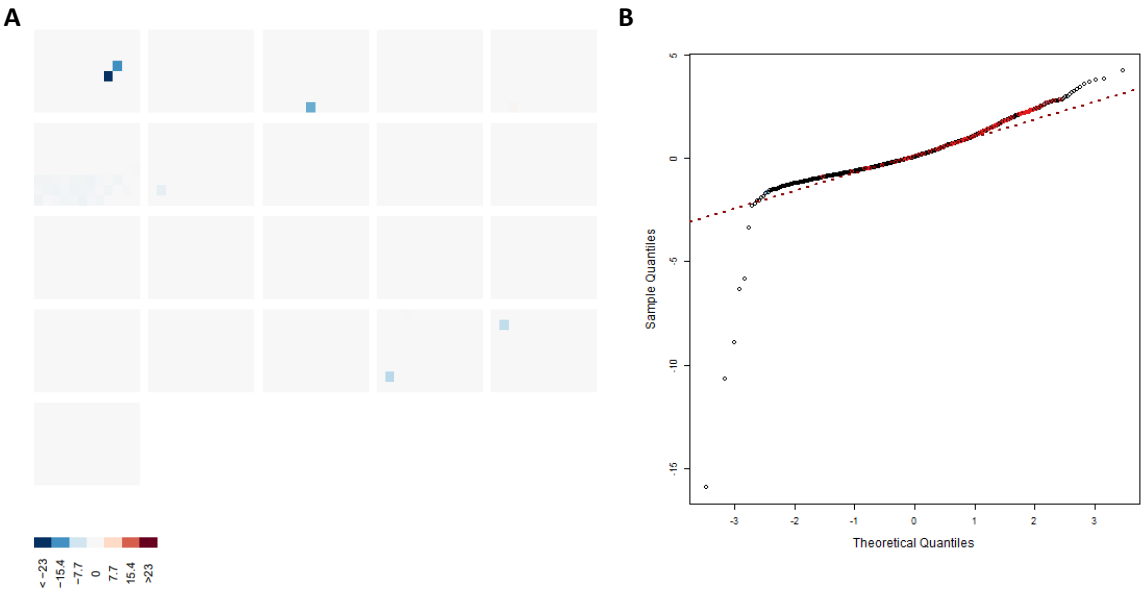

Figure 4.8 – ***Initial analysis showed that outliers needed to be removed.*** **A.** Scored value plot showing only blue significant wells indicating increased number of intracellular bacteria. **B.** Q-Q plot, (quantile-quantile plot), in which the red dotted line depicts theoretical normal distribution.

Table 4.1 contains the hits that resulted in a significant increase in intracellular killing in the compound screen. For some of the compounds listed, work has begun to determine if they are able to be repurposed into antibacterial or antiviral drugs. However, to my knowledge there is no published evidence that work has been carried out for repurposing these drugs to enhance the host response.

This screen is capable of identifying anti-infective agents, some that may have not been explored. This is shown in Table 4.1 as multiple significant hits are antibiotics, with penicillin resulting in the most significant reduction of intracellular bacteria. Antibiotics can be taken up by phagocytes, which brings them in close proximity to their targets and therefore reducing the number of intracellular bacteria albeit at low concentrations (Barcia-Macay *et al.*, 2006). Further investigation of hit compounds would be required to determine if their activity is antibacterial before investigating the effect on enhancing intracellular killing capabilities of macrophages.

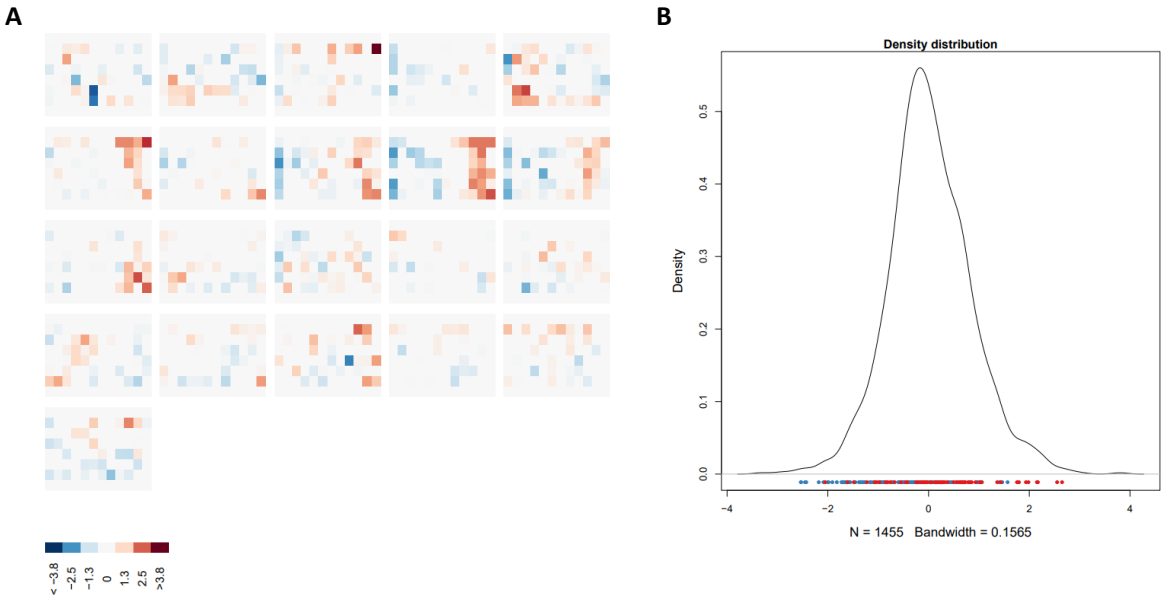

Figure 4.9 – ***Distribution of samples and controls show some overlap of controls but good distribution of data points.*** **A.** Scored value plot after removal of outliers showing increased intracellular bacteria with darker red wells indicating decrease in intracellular bacteria. **B.** Density distribution plot showing distribution of points with blue and red points on the x-axis depicting negative and positive controls, respectively.

Z - Score	Plate	Well	Compound	Class/Activity	Approved use
3.8	3	B12	Penicillin G sodium	Antibiotic	Bacterial Infection
3.01	6	B12	Candesartan cilexetil	Antihypertensive	High blood pressure and heart failure
2.79	5	F03	Aminophylline	Bronchodilator	Brochospasm
2.7	11	F11	Enrofloxacin	Antibiotic	Bacterial Infection
2.65	9	G12	Clemastine	Antihistamine	Allergic response
2.55	11	G12	Clemastine	Antihistamine	Allergic response
2.49	18	B10	Ampicillin Sodium Salt	Antibiotic	Bacterial Infection
2.34	5	F02	Zileuton	Anti-inflammatory	Asthma
2.34	9	C11	Carbocloral	Sedative	Muscle spasm

2.31	9	B11	Modafinil	Nootropic	Sleep apnea / nacrolepsy
2.3	8	D10	Amoxapine	Antidepressant	Depressive disorders
2.3	9	B10	Flurothyl	Nootropic	Chemoconvulsant
2.3	9	B12	Nikethamide	Nootropic	Respiratory stimulant
2.2	9	F10	Mesalamine / mesalazine	Anti-inflammatory	Ulcerative Colitis
2.2	21	B10	Oxibendazole	Anthelminithic	Parasite infection
2.17	8	G12	Clemastine	Antihistamine	Allergic response
2.15	7	G12	Clemastine	Antihistamine	Allergic response
2.15	8	F11	Biperiden Hydrochloride	Antiparkinsonian	Parkinson disease and drug induced movement
2.14	6	B09	Verapamil hydrochloride	Antihypertensive	High blood pressure and angina
2.14	6	B10	Ergoloid Mesylates	Nootropic	Mood and behavioural problems in Alzeimer's disease and stroke
2.12	9	E11	Halcinonide	Anti-inflammatory	Skin conditions including psoriasis and eczema
2.06	8	G11	Piperacetazine	Antipsychotic	Schizophrenia
2.06	9	G11	Fluorometholone Acetate	Glucocorticoid	Eye conditions
2	5	C02	Carbinoxamine Maleate	Antihistamine	Allergic response
1.98	10	E10	Cholecalciferol (Vitamin D3)	Vitamin	Dietary supplement
1.98	17	G12	Clemastine	Antihistamine	Allergic response
1.97	18	B11	Azithromycin	Antibiotic	Bacterial infection
1.96	9	F11	Olsalazine	Anti-inflammatory	Ulcerative Colitis

Table 4.1 – ***Statistically significant hits from screening Johns Hopkins clinical compound library***

4.3 Discussion

The intended model cell for the development of this screen was human monocyte-derived macrophages due to their physiological relevance. However, due to the Covid-19 pandemic, this was not possible due to the shortage of clinicians and nurses able to perform venesection as well as the availability of healthy donors. Therefore, alternative cell types were explored. Initially murine bMDMs were tested but the lack of adherence during the wash steps of the bacterial challenge and staining resulted in very few cells remaining for image analysis. RAW 264.7 cells proved to be more suitable in terms of adherence. The RAW 264.7 cell line is a murine macrophage cell line which is capable of chemotaxis, phagocytosis and intracellular killing and are therefore commonly used to study responses to microbes (Duchesne *et al.*, 2021; Yang *et al.*, 2021). They do have a smaller cytoplasm but with a similar number of lysosomes compared to MDMs (Öhlinger *et al.*, 2020). The use of a cell line removes the effect of donor-to-donor variability as well as the limitations with cell number. However, there was no correlation observed between the responses of RAW 264.7 cells and PBMCs to immunomodulators (Elisia *et al.*, 2018). Compounds that may have an enhancing effect on intracellular killing in MDMs may not have a positive effect in RAW cells therefore, a limitation of this screen may be that some hits are missed due to the cell type used. As the purpose of the screen was to identify compounds that may enhance intracellular killing, a function common to both RAW 264.7 cells and human MDMs, RAW 264.7 cells were deemed suitable for the initial screen, recognising further validation will be required to establish the efficacy of hit compounds in human cells.

As RAW 264.7 cells continue to proliferate, the cell number was determined 2 days after seeding into 96 well plates in order to accurately calculate and add the correct MOI in following experiments. An MOI of 2 was found to give the most consistent results in terms of the percentage reduction of intracellular bacteria. Although there was no significant difference in RAW cell number between the MOIs tested there was a trend towards decreasing cell number with increasing MOI. When determining suitable positive controls, 5µM VPS34 inhibitor and clemastine resulted in a significant reduction in intracellular bacteria. Adding these compounds with the second antibiotic pulse ensured that a reduction of intracellular bacteria compared to negative controls was not as a result of reduced phagocytosis or bactericidal effects of the compounds killing *S. pneumoniae* before it enters the cell. These parameters were then applied to a pilot plate from another compound library

in order to ensure the automation set up was effective as well as the positive and negative controls remaining appropriate. The compound library plates are arrange with column 1 and most of column 12 empty for controls with the remainder of the plate containing compounds. The results of this showed that there were possibly edge effects with some negatives coming up as positive hits. In order to overcome this, negative controls were repositioned to column 1 and positive controls in column 12. This resulted in more consistency and therefore, screening the Johns Hopkins clinical compound library started.

Clemastine appeared in the 28 hits on five occasions. In order to improve this for future work it would be useful to determine the EC50 of VPS34 inhibitor and Clemastine on intracellular killing to ensure the concentration with the biggest effect is being used. Further to this, determining the EC50 of a handful of compounds that were almost significant may reveal another concentration for this screen to be performed at.

Current work in relation to hit compounds for this screen is generally focused on repurposing compounds to function as antibiotics. The limitation with this approach is that the bacteria could still develop advantageous mutations resulting in resistance to treatment. There are also limitations to repurposing compounds in general. Barriers to this can include patents and regulatory boundaries, such as safety characterisation which may require further tests in addition to previous clinical trial data. Some mechanistic work may also be required due to the activity of the drug differing from its prescribed use.

Aminophylline is a bronchodilator used for treatment of asthma and COPD. Addition to bacterial culture medium resulted in a significant decrease in growth rates of a variety of bacterial strains however, *S. aureus* was only susceptible at the highest concentration tested (10mg/ml, equivalent to 25µM) suggesting direct antimicrobial effects (Al-Janabi, 2011). Amoxapine is an antidepressant which has been shown to result in a decrease of *S. aureus* growth in culture medium but not complete inhibition. Co-treatment resulted in a reduction in the MIC of oxacillin, up to 128-fold compared to oxacillin treatment alone. It also may act as a beta-lactamase inhibitor resulting in re-sensitisation of MRSA to the beta-lactam antibiotic, oxacillin. Treatment with amoxapine following treatment with oxacillin, reduced the cleavage of nitrocefin, a chromogenic substrate for beta-lactamases (Wilson, Blackledge and Vigueira, 2018). Verapamil is usually prescribed for treatment of high blood pressure and angina but recently has been show to act as an efflux pump inhibitor which has helped treatment of *M. tuberculosis* acting synergistically with bedaquiline. Bedaquiline is currently

used for the treatment of *M. tuberculosis* but has toxicity effect and can actually increase mortality and lead to liver-related reactions. Like with co-treatment described above, co-treatment with verapamil results in the MIC of bedaquiline being lowered (Gupta, Tyagi and Bishaia, 2015).

Two further compounds have been taken forward from *in vitro* studies to *in vivo* studies displaying antiviral and antibacterial properties. These are carbinoxamine maleate (CAM) and candesartan cilexetil (CC). CAM is an antihistamine that was discovered to have antiviral activity through screening influenza infected MDCK (Madin-Darby canine kidney) cells with an FDA approved drug library. CAM had an IC50 of 3.56μM for inhibiting viral induced cell death with no toxicity effect of the drug until concentrations of 250μM or above. A limitation here is that CAM only inhibits early stage infection of cells by blocking entry of the influenza virus to the cell. When taken forward for in vivo studies mouse survival increased from 22% to 77% when treated with 10mg/kg of CAM compared to PBS treated mice. Lung samples from PBS and CAM treated mice were taken and showed downregulation of viral gene expression as well as maintained alveolar structure and less inflammatory cell infiltrates (Zhang *et al.*, 2018).

Candesartan cilexetil (CC) is a hypertension drug used to treat high blood pressure and heart failure. It has previously been shown to have antiviral properties by inhibiting RNA and protein synthesis of Zika virus (Wing *et al.*, 2019). CC has been further tested for antibacterial effects against a variety of bacteria. It was found to be ineffective in inhibiting growth of Gram-negative bacteria but showed inhibition of growth against a variety of *S. aureus* strains. The MIC was 8-16μg/ml compared to 0.25-4μg/ml with daptomycin, currently a last-resort antibiotic for the treatment of MRSA. A synergistic effect was seen when both CC and gentamicin was added to cultures of *S. aureus*, inhibiting growth when individually at lower concentrations there was no effect on growth rate. Further to this, resistance over 30 days was tested with *S. aureus* which remained as susceptible to CC as it was during initial treatment. Like other antibiotics, CC treatment was shown to result in membrane disruption and ATP leakage. In an *in vivo* skin abscess model, CC reduced bacterial abundance by up to 25-fold at the highest dose compared to vehicle. However, treatment with vancomycin reduced bacterial abundance by 1,000-fold (Leisner *et al.*, 2021).

Further validation would require running the top hits in EC50 experiments in human MDMs to test their activity in a more physiologically relevant cell type and to find their most effective

concentration. Those that show activity in MDMs should be tested in the same format to determine the effect on multiple bacterial species. This would help to determine if this could be a broad treatment or more specific to *S. pneumoniae* infections. Testing these hits on the growth rate of bacterial species would be required to establish if their effect is directly antimicrobial activity or if the intracellular activity is enhanced. It would be interesting to investigate if the compound and vancomycin were working synergistically as shown with candesartan cilexetil and gentamicin (Leisner *et al.*, 2021). It would also be interesting to see if the enhancing effect of these compounds on intracellular killing is also observed in neutrophils. It would also be important to test longer incubation periods and therefore verify any toxicity effects from prolonged treatment before taking compounds forward for *in vivo* studies. The most effective compounds, showing no toxicity effects, could be taken forward for *in vivo* studied. Tracking clearance of GFP-expressing *S. pneumoniae* in infected zebrafish post-treatment could reveal compounds that are candidates for repurposing where improved bacterial clearance and survival is observed.

5 Chapter 5: Development of a human-genome wide siRNA screen to identify novel regulators of intracellular killing

5.1 Introduction

5.1.1 siRNA

siRNA is a useful tool to silence genes, particularly in MDMs as these are terminally differentiated primary cells. The process of gene silencing using this technique begins with dsRNA (double-stranded RNA) (Dana *et al.*, 2017). dsRNA requires a transfection reagent to enter the cell. Lipid based transfection reagents spontaneously form liposomes upon interaction with RNA and DNA. This allows the dsRNA to enter the cell as the liposome fuses with the plasma membrane (Felgner *et al.*, 1987). Once in the cell the dsRNA binds to a protein called Dicer. This protein is part of the RNase III family which cleaves the longer dsRNA into siRNA. RISC, a multi-protein complex, binds the siRNA and separates the strands. The strand with the more stable 5' end remains bound to the RISC complex. The single stranded siRNA then aligns the RISC complex with the target mRNA. The mRNA is then cleaved, recognised as abnormal and degraded (Figure 5.1) (Dana *et al.*, 2017). This prevents translation of the mRNA resulting in gene silencing.

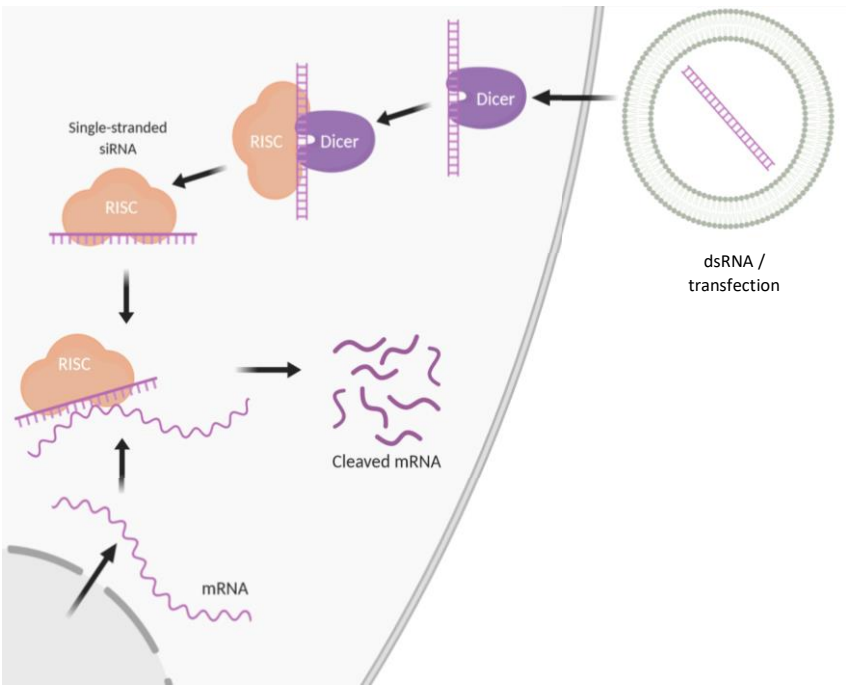

Figure 5.1 – ***Schematic diagram depicting the process of gene silencing by siRNA.*** The transfection/RNA complex fuses with the plasma membrane where the RNA binds to Dicer. Dicer cleaves the RNA to siRNA which then binds the RISC complex. RISC separates the siRNA to leave single strands which then binds to target mRNA. RISC cleaves the target mRNA. Adapted from (Dana *et al.*, 2017) and created using Biorender.com.

5.1.2 siRNA screening

The RNAi facility at the University of Sheffield hold a human genome-wide siRNA library targeting 18,096 genes. This was used herein to screen early microbicidal responses in MDMs. RNAi screens have resulted in the discovery of novel regulators. For example, a collagen-binding receptor, with known roles in immune diseases and tumour metastasis, was identified through a targeted siRNA screen to be a novel regulator of α2β1 integrin trafficking (Eskova *et al.*, 2014).

The increasing rise of antibiotic resistant infections and the difficulty in treating such infections, requires alternative therapeutics. Vaccinations, antibody and phage therapy are limited by their specificity to species of bacteria or even subsets within species. Therefore, therapies targeting the innate immune system may result in exploitation of its broad effectiveness against a wide variety of microbes. In order to determine what genes are required for intracellular killing a genome-wide siRNA library is a useful tool. In this screen, transfected human MDMs (monocyte-derived macrophages) will be exposed to GFP and pHrodo (red) labelled *Streptococcus pneumoniae. S. pneumoniae* usually evades uptake by immune cells due to its polysaccharide capsule however once within the cell it is processed to an acidified phagolysosome where it susceptible to early killing. In this screen a non-encapsulated strain of *S. pneumoniae* will be used to ensure high levels of phagocytosis (Jubrail *et al.*, 2016). *S. pneumoniae* is a useful model organism because it is readily killed in mature phagosomes, is the leading cause of community acquired pneumonia and some strains have now acquired penicillin-resistance (Hakenbeck *et al.*, 2012). As discussed is section 1.3.1 known proteins involved for sequential process of acidification of the phagosome however regulators of this process remain unknown. The aim is to develop an siRNA screen in order to uncover these regulators. Hits that modify the expected decline in intracellular GFP labelled *S. pneumoniae* will be further investigated to confirm if they identify regulators of early microbicidal killing. Utilising pHrodo labelling, which fluoresces in acidified conditions, will predict defects in phagosomal maturation.

5.2 Results

5.2.1 Optimisation of Dissociation and Re-seeding of MDMs

The human siRNA library is stored across 57 384-well plates. It was not possible to seed monocytes directly into these due to unknown effects of transfection on differentiation into monocyte-derived macrophages. Dissociating cells from 6 well plates and re-seeding on day 13 allows the MDMs to fully differentiate. Three different techniques were tested to dissociate the cells from 6 well plates for re-seeding into 384 well plates. Scraping, incubation with pre-warmed PBS and incubation with Accutase were chosen as candidate methods as they have been shown to have no impact on surface markers for M0 macrophages whilst resulting in a high percentage of recovery (Chen *et al.*, 2015). Figures 5.2A and 5.2B show that treatment with Accutase for 20 minutes increases the yield of MDMs when compared to both scraping or incubating with PBS whilst maintaining viability post-dissociation.

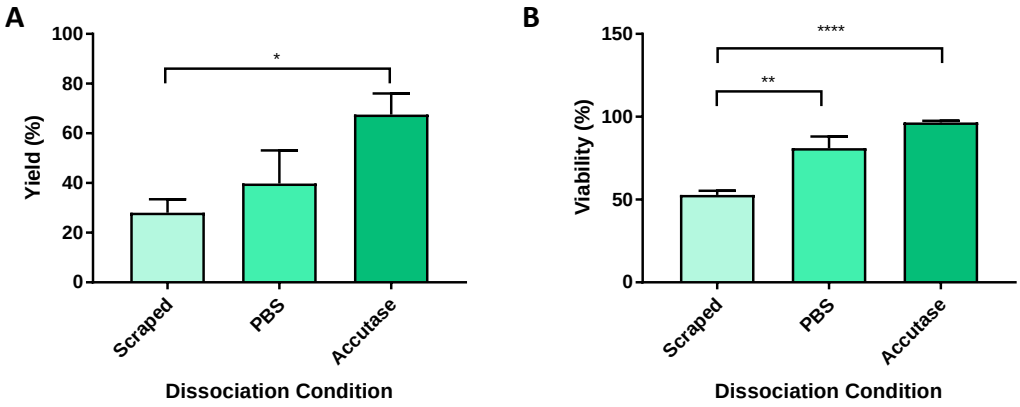

Figure 5.2 – ***Accutase treatment results in the highest viability and yield of MDMs of the dissociation methods tested.*** **A.** Cell counts were performed on dissociated MDMs and compared to the expected number of MDMs per well ($6x10^6$). **B.** Dissociated MDMs were stained with TrypanBlue to determine their viability. Data show the mean ± SEM of 3 individual healthy donors; *P<0.05, **P<0.005, ****P<0.0001 (one-way ANOVA, followed by Tukey's multiple-comparison post-test).

After determining that Accutase treatment achieved good dissociation results, it was necessary to determine the optimal re-seeding density of MDMs to achieve a monolayer of cells with sufficient coverage but without overlapping. After isolation MDMs are plated to obtain a density of $2x10^5$ cells/ml, as a result this density was tested as well as increments to both increase and decrease this density. In order to measure the overlap of the cells, a CellMask Deep Red membrane stain and DAPI nuclei stain was used. The cell membrane stain was used as a mask and the number of nuclei within this was measured. Detection of more

than 1 nuclei per cell indicated overlapping cells. This could skew the data during future infection experiments when outputs will include counting the number of bacteria per cell. Quantification of this data is shown in Figure 5.3. There is no significant difference in the number of nuclei per cell (indicating the level of overlap of cells) between any of the densities, therefore future work will use $2x10^5$ cells/ml, the same seeding density as previously described (Daigneault *et al.*, 2010).

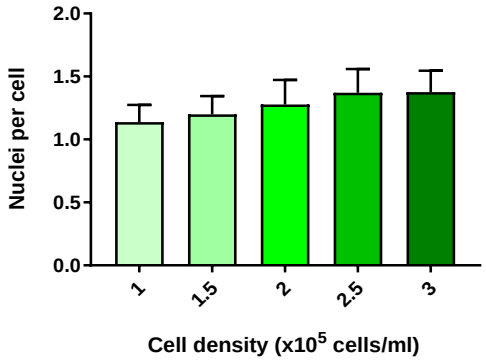

Figure 5.3 – ***Increasing seeding densities had no significant effect on the number of overlapping cells.*** MDMs were dissociated from 6 well plates using Accutase. Viable MDMs were then counted and re-seeded at the given density. After 48 hour incubation cells were stained with CellMask and DAPI before imaging. Data show the mean ± SEM of 4 individual healthy donors ran in at least triplicate wells.

5.2.2 Optimisation of Transfection Reagent

Achieving the highest transfection efficiency is based on using the most suitable transfection reagent, which can differ between cell types and experimental conditions. The RNAi facility at the University of Sheffield frequently recommends using DharmaFect 1 (DF1) for many cells types and has shown to be successful in silencing genes in human MDMs (Behmoaras *et al.*, 2008). Lipofectamine 3000 (Invitrogen) was also used as a comparative transfection reagent. Lipofectamine 2000 has previously been shown to result in high transfection efficiency in bovine MDMs (Jensen, Anderson and Glass, 2014). According to the manufacturer Lipofectamine 3000 was developed to improve transfection efficiency compared to Lipofectamine 2000 and is recommended for use at two different concentrations. Lipofectamine 3000 was used at the lower concentration (A) and higher concentration (B) for comparison with DF1. Cells were also re-seeded (RS) to ensure that there was no significant variation in transfection efficiency due to the process of dissociation. siGLO Green was used to determine transfection efficiency using fluorescence microscopy. After 24 hours, media was replaced or fresh media added to dilute the transfection reagent.

Results in Figure 5.4 show 2 repeats of this with a very slight increase in the number of siGLO positive cells in the media added (MA) condition compared with media changed (MC). Future transfection experiments involved adding media rather than replacing it to avoid reducing the transfection reagent incubation and the risk of losing cells.

Figure 5.5A shows that DF1 and the higher concentration of Lipofectamine 3000 (LP3B) result in the best transfection efficiency. The average cell number per well was calculated to determine if either reagents had any toxicity effects on the cells. Although there was no effect on re-seeded cells, there was a toxicity effect from LP3B on cells that had not been disturbed (Figure 5.5B), therefore future siRNA transfection experiments will be carried out using DF1.

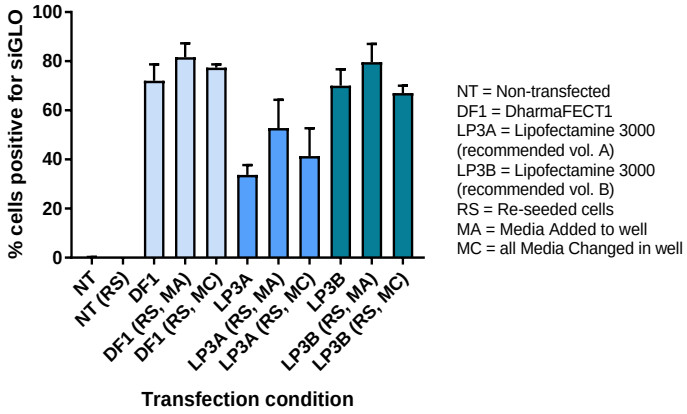

Figure 5.4 – ***Adding fresh media after 24 hours resulted in a slight increase in siGLO positive cells compared to complete replacement of media.*** MDMs were transfected on day 13 using DF1, LP3(A) or LP3(B). 24 hours after transfection media was either replaced entirely (MC) or 100µl media was added (MA). 24 hours later siGLO positive cells were counted. Data show the mean ± SEM of 2 individual healthy donors ran in triplicate wells.

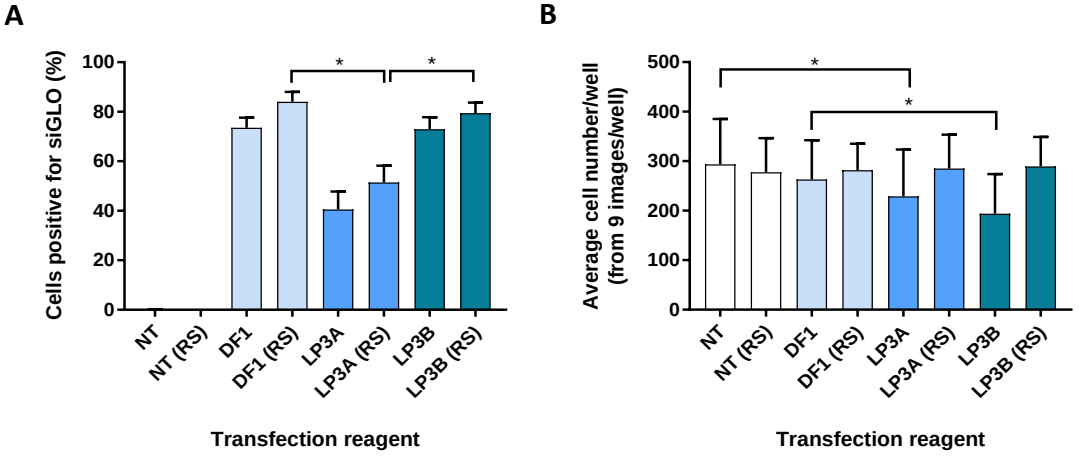

Figure 5.5 – ***DharmaFect 1 resulted in the highest transfection efficiency with no effect on cell number.*** MDMs were transfected using the given transfection reagent, media was added 24 hour later. After a further 24 hours, siGLO positive cells were counted. **A.** Shows the percentage of cells positive for siGLO indicating transfection efficiency. **B.** Shows the average cell number. Data show the mean ± SEM of 2 individual healthy donors; *P<0.05 (one-way ANOVA, followed by Tukey's multiple-comparison post-test).

5.2.3 Confirming siRNA silencing

To confirm that this transfection protocol can successfully result in gene silencing at both mRNA and protein level, MDMs were transfected with 30nM Mcl-1 siRNA using DF1. After 24 hours fresh media was added to the cells (without removing the transfection reagent) which were then incubated for a further 24 hours before RNA or protein extraction. In setting up the qPCR, both primer sets designed (Table 2.6) were first tested for specificity. Figure 5.6A shows that both primer sets were specific as demonstrated by clear single bands on one biological repeat. Figure 5.6B shows primer set 1 tested on the cDNA of the remaining 4 biological replicates.

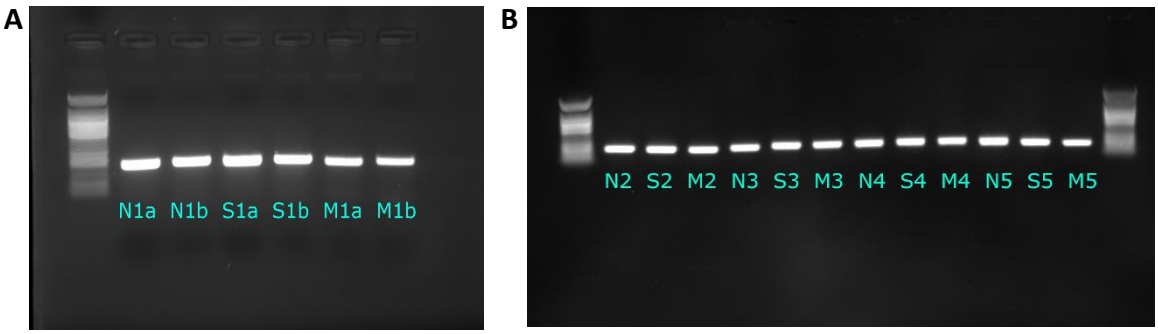

Figure 5.6 – ***A single detectable amplicon after cDNA synthesis was observed using both primer pairs (a and b) and across all samples.*** **A.** N1 = non-transfected sample 1. S = scrambled siRNA (non-targeting). M = Mcl-1 transfected sample. Primer set 1 = a, primer set 2 = b. **B.** Efficiency of primer set 1 tested on all samples. 200bp ladder.

Before running the qPCR, melt curve analysis revealed the primer efficiency for Mcl-1 and 18s was 94% and 91%, respectively. It also showed that the most suitable dilution of cDNA was 1 in 20. Figure 5.7A and B demonstrate clear peaks which are an indication on one amplification product and therefore ideal for qPCR.

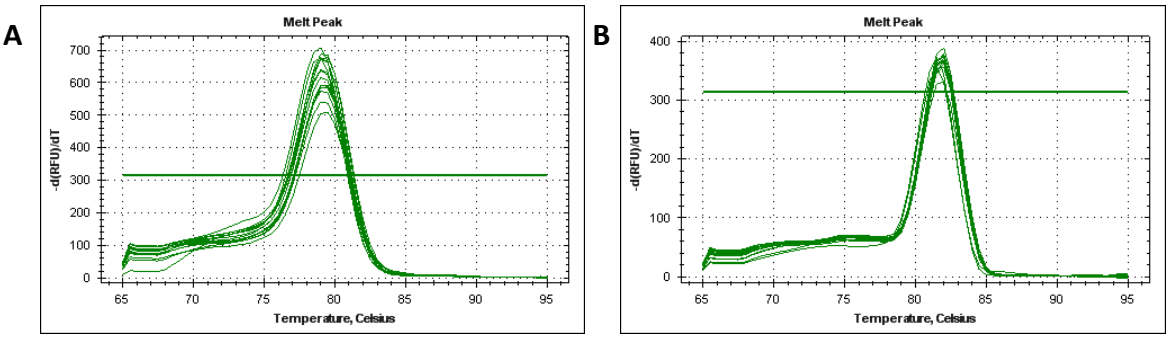

Figure 5.7 – ***qPCR melt curve analysis showing 1 clear amplicon for both primer pairs.*** **A.** 18s and **B.** Mcl-1**.**

qPCR data shown in Figure 5.8A confirm successful Mcl-1 siRNA transfection by a significant reduction in the mRNA levels of Mcl-1, with no effect from transfection using scrambled siRNA. Figure 5.8B shows Western Blot data of 3 representative experiments. This confirms that there is the reduction of Mcl-1 protein as we would expect to see with the reduction of mRNA.

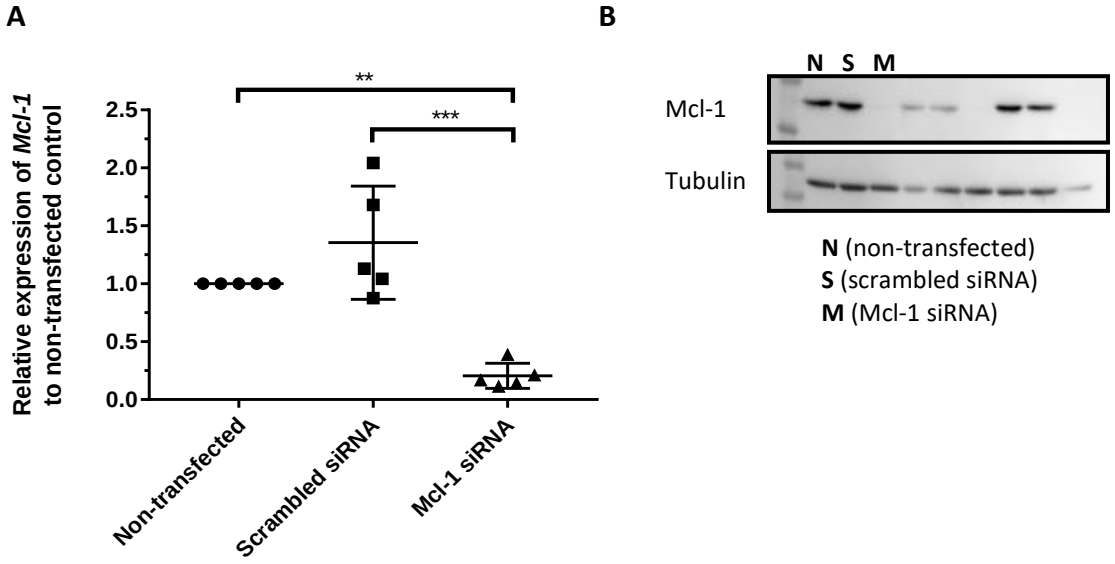

Figure 5.8 – ***Confirmation of successful transfection via qPCR and Western Blot:*** DF1 was the transfection reagent in these experiments with Mcl-1 as the target gene. Successful transfection was confirmed by qPCR (A) and Western Blot (B), showing 5 individual healthy donors with B showing 3 representative experiments. **P<0.005, ***P<0.001 (one-way ANOVA, followed by Tukey's multiple-comparison post-test).

5.2.4 Optimisation of MDM challenge with *S. pneumoniae*: MOI and time-points

MOI (multiplicity of infection) and time-points for required optimisation to determine the optimal condition for observing intracellular killing whilst being suitable for image analysis. If the number of bacteria remaining at the final time-point is too low, the signal to noise ratio will be poor and the image analysis software (MetaXpress) may categorise background signal as GFP positive bacteria. Figure 5.9A shows the timings of the experiment, at each final time-point in bold, MDMs were fixed and stained with CellMask and DAPI.

Non-encapsulated *S. pneumoniae* is rapidly phagocytosed without opsonisation. It also does not alter the maturation of the phagolysosome as previously shown with *S. aureus* (Jubrail et al., 2016). Therefore higher MOIs a required as once *S. pneumoniae* is phagocytosed it is susceptible to intracellular killing. MOIs of 10 and 20 were chosen to ensure high levels of phagocytosis by the first antibiotic pulse with gentamicin and penicillin at 2 and 3 hours, as well as sufficient numbers of bacteria remaining for detection at the 4 and 5 hour

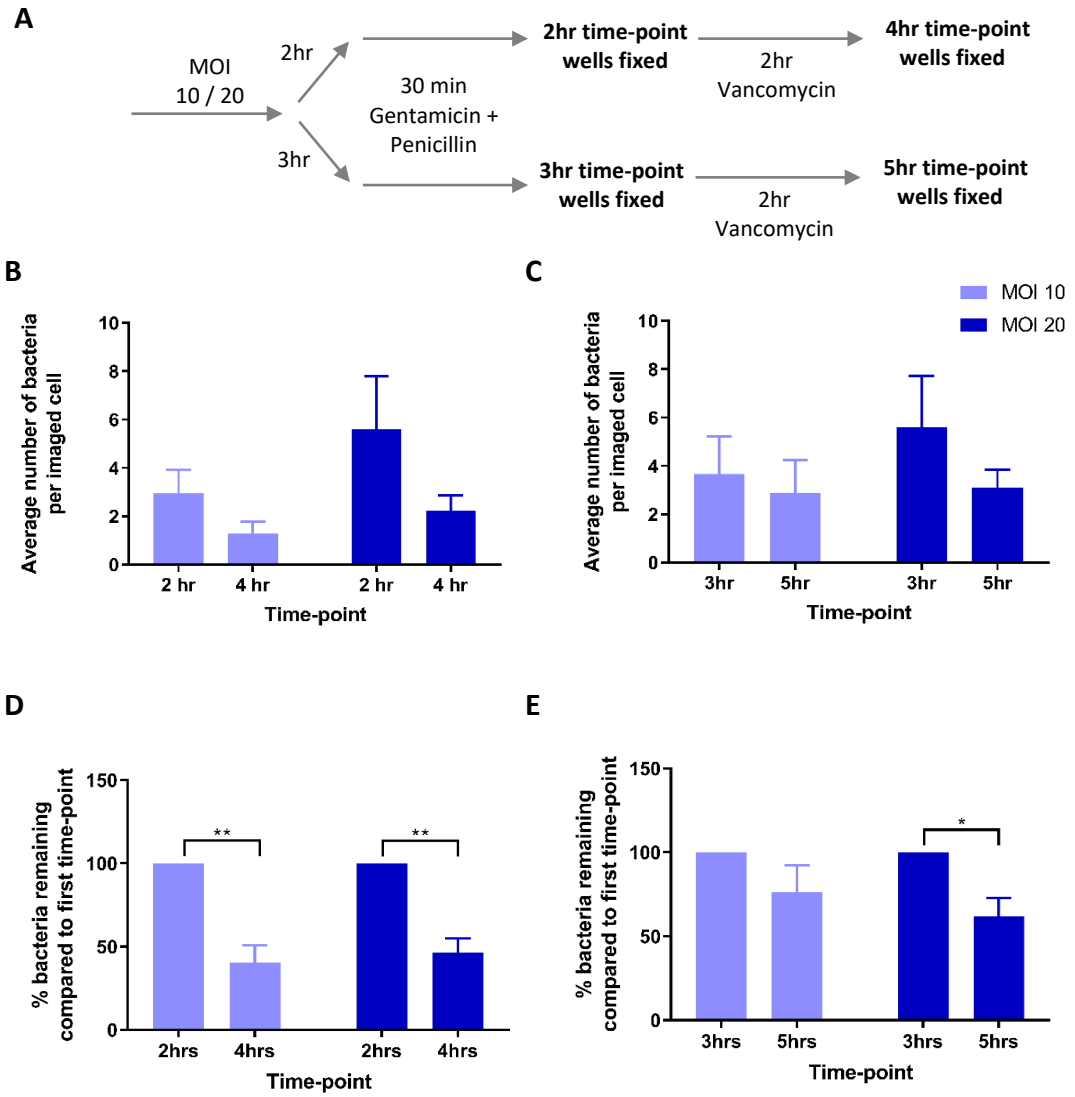

Figure 5.9 – ***Intracellular killing is observed at both time-points tested with a higher number of intracellular bacteria remaining at 5 hours.*** MDMs were challenged with non-encapsulated *S. pneumoniae* at MOI of 10 and 20. MDMs were incubated for 2 or 3 hours before treatment with antibiotic to stop further phagocytosis. The level of intracellular killing was then observed at 4 and 5 hours, respectively. **A.** Schematic illustration of time-points carried out. **B.** Average number of bacteria per MDM cell after image analysis compare between **B.** 2 and 4 hours. And **C.** 3 and 5 hours. **D and E.** Data showing percentage of intracellular bacteria remaining compared to the initial time-point. Data show the mean ± SD of 3 individual healthy donors ran in technical triplicate wells; *P<0.05, **P<0.005 (2way ANOVA, Sikak's multiple comparison test).

time-points by microscopy. Previous work assessing intracellular killing of *S. aureus* in macrophages has been carried out by halting phagocytosis at 4 hours with antibiotic treatment and measuring viable counts after MDM lysis at various time-points. The 4-hour infection period consisted of a 1-hour incubation on ice to allow sedimentation of the bacteria followed by 3 hours at 37°C. The most significant decrease in intracellular bacteria was between 4 and 5.5 hours (Jubrail et al., 2016). The ice step in these optimisation experiments

was replaced with a centrifugation step; 150rcf for 5 minutes. To ensure that the high levels of intracellular killing were not missed, a 2-hour incubation following the centrifugation was used as a comparison.

The expected decrease in intracellular bacteria was observed at both time-points and with both MOIs (Figure 5.9B and C). MDMs from different donors appear to have different capacities in phagocytosis shown by the larger error bars in Figure 5.9B and C. In order to determine if a significant decrease in intracellular bacteria was seen, the bacteria per cell counts were compared to the initial time-point at which gentamicin and penicillin were added to kill extracellular bacteria (Figure 5.9D and 5.9E). A 50-60% decrease in intracellular bacteria is observed at the earlier time-point with both MOI 10 and 20. A 40% decrease is observed at the later time-point with MOI 20 and therefore a higher number of bacteria per cell remaining. This is important as enhancing intracellular killing may lead to problems with signal to noise ratio with the earlier time-points. Therefore, MOI 20 and the final time-point of 5 hours will be used for subsequent experiments.

5.2.5 Traffic-ome pilot plate

The "traffic-ome" siRNA library obtained from the RNAi facility, contains siRNAs targeting genes known to have functions in intracellular trafficking such as Rabs and SNAREs (Poteryaev et al., 2010). DharmaFect 1 was added to all wells and allowed to complex for 30 minutes. Meanwhile, MDMs were dissociated using Accutase on day 13 of differentiation. The cells were then reverse transfected by adding them to the DharmaFect-siRNA complexes with a final density of $2x20^5$/ml. After 24 hours fresh media was added. After a further 24 hours cells were challenged with GFP and pHrodo labelled non-encapsulated *S. pneumoniae* at MOI 20. After 3 hours cells were treated with gentamicin and penicillin to halt further phagocytosis. After a further 2 hours with low dose vancomycin, cells were fixed and stained. The images were be analysed using the CME set up for infections as previously described (section 2.5.3). The data generated were analysed using the R package *cellHTS2* from Bioconductor to assess the number of GFP and pHrodo positive bacteria per cell (Boutros, Hahne and Huber, 2013). As we would expect to see alterations in intracellular killing and phagolysosome acidification from this experiment, it is a suitable test to confirm the automation of the screen process and the analysis.

Figure 5.10A shows the layout of the pilot plate with blue representing non-transfected controls, grey representing siRNAs and white representing empty wells. Due to a lower yield of MDMs in the final repeat, some wells had to be removed to ensure that each data point represented 3 biological replicates. The number of nuclei is first assessed to ensure that the number of cells within the well is not significantly higher or lower which could result in the data being skewed. Figure 5.10B shows that there are wells with significantly less nuclei, indicated by the red wells. These were removed from the data set before further analysis. It

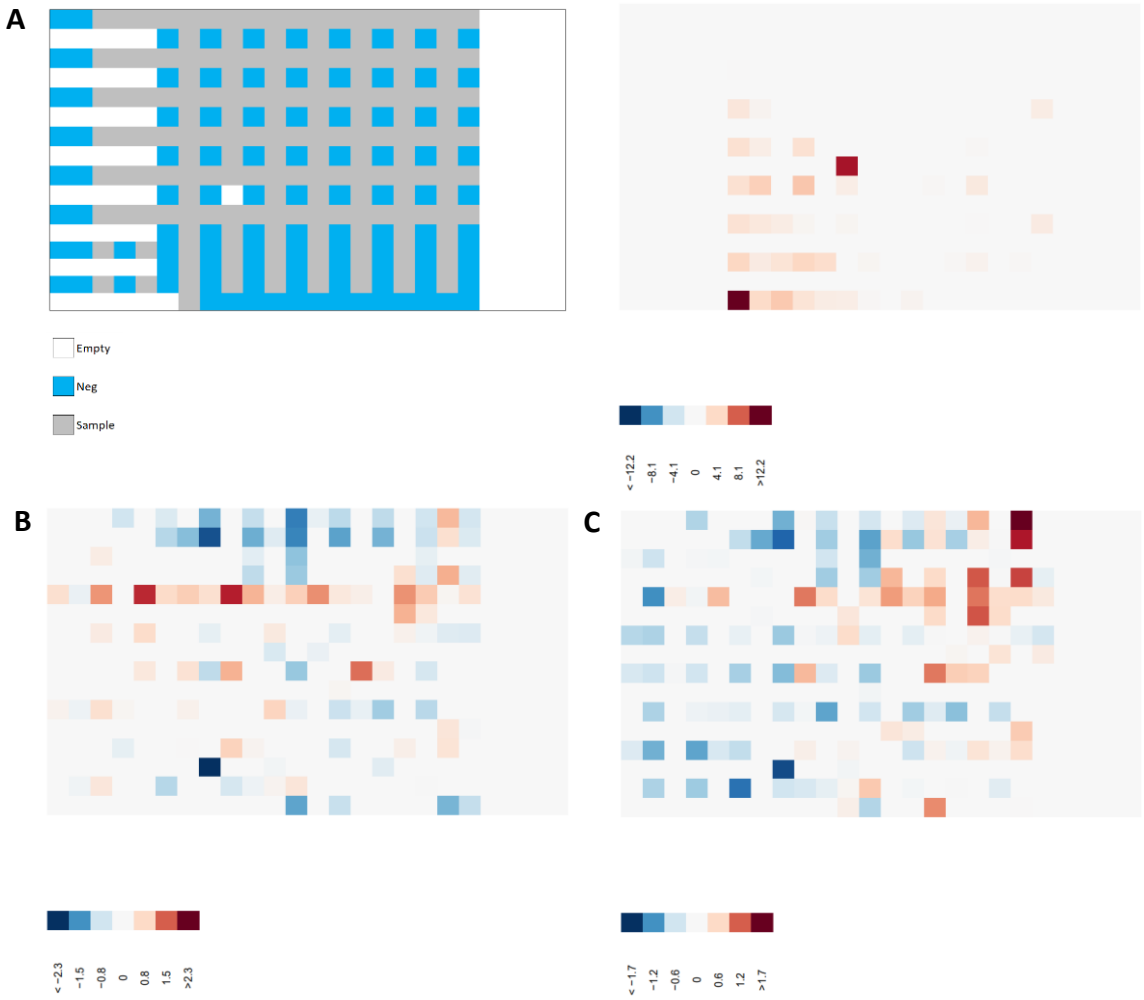

Figure 5.10 – ***Pilot plate revealed no significant hits but showed the need for an alternative cell dispensing method.*** MDMs were reverse transfected on day 13 of differentiation. After 48 hours cells were challenged with GFP and pHrodo labelled *S. pneumoniae*. At 5 hours cells were stained, fixed and imaged to determine the remaining number of intracellular bacteria. **A.** Traffic-ome plate layout. White; empty, blue; negative/non-transfected control, grey; sample. Remaining plots represent high (blue) and low (red) data points. DAPI count only before **(B)** removal of wells with significantly lower nuclei counts. **C.** Representation of the number of GFP positive *S. pneumoniae* per MDM, with blue indicating a higher number of bacteria and red presenting a lower number. **D.** Representation of pHrodo positive *S. pneumoniae* per MDM. Data show n=3 of which each n represents an individual healthy donor.

also indicated that using a multi-drop to dispense the cells may not be suitable as every other row leads to a decrease in cell number so an alternative method for addition of cells will be required. The number of GFP (Figure 5.10C) and pHrodo (Figure 5.10D) positive *S. pneumoniae* was then determined. Blue wells represent a higher number of GFP or pHrodo positive bacteria compared to the median whilst red wells represent a lower number. A score of +/-1.96 indicates a significant alteration in intracellular bacteria. No transfected samples resulted in significant alterations in the number of intracellular bacteria. The darkest blue well in both Figure 5.10A and B corresponded to a non-transfected well. Despite revealing no hits, the pilot plate showed that the methodology and analysis is functional. No negative controls corresponded to wells that had a z score of over 0.7, therefore indicating no enhancing effect on intracellular killing.

5.2.6 Optimisation of a positive control

Since there was no obviously, highly statistically significant hit from the pilot plate, further experiments were required to identify a robust positive control. The same methodology as the pilot plate was applied. The highest-ranking targets from the pilot plate were CLTB and AP2M1 with z-scores of 1.89 and 1.84, respectively. CLTB (clathrin light chain B) associates with clathrin light chain A (CLTA) and clathrin heavy chains to form clathrin-coated vesicles. The function of this is to selectively sort vesicles based on their contents. siRNA and inhibitors have been shown to block particulate uptake as well as lysosome trafficking from the Golgi (Poirier *et al.*, 2009; Huang *et al.*, 2017). This may suggest that the slightly lower number of intracellular bacteria may be due to decreased phagocytosis rather than enhanced killing. AP2M1 encodes a subunit of the assembly protein complex 2 (AP2) which is required for intracellular trafficking and vacuolar ATPase (V-ATPase) activity. siRNA silencing of AP2M1 inhibited Hepatitis C virus entry to cells suggesting the reduction in intracellular bacteria in this data may again be due to decreased phagocytosis (Neveu *et al.*, 2015).

These targets were tested again to confirm findings alongside other targets shown to be important for phagosomal acidification or intracellular killing. Silencing these genes with siRNA would theoretically lead to a decrease in intracellular killing and therefore a higher number of GFP positive cells remaining would be expected. CYBA encodes protein also called p22-PHOX which associates with NOX2, the protein encoded by CYBB, to activate its NADPH oxidase. This leads to the generation of reactive oxygen intermediates (ROI) which can be

converted to H_2O_2 which is important for its bactericidal activity (Singel *et al.*, 2016). V-ATPase is a proton pump consisting of multiple subunits which form the V_1 ATP hydrolysis domain and the V_0 transmembrane domain carrying out proton transport required for the acidification of the phagolysosome (Wang, Cipriano and Forgac, 2007). To determine if silencing one subunit resulted in defects in acidification of the phagosome, 4 genes corresponding to the V_1 domain and 1 gene corresponding to the V_0 domain where chosen. Arginase I (ARG1) is considered anti-inflammatory and associated with M2 macrophage polarisation whereas Arginase II (ARG2) has roles in proinflammatory macrophages and NO production (Yang and Ming, 2014). In zebrafish, macrophages with a mutation in CXCR3, a chemokine receptor, displayed enlarged lysosomes which correlated with increased clearance of bacteria. Therefore a decrease in GFP positive bacteria within macrophages would be expected through silencing of CXCR3 (Sommer *et al.*, 2021).

Figure 5.11 shows the number of GFP positive (A) and pHrodo positive (B) bacteria per cell at the final 5-hour time-point. There is no difference in the number of intracellular bacteria recorded compared to both the non-transfected and the non-targeting siRNA (scrambled) controls. This may be because there are many factors involved in phagolysosome acidification and therefore another pathway may be activated to ensure intracellular killing occurs as it is a fundamental function of the macrophage.

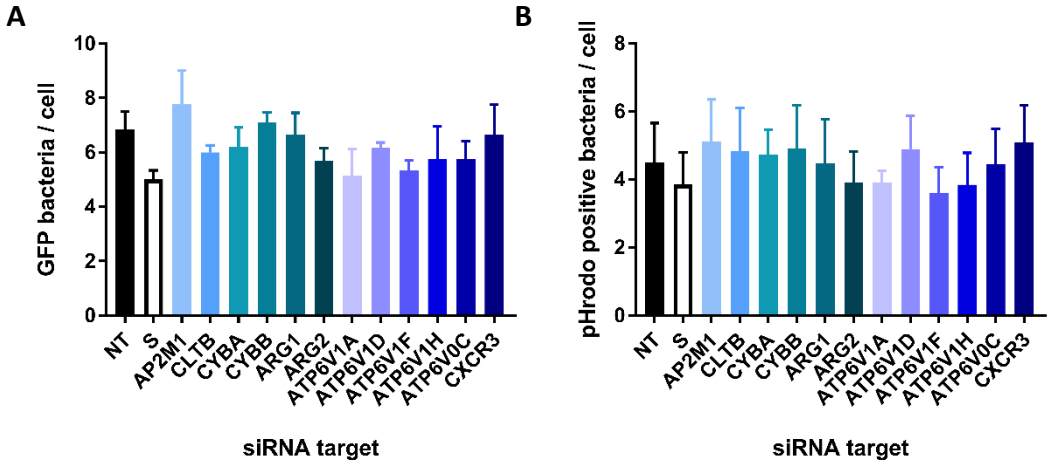

Figure 5.11 – ***siRNAs targeting genes with known roles in phagosomal maturation had no effect on GFP and pHrodo positive bacteria.*** NT = non-transfected, S = scrambled. **A.** GFP positive bacteria per cell **B.** pHrodo positive bacteria per cell. Data show the mean ± SEM of 3 individual healthy donors ran in technical triplicate wells (one-way ANOVA, followed by Tukey's multiple-comparison post-test).

siRNAs targeting known regulators of apoptosis were used to induce cell death as an indirect positive control that siRNA is entering the cell, resulting in the expected effect of reduced cell number, with DAPI counts as the readout. cIAP1/2, AKT1 and PAK1 have all been shown to have anti-apoptotic functions in HeLa cells, whilst c-FLIP has anti-apoptotic activity in human renal cells (Aza-Blanc *et al.*, 2003; Brooks and Sayers, 2005). As before, MDMs were dissociated and reverse transfected. Media was added after 24 hours then the cells were fixed and stained after a further 24 hours. Figure 5.12 shows that no siRNA silencing resulted in a significant reduction in cell number. There appears to be a slight reduction in nuclei count when cFLIP and cIAP2 were targeted compared to non-targeting/scrambled siRNA control. cIAP1 treatment in one repeat resulted in complete cell loss which was not observed in a further two repeats.

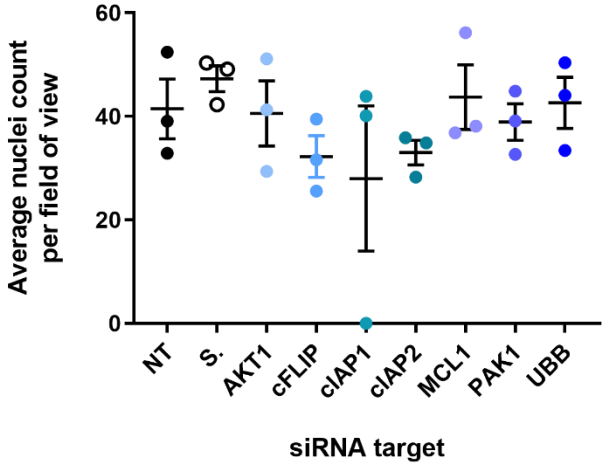

Figure 5.12 – ***siRNA targeting apoptotic regulators did not result in a decrease in cell number.*** MDMs were dissociated on day 13 and reverse transfected. After 48 hours wells were fixed and stained with CellMask and DAPI. NT = non-transfected, S = scrambled. Data show the mean ± SEM of 3 individual healthy donors ran in technical triplicate wells (one-way ANOVA, followed by Tukey's multiple-comparison post-test).

Clemastine and VPS34 inhibitor showed significant enhanced intracellular killing of *S. pneumoniae* in RAW 264.7 cells, presented in section 4.2.3. These were tested in MDMs at the same concentrations alongside their known targets. Silencing HRH1, P2X7R and VPS34 did not result alteration of intracellular GFP and pHrodo positive *S. pneumoniae* (Figure 5.13A and B, respectively). Clemastine at 10µM showed a trend towards decreasing GFP and pHrodo positive cells detected within MDMs (Figure 5.13C and D, respectively). This will be included in the screen but is not the robust positive control sought.

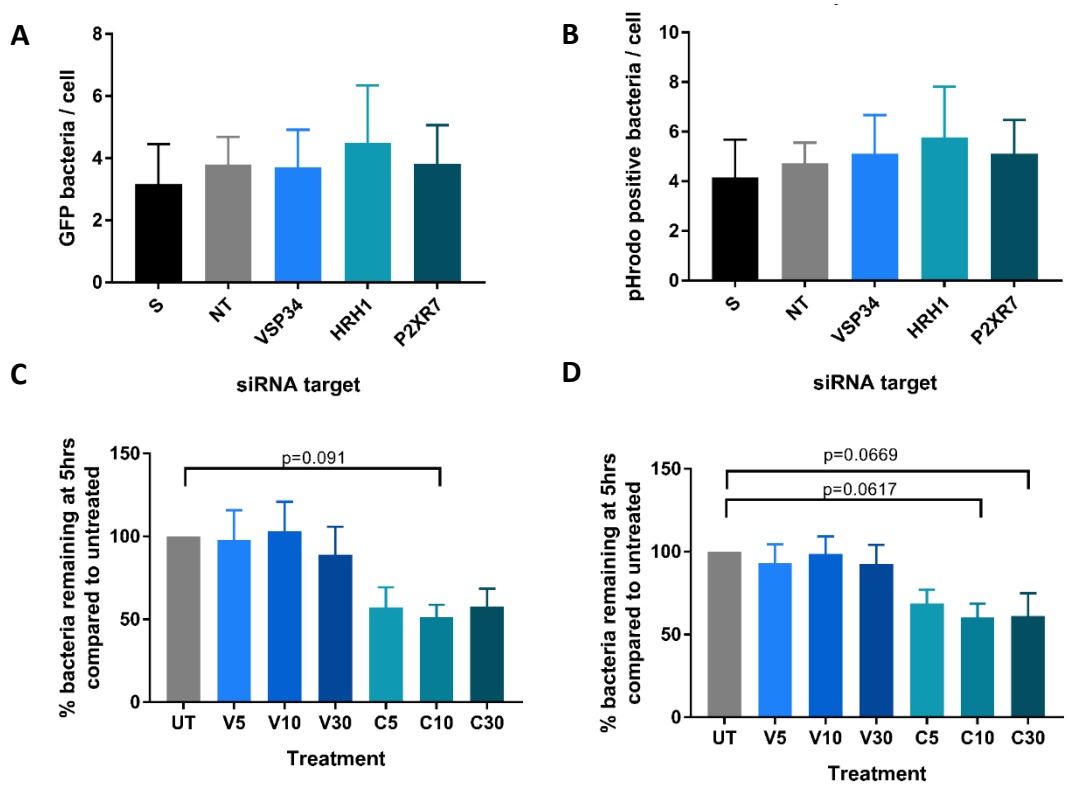

Figure 5.13 – ***Clemastine treatment shows a decrease in intracellular bacteria however silencing its known targets does not.*** NT = non-transfected, S = scrambled, U = untreated, V = VPS34 inhibitor, C = clemastine. MDMs were reverse transfected and after 48 hours were challenged with GFP and pHrodo labelled *S. pneumoniae* at MOI 20. After 5 hours the number of GFP **(A)** and pHrodo **(B)** positive bacteria was assessed. Cells that were not transfected were treated with VPS34 inhibitor or Clemastine at 5, 10 and 30µM with the second round of antibiotic for 2 hours. As before the number of GFP **(C)** and pHrodo **(D)** positive bacteria was assessed. Data show the mean ± SEM of 3 individual healthy donors ran in technical triplicate wells (one-way ANOVA, followed by Tukey's multiple-comparison post-test).

5.2.7 Human siRNA screen, plates 1-13

The siRNA library contains 18,096 siRNAs across 57 384 well plates. To keep variability to a minimum, duplicate plates were analysed on the same day with different donors ensuring MOI and reagents were matched. Assembling all parameters together, MDMs were dissociated on day 13 with Accutase treatment for 20 minutes. Meanwhile DharmaFect 1 was added to siRNA plates and allowed to complex for 30 minutes. Cells were seeded to a final volume of $2x10^5$ cells/ml resulting in 5,000 cells per well. After 24 hours an equal volume of fresh media was added. After a further 24 hours MDMs were challenged with non-encapsulated GFP and pHrodo labelled *S. pneumoniae* with an MOI of 20. After the second antibiotic treatment and addition of Clemastine, cells were fixed and stained for high-content imaging. Images were analysed using CME in MetaXpress. Data generated from MetaXpress was analysed using the R package *cellHTS2* (Boutros, Hahne and Huber, 2013). Columns 1 and

24 were excluded from every plate due to edge effects resulting in cell loss. First nuclei, counts were assessed which are represented in Figure 5.14, with red wells representing low data points and blue wells representing high data points. The scale bar shows the associated z-score with the intensity of the colour. A z-score above 1.96 is considered statistically significant. Wells were detected with significant cell loss across all plates, indicated by red wells representing significantly low data points (Figure 5.14A). After removal of these wells it was clear that there were edge effects on plate 9 whereby the outer edge had significantly higher number of cells (indicated by the blue wells) compared to the middle wells (Figure 5.14B). Although this effect was only seen in one plate out of the two tested, both were removed from analysis as hits from plate 9 would be unreliable as they would be based on data from only one donor. Figure 5.14C shows a more even distribution of points with no wells displaying a significant difference in cell number.

After eliminating wells with low cell counts, the number of GFP and pHrodo positive intracellular *S. pneumoniae* could be assessed. Figure 5.15A and 5.16A show representation of significant hits across the plates. Hits with a positive z-score above 1.96 correspond to wells with a significantly lower number of GFP or pHrodo bacteria compared to the median, these are represented by red wells. The deeper red indicates statistically significant hits as indicated by the scale bar. Plate 7 was removed from analysis due to the obvious edge effects displayed by grouped, highly significant wells in the bottom right corner in Figure 5.15A. The removal is represented by a blank plate in Figure 5.16A. The significant decrease in intracellular GFP and pHrodo bacteria could be due to enhanced intracellular killing or disrupted phagocytosis pathways which would require further determination. In addition, where there is a decrease in the pHrodo but not in GFP signal could suggest disruption of phagolysosome acidification. A z-score of -1.96 or below suggests significantly higher numbers of intracellular bacteria, which may indicate disruption of a pathway essential for intracellular killing. Where there is a high number of GFP and pHrodo bacteria, acidification may not be disrupted but bacterial killing may be delayed or disrupted due to reduction of trafficking of lysosomes containing degradative enzymes. It also may also suggest an increase in phagocytosis. These wells are represented in blue according to the scale in Figure 5.15A and Figure 5.16A. Figure 5.15B and 5.16B show density distribution plots in which we can see that the data is normally distributed. The red and blue points on the bottom axis represent positive and negative controls respectively. As noted in section 1.2.6, Clemastine did not lead to a strong reduction

in intracellular bacteria so therefore the lack distinction between of controls was expected. There are a small number of outliers in Figure 5.15B in which both positive and negative that are identified as having the opposite effect to that expected. This does not affect the data as it is not normalised to controls.

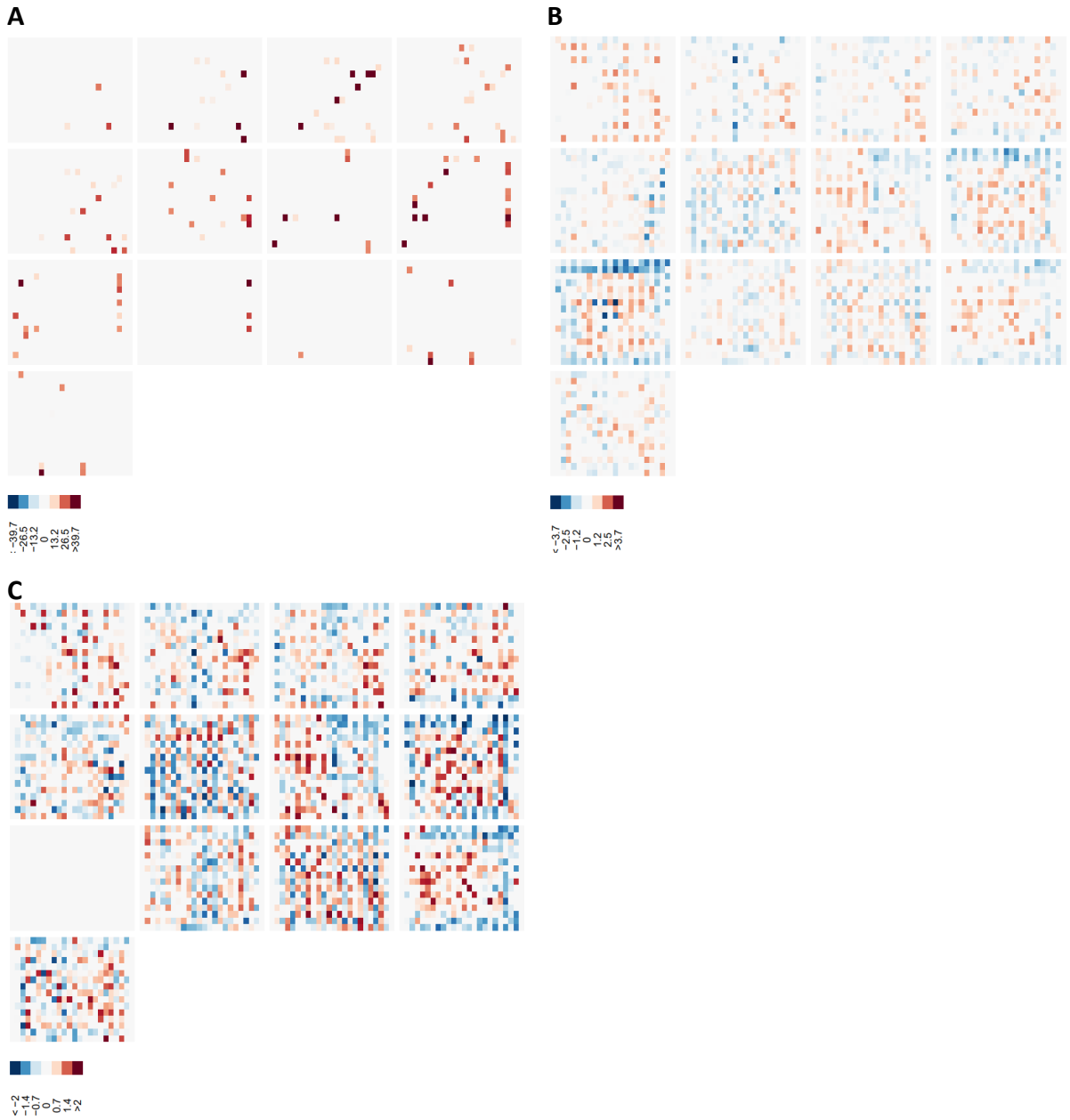

Figure 5.14 – ***Data from wells that had a significantly low number of MDMs required removal before subsequent analysis of intracellular bacteria.*** Representation of MDM cell counts in each well with blue representing a higher cell count and red representing a lower cell count with z-score scales below each collective image. **A.** Initial DAPI counts. **B.** After removal of wells with significantly low cell counts. **C.** After removal of plates with edge effects.

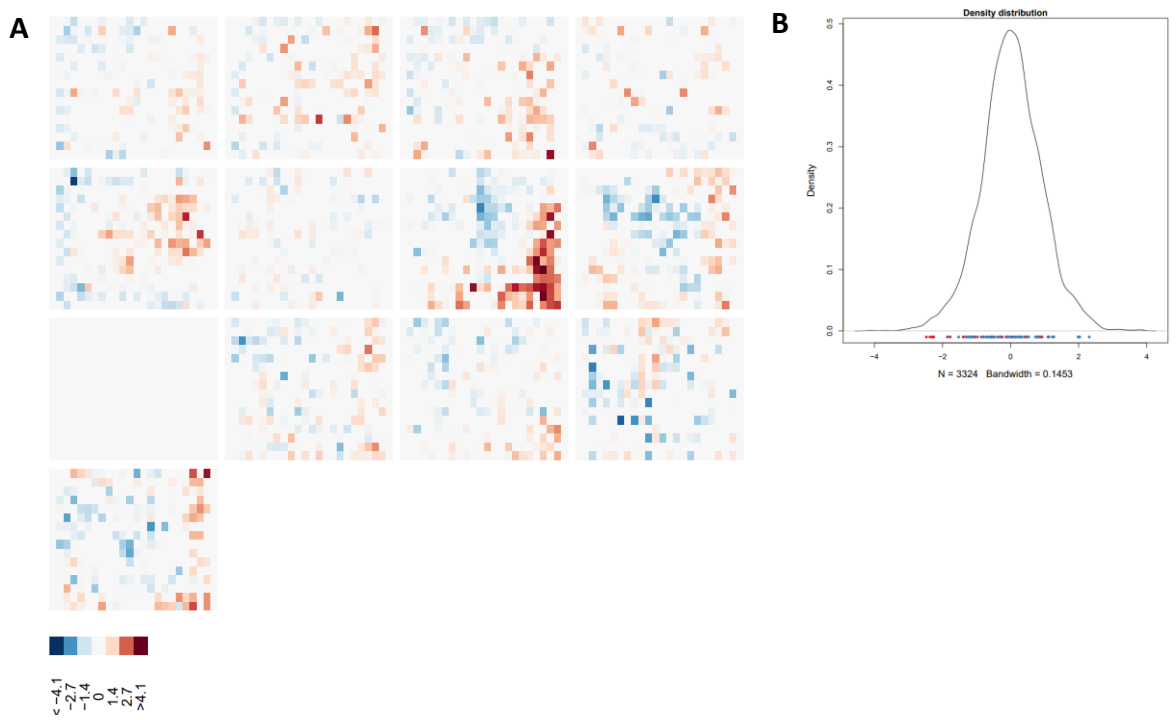

Figure 5.15 – ***Distribution of GFP positive*** **S. pneumoniae** ***data.*** **A.** Representation of GFP positive *S. pneumoniae* counts in each well across 13 plates with plate 9 being excluded previously. Blue wells represent a higher number of GFP *S. pneumoniae* whilst red wells represent a lower cell count. The shade represents the associated z-score. **B.** Density distribution plot showing the distribution of the data points shown in A. Blue and red dots along the x axis represent negative and positive controls, respectively.

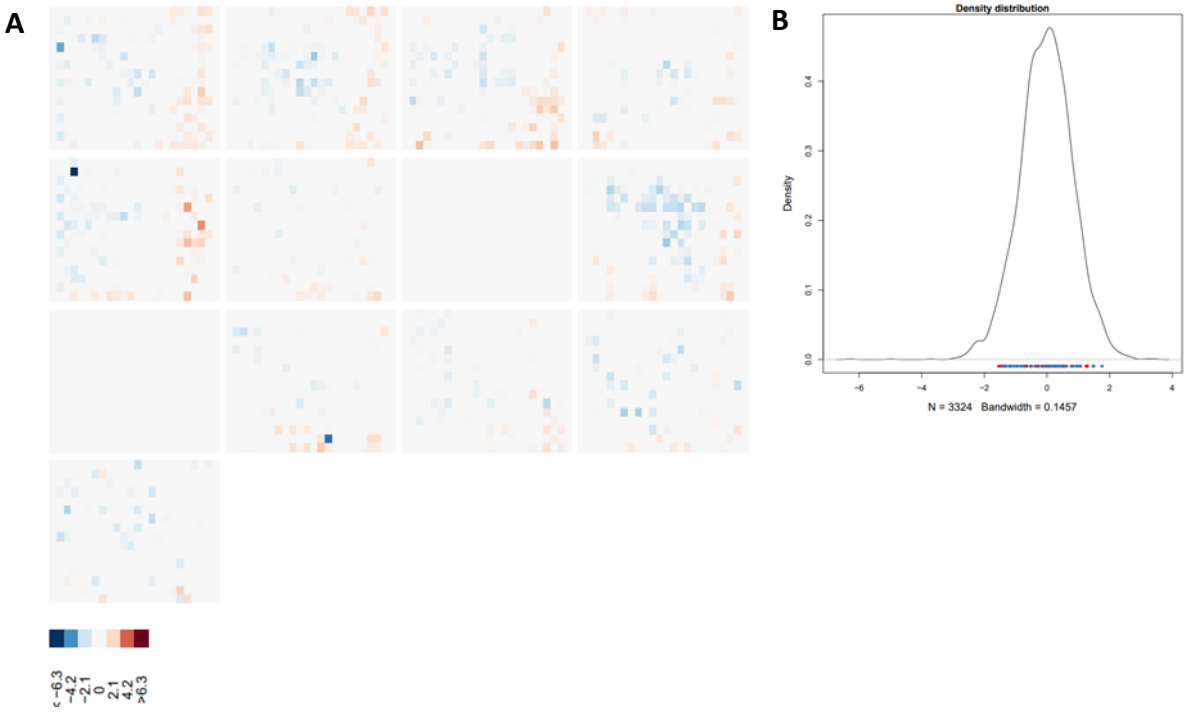

Figure 5.16 – ***Distribution of pHrodo positive*** **S. pneumoniae** ***data.*** **A.** Representation of pHrodo positive *S. pneumoniae* counts in each well across 13 plates with plates 7 and 9 previously excluded. Blue wells represent a higher number of pHrodo *S. pneumoniae* whilst red wells represent a lower cell count. The shade represents the associated z-score. **B.** Density distribution plot showing the distribution of the data points shown in A. Blue and red dots along the x axis represent negative and positive controls, respectively.

	Significantly increased signal (blue wells)		Significantly decreased signal (red wells)	
	GFP	pHrodo	GFP	pHrodo
Enhanced intracellular killing				
Enhanced intracellular killing				
Enhanced phagosome acidification				
Disrupted phagosome acidification				
Disrupted phagosome acidification				
Defects in intracellular killing				
Defects in lysosome trafficking				
Disrupted phagocytosis				

Figure 5.17 – ***The possible causes of significant alterations in GFP and pHrodo signal.*** Each row represents a different cause with each column indicating hits in green.

The manner in which hits correlate with one another could give indication as to what function may have been disrupted or enhanced. These are displayed in Figure 5.17. There were 63 and 29 hits that showed a significant reduction in the number of GFP and pHrodo positive bacteria, respectively. 11 of these were common to both. A significant decrease in the number of intracellular GFP bacteria coupled with a significant decrease in pHrodo signal could either be due to enhanced killing, also resulting in the dispersion of the pHrodo fluorophore, or due to disrupted phagocytosis. The top 3 common to both decreased GFP and pHrodo, indicating enhanced killing or reduced phagocytosis, are DAZ2 (Deleted in Azoospermia 2), FOXA3 (Forkhead Box A3, also known as Hepatocyte Nuclear Factor 3-Gamma) and REXO1 (RNA Exonuclease 1 Homolog). Whether enhanced intracellular killing could result in a significant decrease in GFP positive bacteria with no significant effect on pHrodo signal requires further investigation. A significant reduction in pHrodo signal without GFP reduction may indicate disrupted phagosome acidification and diminished intracellular killing capabilities.

5.2.8 STRING analysis

STRING analysis (version 11.5) aims to give information about interactions and associations between a specified set of proteins, whether direct binding or indirect associations such as being involved in the same signalling pathway. The information given is drawn from data mining, experimental data and literature. If protein interactions and associations are found, lines linking the two (or more) proteins together are shown. These associations are given a score which only indicates the confidence of this interaction.

STRING analysis was carried out in order to determine any known connections between hits described in section 5.2.7. The hits were separated by readout (GFP and pHrodo) as well as whether a significant increase or decrease in the signal was observed. The confidence score specified for this data was 'medium' (0.4 or greater) with the thicker line representing a greater score. Figure 5.18A and 5.19A show the siRNA targets that resulted in a significant reduction of intracellular GFP or pHrodo positive bacteria, respectively. The connections in both these figures represent targets that were co-mentioned in abstracts. The exceptions to this are those that are co-expressed. In Figure 5.18A these are YJEFN3 (YjeF N-Terminal Domain Containing 3) and OGFOD2 (2-Oxoglutarate And Iron Dependent Oxygenase Domain Containing 2), whilst in Figure 5.19A these are NDUFS5 (NADH:Ubiquinone Oxidoreductase Subunit S5) and COX5B (Cytochrome C Oxidase Subunit 5B).

On the other hand, there were 53 hits showing a significant increase in intracellular GFP and pHrodo *S. pneumoniae*, respectively (Figure 5.18B and 5.19B), in which 28 genes were common. Connections between siRNA targets in Figure 5.18B were all co-mentioned in abstracts whilst PPIA and TUBA1B have been shown to be co-expressed. The most significant associations between pHrodo hits, showing an increase in signal, are shown with thick lines in Figure 5.19B. These genes have all been shown to be co-expressed, along with all genes connected to UBC.

An increase in GFP coupled with an increase in pHrodo signal could be due to defects in intracellular killing, such as lysosome trafficking of degradative enzymes, but not phagosome acidification. However, phagolysosome acidification has previously been showed to be essential for *S. pnuemoniae* killing in zebrafish (Prajsnar *et al.*, 2022). An increase in intracellular GFP positive bacteria without pHrodo signal may indicate impaired killing due to defects in phagosomal maturation.

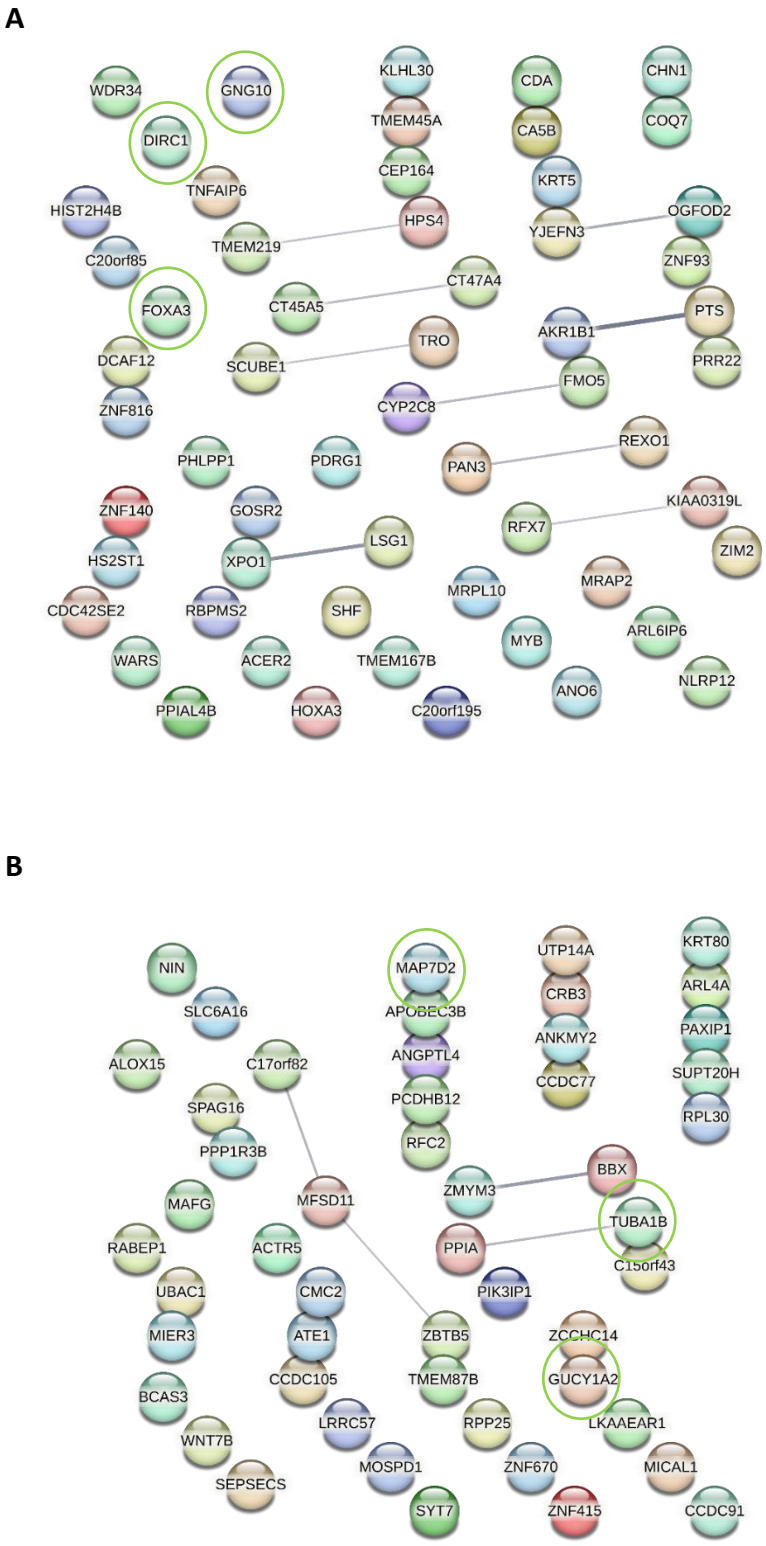

Figure 5.18 – ***STRING analysis of hits that significantly altered the number of intracellular GFP bacteria.*** Lines between genes represent connections, with the thickness correlating to significance. Circled in green are the top 3 most significant hits. **A.** siRNA targets that resulted in a significant reduction in GFP bacteria and had a z-score>1.96, **B.** siRNA targets correlating to a increase in GFP bacteria with a z-score<-1.96.

A

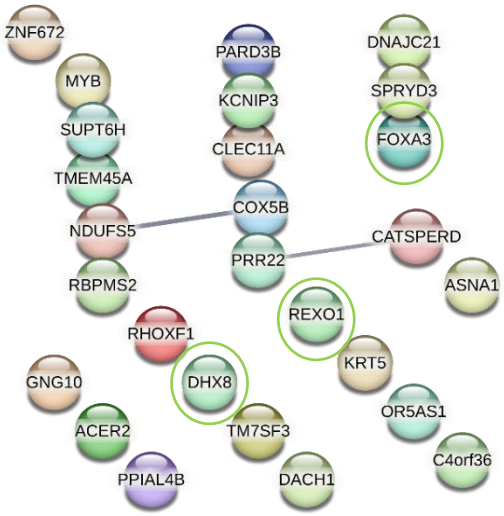

B

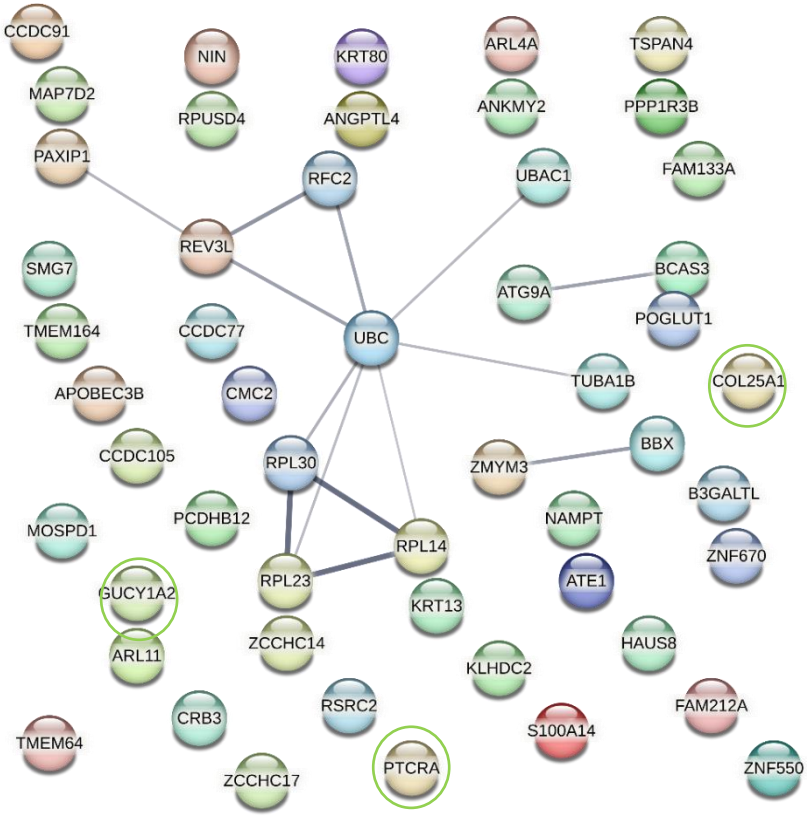

Figure 5.19 – ***STRING analysis of hits that significantly altered the number of intracellular pHrodo* S. pneumoniae.** Lines between genes represent connections, with the thickness correlating to significance. Circled in green are the top 3 most significant hits. **A.** siRNA targets that resulted in a significant reduction in pHrodo bacteria and had a z-score>1.96, **B.** siRNA targets correlating to a increase in pHrodo bacteria with a z-score<-1.96.

5.3 Discussion

5.3.1 Summary of findings

Transfecting cells with siRNA is a useful tool for assessing the functional effects on a particular phenotype after silencing specific genetic targets. Demonstrated here is the development of a genome-wide siRNA library containing over 18,000 siRNAs, used for assessing the effect of gene silencing on the ability of MDMs to kill *S. pneumoniae* intracellularly. Prior to running the siRNA screen several parameters required optimisation. As the siRNAs are contained within 384 well plates, MDMs required dissociation and re-seeding after maturations due to the unknown effects of siRNAs on differentiation. Treatment with Accutase lead to the best yield and viability of cells post-dissociation compared to other methods tested with no changes in re-seeding density. DharmaFECT 1 and Lipofectamine 3000 transfection reagents have been shown to result in high transfection efficiency across a range of cell type. Both resulted in approximately 85% transfection efficiency using cells positive for siGLO. However, Lipofectamine showed a reduction in cell number at the highest concentration tested therefore, DharmaFECT 1 was selected as the most suitable transfection reagent. To confirm the transfection efficiency observed correlated with gene silencing, MDMs were transfected using the same protocol with siRNA targeting *MCL1* which encodes an anti-apoptotic protein. A reduction was seen at both mRNA and protein level, assessed by qPCR and Western Blot. Finally, the most suitable MOI and time-points for observing early intracellular killing whilst leaving enough remaining bacteria for observation of enhanced killing without signal to noise ratio problems was determined. As non-encapsulated *S. pneumoniae* is known to be easily phagocytosed and killed intracellularly via phagosome acidification the most suitable MOI was found to be 20 with a final time-point of 5 hours. A pilot plate was used containing siRNAs targeting gene with known functions in intracellular trafficking in order to test the optimised parameters. Although alterations in the expected decline of intracellular GFP were observed, no significant difference was detected. Further work aimed to find a robust positive control. Genes with known roles in acidification were tested but no alterations in GFP or pHrodo signal were observed. siRNAs targeting genes encoding apoptosis inhibitors were tested as an indirect positive control but no effect was seen on cell number. A VPS34 inhibitor and Clemastine had been shown to enhance intracellular killing in neutrophil and MDMs by other colleagues, as well as in RAW 264.7 cells here in optimisation of the compound screen in Chapter 4. Therefore, these compounds were

tested in this setting as well as their targets. No effect on intracellular killing was observed when targeting VPS34 with the inhibitor or siRNA however treating MDMs with Clemastine at a final concentration of 30μM which, although not significant (p = 0.06), did result in a trend towards enhanced intracellular killing.

30μM Clemastine was added to each plate that was screened. 13 out of total of 57 plates were screened in duplicate as shown in section 5.2.7. Hits were identified after high-content microscopy, image analysis and subsequent data analysis utilising the *cellHTS2* R package from Bioconductor. siRNA targets that resulted in a z-score greater than 1.96 or less than -1.96 were categorised as hits indicating a significant decrease or increase in intracellular bacteria, respectively. There were 116 hits that showed an alteration in the expected decline of GFP signal, 63 of these showed a decrease in intracellular GFP positive *S. pneumoniae* whilst 53 showed an increase in signal. There were 82 hits in relation to pHrodo positive bacteria in which the signal was significantly reduced in 29 hits and significantly increased in 53. A significant decrease in the number of intracellular GFP and pHrodo bacteria could either be due to enhanced killing or due to disrupted phagocytosis. Imaging after the addition of the first antibiotic may elucidate this. Alternatively, challenge with fluorescent beads that will not be subject to degradation and comparison of the number of intracellular beads will determine if gene silencing by these hits is due to reduced phagocytosis or enhanced killing.

Interestingly, two hits that resulted in a decrease in GFP signal were also found to be significantly downregulated in MDMs that had phagocytosed 3 or beads at 2 hours in RNA sequencing data in section 3.2.7. This finding indicates that silencing of these genes does not result in reduced phagocytosis and therefore possibly enhances intracellular killing. These genes are RNA Binding Protein, mRNA Processing Factor 2 (RBPMS2) and Chimerin 1 (CHN1). Low expression of RBPMS2 is associated with gastric cancer with high immune cell infiltration but expression within macrophages and its role in infection response is unknown and therefore required investigation in this context (Chen *et al.*, 2022). Mutations in CHN1 can cause Duane's reaction syndrome 2 whilst expression of CHN1 induced by miR-205 has been associated with aggressive cervical cancer (Miyake *et al.*, 2008; Liu *et al.*, 2020).

5.3.2 siRNA screen limitations

Gene redundancy, in which another gene with the same or similar function is expressed, may mask the effect of targeting one gene especially as intracellular killing is a fundamental

function of the macrophage. Therefore, interesting targets and pathways may not be recognised as a 'hit' thus a possible limitation of this screen may be targeting one gene. This was possibly evident in the context of positive control optimisation. It may have been useful to test two siRNA targets together to yield a strong positive controls, such as the two proteins that form the NOX2-complex, cyba and cybb. However, it was intended to use a single siRNA target as that is the basis of the screen.

The readout for the screen related to phagosomal acidification, and other modes of killing such as apoptosis-mediated killing, might not be fully captured by this methodology. However, phagosomal acidification reflects phagosomal maturation and will be relevant to the intracellular execution of a range of pathogens, whilst apoptosis-associated killing is more specialised to the pneumococcus. In addition, it is important for a high-throughput screen to have a readout that can be readily detected by imaging/image processing, and the use of GFP/pHrodo labelled bacteria is adaptable to this methodology whilst apoptosis-associated killing would not be easily assessed at this level.

Plates did require elimination from analysis due to edge effects, these were reduced through automated liquid handling however, it is plausible that hits will have been missed from these plates.

As discussed, MDMs were differentiated from isolated PBMCs and as this screen required a large number of cells it will be subject to donor-to-donor variability. Some donors may respond differently to bacterial challenge than others, however, running in duplicate should reduce the effect of false positives or false negatives. Equivalent MOIs per plate were assumed but small variations may have occurred due to bacterial cell loss due to pHrodo. Previous work, not shown here, has been carried out to keep this variability to a minimum. Normalisation of data to the median value has been carried out as part of data analysis utilising the R package *cellHTS2* which will further minimise variation between plates and repeats.

5.3.3 COVID-19 impact on the completion of the siRNA screen

Due to the COVID-19 pandemic, work on the screen had to be paused because of the difficulties in recruiting donors combined with the unavailability of clinicians and nurses for performing venesection. It would not have been possible to change to another cell type or cell line as all the previous optimisation up to that point would have to be repeated. The

alternative cell type may respond differently to bacteria and most importantly the transfection reagent may not be suitable or result in a high transfection efficiency. It would also have to be a human derived cell line or type due to the siRNA library targeting human genes. Progress throughout 2021 remained slow due to the intermittent availability of both donors and nurses. Prior to the pandemic, cells from some donors would occasionally fail to result in the expected number of mature MDMs at day 14 however, post-pandemic the occurrence of this hugely increased. These cells were not used for subsequent experiments due to the unknown effect of sparse cells on macrophage function and inability to yield sufficient MDMs for one 384 well plate. Whether or not the lack of MDMs was due to prior COVID-19 infection or recent vaccination is unknown. Our criteria for donors remained the same, whereby donors that were vaccinated within the last week or had recent infection were excluded.

5.3.4 Future work

Completion of the screen may reveal more, highly significant hits that show enhanced intracellular killing through silencing. STRING analysis on all hits from the completed screen may reveal common hits in shared pathways. To determine if the reduction in GFP and / or pHrodo signal is due to a disrupted phagocytosis it would be useful to compare hits to the RNA sequencing data generated in the previous chapter. Genes that are significantly downregulated in the phagocytic groups compared to their non-phagocytic counterpart could suggest that these hits are not due to a reduction in the number of bacteria being phagocytosed. As mentioned, RBPMS2 and CHN1 fit this criteria but determining if therapeutically inhibiting these targets results in enhanced intracellular killing requires further investigation. Also as discussed in the previous section, challenging transfected MDMs with inert beads would confirm the effect of siRNA silencing on phagocytosis. The hits that do not correlated with defects in phagocytosis can be taken forward for further investigation into their effects on intracellular killing. Validation of selected hits could be taken forward for killing assays in which transfected MDMs are lysed post-infection and antibiotic treatment, lysates are plated onto agar plates as the CFU can be calculated and compared to non-transfected or non-targeting siRNA controls. These assays would also be useful to test in other bacteria, both Gram-negative and bacteria such as *S. aureus* which is known to subvert the acidification of the phagosome. To confirm silencing has occurred, a handful of hits should be

validated via qPCR or Western Blot. The most effective and biologically relevant hits could be taken forward into zebrafish *in vivo* studies in which clearance of fluorescent bacteria can be tracked as well as improved survival.

6 Discussion

Most current methodologies for enhancing immune responses and creating alternative treatments to antibiotics are limited to specific species or strains of bacteria or focus on antimicrobial properties which are still vulnerable to the risk of resistance. Vaccinations are generally very successful at preventing disease but are developed with high specificity to strains within species of bacteria. Phage-directed therapy, whereby viruses with selectivity for bacteria, can result in the lysis of both Gram-positive and Gram-negative bacteria. The limitation of species specificity, similar to vaccinations, exists as well as lack of information for treatment duration and the development of phage-resistance by the bacterium (Alaoui Mdarhri *et al.*, 2022). Studies are also underway to repurpose existing drugs to treat infections as developing new antibiotics is not an effective or profitable option for the pharmaceutical industry due to the time and cost associated with drug discovery with the added risk of antibiotic resistance. However, screening clinical compound libraries in these instances is focused on antimicrobial activity rather than utilising the broad effectiveness of the innate immune system against a wide variety of bacteria. Demonstrated here are multiple avenues that have led to the identification of multiple targets for further investigation to modulate the immune system in response to infection. To identify molecular regulators of phagocytosis and intracellular killing, RNA sequencing and siRNA screening were employed, respectively. Additionally a compound screen was developed using a library of approved drugs was used to screen macrophages for enhanced intracellular killing.

Firstly, heterogeneity in the phagocytic capacity of macrophages and neutrophils was found to be a feature that is pre-programmed or inherent to the phagocytic cells supporting previously published work (Hellebrekers *et al.*, 2017). Indeed neutrophils displayed a 'super-ingester' phenotype. To begin to investigate the molecular signatures behind these phenotypes, both macrophages and neutrophils were sorted based on the number of beads that they had phagocytosed for subsequent RNA sequencing. Neutrophils only showed a total of 18 differentially expressed genes (DEGs) between phagocytic and non-phagocytic cells. However, macrophages at both 2 and 4 hours after challenge with opsonised beads showed over 1,000 DEGs. Further investigation is required to narrow down these hits before studying manipulation in the expression of these target genes and the following effects on phagocytic capacity and heterogeneity previously observed. Whether this increases the intracellular killing and clearance of bacteria remains to be determined.

A compound screen was developed to assess any enhancement of the expected decline of intracellular *S. pneumoniae*. The Johns Hopkins Clinical compound library (JHCCL) containing 1,690 approved drugs was used to treat infected RAW 264.7 macrophages for 2 hour, after which the remaining intracellular bacteria was quantified. 23 compounds were found to show a significant decrease in the number of intracellular GFP positive *S. pneumoniae.* The ability of this screen to identify anti-infectives is evident through the presence of known antibiotics, such as penicillin and ampicillin, and other compounds that are currently being investigated for their antimicrobial properties within the list of hits. These include carbinoxamine maleate (CAM) and candesartan cilexetil (CC) which have recently been tested *in vivo* revealing improved bacterial clearance (Zhang *et al.*, 2018; Loe, Lee and Chu, 2019; Leisner *et al.*, 2021).

The final approach to explore immunomodulatory avenues for enhancement of the immune system was the development of an siRNA screen. GFP expressing *S. pneumoniae* was also labelled with pHrodo to determine effects of gene silencing on both the number of intracellular bacteria and acidification of the phagosome. Thirteen plates from the genome-wide siRNA library were used for screening infected MDMs. Hits were classified as having significantly altered the expected decline of GFP signal whilst monitoring any defects in phagosomal acidification. 116 hits that showed significant difference in GFP signal, whilst 82 hits showed alterations in pHrodo positive bacteria. STRING analysis did not reveal any common pathways however, completion of the screen may reveal key pathways. All three approaches demonstrate avenues for further investigation into modulating key antimicrobial features of macrophages and neutrophils.

6.1 Limitations

Neutrophil have a lower gene expression profile than other cells, which may have a negative impact on the low number of DEGs detected through RNA sequencing (Garratt, 2021). The effect on the age of the circulating neutrophil prior to isolation may also have an effect of gene expression. Other methods, such as surface marker staining, may be required to determine the phenotypic variability in neutrophils phagocytic capacities.

GFP expressing *S. pneumoniae,* modified with a capsule deletion, was used to study intracellular killing due to the ability of macrophages to readily phagocytose the bacterium without the need for antibody or complement opsonisation. The hits from both the siRNA screen and the compound screen were both based on the assumption that quenching of the

GFP signal correlates with bacterial cell death therefore, further validation would be required to confirm findings.

Variation within the screens was limited where possible from automated liquid handling, batch effects and even positioning in the incubator, further minimised through normalisation during data analysis. However, data points still required removal from analysis due to edge effects and outliers. In the case of the compound screen, this was due to cell number abnormalities in plate 10 and outliers due to fluorescence interference of compounds.

Delays due to the COVID-19 pandemic occurred at many points within this project. Lockdown prevented the shipment of cell lysate samples for RNA sequencing whilst the limited availability of primary cells halted progress on the development of the siRNA screen. An alternative cell line, RAW 264.7 murine macrophages, was used in place of human MDMs for the development of the compound screen. In terms of screening, this was a suitable substitute as these cells were capable of phagocytosing and killing *S. pneumoniae* intracellularly. However, in published data the effects of immunomodulators do not correlate between RAW 264.7 cells and PBMCs (Elisia *et al.*, 2018). As a result, compounds that resulted in enhanced intracellular killing may not have the same effective in MDMs. The same applies for compounds that did not result in a significant decrease in intracellular bacteria, may have done so if MDMs were used for the primary screen.

6.2 Future work

All methodologies used here demonstrate the opportunity that the innate immune system offers for modulation of phagocytosis and intracellular killing. The compound screen was able to identify anti-infectives. Screening compounds for effects on intracellular killing is a viable approach to finding existing drugs that may be able to modulate this fundamental function of professional phagocytes. Further libraries could be screened and hits could be taken forward to evaluate effectiveness in primary human phagocytes such as monocyte-derived macrophages and neutrophils.

Completion of the siRNA screen may reveal further targets common to essential pathways for intracellular killing. These targets could initially be compared with the RNAseq data set. Targets that result in a significant reduction of intracellular GFP bacteria may not be due to disrupted phagocytosis if they correlate with significantly downregulated genes in phagocytic MDMs. These would be particularly interesting targets to take forward for validation as it may

reveal that driving non-phagocytic macrophages into phagocytosing leads to further enhanced killing rather than over-activation.

Hits that show effectiveness against a variety of bacteria *in vitro,* whether enhanced phagocytosis or enhanced killing, should be taken forward for *in vivo* studies. The zebrafish infection model is genetically malleable and optically transparent. It is therefore ideal for tracking the clearance of fluorescent bacteria by labelled macrophages or neutrophils as well as concluding that hits lead to enhanced survival.

6.3 Conclusion

The overarching aim of this project was to uncover molecular signatures and regulators of phagocytosis and intracellular killing that are therapeutically targetable to modulate the innate immune system, providing an alternative avenue for treating infections. The prevalence of antibiotic resistant infections has increased over time and continues to do so due to both the required use combined with the misuse of antibiotics. The staggering estimation of 10 million deaths per year globally by 2050 emphasises the requirement for effective, novel therapeutic strategies (HM Government, 2019). The findings described and summarised here offer targets of interest for further investigation to exploit and enhance innate immune response as an alternative therapeutic method to antibiotic treatment, particularly in the case of antibiotic resistant infections.

7 References

Abdel-Latif, D. *et al.* (2004) 'Rac2 is critical for neutrophil primary granule exocytosis.', *Blood*. American Society of Hematology, 104(3), pp. 832–9. doi: 10.1182/blood-2003-07-2624.

Afroz, S. *et al.* (2016) 'Transcriptome meta-analysis reveals a dysregulation in extra cellular matrix and cell junction associated gene signatures during Dengue virus infection', *Scientific Reports*. Nature Publishing Group, 6. doi: 10.1038/srep33752.

Al-Janabi, A. A. H. S. (2011) 'Potential Activity of the Purine Compounds Caffeine and Aminophylline on Bacteria', *Journal of Global Infectious Diseases*. Wolters Kluwer -- Medknow Publications, 3(2), p. 133. doi: 10.4103/0974-777X.81689.

Alaoui Mdarhri, H. *et al.* (2022) 'Alternatives Therapeutic Approaches to Conventional Antibiotics: Advantages, Limitations and Potential Application in Medicine', *Antibiotics*, 11(12). doi: 10.3390/antibiotics11121826.

Aljawai, Y. *et al.* (2014) 'β-Catenin/TCF-4 Signaling Regulates Susceptibility of Macrophages and Resistance of Monocytes to HIV-1 Productive Infection', *Current HIV Research*. Bentham Science Publishers Ltd., 12(3), pp. 164–173. doi: 10.2174/1570162x12666140526122249.

Amulic, B. *et al.* (2017) 'Cell-Cycle Proteins Control Production of Neutrophil Extracellular Traps Article Cell-Cycle Proteins Control Production of Neutrophil Extracellular Traps', *Developmental Cell*. Elsevier Inc., 43(4), pp. 449-462.e5. doi: 10.1016/j.devcel.2017.10.013.

Arafa, E. I. *et al.* (2022) 'Recruitment and training of alveolar macrophages after pneumococcal pneumonia', *JCI Insight*, 7(5). doi: 10.1172/jci.insight.150239.

Atri, C., Guerfali, F. Z. and Laouini, D. (2018) 'Role of Human Macrophage Polarization in Inflammation during Infectious Diseases.', *International journal of molecular sciences*. Multidisciplinary Digital Publishing Institute (MDPI), 19(6). doi: 10.3390/ijms19061801.

Aydin, M. A. *et al.* (2023) 'Microbiological and clinical characteristics of Streptococcus pneumoniae serotype 3 infection and risk factors for severe outcome : A multicenter observational study', *Journal of Microbiology, Immunology and Infection*. Elsevier Taiwan LLC, pp. 1–7. doi: 10.1016/j.jmii.2023.01.013.

Aynacıoğlu, A. Ş., Bilir, A. and Tuna, M. Y. (2019) 'Involvement of midkine in autoimmune and autoinflammatory diseases', *Modern Rheumatology*. Taylor and Francis Ltd, pp. 567–571. doi: 10.1080/14397595.2018.1523701.

Aza-Blanc, P. *et al.* (2003) 'Identification of modulators of TRAIL-induced apoptosis via RNAi-based phenotypic screening', *Molecular Cell*, 12(3), pp. 627–637. doi: 10.1016/S1097-2765(03)00348-4.

Bain, C. C. *et al.* (2015) 'Constant replenishment from circulating monocytes maintains the macrophage pool in adult intestine', *Europe PMC Funders*, 15(10), pp. 929–937. doi: 10.1038/ni.2967.Constant.

Barcia-Macay, M. *et al.* (2006) 'Pharmacodynamic evaluation of the intracellular activities of antibiotics against Staphylococcus aureus in a model of THP-1 macrophages', *Antimicrobial Agents and Chemotherapy*. American Society for Microbiology, 50(3), pp. 841–851. doi:

10.1128/AAC.50.3.841-851.2006/ASSET/46804A4E-7380-418C-BA91-D625C13FCBF4/ASSETS/GRAPHIC/ZAC0030656230006.JPEG.

Behmoaras, J. *et al.* (2008) 'Jund is a determinant of macrophage activation and is associated with glomerulonephritis susceptibility', *Nature Genetics*, 40(5), pp. 553–559. doi: 10.1038/ng.137.

Behura, A. *et al.* (2021) 'ESAT-6 impedes IL-18 mediated phagosome lysosome fusion via microRNA-30a upon Calcimycin treatment in mycobacteria infected macrophages', *International Immunopharmacology*. Elsevier B.V., 101(PA), p. 108319. doi: 10.1016/j.intimp.2021.108319.

Benard, E. L. *et al.* (2014) 'Phagocytosis of mycobacteria by zebrafish macrophages is dependent on the scavenger receptor Marco, a key control factor of pro-inflammatory signalling', *Developmental and Comparative Immunology*. Elsevier Ltd, 47(2), pp. 223–233. doi: 10.1016/j.dci.2014.07.022.

Benoit, M., Desnues, B. and Mege, J.-L. (2008) 'Macrophage Polarization in Bacterial Infections', *The Journal of Immunology*. American Association of Immunologists, 181(6), pp. 3733–3739. doi: 10.4049/JIMMUNOL.181.6.3733.

Bewley, M. A. *et al.* (2011) 'A Cardinal Role for Cathepsin D in Co-Ordinating the Host-Mediated Apoptosis of Macrophages and Killing of Pneumococci', *PLoS Pathogens*. Public Library of Science, 7(1). doi: 10.1371/JOURNAL.PPAT.1001262.

Blériot, C., Chakarov, S. and Ginhoux, F. (2020) 'Determinants of Resident Tissue Macrophage Identity and Function', *Immunity*, 52(6), pp. 957–970. doi: 10.1016/j.immuni.2020.05.014.

Borregaard, N. and Cowland, J. B. (1997) 'Granules of the Human Neutrophilic Polymorphonuclear Leukocyte', *Blood*. American Society of Hematology, 89(10), pp. 3503–3521. Available at: http://www.ncbi.nlm.nih.gov/pubmed/2153038 (Accessed: 25 June 2019).

Bou Ghanem, E. N. *et al.* (2015) 'Extracellular Adenosine Protects against Streptococcus pneumoniae Lung Infection by Regulating Pulmonary Neutrophil Recruitment', *PLoS Pathogens*, 11(8), pp. 1–23. doi: 10.1371/journal.ppat.1005126.

Boutros, M., Hahne, F. and Huber, W. (2013) 'End-to-end analysis of cell-based screens : from raw intensity readings to the annotated hit list', *Bioconductor*, pp. 1–48.

Bowdish, D. *et al.* (2007a) 'Macrophage receptors implicated in the "'adaptive'" form of innate immunity'. doi: 10.1016/j.micinf.2007.09.002.

Bowdish, D. *et al.* (2007b) 'Macrophage receptors implicated in the "'adaptive'" form of innate immunity'. doi: 10.1016/j.micinf.2007.09.002.

Branzk, N. *et al.* (2014) 'Neutrophils sense microbe size and selectively release neutrophil extracellular traps in response to large pathogens', *Nature Immunology*. Nature Publishing Group, 15(11), pp. 1017–1025. doi: 10.1038/ni.2987.

Brinkmann, V. *et al.* (2004) 'Neutrophil Extracellular Traps Kill Bacteria', *Science*, 303(5663), pp. 1532–1535.

Brogden, K. A. (2005) 'Antimicrobial peptides: pore formers or metabolic inhibitors in bacteria?', *Nature Reviews Microbiology*. Nature Publishing Group, 3(3), pp. 238–250. doi: 10.1038/nrmicro1098.

Brooks, A. D. and Sayers, T. J. (2005) 'Reduction of the antiapoptotic protein cFLIP enhances the susceptibility of human renal cancer cells to TRAIL apoptosis', *Cancer Immunology, Immunotherapy*, 54(5), pp. 499–505. doi: 10.1007/s00262-004-0595-8.

Byrne, A. J. *et al.* (2020) 'Dynamics of human monocytes and airway macrophages during healthy aging and after transplant', *Journal of Experimental Medicine*, 217(3), pp. 1–11. doi: 10.1084/jem.20191236.

Cabral, W. A. *et al.* (2016) 'Absence of the ER Cation Channel TMEM38B/TRIC-B Disrupts Intracellular Calcium Homeostasis and Dysregulates Collagen Synthesis in Recessive Osteogenesis Imperfecta', *PLoS Genetics*. Public Library of Science, 12(7). doi: 10.1371/journal.pgen.1006156.

Cano, C. E. *et al.* (2012) 'Homotypic cell cannibalism, a cell-death process regulated by the nuclear protein 1, opposes to metastasis in pancreatic cancer', *EMBO Molecular Medicine*. Blackwell Publishing Ltd, 4(9), pp. 964–979. doi: 10.1002/emmm.201201255.

Caputo, M. *et al.* (2022) 'Duplication of exons 15 and 16 in Matrin-3: a phenotype bridging amyotrophic lateral sclerosis and immune-mediated disorders', *Neurological Sciences*. Springer-Verlag Italia s.r.l., 43(2), pp. 1419–1421. doi: 10.1007/s10072-021-05669-2.

Chaplin, D. D. (2010) 'Overview of the immune response.', *The Journal of allergy and clinical immunology*. NIH Public Access, 125(2 Suppl 2), pp. S3-23. doi: 10.1016/j.jaci.2009.12.980.

El Chemaly, A. *et al.* (2010) 'VSOP/Hv1 proton channels sustain calcium entry, neutrophil migration, and superoxide production by limiting cell depolarization and acidification', *Journal of Experimental Medicine*, 207(1), pp. 129–139. doi: 10.1084/jem.20091837.

Chen, L. *et al.* (2020) 'Effect of alkylglycerone phosphate synthase on the expression levels of lncRNAs in glioma cells and its functional prediction', *Oncology Letters*. Spandidos Publications, 20(4). doi: 10.3892/ol.2020.11927.

Chen, S. *et al.* (2015) 'Impact of Detachment Methods on M2 Macrophage Phenotype and Function', *Journal of Immunological Methods*. Elsevier B.V., 426, pp. 56–61. doi: 10.1016/j.jim.2015.08.001.

Chen, S. *et al.* (2022) 'Identification of lncRNAs based on different patterns of immune infiltration in gastric cancer', *Journal of Gastrointestinal Oncology*, 13(1), pp. 102–116. doi: 10.21037/jgo-21-833.

Cheng, Y. *et al.* (2020) 'Host cytosolic RNA sensing pathway promotes T Lymphocyte-mediated mycobacterial killing in macrophages', *PLoS Pathogens*. Public Library of Science, 16(5). doi: 10.1371/journal.ppat.1008569.

Chhiba, K. D. *et al.* (2017) 'Transcriptional Heterogeneity of Mast Cells and Basophils upon Activation.', *Journal of immunology (Baltimore, Md. : 1950)*. American Association of Immunologists, 198(12), pp. 4868–4878. doi: 10.4049/jimmunol.1601825.

Clardy, J., Fischbach, M. A. and Currie, C. R. (2009) 'The natural history of antibiotics', *Current Biology*, 19, pp. 437–441.

Colom, B. *et al.* (2015) 'Leukotriene B4-Neutrophil Elastase Axis Drives Neutrophil Reverse Transendothelial Cell Migration InVivo', *Immunity*. The Authors, 42(6), pp. 1075–1086. doi: 10.1016/j.immuni.2015.05.010.

Daigneault, M. *et al.* (2010) 'The identification of markers of macrophage differentiation in PMA-stimulated THP-1 cells and monocyte-derived macrophages', *PLoS ONE*, 5(1). doi: 10.1371/journal.pone.0008668.

Daitoku, H. *et al.* (2021) 'siRNA screening identifies METTL9 as a histidine Nπ-methyltransferase that targets the proinflammatory protein S100A9', *Journal of Biological Chemistry*. American Society for Biochemistry and Molecular Biology Inc., 297(5), p. 101230. doi: 10.1016/j.jbc.2021.101230.

Dana, H. *et al.* (2017) 'Molecular Mechanisms and Biological Functions of siRNA.', *International journal of biomedical science : IJBS*, 13(2), pp. 48–57. Available at: http://www.ncbi.nlm.nih.gov/pubmed/28824341%0Ahttp://www.pubmedcentral.nih.gov/articlerender.fcgi?artid=PMC5542916.

Davies, L. C. *et al.* (2013) 'Tissue-resident macrophages.', *Nature immunology*. Europe PMC Funders, 14(10), pp. 986–95. doi: 10.1038/ni.2705.

Davydova, E. *et al.* (2021) 'The methyltransferase METTL9 mediates pervasive 1-methylhistidine modification in mammalian proteomes', *Nature Communications*. Nature Research, 12(1), pp. 1–14. doi: 10.1038/s41467-020-20670-7.

Deniset, J. F. and Kubes, P. (2018) 'Neutrophil heterogeneity: Bona fide subsets or polarization states?', *Journal of Leukocyte Biology*, 103(5), pp. 829–838. doi: 10.1002/JLB.3RI0917-361R.

Dockrell, D. H., Whyte, M. K. B. and Mitchell, T. J. (2012) 'Pneumococcal pneumonia: mechanisms of infection and resolution.', *Chest*. American College of Chest Physicians, 142(2), pp. 482–491. doi: 10.1378/chest.12-0210.

Domenech, M. *et al.* (2013) 'Biofilm formation avoids complement immunity and phagocytosis of Streptococcus pneumoniae', *Infection and Immunity*, 81(7), pp. 2606–2615. doi: 10.1128/IAI.00491-13.

Domon, H. and Terao, Y. (2021) 'The Role of Neutrophils and Neutrophil Elastase in Pneumococcal Pneumonia', *Frontiers in Cellular and Infection Microbiology*, 11(March), pp. 1–9. doi: 10.3389/fcimb.2021.615959.

Duchesne, C. *et al.* (2021) 'Cold Atmospheric Plasma Promotes Killing of Staphylococcus aureus by Macrophages', *mSphere*. American Society for Microbiology (ASM), 6(3). doi: 10.1128/MSPHERE.00217-21.

Elisia, I. *et al.* (2018) 'Comparison of RAW264.7, human whole blood and PBMC assays to screen for immunomodulators', *Journal of Immunological Methods*. Elsevier, 452, pp. 26–31. doi: 10.1016/J.JIM.2017.10.004.

Ellis, M. J. *et al.* (2019) 'A macrophage-based screen identifies antibacterial compounds selective for intracellular Salmonella Typhimurium', *Nature Communications*. Springer US, 10(1). doi: 10.1038/s41467-018-08190-x.

Eskova, A. *et al.* (2014) 'An RNAi screen identifies KIF15 as a novel regulator of the endocytic

trafficking of integrin', *Journal of Cell Science*, 127(11), pp. 2433–2447. doi: 10.1242/jcs.137281.

Fagiani, E. and Christofori, G. (2013) 'Angiopoietins in angiogenesis', *Cancer Letters*. Elsevier Ireland Ltd, pp. 18–26. doi: 10.1016/j.canlet.2012.08.018.

Felgner, P. L. *et al.* (1987) 'Lipofection: a highly efficient, lipid-mediated DNA-transfection procedure.', *Proceedings of the National Academy of Sciences of the United States of America*, 84(21), pp. 7413–7417. doi: 10.1073/pnas.84.21.7413.

Flannagan, R., Heit, B. and Heinrichs, D. (2015) 'Antimicrobial Mechanisms of Macrophages and the Immune Evasion Strategies of Staphylococcus aureus', *Pathogens*. Multidisciplinary Digital Publishing Institute, 4(4), pp. 826–868. doi: 10.3390/pathogens4040826.

Folco, E. J. *et al.* (2009) 'Adiponectin inhibits pro-inflammatory signaling in human macrophages independent of interleukin-10', *Journal of Biological Chemistry*, 284(38), pp. 25569–25575. doi: 10.1074/jbc.M109.019786.

Foster, J. W. and Slonczewski, J. L. (2011) *Microbiology: An Evolving Science*. 2nd edn. Norton.

Freeman, S. A. and Grinstein, S. (2014) 'Phagocytosis: receptors, signal integration, and the cytoskeleton', *Immunological Reviews*. John Wiley & Sons, Ltd (10.1111), 262(1), pp. 193–215. doi: 10.1111/imr.12212.

Fuchs, T. A. *et al.* (2007) 'Novel cell death program leads to neutrophil extracellular traps', *The Journal of Cell Biology*. Rockefeller University Press, 176(2), pp. 231–241. doi: 10.1083/JCB.200606027.

Ganaie, F. *et al.* (2021) 'Structural, Genetic, and Serological Elucidation of Streptococcus pneumoniae Serogroup 24 Serotypes: Discovery of a New Serotype, 24C, with a Variable Capsule Structure'. doi: 10.1128/JCM.00540-21.

Garratt, L. W. (2021) 'Current Understanding of the Neutrophil Transcriptome in Health and Disease', *Cells*. Multidisciplinary Digital Publishing Institute (MDPI), 10(9). doi: 10.3390/CELLS10092406.

Ghofrani, H. A., Osterloh, I. H. and Grimminger, F. (2006) 'Sildenafil: From angina to erectile dysfunction to pulmonary hypertension and beyond', *Nature Reviews Drug Discovery*, 5(8), pp. 689–702. doi: 10.1038/nrd2030.

Gillen, A. E. *et al.* (2017) 'Alternative polyadenylation of PRELID1 regulates mitochondrial ros signaling and cancer outcomes', *Molecular Cancer Research*. American Association for Cancer Research Inc., 15(12), pp. 1741–1751. doi: 10.1158/1541-7786.MCR-17-0010.

Gong, B. *et al.* (2021) 'A Golgi-derived vesicle potentiates PtdIns4P to PtdIns3P conversion for endosome fission', *Nature Cell Biology*. Nature Research, 23(7), pp. 782–795. doi: 10.1038/s41556-021-00704-y.

Gong, J. L. *et al.* (1994) 'Interstitial lung macrophages interact with dendritic cells to present antigenic peptides derived from particulate antigens to T cells.', *Immunology*, 81(3), pp. 343–51. Available at: http://www.ncbi.nlm.nih.gov/pubmed/8206508%0Ahttp://www.pubmedcentral.nih.gov/articlerender.fcgi?artid=PMC1422342.

Gordon, E. *et al.* (2000) 'The crystal structure of the penicillin-binding protein 2x from Streptococcus pneumoniae and its acyl-enzyme form: Implication in drug resistance', *Journal of Molecular Biology*, 299(2), pp. 477–485. doi: 10.1006/jmbi.2000.3740.

Gou, X. *et al.* (2020) 'IL-6 During Influenza-Streptococcus pneumoniae Co-Infected Pneumonia—A Protector', *Frontiers in Immunology*, 10(January), pp. 1–13. doi: 10.3389/fimmu.2019.03102.

Greenlee-Wacker, M. C. and Nauseef, W. M. (2017) ' IFN-γ targets macrophage-mediated immune responses toward Staphylococcus aureus ', *Journal of Leukocyte Biology*, 101(3), pp. 751–758. doi: 10.1189/jlb.4a1215-565rr.

Gupta, S., Tyagi, S. and Bishaia, W. R. (2015) 'Verapamil Increases the Bactericidal Activity of Bedaquiline against Mycobacterium tuberculosis in a Mouse Model', *Antimicrobial Agents and Chemotherapy*. American Society for Microbiology (ASM), 59(1), p. 673. doi: 10.1128/AAC.04019-14.

Guthrie, L. A. *et al.* (1984) 'Priming of neutrophils for enhanced release of oxygen metabolites by bacterial lipopolysaccharide: Evidence for increased activity of the superoxide-producing enzyme', *Journal of Experimental Medicine*, 160(6), pp. 1656–1671. doi: 10.1084/jem.160.6.1656.

Hahn, I. *et al.* (2011) 'Cathepsin G and neutrophil elastase play critical and nonredundant roles in lung-protective immunity against Streptococcus pneumoniae in mice', *Infection and Immunity*, 79(12), pp. 4893–4901. doi: 10.1128/IAI.05593-11.

Hakenbeck, R. *et al.* (2012) 'Molecular mechanisms of b -lactam resistance in', *Future Microbiology*, 7(3), pp. 395–410. doi: 10.2217/fmb.12.2.

Harber, K. J. *et al.* (2020) 'Succinate is an inflammation-induced immunoregulatory metabolite in macrophages', *Metabolites*. MDPI AG, 10(9), pp. 1–14. doi: 10.3390/metabo10090372.

Harrison, R. E. *et al.* (2003) 'Phagosomes Fuse with Late Endosomes and/or Lysosomes by Extension of Membrane Protrusions along Microtubules: Role of Rab7 and RILP', *Molecular and Cellular Biology*. American Society for Microbiology Journals, 23(18), pp. 6494–6506. doi: 10.1128/MCB.23.18.6494-6506.2003.

Hashiguchi, M.-J. 2022/Papers to download via mendeley/1-s2. .-S. pd. *et al.* (2018) 'Tumor necrosis factor superfamily member (TNFSF) 13 (APRIL) and TNFSF13B (BAFF) downregulate homeostatic immunoglobulin production in the intestines', *Cellular Immunology*. Elsevier, 323(June 2017), pp. 41–48. doi: 10.1016/j.cellimm.2017.10.009.

Hellebrekers, P. *et al.* (2017) 'Neutrophil Functional Heterogeneity: Identification of Competitive Phagocytosis', *Frontiers in Immunology*. Frontiers, 8, p. 1498. doi: 10.3389/fimmu.2017.01498.

Hesselink, L. *et al.* (2020) 'New automated analysis to monitor neutrophil function point-of-care in the intensive care unit after trauma', *Intensive Care Medicine Experimental* . Intensive Care Medicine Experimental, 8(1), pp. 1–12. doi: 10.1186/s40635-020-0299-1.

Hlaka, L. *et al.* (2021) 'IL-4i1 Regulation of Immune Protection during Mycobacterium tuberculosis Infection', *Journal of Infectious Diseases*, 224(12), pp. 2170–2180. doi:

10.1093/infdis/jiab558.

HM Government (2019) 'The UK's five-year national action plan', (January). Available at: https://assets.publishing.service.gov.uk/government/uploads/system/uploads/attachment_data/file/784894/UK_AMR_5_year_national_action_plan.pdf.

Hoebe, K., Janssen, E. and Beutler, B. (2004) 'The interface between innate and adaptive immunity', *Nature immunology*, 5(10), pp. 971–974.

van den Homberg, D. A. L. *et al.* (2022) 'N-6-Methyladenosine in Vasoactive microRNAs during Hypoxia; A Novel Role for METTL4', *International Journal of Molecular Sciences*. MDPI, 23(3). doi: 10.3390/ijms23031057.

Huang, R. *et al.* (2017) 'Betanodavirus-like particles enter host cells via clathrin-mediated endocytosis in a cholesterol-, pH- and cytoskeleton-dependent manner', *Veterinary Research*. BioMed Central, 48(1). doi: 10.1186/S13567-017-0412-Y.

Hughes, J. P. *et al.* (2011) 'Principles of early drug discovery', *British Journal of Pharmacology*, 162(6), pp. 1239–1249. doi: 10.1111/j.1476-5381.2010.01127.x.

Hui, M. *et al.* (2020) 'KDELR2 is an unfavorable prognostic biomarker and regulates CCND1 to promote tumor progression in glioma', *Pathology Research and Practice*. Elsevier GmbH, 216(7). doi: 10.1016/j.prp.2020.152996.

Huynh, K. K. *et al.* (2007) 'LAMP proteins are required for fusion of lysosomes with phagosomes', *EMBO Journal*, 26(2), pp. 313–324. doi: 10.1038/sj.emboj.7601511.

Ikuta, K. S. *et al.* (2022a) 'Global mortality associated with 33 bacterial pathogens in 2019: a systematic analysis for the Global Burden of Disease Study 2019', *The Lancet*. Elsevier B.V., 400(10369), pp. 2221–2248. doi: 10.1016/S0140-6736(22)02185-7.

Ikuta, K. S. *et al.* (2022b) 'Global mortality associated with 33 bacterial pathogens in 2019: a systematic analysis for the Global Burden of Disease Study 2019', *The Lancet*, 400(10369), pp. 2221–2248. doi: 10.1016/S0140-6736(22)02185-7.

Italiani, P. and Boraschi, D. (2014) 'From Monocytes to M1/M2 Macrophages: Phenotypical vs. Functional Differentiation.', *Frontiers in immunology*. Frontiers Media SA, 5, p. 514. doi: 10.3389/fimmu.2014.00514.

Iwasaki, A. and Medzhitov, R. (2010) 'Regulation of Adaptive Immunity by the Innate Immune System', *Science*, 327(5963), pp. 291–295.

Janeway, C. A. (1989) 'Approaching the asymptote? Evolution and revolution in immunology.', *Cold Spring Harbor symposia on quantitative biology*, 54, pp. 1–13. Available at: http://www.ncbi.nlm.nih.gov/pubmed/24141854.

Jensen, K., Anderson, J. A. and Glass, E. J. (2014) 'Comparison of small interfering RNA (siRNA) delivery into bovine monocyte-derived macrophages by transfection and electroporation', *Veterinary Immunology and Immunopathology*. Elsevier B.V., 158(3–4), pp. 224–232. doi: 10.1016/j.vetimm.2014.02.002.

Jeon, S. T. *et al.* (2010) 'Reverse signaling through BAFF differentially regulates the expression of inflammatory mediators and cytoskeletal movements in THP-1 cells', *Immunology and Cell Biology*, 88(2), pp. 148–156. doi: 10.1038/icb.2009.75.

Jog, N. R. *et al.* (2007) 'The actin cytoskeleton regulates exocytosis of all neutrophil granule subsets', *American Journal of Physiology-Cell Physiology*. American Physiological Society, 292(5), pp. C1690–C1700. doi: 10.1152/ajpcell.00384.2006.

Johnson, J. L. *et al.* (2011) 'Munc13-4 restricts motility of Rab27a-expressing vesicles to facilitate lipopolysaccharide-induced priming of exocytosis in neutrophils.', *The Journal of biological chemistry*. American Society for Biochemistry and Molecular Biology, 286(7), pp. 5647–56. doi: 10.1074/jbc.M110.184762.

Jubrail, J. *et al.* (2016) 'Inability to sustain intraphagolysosomal killing of Staphylococcus aureus predisposes to bacterial persistence in macrophages', *Cellular Microbiology*, 18(1), pp. 80–96. doi: 10.1111/cmi.12485.

Karthikeyan, R. S. G. *et al.* (2013) 'Host Response and Bacterial Virulence Factor Expression in Pseudomonas aeruginosa and Streptococcus pneumoniae Corneal Ulcers', *PLoS ONE*, 8(6), pp. 2–9. doi: 10.1371/journal.pone.0064867.

Kennedy, A. D. and DeLeo, F. R. (2009) 'Neutrophil apoptosis and the resolution of infection', *Immunologic Research*. Humana Press Inc, 43(1–3), pp. 25–61. doi: 10.1007/s12026-008-8049-6.

Khan, A. I. *et al.* (2004) 'Role of CD44 and hyaluronan in neutrophil recruitment.', *Journal of immunology (Baltimore, Md. : 1950)*. American Association of Immunologists, 173(12), pp. 7594–601. doi: 10.4049/jimmunol.173.12.7594.

Kishore, U. *et al.* (2020) 'Phagocytosis: Our Current Understanding of a Universal Biological Process', *Frontiers in Immunology | www.frontiersin.org*, 1, p. 1066. doi: 10.3389/fimmu.2020.01066.

Kitchen, E. *et al.* (1996) 'Demonstration of reversible priming of human neutrophils using platelet- activating factor', *Blood*, 88(11), pp. 4330–4337. Available at: http://www.bloodjournal.org/content/88/11/4330.long?sso-checked=true (Accessed: 14 June 2019).

Kobayashi, S. D. *et al.* (2005) 'Neutrophils in the innate immune response', *Archivum immunologiae et therapiae experimentalis*, 53(6), pp. 505–517.

Koo, J. Il *et al.* (2019) 'The pivotal role of long noncoding RNA RAB5IF in the proliferation of hepatocellular carcinoma via LGR5 mediated β-catenin and c-Myc signaling', *Biomolecules*. MDPI AG, 9(11). doi: 10.3390/biom9110718.

Kraal, G. *et al.* (2000) 'The macrophage receptor MARCO', *Microbes and Infection*. Elsevier Masson SAS, pp. 313–316. doi: 10.1016/S1286-4579(00)00296-3.

Lämmermann, T. *et al.* (2013) 'Neutrophil swarms require LTB4 and integrins at sites of cell death in vivo', *Nature*, 498(7454). doi: 10.1038/nature08365.Reconstructing.

Lees, M. P. *et al.* (2010) 'P2X7 receptor-mediated killing of an intracellular parasite, Toxoplasma gondii, by human and murine macrophages', *Journal of immunology (Baltimore, Md. : 1950)*. NIH Public Access, 184(12), p. 7040. doi: 10.4049/JIMMUNOL.1000012.

Leisner, J. J. *et al.* (2021) 'Repurposing Candesartan Cilexetil as Antibacterial Agent for MRSA Infection'. doi: 10.3389/fmicb.2021.688772.

Li, W. *et al.* (2018) 'DEPP/DEPP1/C10ORF10 regulates hepatic glucose and fat metabolism partly *via* ROS-induced FGF21', *The FASEB Journal*. FASEB, 32(10), pp. 5459–5469. doi: 10.1096/fj.201800357R.

Liepelt, A. *et al.* (2020) 'Differential gene expression in circulating CD14+ monocytes indicates the prognosis of critically ill patients with sepsis', *Journal of Clinical Medicine*. MDPI, 9(1). doi: 10.3390/jcm9010127.

Lim, S. G. *et al.* (2017) 'Crosstalk between signals initiated from TLR4 and cell surface BAFF results in synergistic induction of proinflammatory mediators in THP-1 cells', *Scientific Reports*. Nature Publishing Group, 7. doi: 10.1038/srep45826.

Liu, J. *et al.* (2020) 'Upregulation of miR-205 induces CHN1 expression, which is associated with the aggressive behaviour of cervical cancer cells and correlated with lymph node metastasis', *BMC Cancer*. BMC Cancer, 20(1), pp. 1–13. doi: 10.1186/s12885-020-07478-w.

Locati, M., Curtale, G. and Mantovani, A. (no date) 'Diversity, Mechanisms and Significance of Macrophage Plasticity'. doi: 10.1146/annurev-pathmechdis-012418-012718.

Loe, M. W. C., Lee, R. C. H. and Chu, J. J. H. (2019) 'Antiviral activity of the FDA-approved drug candesartan cilexetil against Zika virus infection', *Antiviral Research*. Elsevier, 172, p. 104637. doi: 10.1016/J.ANTIVIRAL.2019.104637.

Marriott, H. M. *et al.* (2005) 'Dynamic changes in Mcl-1 expression regulate macrophage viability or commitment to apoptosis during bacterial clearance.', *The Journal of clinical investigation*. American Society for Clinical Investigation, 115(2), pp. 359–68. doi: 10.1172/JCI21766.

Marriott, H. M. *et al.* (2008) 'Reactive oxygen species regulate neutrophil recruitment and survival in pneumococcal pneumonia', *American Journal of Respiratory and Critical Care Medicine*, 177(8), pp. 887–895. doi: 10.1164/rccm.200707-990OC.

Martinez, P. J. *et al.* (2019) 'PspA facilitates evasion of pneumococci from bactericidal activity of neutrophil extracellular traps (NETs)', *Microbial Pathogenesis*. Elsevier Ltd, 136(August), p. 103653. doi: 10.1016/j.micpath.2019.103653.

Matty, M. A. *et al.* (2019) 'Potentiation of P2RX7 as a host-directed strategy for control of mycobacterial infection', *eLife*. NLM (Medline), 8. doi: 10.7554/eLife.39123.

May, R. C. *et al.* (2000) 'Involvement of the Arp2/3 complex in phagocytosis mediated by FcγR or CR3', *Nature Cell Biology*. Nature Publishing Group, 2(4), pp. 246–248. doi: 10.1038/35008673.

McPhail, L. C., Clayton, C. C. and Snyderman, R. (1984) 'The NADPH Oxidase of Human Polymorphonuclear Leukocytes', *The Jounal of Biological Chemistry*, 259(9), pp. 5768–5775.

Medzhitov, R. (2007) 'Recognition of microorganisms and activation of the immune response.', *Nature*, 449(7164), pp. 819–26. doi: 10.1038/nature06246.

Meghraoui-Kheddar, A. *et al.* (2022) 'Two New Neutrophil Subsets Define a Discriminating Sepsis Signature', *American Journal of Respiratory and Critical Care Medicine*. American Thoracic Society, 205(1), pp. 46–59. doi: 10.1164/RCCM.202104-1027OC.

Metzler, K. D. *et al.* (2014) 'Myeloperoxidase-containing complex regulates neutrophil

elastase release and actin dynamics during NETosis', *Cell Reports*. The Authors, 8(3), pp. 883–896. doi: 10.1016/j.celrep.2014.06.044.

Mills, C. D. *et al.* (2000) 'M-1/M-2 macrophages and the Th1/Th2 paradigm.', *Journal of immunology (Baltimore, Md. : 1950)*. American Association of Immunologists, 164(12), pp. 6166–73. doi: 10.4049/jimmunol.164.12.6166.

Minakami, R. *et al.* (2010) 'Membrane phospholipid metabolism during phagocytosis in human neutrophils', *Genes to Cells*, 15(5), pp. 409–424. doi: 10.1111/j.1365-2443.2010.01393.x.

Miralda, I., Uriarte, S. M. and McLeish, K. R. (2017) 'Multiple Phenotypic Changes Define Neutrophil Priming', *Frontiers in Cellular and Infection Microbiology*. Frontiers, 7, p. 217. doi: 10.3389/fcimb.2017.00217.

Miyake, N. *et al.* (2008) ' Human CHN1 mutations hyperactivate alpha2-chimaerin and cause Duane's retraction syndrome. Science (New York, N.Y.), 321(5890), 839-43. doi:10.1126/s', *Science (New York, N.Y.)*, 321(5890), pp. 839–43. doi: 10.1126/science.1156121.Human.

Miyauchi, J. *et al.* (1985) 'Ultrastructural immunocytochemical localization of lysozyme in human monocytes and macrophages', *Cell and Tissue Research*. Springer-Verlag, 242(2), pp. 269–277. doi: 10.1007/BF00214539.

Mojakgomo, R., Mbita, Z. and Dlamini, Z. (2015) 'Linking the ceramide synthases (CerSs) 4 and 5 with apoptosis, endometrial and colon cancers', *Experimental and Molecular Pathology*. Academic Press Inc., 98(3), pp. 585–592. doi: 10.1016/j.yexmp.2015.03.019.

Molinier-Frenkel, V., Prévost-Blondel, A. and Castellano, F. (2019) 'The il4i1 enzyme: A new player in the immunosuppressive tumor microenvironment', *Cells*. MDPI. doi: 10.3390/cells8070757.

Moore, K. L. *et al.* (1995) 'P-selectin glycoprotein ligand-1 mediates rolling of human neutrophils on P-selectin.', *The Journal of cell biology*. The Rockefeller University Press, 128(4), pp. 661–71. doi: 10.1083/jcb.128.4.661.

Morawska-Pucinska, E., Szymanska, M. and Blitek, A. (2014) 'Expression profile and role of prostacyclin receptor (PTGIR) in peri-implantation porcine conceptuses', *Theriogenology*. Elsevier Inc., 82(4), pp. 546–556. doi: 10.1016/j.theriogenology.2014.05.014.

Morimoto, K. *et al.* (2006) 'Lovastatin Enhances Clearance of Apoptotic Cells (Efferocytosis) with Implications for Chronic Obstructive Pulmonary disease', *The Journal of Immunology*, 176(12), pp. 7657–7665.

Munita, J. M. and Arias, C. A. (2016) 'Mechanisms of antibiotic resistance', *Virulence Mechanisms of Bacterial Pathogens*, (6), pp. 481–511. doi: 10.1128/9781555819286.ch17.

Nagata, S. *et al.* (2016) 'Exposure of phosphatidylserine on the cell surface'. doi: 10.1038/cdd.2016.7.

Neira, J. L. *et al.* (2020) 'A phosphorylation-induced switch in the nuclear localization sequence of the intrinsically disordered nupr1 hampers binding to importin', *Biomolecules*. MDPI AG, 10(9), pp. 1–22. doi: 10.3390/biom10091313.

Neveu, G. *et al.* (2015) 'AP-2-associated protein kinase 1 and cyclin G-associated kinase

regulate hepatitis C virus entry and are potential drug targets', *Journal of virology*. J Virol, 89(8), pp. 4387–4404. doi: 10.1128/JVI.02705-14.

Nordenfelt, P. and Tapper, H. (2011) 'Phagosome dynamics during phagocytosis by neutrophils.', *Journal of leukocyte biology*, 90(2), pp. 271–84. doi: 10.1189/jlb.0810457.

Nörenberg, W. *et al.* (2011) 'Clemastine potentiates the human P2X7 receptor by sensitizing it to lower ATP concentrations', *Journal of Biological Chemistry*, 286(13), pp. 11067–11081. doi: 10.1074/jbc.M110.198879.

Nunes, P., Guido, D. and Demaurex, N. (2015) 'Measuring phagosome ph by ratiometric fluorescence microscopy', *Journal of Visualized Experiments*, 2015(106), pp. 1–9. doi: 10.3791/53402.

Öhlinger, K. *et al.* (2020) 'Different sensitivity of macrophages to phospholipidosis induction by amphiphilic cationic drugs', *International Journal of Molecular Sciences*, 21(21), pp. 1–20. doi: 10.3390/ijms21218391.

Ostendorf, T. *et al.* (2020) 'Immune Sensing of Synthetic, Bacterial, and Protozoan RNA by Toll-like Receptor 8 Requires Coordinated Processing by RNase T2 and RNase 2', *Immunity*. Cell Press, 52(4), pp. 591-605.e6. doi: 10.1016/j.immuni.2020.03.009.

Paton, J. C. and Trappetti, C. (2019) ' Streptococcus pneumoniae Capsular Polysaccharide ', *Microbiology Spectrum*. American Society for Microbiology, 7(2). doi: 10.1128/MICROBIOLSPEC.GPP3-0019-2018/ASSET/0CEFC64C-B7B7-4947-B5E6-B57534FAB696/ASSETS/GRAPHIC/GPP3-0019-2018-FIG2.GIF.

Patro, R. *et al.* (2017) 'Salmon provides fast and bias-aware quantification of transcript expression', *Nature Methods*. Nature Publishing Group, 14(4), pp. 417–419. doi: 10.1038/nmeth.4197.

Paul-Clark, M. J. *et al.* (2006) 'Differential effects of Gram-positive versus Gram-negative bacteria on NOSII and TNFα in macrophages: role of TLRs in synergy between the two', *British Journal of Pharmacology*. Wiley-Blackwell, 148(8), p. 1067. doi: 10.1038/SJ.BJP.0706815.

Pereira, J. M. *et al.* (2022) 'The Yin and Yang of Pneumolysin During Pneumococcal Infection', *Frontiers in Immunology*, 13(April), pp. 1–21. doi: 10.3389/fimmu.2022.878244.

Perland, E. *et al.* (2017) 'Structural prediction of two novel human atypical SLC transporters, MFSD4A and MFSD9, and their neuroanatomical distribution in mice', *PLoS ONE*. Public Library of Science, 12(10). doi: 10.1371/journal.pone.0186325.

Pinder, E. M. *et al.* (2018) 'Randomised controlled trial of GM-CSF in critically ill patients with impaired neutrophil phagocytosis', *Thorax*, 73(10), pp. 918–925. doi: 10.1136/thoraxjnl-2017-211323.

Poirier, S. *et al.* (2009) 'Dissection of the Endogenous Cellular Pathways of PCSK9-induced Low Density Lipoprotein Receptor Degradation EVIDENCE FOR AN INTRACELLULAR ROUTE * □ S'. doi: 10.1074/jbc.M109.037085.

Porcheray, F. *et al.* (2005) 'Macrophage activation switching: an asset for the resolution of inflammation.', *Clinical and experimental immunology*. Wiley-Blackwell, 142(3), pp. 481–9. doi: 10.1111/j.1365-2249.2005.02934.x.

Prajsnar, T. K. *et al.* (2022) 'Phagosomal Acidification Is Required to Kill Streptococcus pneumoniae in a Zebrafish Model', *Cellular Microbiology*. Wiley-Hindawi, 2022. doi: 10.1155/2022/9429516.

Puiffe, M. L. *et al.* (2013) 'Antibacterial Properties of the Mammalian L-Amino Acid Oxidase IL4I1', *PLoS ONE*, 8(1), pp. 2–9. doi: 10.1371/journal.pone.0054589.

Pushpakom, S. *et al.* (2018) 'Drug repurposing: Progress, challenges and recommendations', *Nature Reviews Drug Discovery*. Nature Publishing Group, 18(1), pp. 41–58. doi: 10.1038/nrd.2018.168.

Ravetch, J. V. and Bolland, S. (2001) 'IgG Fc Receptors', *Annual Review of Immunology*. Annual Reviews 4139 El Camino Way, P.O. Box 10139, Palo Alto, CA 94303-0139, USA, 19(1), pp. 275–290. doi: 10.1146/annurev.immunol.19.1.275.

Rosales, C. and Uribe-Querol, E. (2017) 'Phagocytosis: A Fundamental Process in Immunity.', *BioMed research international*. Hindawi Limited, 2017, p. 9042851. doi: 10.1155/2017/9042851.

Roth, K., Strickland, J. and Copple, B. L. (2020) 'Regulation of macrophage activation in the liver after acute injury: Role of the fibrinolytic system', *World Journal of Gastroenterology*, 26(16), pp. 1879–1887. doi: 10.3748/WJG.V26.I16.1879.

Schlame, M. and Xu, Y. (2020) 'The Function of Tafazzin, a Mitochondrial Phospholipid–Lysophospholipid Acyltransferase', *Journal of Molecular Biology*. Academic Press, pp. 5043–5051. doi: 10.1016/j.jmb.2020.03.026.

Schulthess, J. *et al.* (2019) 'The Short Chain Fatty Acid Butyrate Imprints an Antimicrobial Program in Macrophages', *Immunity*. Elsevier, 50(2), p. 432. doi: 10.1016/J.IMMUNI.2018.12.018.

Schulz, D. *et al.* (2019) 'In-Depth Characterization of Monocyte-Derived Macrophages using a Mass Cytometry-Based phagocytosis Assay', *Scientific Reports*, 9(1925), p. 12. doi: 10.1038/s41598-018-38127-9.

Segal, A. W. *et al.* (1981) 'The respiratory burst of phagocytic cells is associated with a rise in vacuolar pH', *Nature 1981 290:5805*. Nature Publishing Group, 290(5805), pp. 406–409. doi: 10.1038/290406a0.

Sengeløv, H., Kjeldsen, L. and Borregaard, N. (1993) 'Control of exocytosis in early neutrophil activation', *Journal of immunology (Baltimore, Md. : 1950)*, 150(4), pp. 1535–43.

Shepard, H. M. *et al.* (2017) 'Developments in therapy with monoclonal antibodies and related proteins', *Clinical Medicine, Journal of the Royal College of Physicians of London*, 17(3), pp. 220–232. doi: 10.7861/clinmedicine.17-3-220.

Simard, J.-C. *et al.* (2011) 'Damage-Associated Molecular Pattern S100A9 Increases Bactericidal Activity of Human Neutrophils by Enhancing Phagocytosis', *The Journal of Immunology*, 186(6), pp. 3622–3631. doi: 10.4049/jimmunol.1002956.

Singel, K. L. *et al.* (2016) 'NOX2-dependent regulation of inflammation THE NADPH OXIDASE FAMILY HHS Public Access Author manuscript', *Clin Sci (Lond)*, 130(7), pp. 479–490. doi: 10.1042/CS20150660.

Sjöström, K. *et al.* (2006) 'Clonal and capsular types decide whether pneumococci will act as a primary or opportunistic pathogen', *Clinical Infectious Diseases*, 42(4), pp. 451–459. doi: 10.1086/499242.

Skytthe, M. K., Graversen, J. H. and Moestrup, S. K. (2020) 'Targeting of cd163+ macrophages in inflammatory and malignant diseases', *International Journal of Molecular Sciences*, 21(15), pp. 1–31. doi: 10.3390/ijms21155497.

Smith, T. D. *et al.* (2016) 'Regulation of macrophage polarization and plasticity by complex activation signals.', *Integrative biology : quantitative biosciences from nano to macro*. NIH Public Access, 8(9), pp. 946–55. doi: 10.1039/c6ib00105j.

Soehnlein, O. (2009) 'Direct and alternative antimicrobial mechanisms of neutrophil-derived granule proteins', *Journal of Molecular Medicine*. Springer-Verlag, 87(12), pp. 1157–1164. doi: 10.1007/s00109-009-0508-6.

Sommer, F. *et al.* (2021) 'Disruption of Cxcr3 chemotactic signaling alters lysosomal function and renders macrophages more microbicidal', *Cell Reports*. ElsevierCompany., 35(2), p. 109000. doi: 10.1016/j.celrep.2021.109000.

Standish, A. J. and Weiser, J. N. (2009) ' Human Neutrophils Kill Streptococcus pneumoniae via Serine Proteases ', *The Journal of Immunology*, 183(4), pp. 2602–2609. doi: 10.4049/jimmunol.0900688.

Storisteanu, D. M. L. *et al.* (2017) 'Evasion of neutrophil extracellular traps by respiratory pathogens', *American Journal of Respiratory Cell and Molecular Biology*, 56(4), pp. 423–431. doi: 10.1165/rcmb.2016-0193PS.

Studer, D. *et al.* (2012) 'Ribosomal protein L13a as a reference gene for human bone marrow-derived mesenchymal stromal cells during expansion, adipo-, chondro-, and osteogenesis', *Tissue Engineering - Part C: Methods*, 18(10), pp. 761–771. doi: 10.1089/ten.tec.2012.0081.

Sun, B. *et al.* (2014) 'Phosphatase Wip1 Negatively Regulates Neutrophil Migration and Inflammation', *The Journal of Immunology*. The American Association of Immunologists, 192(3), pp. 1184–1195. doi: 10.4049/jimmunol.1300656.

Suzuki, J., Imanishi, E. and Nagata, S. (2016) 'Xkr8 phospholipid scrambling complex in apoptotic phosphatidylserine exposure', *Proceedings of the National Academy of Sciences of the United States of America*. National Academy of Sciences, 113(34), pp. 9509–9514. doi: 10.1073/pnas.1610403113.

Tan, Y. *et al.* (2019) 'PSMD1 and PSMD2 regulate HepG2 cell proliferation and apoptosis via modulating cellular lipid droplet metabolism', *BMC Molecular Biology*. BioMed Central Ltd., 20(1). doi: 10.1186/s12867-019-0141-z.

Tang, X. Z. *et al.* (2022) 'Bronchus-associated macrophages efficiently capture and present soluble inhaled antigens and are capable of local Th2 cell activation', *eLife*, 11, pp. 1–36. doi: 10.7554/eLife.63296.

Tao, H. *et al.* (2021) 'Macrophage SR-BI modulates autophagy via VPS34 complex and PPARα transcription of TFEB in atherosclerosis', *Journal of Clinical Investigation*, 131(7), pp. 1–16. doi: 10.1172/JCI94229.

Thiriot, J. D. *et al.* (2020) 'Hacking the host: exploitation of macrophage polarization by intracellular bacterial pathogens', *FEMS*, 78, p. 9. doi: 10.1093/femspd/ftaa009.

Tiwarekar, V., Fehrholz, M. and Schneider-Schaulies, J. (2019) 'Kdelr2 competes with measles virus envelope proteins for cellular chaperones reducing their chaperone-mediated cell surface transport', *Viruses*. MDPI AG, 11(1). doi: 10.3390/v11010027.

Vieira, O. V. *et al.* (2001) 'Distinct roles of class I and class III phosphatidylinositol 3-kinases in phagosome formation and maturation', *Journal of Cell Biology*, 155(1), pp. 19–25. doi: 10.1083/jcb.200107069.

Villadangos, J. A. and Schnorrer, P. (2007) 'Intrinsic and cooperative antigen-presenting functions of dendritic-cell subsets in vivo', *Nature Reviews Immunology*, 7(7), pp. 543–555. doi: 10.1038/nri2103.

Villani, A. C. *et al.* (2017) 'Single-cell RNA-seq reveals new types of human blood dendritic cells, monocytes, and progenitors', *Science*. American Association for the Advancement of Science, 356(6335). doi: 10.1126/science.aah4573.

Vogt, K. L. *et al.* (2018) 'Priming and de-priming of neutrophil responses in vitro and in vivo', *European Journal of Clinical Investigation*, 48(January), pp. 1–9. doi: 10.1111/eci.12967.

Vono, M. *et al.* (2017) 'Neutrophils acquire the capacity for antigen presentation to memory CD4+ T cells in vitro and ex vivo', *Blood*. The American Society of Hematology, 129(14), p. 1991. doi: 10.1182/BLOOD-2016-10-744441.

Vorobjeva, N. V. and Chernyak, B. V. (2020) 'NETosis: Molecular Mechanisms, Role in Physiology and Pathology', *Biochemistry (Moscow)*, 85(10), pp. 1178–1190. doi: 10.1134/S0006297920100065.

Wade, N. *et al.* (2001) 'Syntaxin 7 Complexes with Mouse Vps10p Tail Interactor 1b, Syntaxin 6, Vesicle-associated Membrane Protein (VAMP)8, and VAMP7 in B16 Melanoma Cells', *Journal of Biological Chemistry*. American Society for Biochemistry and Molecular Biology, 276(23), pp. 19820–19827. doi: 10.1074/JBC.M010838200.

Wang, K. *et al.* (2022) 'Locally organised and activated Fth1hi neutrophils aggravate inflammation of acute lung injury in an IL-10-dependent manner', *Nature Communications*. Springer US, 13(1). doi: 10.1038/s41467-022-35492-y.

Wang, Y., Cipriano, D. J. and Forgac, M. (2007) 'Arrangement of subunits in the proteolipid ring of the V-ATPase', *The Journal of biological chemistry*. NIH Public Access, 282(47), p. 34058. doi: 10.1074/JBC.M704331200.

Weinberger, R. *et al.* (2018) 'Invasive pneumococcal disease in children under 16 years of age: Incomplete rebound in incidence after the maximum effect of PCV13 in 2012/13 in Germany', *Vaccine*. Elsevier Ltd, 36(4), pp. 572–577. doi: 10.1016/j.vaccine.2017.11.085.

Weischenfeldt, J. and Porse, B. (2008) 'Bone marrow-derived macrophages (BMM): Isolation and applications', *Cold Spring Harbor Protocols*, 3(12), pp. 1–7. doi: 10.1101/pdb.prot5080.

Wigerblad, G. *et al.* (2022) 'Single-Cell Analysis Reveals the Range of Transcriptional States of Circulating Human Neutrophils', *The Journal of Immunology*, 209(4), pp. 772–782. doi: 10.4049/jimmunol.2200154.

Wilson, H. L. *et al.* (2004) 'Secretion of Intracellular IL-1 Receptor Antagonist (Type 1) Is Dependent on P2X7 Receptor Activation', *The Journal of Immunology*. American Association of Immunologists, 173(2), pp. 1202–1208. doi: 10.4049/JIMMUNOL.173.2.1202.

Wilson, T. J., Blackledge, M. S. and Vigueira, P. A. (2018) 'Resensitization of methicillin-resistant Staphylococcus aureus by amoxapine, an FDA-approved antidepressant', *Heliyon*. Heliyon, 4(1). doi: 10.1016/J.HELIYON.2017.E00501.

Wing, M. *et al.* (2019) 'Antiviral activity of the FDA-approved drug candesartan cilexetil against Zika virus infection'. doi: 10.1016/j.antiviral.2019.104637.

Wood, A. J. T. *et al.* (2020) 'C5a impairs phagosomal maturation in the neutrophil through phosphoproteomic remodeling', *JCI Insight*, 5(15), pp. 1–16. doi: 10.1172/jci.insight.137029.

Wu, L. *et al.* (2020) 'Targeting DUSP7 signaling alleviates hepatic steatosis, inflammation and oxidative stress in high fat diet (HFD)-fed mice via suppression of TAK1', *Free Radical Biology and Medicine*. Elsevier Inc., 153, pp. 140–158. doi: 10.1016/j.freeradbiomed.2020.04.009.

Wu, M. *et al.* (2017) 'Immunomodulators targeting MARCO expression improve resistance to postinfluenza bacterial pneumonia', *American Journal of Physiology - Lung Cellular and Molecular Physiology*, 313(1), pp. L138–L153. doi: 10.1152/ajplung.00075.2017.

Wu, Y. *et al.* (2016) 'The transcriptional foundations of sp110-mediated macrophage (RAW264.7) resistance to mycobacterium tuberculosis H37Ra', *Scientific Reports*. Nature Publishing Group, 6(August 2015), pp. 1–15. doi: 10.1038/srep22041.

Yang, Z. *et al.* (2021) 'Major Outer Membrane Protein from Legionella pneumophila Inhibits Phagocytosis but Enhances Chemotaxis of RAW 264.7 Macrophages by Regulating the FOXO1/Coronin-1 Axis', *Journal of Immunology Research*, 2021. doi: 10.1155/2021/9409777.

Yang, Z. and Ming, X. F. (2014) 'Functions of arginase isoforms in macrophage inflammatory responses: Impact on cardiovascular diseases and metabolic disorders', *Frontiers in Immunology*, 5(OCT), pp. 1–10. doi: 10.3389/fimmu.2014.00533.

Yin, C. and Heit, B. (2018) 'Armed for destruction: formation, function and trafficking of neutrophil granules', *Cell and Tissue Research*. Springer Berlin Heidelberg, 371(3), pp. 455–471. doi: 10.1007/s00441-017-2731-8.

Yipp, B. G. and Kubes, P. (2013) 'NETosis: how vital is it?', *Blood*. American Society of Hematology, 122(16), pp. 2784–94. doi: 10.1182/blood-2013-04-457671.

Yu, L. *et al.* (2023) 'Heterogeneity of macrophages in atherosclerosis revealed by single-cell RNA sequencing.', *FASEB journal : official publication of the Federation of American Societies for Experimental Biology*, 37(3), p. e22810. doi: 10.1096/fj.202201932RR.

Yue, Y. *et al.* (2015) 'IL4I1 is a novel regulator of M2 macrophage polarization that can inhibit t cell activation via L-tryptophan and arginine depletion and IL-10 production', *PLoS ONE*, 10(11), pp. 1–19. doi: 10.1371/journal.pone.0142979.

Zagon, I. S. and McLaughlin, P. J. (2018) 'Intermittent blockade of OGFr and treatment of autoimmune disorders', *Experimental Biology and Medicine*. SAGE Publications Inc., pp. 1323–1330. doi: 10.1177/1535370218817746.

Zhang, H. *et al.* (2021) 'Exploration of novel candidate genes involved in epidermal keratinocyte differentiation and skin barrier repair in man', *Differentiation*. Elsevier Ltd, 119, pp. 19–27. doi: 10.1016/j.diff.2021.04.001.

Zhang, Q. *et al.* (2018) 'The Antihistamine Drugs Carbinoxamine Maleate and Chlorpheniramine Maleate Exhibit Potent Antiviral Activity Against a Broad Spectrum of Influenza Viruses'. doi: 10.3389/fmicb.2018.02643.

Zhao, C. *et al.* (2021) 'Identification of an alveolar macrophage-related core gene set in acute respiratory distress syndrome', *Journal of Inflammation Research*. Dove Medical Press Ltd, 14, pp. 2353–2361. doi: 10.2147/JIR.S306136.

Zhou, A. *et al.* (2021) 'Comprehensive Transcriptomic Analysis Identifies Novel Antiviral Factors Against Influenza A Virus Infection', *Frontiers in Immunology*. Frontiers Media S.A., 12, p. 632798. doi: 10.3389/fimmu.2021.632798.

Zwolak, A. *et al.* (2013) 'CARMIL leading edge localization depends on a non-canonical PH domain and dimerization', *Nature Communications*. NIH Public Access, 4, p. 2523. doi: 10.1038/ncomms3523.

8 Appendix A: RNA sequencing analysis code

Analysis code for RNA sequencing analysis in R Studio, adapted from courses delivered by Sheffield Bioinformatics Core.

```
```{r}
if (!requireNamespace("BiocManager", quietly = TRUE))
install.packages("BiocManager")
BiocManager::install("ensembldb")

if(!require(BiocManager)) install.packages("BiocManager")
BiocManager::install(c("limma",
         "org.Hs.eg.db",
         "RColorBrewer",
         "TxDb.Hsapiens.UCSC.hg38.knownGene",
         "goseq",
         "fgsea",
         "DESeq2",
         "pheatmap",
         "rmarkdown",
         "tximport",
         "clusterProfiler",
         "DOSE",
         "pathview",
         "biomaRt",
         "dplyr",
         "ggplot2"),suppressUpdates=TRUE)
```
```{r}
library(tximport)
dir <- "/Users/UOS/Documents/RNAseq project/MDM-2hr-
analysis/MDM2hr"
list.files(dir)
samples <- read.table(file.path(dir, "sample-info-MDM-
2hr.txt"), header = TRUE)
samples
```
```{r}
sampleinfo <- read.delim("/Users/UOS/Documents/RNAseq
project/MDM-2hr-analysis/MDM2hr/sample-info-MDM-2hr.txt")
```
```{r}
```
```

```
dirs <- dir("MDM2hr/quant")
quant_files <- list.files("MDM2hr/quant", pattern="quant.sf",
recursive = TRUE, full.names = TRUE)
names(quant_files) <- dirs
```
```{r}
install.packages("tidyverse")
```
```{r}
library(readr)
quants <- read_tsv(quant_files[1])
```
```{r}
gtf_file <- "Homo_sapiens.GRCh38.104.gft.gz"
```
```{r}
download.file("http://ftp.ensembl.org/pub/release-
104/gtf/homo_sapiens/Homo_sapiens.GRCh38.104.gtf.gz", destfile
= gtf_file)
file.exists(gtf_file)
```
```{r}
library(GenomicFeatures)
```
```{r}
txdb <- makeTxDbFromGFF(format="gtf", gtf_file)
```
```{r}
k <- keys(txdb, keytype = "TXNAME")
tx_map <- select(txdb, keys = k, columns="GENEID", keytype =
"TXNAME")
head(tx_map)
```
```{r}
tx2gene <- tx_map
txi <- tximport(quant_files,type="salmon",tx2gene =
tx2gene,ignoreTxVersion = TRUE)
```
```{r}
library(tidyr)
library(dplyr)
```

```{r}
quants<-separate(quants, Name, c("TXNAME", "Number"), remove =
FALSE)
head(quants)
```
```{r}
quants <- left_join(quants, tx_map, by="TXNAME")
head(quants)
```
```{r}
tx2gene <- dplyr:::select(quants, Name, GENEID)
head(tx2gene)
```
```{r}
any(is.na(tx2gene$GENEID))
```
```{r}
tx2gene <- filter(tx2gene, !is.na(GENEID))
```
```{r}
txi <- tximport(quant_files,type="salmon",tx2gene = tx2gene)
```
```{r}
all(rownames(sampleinfo) == colnames(txi$counts))
```
```{r}
library(DESeq2)
```
```{r}
dds <- DESeqDataSetFromTximport(txi,
                                colData = sampleinfo,
                                design <- ~Bead)
```
```{r}
library(RColorBrewer)
library(pheatmap)
library(tibble)
```
```{r}
colData(dds)
tmp <- txi$abundance
write.csv(tmp, file="tmp_values.csv", quote=FALSE)
```

```
```{r}
sum(assay(dds)[,1])
colSums(assay(dds))
```
```{r}
library(ggplot2)
library(ggrepel)
```
```{r}
barplot(colSums(assay(dds)), names = sampleinfo$Run)
```
```{r}
is_expressed <- assay(dds) >= 5
hist(rowSums(is_expressed),main="Number of samples a gene is
expressed in",xlab="Sample Count")
```
```{r}
keep <- rowSums(assay(dds) >= 5) >= 2
table(keep)
```
```{r}
dds <- dds[keep,]
boxplot(assay(dds))
```
```{r}
vsd <- vst(dds, blind=TRUE)
boxplot(assay(vsd), xlab="", ylab="Log2 counts per million",
las=2, main="Normalised Distribution")
abline(h=median(assay(vsd)), col="blue")
```
```{r}
sampleDists <- dist(t(assay(vsd)))
```
```{r}
library(RColorBrewer)
library(pheatmap)
```
```{r}
sampleDistMatrix <- as.matrix(sampleDists)
rownames(sampleDistMatrix) <- paste(colData(dds)$Bead, sep="-
")
```
```

```
colnames(sampleDistMatrix) <- colData(dds)$Name
colors <- colorRampPalette( rev(brewer.pal(9, "Blues")) )(255)
pheatmap(sampleDistMatrix,
         col=colors)
```
```{r}
plotPCA(vsd,intgroup="Bead") + geom_text_repel(aes(label =
sampleinfo$Run))
```
```{r}
install.packages(c("FactoMineR", "factoextra"))
library(FactoMineR)
library(factoextra)
```
```{r}
install.packages('ggfortify')
library(ggfortify)
df <- iris[1:4]
```
```{r}
design(dds) <- ~Bead
de.Bead <- DESeq(dds)
```
```{r}
library(tibble)
```
```{r}
results.Bead <- as.data.frame(results(de.Bead)) %>%
  rownames_to_column("GeneID")
results.Bead
```
```{r}
arrange(results.Bead, padj) %>%
  head(n=10)
```
```{r}
arrange(results.Bead, padj) %>%
write.csv("MDM2hr_all.csv")
```
```{r}
arrange(results.Bead, padj) %>%
  filter(padj < 0.05) %>%
```

```
  write.csv("MDM2hr_DE.csv")
```
```{r}
results.BeadZeroThree <- as.data.frame(results(de.Bead,
contrast=c("Bead","zero", "three"))) %>%
  rownames_to_column("ENSEMBL")
results.orderedZeroThree <- arrange(results.BeadZeroThree,
padj)
head(results.orderedZeroThree)
arrange(results.BeadZeroThree, padj) %>%
  filter(padj < 0.05) %>%
  write.csv("MDM2hr_zero_vs_three.csv")
```
```{r}
results.BeadOneThree <- as.data.frame(results(de.Bead,
contrast=c("Bead","one", "three"))) %>%
  rownames_to_column("ENSEMBL")
results.orderedOneThree <- arrange(results.BeadOneThree, padj)
head(results.orderedOneThree)
arrange(results.BeadOneThree, padj) %>%
  filter(padj < 0.05) %>%
  write.csv("MDM2hr_one_vs_three.csv")
```
```{r}
results.BeadZeroOne <- as.data.frame(results(de.Bead,
contrast=c("Bead","zero", "one"))) %>%
  rownames_to_column("ENSEMBL")
results.orderedZeroOne <- arrange(results.BeadZeroOne, padj)
head(results.orderedZeroOne)
arrange(results.BeadZeroOne, padj) %>%
  filter(padj < 0.05) %>%
  write.csv("MDM2hr_zero_vs_one.csv")
```
```{r}
BiocManager::install("org.Hs.eg.db")
library(org.Hs.eg.db)
columns(org.Hs.eg.db)
```
```{r}
keys(org.Hs.eg.db, keytype="ENSEMBL")[1:10]
```

#0 v 3 – analysis for DEGs between non-phagocytic cells (zero/0) and super-ingester cells (three/3). Subsequent analysis code is not included for ‘zero’ v. ‘one’.

```{r}
anno0_3 <-
AnnotationDbi::select(org.Hs.eg.db,keys=results.BeadZeroThree$
ENSEMBL,
              columns=c("SYMBOL","GENENAME"),
              keytype="ENSEMBL")
```
```{r}
dim(anno0_3)
```
```{r}
dim(results.orderedZeroThree)
```
```{r}
dup_ids0_3 <- anno0_3$ENSEMBL[duplicated(anno0_3$ENSEMBL)]
filter(anno0_3, ENSEMBL %in% dup_ids0_3) %>%
  arrange(ENSEMBL) %>% head
```
```{r}
anno0_3 <-
AnnotationDbi::select(org.Hs.eg.db,keys=results.orderedZeroThr
ee$ENSEMBL,
columns=c("ENSEMBL","SYMBOL","GENENAME","ENTREZID"),
              keytype="ENSEMBL") %>%
  filter(!duplicated(ENSEMBL))
dim(anno0_3)
```
```{r}
results.annotated0_3 <- left_join(results.orderedZeroThree,
anno0_3,by="ENSEMBL")
head(results.annotated0_3)
```
```{r}
write.csv(results.annotated0_3,file="MDM2hr_Zero_v_Three_DESeq
_annotated.csv",row.names=FALSE)
```
```{r}
top_genes0_3 <- results.annotated0_3$ENSEMBL[1:10]
vsd <- vst(dds)
```

```
pheatmap(assay(vsd)[top_genes0_3,])
```
```{r}
png("heatmap_top10_genes_MDM2hr_0_3.png",width=800,height=800)
pheatmap(assay(vsd)[top_genes0_3,])
```
```{r}
N <- 10
top_genes0_3 <- results.annotated0_3$ENSEMBL[1:N]
results.annotated0_3 %>%
  mutate(Label = ifelse(ENSEMBL %in% top_genes0_3, "SYMBOL"))
%>%
  pheatmap(assay(vsd)[top_genes0_3,])
```
```{r}
if(!require(ggrepel)) install.packages("ggrepel")
results.annotated0_3 %>%
  mutate(Label = ifelse(ENSEMBL %in% top_genes0_3, SYMBOL,
"")) %>%
  ggplot(aes(x = log2FoldChange, y = -log10(padj),
label=Label)) + geom_point(alpha=0.4) +
geom_text_repel(col="blue")
```
```{r}
if (!requireNamespace("BiocManager", quietly = TRUE))
    install.packages("BiocManager")
BiocManager::install("Glimma")
library(Glimma)
```
```{r}
results <- results.BeadZeroThree
anno0_3 <-
AnnotationDbi::select(org.Hs.eg.db,keys=rownames(results),
              columns=c("SYMBOL","GENENAME"),
              keytype="ENSEMBL") %>%
  filter(!duplicated(ENSEMBL))
```
```{r}
dds <- estimateSizeFactors(dds)
```
```{r}
glMDPlot(results,
```

```
        anno0_3,
        groups = colData(dds)$Bead,
        counts = counts(dds,normalized=TRUE),
        transform = TRUE,
        side.main = "ENSEMBL")
```
```{r}
gseaInput0_3 <- filter(results.annotated0_3, !is.na(ENTREZID))
%>%
  arrange(stat)
ranks0_3 <- pull(gseaInput0_3,stat)
names(ranks0_3) <- gseaInput0_3$ENTREZID
```
```{r}
load("human_H_v5p2.rdata")
pathways <- Hs.H
```
```{r}
library(fgsea)
fgseaRes0_3 <- fgsea(pathways, ranks0_3, minSize=15, maxSize =
500, nperm=1000)
```
```{r}
dim(fgseaRes0_3)
```
```{r}
fgseaResTidy0_3 <- fgseaRes0_3 %>%
  as_tibble() %>%
  arrange(desc(NES))
fgseaResTidy0_3
```

```{r}
library(ggplot2)
ggplot(fgseaResTidy0_3, aes(reorder(pathway, NES), NES)) +
  geom_col(aes(fill=padj<0.05)) +
  coord_flip() +
  labs(x="Pathway", y="Normalized Enrichment Score",
       title="Hallmark pathways NES from GSEA")
```
```{r}
library(pheatmap)
```

```
my_genes0_3 <- filter(results.annotated0_3, ENTREZID %in%
pathways[["HALLMARK_MYC_TARGETS_V1"]]) %>%
  pull(ENSEMBL)
```
```{r}
mat0_3 <- assay(vsd)[my_genes0_3,]
mat0_3 <- mat0_3 - rowMeans(mat0_3)
dim(mat0_3)
```
```{r}
rownames(sampleinfo) <- sampleinfo$run
pheatmap(mat0_3)
```
```{r}
library(clusterProfiler)
universe0_3 <- results.annotated0_3 %>% pull(ENTREZID)
sigGenes0_3 <- results.annotated0_3 %>%
  filter(padj < 0.05, !is.na(ENTREZID)) %>% pull(ENTREZID)
enrich_go0_3 <- enrichGO(
  gene= sigGenes0_3,
  OrgDb = org.Hs.eg.db,
  keyType = "ENTREZID",
  ont = "BP",
  universe = universe0_3,
  qvalueCutoff = 0.05,
  readable=TRUE
)
```
```{r}
dotplot(enrich_go0_3)
```

9 Appendix B: RNA sequencing data

All differentially expressed genes shown in Appendix B are compared to non-phagocytic MDMs at the stated time-point. DEGs were classified as significant if they fit the criteria of $p<0.05$ and $|\log_2FC|>1$. However, shown here are DEGs that have associated padj values<0.05 and $|\log_2FC|>2$ or $|\log_2FC|<-2$. A negative fold change value represents genes that are significantly downregulated.

Table B1: DEGs in MDMs that have phagocytosed 1-2 beads compared to non-phagocytic MDMs at 2 hours post-challenge with latex beads.

Gene symbol	Gene name	padj	Log2FC
TRIM54	tripartite motif containing 54	4.74E-13	-3.379
KCNJ1	potassium inwardly rectifying channel subfamily J member 1	8.00E-13	-3.063
ANKRD36B	ankyrin repeat domain 36B	1.45E-10	-2.022
ATL1	atlastin GTPase 1	3.52E-09	-2.648
RNASE2	ribonuclease A family member 2	1.90E-08	2.263
PLCL1	phospholipase C like 1 (inactive)	6.38E-08	-2.805
SH3RF2	SH3 domain containing ring finger 2	6.38E-08	-2.932
FCN1	ficolin 1	9.07E-08	3.096
MARCO	macrophage receptor with collagenous structure	2.08E-07	3.036
RNF128	ring finger protein 128	2.14E-07	-2.310
MAP7	microtubule associated protein 7	6.35E-07	-2.428
COLQ	collagen like tail subunit of asymmetric acetylcholinesterase	9.31E-07	-2.527
DGCR6	DiGeorge syndrome critical region gene 6	1.69E-06	2.639
C11orf45	chromosome 11 open reading frame 45	2.68E-06	-2.024
SLC1A2	solute carrier family 1 member 2	3.55E-06	-2.206
CSRP2	cysteine and glycine rich protein 2	4.39E-06	-2.724
DSP	desmoplakin	4.85E-06	-3.507
SUCNR1	succinate receptor 1	5.04E-06	-2.440
MMP2	matrix metallopeptidase 2	5.04E-06	4.740
SLC30A3	solute carrier family 30 member 3	5.14E-06	-2.200
BNC2	basonuclin 2	1.06E-05	2.209
GPER1	G protein-coupled estrogen receptor 1	2.95E-05	-2.392
SYNC	syncoilin, intermediate filament protein	4.78E-05	-6.828
P2RY6	pyrimidinergic receptor P2Y6	9.34E-05	5.393
GALNT12	polypeptide N-acetylgalactosaminyltransferase 12	0.00015	-2.279
IGF1	insulin like growth factor 1	0.00015	3.211
NCF1B	neutrophil cytosolic factor 1B pseudogene	0.00016	3.291
STAB1	stabilin 1	0.00022	2.466
TEAD3	TEA domain transcription factor 3	0.00025	-4.071
IFNAR2	interferon alpha and beta receptor subunit 2	0.00060	2.601

NCKAP1	NCK associated protein 1	0.00100	-2.160
NFKBIA	NFKB inhibitor alpha	0.00116	5.190
ITM2B	integral membrane protein 2B	0.00151	2.100
CCL4	C-C motif chemokine ligand 4	0.00170	3.216
CARMIL1	capping protein regulator and myosin 1 linker 1	0.00171	-2.449
NHSL2	NHS like 2	0.00180	-2.522
MMP12	matrix metallopeptidase 12	0.00184	-2.271
NPR1	natriuretic peptide receptor 1	0.00188	-3.266
RYR1	ryanodine receptor 1	0.00217	-2.528
KIAA1210	KIAA1210	0.00233	-2.123
ADRA2B	adrenoceptor alpha 2B	0.00261	-2.315
SLC46A1	solute carrier family 46 member 1	0.00289	2.512
PLS1	plastin 1	0.00289	-2.959
CD14	CD14 molecule	0.00295	3.411
CPEB1	cytoplasmic polyadenylation element binding protein 1	0.00431	-2.361
PPM1E	protein phosphatase, Mg2+/Mn2+ dependent 1E	0.00451	-3.589
CD79A	CD79a molecule	0.00574	-2.294
TMEM26	transmembrane protein 26	0.00641	3.552
TIMP4	TIMP metallopeptidase inhibitor 4	0.00769	-3.365
DAAM1	dishevelled associated activator of morphogenesis 1	0.00798	-2.126
SYT1	synaptotagmin 1	0.00812	2.542
B3GALNT1	beta-1,3-N-acetylgalactosaminyltransferase 1 (globoside blood group)	0.00857	2.320
CETP	cholesteryl ester transfer protein	0.01013	2.375
FANCE	FA complementation group E	0.01013	-2.324
KCNA10	potassium voltage-gated channel subfamily A member 10	0.01020	-2.302
SHISA2	shisa family member 2	0.01116	-2.148
ATP2B4	ATPase plasma membrane Ca2+ transporting 4	0.01116	-2.235
HPD	4-hydroxyphenylpyruvate dioxygenase	0.01116	-3.987
CFP	complement factor properdin	0.01116	2.671
CCL22	C-C motif chemokine ligand 22	0.01133	-2.344
MAP1A	microtubule associated protein 1A	0.01513	-2.071
FER1L6	fer-1 like family member 6	0.01659	-5.468
KCNJ10	potassium inwardly rectifying channel subfamily J member 10	0.01726	2.296
HS3ST1	heparan sulfate-glucosamine 3-sulfotransferase 1	0.02179	3.696
PLAU	plasminogen activator, urokinase	0.02194	2.385
SEC14L2	SEC14 like lipid binding 2	0.02389	-2.118
PRSS30P	serine protease 30, pseudogene	0.02524	-3.437
SORBS1	sorbin and SH3 domain containing 1	0.02889	-3.169
C1QB	complement C1q B chain	0.02923	2.097
CCNA1	cyclin A1	0.02942	-2.162
COL11A2	collagen type XI alpha 2 chain	0.02960	-3.737
CCL2	C-C motif chemokine ligand 2	0.03029	2.070
AIF1	allograft inflammatory factor 1	0.03171	4.264
EXT1	exostosin glycosyltransferase 1	0.03171	2.283

TMEM114	transmembrane protein 114	0.03216	-2.148
DUSP13	dual specificity phosphatase 13	0.03467	-2.119
ALPK3	alpha kinase 3	0.03467	-2.805
SUSD4	sushi domain containing 4	0.03486	-4.747
PRG2	proteoglycan 2, pro eosinophil major basic protein	0.03885	-3.861
MS4A6A	membrane spanning 4-domains A6A	0.03968	2.318
MRGPRF	MAS related GPR family member F	0.04003	-2.209
GNAL	G protein subunit alpha L	0.04174	-2.165
PCDHGC3	protocadherin gamma subfamily C, 3	0.04232	-2.208
C1QC	complement C1q C chain	0.04397	3.588
C1QA	complement C1q A chain	0.04428	2.310
CYP4X1	cytochrome P450 family 4 subfamily X member 1	0.04541	-2.104
OCSTAMP	osteoclast stimulatory transmembrane protein	0.04541	-2.414
TMEM37	transmembrane protein 37	0.04541	2.808
ZC2HC1C	zinc finger C2HC-type containing 1C	0.04611	-2.264
RHBDF1	rhomboid 5 homolog 1	0.04837	-2.032

Table B2: DEGs in MDMs that have phagocytosed 3 beads compared to non-phagocytic MDMs at 2 hours post-challenge with latex beads.

Gene symbol	Gene name	padj	Log2FC
ANKRD36B	ankyrin repeat domain 36B	2.76E-24	-3.067
TRIM54	tripartite motif containing 54	2.98E-24	-6.299
KCNJ1	potassium inwardly rectifying channel subfamily J member 1	4.10E-22	-4.406
STMN1	stathmin 1	4.93E-21	2.177
C1QC	complement C1q C chain	5.49E-20	4.723
C11orf45	chromosome 11 open reading frame 45	1.17E-19	-3.462
CTTN	cortactin	3.43E-17	-2.653
C1QA	complement C1q A chain	3.87E-17	4.372
CSRP2	cysteine and glycine rich protein 2	3.06E-16	-4.350
CCL2	C-C motif chemokine ligand 2	1.03E-15	5.666
TSPAN4	tetraspanin 4	5.40E-15	2.437
TBC1D2B	TBC1 domain family member 2B	1.45E-14	-2.561
PLCD1	phospholipase C delta 1	1.45E-14	-2.800
TMEM273	transmembrane protein 273	1.70E-14	2.511
CYP27B1	cytochrome P450 family 27 subfamily B member 1	5.45E-14	-2.330
EFR3B	EFR3 homolog B	6.47E-14	-2.673
SLC30A3	solute carrier family 30 member 3	6.47E-14	-3.676
RNF128	ring finger protein 128	1.57E-13	-3.169
SLC1A2	solute carrier family 1 member 2	1.57E-13	-3.204
TMEM37	transmembrane protein 37	2.17E-13	2.670
CD74	CD74 molecule	5.18E-13	2.535
MS4A6A	membrane spanning 4-domains A6A	1.23E-12	3.481
GPER1	G protein-coupled estrogen receptor 1	1.87E-12	-4.069
KIAA1210	KIAA1210	2.24E-12	-4.146
AIF1	allograft inflammatory factor 1	2.41E-12	3.088
SLC28A3	solute carrier family 28 member 3	3.78E-12	-3.089
MAP7	microtubule associated protein 7	3.78E-12	-3.176
IL18	interleukin 18	3.96E-12	2.719
ATL1	atlastin GTPase 1	4.19E-12	-2.883
GPC4	glypican 4	6.60E-12	-5.204
IL4I1	interleukin 4 induced 1	7.72E-12	2.646
NCAPH	non-SMC condensin I complex subunit H	8.21E-12	-3.149
FCGR3A	Fc fragment of IgG receptor IIIa	1.28E-11	2.479
PLCL1	phospholipase C like 1 (inactive)	2.41E-11	-3.298
GALNT12	polypeptide N-acetylgalactosaminyltransferase 12	2.41E-11	-3.505
PLAU	plasminogen activator, urokinase	3.72E-11	3.730
COLQ	collagen like tail subunit of asymmetric acetylcholinesterase	3.72E-11	-3.181
NCKAP1	NCK associated protein 1	3.88E-11	-3.611
RETREG1	reticulophagy regulator 1	7.05E-11	-4.381
PSD3	pleckstrin and Sec7 domain containing 3	1.08E-10	-2.465
ASPHD1	aspartate beta-hydroxylase domain containing 1	1.47E-10	-2.365

SH3RF2	SH3 domain containing ring finger 2	1.73E-10	-3.212
LRRC8A	leucine rich repeat containing 8 VRAC subunit A	4.06E-10	-2.536
MPEG1	macrophage expressed 1	5.77E-10	2.636
DHRS9	dehydrogenase/reductase 9	7.76E-10	-2.746
RHOC	ras homolog family member C	8.58E-10	-2.116
CSPG4	chondroitin sulfate proteoglycan 4	9.49E-10	-4.068
CCL22	C-C motif chemokine ligand 22	1.66E-09	-4.241
C1QB	complement C1q B chain	3.42E-09	4.397
ECE1	endothelin converting enzyme 1	3.57E-09	-2.763
TGFBI	transforming growth factor beta induced	3.60E-09	3.673
AOC1	amine oxidase copper containing 1	3.93E-09	-2.439
DSP	desmoplakin	3.93E-09	-4.376
MARCKS	myristoylated alanine rich protein kinase C substrate	4.07E-09	2.859
TIE1	tyrosine kinase with immunoglobulin like and EGF like domains 1	5.04E-09	-2.226
MRC2	mannose receptor C type 2	5.18E-09	2.358
COL8A2	collagen type VIII alpha 2 chain	5.18E-09	-2.356
TSPAN17	tetraspanin 17	5.54E-09	-3.186
ADRA2B	adrenoceptor alpha 2B	5.81E-09	-3.718
CLU	clusterin	1.04E-08	-3.029
CCL3	C-C motif chemokine ligand 3	1.13E-08	2.904
C3AR1	complement C3a receptor 1	1.45E-08	2.452
KCTD9	potassium channel tetramerization domain containing 9	1.93E-08	-2.561
CCNA1	cyclin A1	2.13E-08	-4.320
RPS13	ribosomal protein S13	2.25E-08	2.073
EMP3	epithelial membrane protein 3	2.53E-08	2.117
MMP12	matrix metallopeptidase 12	2.59E-08	-3.378
RPL18A	ribosomal protein L18a	3.28E-08	2.228
STEAP3	STEAP3 metalloreductase	3.28E-08	2.181
TMEM114	transmembrane protein 114	4.74E-08	-4.242
HS3ST1	heparan sulfate-glucosamine 3-sulfotransferase 1	5.04E-08	3.499
RPLP1	ribosomal protein lateral stalk subunit P1	5.04E-08	2.457
IL1RN	interleukin 1 receptor antagonist	5.72E-08	-2.709
OCSTAMP	osteoclast stimulatory transmembrane protein	6.67E-08	-5.319
MDK	midkine	7.72E-08	-3.237
SYNGR1	synaptogyrin 1	8.06E-08	-3.056
SSBP3	single stranded DNA binding protein 3	9.94E-08	-2.766
CD79A	CD79a molecule	1.01E-07	-4.397
DOCK3	dedicator of cytokinesis 3	1.03E-07	-2.129
ARHGEF10L	Rho guanine nucleotide exchange factor 10 like	1.39E-07	2.270
TNFSF13B	TNF superfamily member 13b	1.88E-07	2.250
CPEB1	cytoplasmic polyadenylation element binding protein 1	1.90E-07	-4.098
TEAD3	TEA domain transcription factor 3	2.21E-07	-6.137
GAL	galanin and GMAP prepropeptide	2.34E-07	-9.740
CRABP2	cellular retinoic acid binding protein 2	2.58E-07	-3.330
FANCE	FA complementation group E	2.60E-07	-4.300

CMKLR1	chemerin chemokine-like receptor 1	2.62E-07	2.464
MARCO	macrophage receptor with collagenous structure	2.81E-07	4.222
FCGR2B	Fc fragment of IgG receptor IIb	2.95E-07	2.509
ZFP36	ZFP36 ring finger protein	3.23E-07	2.354
SIGLEC11	sialic acid binding Ig like lectin 11	3.43E-07	2.640
RGS20	regulator of G protein signaling 20	4.31E-07	-2.881
RPLP0	ribosomal protein lateral stalk subunit P0	4.90E-07	2.195
LDLRAP1	low density lipoprotein receptor adaptor protein 1	5.16E-07	-2.503
FPR3	formyl peptide receptor 3	5.20E-07	2.572
COL9A2	collagen type IX alpha 2 chain	5.46E-07	-4.262
ACP6	acid phosphatase 6, lysophosphatidic	6.24E-07	-3.049
PLS1	plastin 1	7.20E-07	-4.213
EHD3	EH domain containing 3	8.13E-07	-2.967
RPL28	ribosomal protein L28	8.90E-07	2.464
RPS12	ribosomal protein S12	1.01E-06	2.845
METTL9	methyltransferase like 9	1.01E-06	-3.467
CD14	CD14 molecule	1.07E-06	3.721
PCDHGC3	protocadherin gamma subfamily C, 3	1.10E-06	-4.815
FUCA1	alpha-L-fucosidase 1	1.21E-06	2.525
RPL13	ribosomal protein L13	1.21E-06	2.250
EEF1G	eukaryotic translation elongation factor 1 gamma	1.21E-06	2.027
TIMP1	TIMP metallopeptidase inhibitor 1	1.27E-06	2.189
SELENOP	selenoprotein P	1.29E-06	2.999
USP2	ubiquitin specific peptidase 2	1.29E-06	-2.160
RPL10	ribosomal protein L10	1.40E-06	2.235
MMD	monocyte to macrophage differentiation associated	1.41E-06	2.664
RPL10A	ribosomal protein L10a	1.71E-06	2.115
RPS16	ribosomal protein S16	1.73E-06	2.322
PHACTR1	phosphatase and actin regulator 1	1.88E-06	2.318
ETV5	ETS variant transcription factor 5	1.95E-06	2.325
CFP	complement factor properdin	2.10E-06	2.652
CARMIL1	capping protein regulator and myosin 1 linker 1	2.10E-06	-3.127
LRRC8B	leucine rich repeat containing 8 VRAC subunit B	2.50E-06	-2.739
IFI30	IFI30 lysosomal thiol reductase	2.52E-06	2.380
RPS3A	ribosomal protein S3A	2.55E-06	2.400
RPL4	ribosomal protein L4	3.11E-06	2.158
RPS3	ribosomal protein S3	3.22E-06	2.141
CETP	cholesteryl ester transfer protein	3.71E-06	3.968
MYOZ1	myozenin 1	3.71E-06	-2.272
CCL4	C-C motif chemokine ligand 4	3.74E-06	3.347
SUCNR1	succinate receptor 1	3.74E-06	-2.302
B3GALNT1	beta-1,3-N-acetylgalactosaminyltransferase 1 (globoside blood group)	3.79E-06	3.224
DUSP13	dual specificity phosphatase 13	3.84E-06	-3.531
RPL6	ribosomal protein L6	3.93E-06	2.086
NPR1	natriuretic peptide receptor 1	4.14E-06	-5.438

RPS23	ribosomal protein S23	4.22E-06	2.461
SHISA2	shisa family member 2	4.26E-06	-3.288
IGFBP6	insulin like growth factor binding protein 6	4.42E-06	-3.317
VIM	vimentin	4.56E-06	2.418
OSM	oncostatin M	4.78E-06	2.779
RAI14	retinoic acid induced 14	4.88E-06	-2.225
STAB1	stabilin 1	4.90E-06	3.610
RNASE2	ribonuclease A family member 2	4.91E-06	5.612
LAT	linker for activation of T cells	5.06E-06	-2.722
TMSB4XP4	TMSB4X pseudogene 4	5.37E-06	2.273
RGS16	regulator of G protein signaling 16	5.37E-06	-2.742
PHKA1	phosphorylase kinase regulatory subunit alpha 1	5.88E-06	-3.449
ADM	adrenomedullin	5.92E-06	2.071
RPL12	ribosomal protein L12	5.92E-06	2.031
TOGARAM2	TOG array regulator of axonemal microtubules 2	5.93E-06	-2.067
RND3	Rho family GTPase 3	8.26E-06	3.326
MATK	megakaryocyte-associated tyrosine kinase	8.26E-06	-2.492
RPS29	ribosomal protein S29	8.77E-06	2.052
CTSC	cathepsin C	8.91E-06	2.062
MMP7	matrix metallopeptidase 7	9.99E-06	-3.676
EXT1	exostosin glycosyltransferase 1	1.03E-05	4.167
NPC2	NPC intracellular cholesterol transporter 2	1.10E-05	2.029
SCG5	secretogranin V	1.10E-05	-3.525
ADA	adenosine deaminase	1.11E-05	2.029
RPL15	ribosomal protein L15	1.16E-05	2.068
EEF1B2	eukaryotic translation elongation factor 1 beta 2	1.19E-05	2.161
MRGPRF	MAS related GPR family member F	1.20E-05	-3.773
RPLP2	ribosomal protein lateral stalk subunit P2	1.22E-05	2.094
RPS15A	ribosomal protein S15a	1.23E-05	2.096
TLN2	talin 2	1.31E-05	-2.711
MTMR1	myotubularin related protein 1	1.38E-05	-2.144
LAYN	layilin	1.44E-05	-3.366
RPL31	ribosomal protein L31	1.51E-05	2.352
RACK1	receptor for activated C kinase 1	1.51E-05	2.011
SLC6A12	solute carrier family 6 member 12	1.51E-05	-2.760
PPM1E	protein phosphatase, Mg2+/Mn2+ dependent 1E	1.51E-05	-5.339
ELOVL6	ELOVL fatty acid elongase 6	1.54E-05	-2.381
RPS25	ribosomal protein S25	1.58E-05	2.100
ALPK3	alpha kinase 3	1.65E-05	-4.702
RPL13A	ribosomal protein L13a	1.70E-05	2.301
RPS8	ribosomal protein S8	1.70E-05	2.276
TPT1	tumor protein, translationally-controlled 1	1.94E-05	2.268
RPL32	ribosomal protein L32	1.96E-05	2.040
RPS24	ribosomal protein S24	2.02E-05	2.404
DHRS11	dehydrogenase/reductase 11	2.03E-05	-2.886
MAP1A	microtubule associated protein 1A	2.05E-05	-2.971

ANXA6	annexin A6	2.07E-05	2.378
RPS6	ribosomal protein S6	2.07E-05	2.266
KCNA10	potassium voltage-gated channel subfamily A member 10	2.53E-05	-3.282
C2orf92	chromosome 2 open reading frame 92	2.79E-05	-2.275
RPS18	ribosomal protein S18	3.16E-05	2.100
INO80E	INO80 complex subunit E	3.33E-05	3.394
RPL27A	ribosomal protein L27a	3.39E-05	2.206
RPL3	ribosomal protein L3	3.43E-05	2.097
RPL24	ribosomal protein L24	3.44E-05	2.105
FCGR1B	Fc fragment of IgG receptor Ib	3.65E-05	2.237
SEMA7A	semaphorin 7A (John Milton Hagen blood group)	3.66E-05	-3.338
DEPP1	DEPP1 autophagy regulator	3.73E-05	-2.424
PMP22	peripheral myelin protein 22	3.76E-05	2.369
RAB5IF	RAB5 interacting factor	3.84E-05	-3.567
FCN1	ficolin 1	3.92E-05	4.250
GDA	guanine deaminase	3.97E-05	-2.028
RPL39	ribosomal protein L39	4.11E-05	2.192
GPC3	glypican 3	4.32E-05	-5.310
SLAMF7	SLAM family member 7	4.46E-05	-2.354
PLTP	phospholipid transfer protein	4.85E-05	2.618
RAB6B	RAB6B, member RAS oncogene family	5.06E-05	-3.960
TMEM26	transmembrane protein 26	5.46E-05	4.319
PERP	p53 apoptosis effector related to PMP22	5.59E-05	-3.875
TIMP4	TIMP metallopeptidase inhibitor 4	5.66E-05	-4.812
KCNA2	potassium voltage-gated channel subfamily A member 2	5.68E-05	-2.728
ANO5	anoctamin 5	5.81E-05	-2.924
SPR	sepiapterin reductase	6.17E-05	-4.208
MCOLN2	mucolipin TRP cation channel 2	6.26E-05	2.448
SLC6A7	solute carrier family 6 member 7	6.26E-05	-3.677
HPD	4-hydroxyphenylpyruvate dioxygenase	6.38E-05	-5.719
TRPV4	transient receptor potential cation channel subfamily V member 4	6.81E-05	2.574
SERPINA1	serpin family A member 1	6.83E-05	2.124
FXYD6	FXYD domain containing ion transport regulator 6	6.94E-05	2.508
GAPDH	glyceraldehyde-3-phosphate dehydrogenase	6.96E-05	2.179
RPS17	ribosomal protein S17	7.04E-05	2.269
RYR1	ryanodine receptor 1	7.49E-05	-2.872
DAAM1	dishevelled associated activator of morphogenesis 1	8.38E-05	-2.700
RPL36A	ribosomal protein L36a	0.00011	2.488
DIXDC1	DIX domain containing 1	0.00011	-2.289
RPS7	ribosomal protein S7	0.00012	2.035
MMP2	matrix metallopeptidase 2	0.00012	3.257
CD163	CD163 molecule	0.00013	4.165
CXCL2	C-X-C motif chemokine ligand 2	0.00014	3.314
RAB11FIP4	RAB11 family interacting protein 4	0.00014	-2.267
SDC1	syndecan 1	0.00015	-5.577

HSPB7	heat shock protein family B (small) member 7	0.00017	-6.702
SLAMF6	SLAM family member 6	0.00017	-2.105
PLA2G2D	phospholipase A2 group IID	0.00019	3.023
GPR183	G protein-coupled receptor 183	0.00019	2.708
MYCL	MYCL proto-oncogene, bHLH transcription factor	0.00020	-2.759
CYP4X1	cytochrome P450 family 4 subfamily X member 1	0.00020	-3.231
HLA-DPA1	major histocompatibility complex, class II, DP alpha 1	0.00021	2.554
RPL23A	ribosomal protein L23a	0.00021	2.124
OLFML2B	olfactomedin like 2B	0.00022	3.201
ZNF480	zinc finger protein 480	0.00023	2.517
MYH10	myosin heavy chain 10	0.00023	-4.139
RPL37	ribosomal protein L37	0.00024	2.059
TERF2IP	TERF2 interacting protein	0.00024	-3.162
CD38	CD38 molecule	0.00024	2.375
RPL9	ribosomal protein L9	0.00026	2.064
TDRD9	tudor domain containing 9	0.00029	-2.597
UGT3A1	UDP glycosyltransferase family 3 member A1	0.00030	-3.859
CTSL	cathepsin L	0.00031	2.155
CHPF	chondroitin polymerizing factor	0.00032	-3.497
ADARB1	adenosine deaminase RNA specific B1	0.00035	-2.442
RPL14	ribosomal protein L14	0.00036	2.067
BAG3	BAG cochaperone 3	0.00038	-2.619
TIFAB	TIFA inhibitor	0.00039	2.329
BCAN	brevican	0.00039	-5.295
RPS27A	ribosomal protein S27a	0.00040	2.291
EPHB1	EPH receptor B1	0.00044	-2.563
ATP2B4	ATPase plasma membrane Ca2+ transporting 4	0.00044	-2.580
ZBTB7C	zinc finger and BTB domain containing 7C	0.00044	-3.392
TMEM163	transmembrane protein 163	0.00046	2.460
RPL11	ribosomal protein L11	0.00048	2.124
H2BC4	H2B clustered histone 4	0.00049	-2.464
STK17A	serine/threonine kinase 17a	0.00051	-2.885
PTGIR	prostaglandin I2 receptor	0.00052	2.412
SPON2	spondin 2	0.00052	-3.060
MFSD4A	major facilitator superfamily domain containing 4A	0.00052	-2.256
CDIPT	CDP-diacylglycerol--inositol 3-phosphatidyltransferase	0.00054	-2.484
SORBS1	sorbin and SH3 domain containing 1	0.00056	-4.482
SPINT1	serine peptidase inhibitor, Kunitz type 1	0.00058	-2.002
CCDC27	coiled-coil domain containing 27	0.00060	2.152
ACAT2	acetyl-CoA acetyltransferase 2	0.00068	-2.487
SLC49A3	solute carrier family 49 member 3	0.00073	-3.256
JDP2	Jun dimerization protein 2	0.00074	2.185
RHBDF1	rhomboid 5 homolog 1	0.00078	-2.693
IQGAP3	IQ motif containing GTPase activating protein 3	0.00079	-2.661
EEF1A1	eukaryotic translation elongation factor 1 alpha 1	0.00081	2.436
CAVIN1	caveolae associated protein 1	0.00083	-2.648

TBX21	T-box transcription factor 21	0.00085	-4.856
FOSL1	FOS like 1, AP-1 transcription factor subunit	0.00088	2.149
CHMP4C	charged multivesicular body protein 4C	0.00088	-2.035
DNTTIP1	deoxynucleotidyltransferase terminal interacting protein 1	0.00090	-2.479
AFAP1L1	actin filament associated protein 1 like 1	0.00092	-2.797
GAL3ST4	galactose-3-O-sulfotransferase 4	0.00096	2.543
TOMM40	translocase of outer mitochondrial membrane 40	0.00097	-2.997
KCNJ10	potassium inwardly rectifying channel subfamily J member 10	0.00098	4.734
MEP1A	meprin A subunit alpha	0.00099	-3.048
OTOAP1	OTOA pseudogene 1	0.00105	2.232
COL11A2	collagen type XI alpha 2 chain	0.00106	-4.891
HAMP	hepcidin antimicrobial peptide	0.00111	2.236
P2RY6	pyrimidinergic receptor P2Y6	0.00114	2.711
HPGDS	hematopoietic prostaglandin D synthase	0.00118	-2.219
DUSP2	dual specificity phosphatase 2	0.00140	-2.265
TMEM102	transmembrane protein 102	0.00141	-6.291
CD93	CD93 molecule	0.00143	3.132
PDGFRA	platelet derived growth factor receptor alpha	0.00161	-3.486
ITGB3	integrin subunit beta 3	0.00161	-2.423
MAP3K11	mitogen-activated protein kinase kinase kinase 11	0.00162	-2.082
LILRB5	leukocyte immunoglobulin like receptor B5	0.00162	2.274
HPSE	heparanase	0.00172	2.625
LTB4R	leukotriene B4 receptor	0.00173	-3.301
UBTD1	ubiquitin domain containing 1	0.00178	-2.163
RNASE1	ribonuclease A family member 1, pancreatic	0.00179	3.989
RPL5	ribosomal protein L5	0.00179	2.454
CPNE6	copine 6	0.00179	-4.675
DUSP7	dual specificity phosphatase 7	0.00183	-2.112
PROS1	protein S	0.00192	-2.482
MYL9	myosin light chain 9	0.00193	-2.490
FCMR	Fc fragment of IgM receptor	0.00196	-2.452
TIMP3	TIMP metallopeptidase inhibitor 3	0.00196	-2.197
EBI3	Epstein-Barr virus induced 3	0.00207	3.450
SEPTIN4	septin 4	0.00214	-4.302
NCF1B	neutrophil cytosolic factor 1B pseudogene	0.00214	2.353
SIGLEC15	sialic acid binding Ig like lectin 15	0.00240	-4.151
CACNA2D4	calcium voltage-gated channel auxiliary subunit alpha2delta 4	0.00241	2.235
SEC14L2	SEC14 like lipid binding 2	0.00243	-2.353
FBXO32	F-box protein 32	0.00248	-3.098
EPDR1	ependymin related 1	0.00256	-3.427
GPAT2	glycerol-3-phosphate acyltransferase 2, mitochondrial	0.00269	-2.662
ALPL	alkaline phosphatase, biomineralization associated	0.00271	-5.199
SH3PXD2B	SH3 and PX domains 2B	0.00281	2.604
ARFGEF3	ARFGEF family member 3	0.00281	-2.538

EPSTI1	epithelial stromal interaction 1	0.00283	2.171
THEM6	thioesterase superfamily member 6	0.00292	-2.801
OGFR	opioid growth factor receptor	0.00298	-3.342
TRADD	TNFRSF1A associated via death domain	0.00311	-3.464
SPSB1	splA/ryanodine receptor domain and SOCS box containing 1	0.00314	-2.746
VWF	von Willebrand factor	0.00339	-2.836
IGF1	insulin like growth factor 1	0.00354	2.221
DNAJC1	DnaJ heat shock protein family (Hsp40) member C1	0.00354	-3.051
AKR7A2	aldo-keto reductase family 7 member A2	0.00356	-3.639
TMIGD3	transmembrane and immunoglobulin domain containing 3	0.00360	2.151
TMEM119	transmembrane protein 119	0.00360	3.497
ACAP3	ArfGAP with coiled-coil, ankyrin repeat and PH domains 3	0.00362	-4.126
HTR7	5-hydroxytryptamine receptor 7	0.00364	4.178
KLK13	kallikrein related peptidase 13	0.00376	-3.871
IL24	interleukin 24	0.00377	-2.095
MEIKIN	meiotic kinetochore factor	0.00377	-2.205
RAP1GAP	RAP1 GTPase activating protein	0.00378	-2.813
EMILIN1	elastin microfibril interfacer 1	0.00384	-4.267
SH2D3C	SH2 domain containing 3C	0.00388	-2.177
LYPD1	LY6/PLAUR domain containing 1	0.00411	3.970
GCNT4	glucosaminyl (N-acetyl) transferase 4	0.00416	-3.656
FDX1	ferredoxin 1	0.00432	-2.498
RBPMS2	RNA binding protein, mRNA processing factor 2	0.00440	-4.920
CXCL3	C-X-C motif chemokine ligand 3	0.00454	2.961
CCL8	C-C motif chemokine ligand 8	0.00455	3.505
FA2H	fatty acid 2-hydroxylase	0.00457	-3.866
RPL9P8	ribosomal protein L9 pseudogene 8	0.00464	2.213
ROCK1P1	Rho associated coiled-coil containing protein kinase 1 pseudogene 1	0.00483	-4.435
AGPS	alkylglycerone phosphate synthase	0.00488	-2.190
VSIG4	V-set and immunoglobulin domain containing 4	0.00492	2.380
TUBA1C	tubulin alpha 1c	0.00536	2.235
NEFH	neurofilament heavy chain	0.00536	-2.325
VAT1L	vesicle amine transport 1 like	0.00548	-3.845
HECTD3	HECT domain E3 ubiquitin protein ligase 3	0.00553	-2.218
CLEC5A	C-type lectin domain containing 5A	0.00577	3.495
SIGLEC1	sialic acid binding Ig like lectin 1	0.00581	2.637
GJA5	gap junction protein alpha 5	0.00584	-3.331
SLC25A38	solute carrier family 25 member 38	0.00587	2.729
HPCAL1	hippocalcin like 1	0.00601	-2.554
SDF4	stromal cell derived factor 4	0.00640	-4.444
AP1M2	adaptor related protein complex 1 subunit mu 2	0.00665	-3.970
HPGD	15-hydroxyprostaglandin dehydrogenase	0.00669	-2.006
SYNC	syncoilin, intermediate filament protein	0.00676	-3.667
MYC	MYC proto-oncogene, bHLH transcription factor	0.00683	2.317
LANCL3	LanC like 3	0.00711	-2.367

CSNK1G3	casein kinase 1 gamma 3	0.00746	-2.330
LILRA2	leukocyte immunoglobulin like receptor A2	0.00746	-2.717
ZC2HC1C	zinc finger C2HC-type containing 1C	0.00789	-2.372
TRIB2	tribbles pseudokinase 2	0.00827	5.912
RAB37	RAB37, member RAS oncogene family	0.00869	-2.059
NCF1C	neutrophil cytosolic factor 1C pseudogene	0.00872	2.041
RPP25	ribonuclease P and MRP subunit p25	0.00886	-3.224
KLHDC2	kelch domain containing 2	0.00896	-2.083
KIAA1522	KIAA1522	0.00921	-2.742
SLC9A7P1	solute carrier family 9 member 7 pseudogene 1	0.00932	-2.249
MEN1	menin 1	0.00966	-3.118
DUSP4	dual specificity phosphatase 4	0.00999	2.447
BAALC	BAALC binder of MAP3K1 and KLF4	0.00999	-2.995
NHSL2	NHS like 2	0.01006	-2.018
UBXN10	UBX domain protein 10	0.01008	-4.028
DEPDC1B	DEP domain containing 1B	0.01055	2.255
ZNF827	zinc finger protein 827	0.01090	-3.081
POTEJ	POTE ankyrin domain family member J	0.01129	3.929
DEXI	Dexi homolog	0.01141	-3.980
STAC	SH3 and cysteine rich domain	0.01176	-4.213
XBP1	X-box binding protein 1	0.01184	-2.270
VCAM1	vascular cell adhesion molecule 1	0.01260	2.549
NIPAL2	NIPA like domain containing 2	0.01263	-2.196
S1PR4	sphingosine-1-phosphate receptor 4	0.01291	-3.356
HTR2B	5-hydroxytryptamine receptor 2B	0.01307	2.659
AKIRIN1	akirin 1	0.01317	-2.196
CHST13	carbohydrate sulfotransferase 13	0.01347	-4.022
KCTD5	potassium channel tetramerization domain containing 5	0.01350	-2.054
OR6C75	olfactory receptor family 6 subfamily C member 75	0.01351	-2.192
RASAL1	RAS protein activator like 1	0.01371	2.562
NES	nestin	0.01384	-3.591
GOLPH3	golgi phosphoprotein 3	0.01415	-2.550
LTBP2	latent transforming growth factor beta binding protein 2	0.01416	2.466
GPA33	glycoprotein A33	0.01424	-2.375
ACAA1	acetyl-CoA acyltransferase 1	0.01426	-2.113
FUT7	fucosyltransferase 7	0.01454	4.297
ANKRD6	ankyrin repeat domain 6	0.01454	-2.427
ABTB2	ankyrin repeat and BTB domain containing 2	0.01454	-3.253
C8orf44-SGK3	C8orf44-SGK3 readthrough	0.01503	-5.028
STRADB	STE20 related adaptor beta	0.01561	-2.161
EMC8	ER membrane protein complex subunit 8	0.01587	-2.578
MTARC1	mitochondrial amidoxime reducing component 1	0.01605	-2.537
MYEOV	myeloma overexpressed	0.01660	-2.460
LOC642929	general transcription factor II, i pseudogene	0.01660	-3.435
SCUBE2	signal peptide, CUB domain and EGF like domain containing 2	0.01690	-3.568

FN1	fibronectin 1	0.01714	2.032
MTCH1	mitochondrial carrier 1	0.01719	-2.074
ZNF213	zinc finger protein 213	0.01750	-2.202
STAR	steroidogenic acute regulatory protein	0.01798	-2.952
REM1	RRAD and GEM like GTPase 1	0.01808	5.795
PLXNA2	plexin A2	0.01808	-3.191
BMS1P3	BMS1 pseudogene 3	0.01822	-4.314
RPL32P29	ribosomal protein L32 pseudogene 29	0.01825	2.699
PDE4D	phosphodiesterase 4D	0.01828	-2.434
EPHX4	epoxide hydrolase 4	0.01849	-4.334
NUDT18	nudix hydrolase 18	0.01877	-3.223
DEGS2	delta 4-desaturase, sphingolipid 2	0.01922	-3.872
LOC100420050	DNA replication fork stabilization factor DONSON pseudogene	0.01953	-3.553
MAGEF1	MAGE family member F1	0.01992	-2.698
TRIM9	tripartite motif containing 9	0.02009	-3.641
CFAP61	cilia and flagella associated protein 61	0.02063	-3.031
SELENON	selenoprotein N	0.02137	-2.886
NDUFAF8	NADH:ubiquinone oxidoreductase complex assembly factor 8	0.02144	-2.973
LSR	lipolysis stimulated lipoprotein receptor	0.02180	-2.698
MAF1	MAF1 homolog, negative regulator of RNA polymerase III	0.02203	-2.871
ARL4C	ADP ribosylation factor like GTPase 4C	0.02237	2.024
IL1B	interleukin 1 beta	0.02338	2.798
PNMA8B	PNMA family member 8B	0.02340	-4.194
TUBAP2	tubulin alpha pseudogene 2	0.02359	3.785
C4orf48	chromosome 4 open reading frame 48	0.02361	-5.912
RALGPS1	Ral GEF with PH domain and SH3 binding motif 1	0.02363	-2.639
CLCN4	chloride voltage-gated channel 4	0.02426	3.841
CD163L1	CD163 molecule like 1	0.02439	2.339
BIRC7	baculoviral IAP repeat containing 7	0.02447	3.456
H2BC5	H2B clustered histone 5	0.02450	-2.266
GALNT14	polypeptide N-acetylgalactosaminyltransferase 14	0.02501	-2.205
MGAT4B	alpha-1,3-mannosyl-glycoprotein 4-beta-N-acetylglucosaminyltransferase B	0.02501	-2.804
CRTAP	cartilage associated protein	0.02515	-2.124
ALKBH6	alkB homolog 6	0.02532	-2.901
METTL7B	methyltransferase like 7B	0.02571	-3.802
CCL20	C-C motif chemokine ligand 20	0.02585	3.222
FAM120C	family with sequence similarity 120C	0.02601	-2.537
CXCL1	C-X-C motif chemokine ligand 1	0.02752	2.939
C11orf65	chromosome 11 open reading frame 65	0.02762	-3.363
ADGRD1	adhesion G protein-coupled receptor D1	0.02864	-2.171
LMBR1	limb development membrane protein 1	0.02931	-2.260
REEP1	receptor accessory protein 1	0.02934	-3.616
DPYSL3	dihydropyrimidinase like 3	0.02949	-2.231
CHAC2	ChaC glutathione specific gamma-glutamylcyclotransferase 2	0.03032	2.601

HOMER2	homer scaffold protein 2	0.03075	-2.304
KLK4	kallikrein related peptidase 4	0.03148	-3.831
CAMK1G	calcium/calmodulin dependent protein kinase IG	0.03167	3.489
FER1L6	fer-1 like family member 6	0.03190	-4.168
S100B	S100 calcium binding protein B	0.03307	2.431
EFNB1	ephrin B1	0.03307	-2.809
SLC25A48	solute carrier family 25 member 48	0.03346	-3.510
SLC35E4	solute carrier family 35 member E4	0.03444	-2.175
ATP5F1D	ATP synthase F1 subunit delta	0.03547	-2.049
TSPAN12	tetraspanin 12	0.03561	-2.335
ST20-MTHFS	ST20-MTHFS readthrough	0.03687	-2.037
KCNH4	potassium voltage-gated channel subfamily H member 4	0.03715	-4.389
GFI1	growth factor independent 1 transcriptional repressor	0.03752	-4.777
PXYLP1	2-phosphoxylose phosphatase 1	0.03766	-2.117
MME	membrane metalloendopeptidase	0.03853	-2.050
XDH	xanthine dehydrogenase	0.03871	-4.058
PRSS36	serine protease 36	0.03888	-2.211
SPTBN2	spectrin beta, non-erythrocytic 2	0.03903	-4.221
NPM1P40	nucleophosmin 1 pseudogene 40	0.03924	-4.011
GIPR	gastric inhibitory polypeptide receptor	0.03939	-2.333
CHN1	chimerin 1	0.03939	-3.274
ISLR2	immunoglobulin superfamily containing leucine rich repeat 2	0.03947	-3.413
WHRN	whirlin	0.03954	-4.002
GUCY2D	guanylate cyclase 2D, retinal	0.04019	-3.779
LRGUK	leucine rich repeats and guanylate kinase domain containing	0.04025	-2.525
DTX1	deltex E3 ubiquitin ligase 1	0.04175	2.660
PRSS30P	serine protease 30, pseudogene	0.04199	-2.815
ADAMTS2	ADAM metallopeptidase with thrombospondin type 1 motif 2	0.04567	4.051
PDPK2P	3-phosphoinositide dependent protein kinase 2, pseudogene	0.04568	-2.571
CAMK2B	calcium/calmodulin dependent protein kinase II beta	0.04576	-2.843
ATP9A	ATPase phospholipid transporting 9A (putative)	0.04594	-2.754
CENPS-CORT	CENPS-CORT readthrough	0.04604	2.846
TANC1	tetratricopeptide repeat, ankyrin repeat and coiled-coil containing 1	0.04674	-3.488
GRAMD1C	GRAM domain containing 1C	0.04758	-3.543
KANK3	KN motif and ankyrin repeat domains 3	0.04764	-3.016
SLC1A7	solute carrier family 1 member 7	0.04764	-3.094
SERPINI1	serpin family I member 1	0.04775	-2.291
IGF2BP2	insulin like growth factor 2 mRNA binding protein 2	0.04838	-2.537

Table B3: DEGs in MDMs that have phagocytosed 1-2 beads compared to non-phagocytic MDMs at 4 hours post-challenge with latex beads.

Gene symbol	Gene name	padj	Log2FC
THBD	thrombomodulin	2.22E-06	2.390
ADORA2A	adenosine A2a receptor	8.97E-05	6.373
MARCO	macrophage receptor with collagenous structure	9.20E-05	2.127
MCUB	mitochondrial calcium uniporter dominant negative subunit beta	0.00029	2.456
SLC39A8	solute carrier family 39 member 8	0.00033	2.013
TYMS	thymidylate synthetase	0.00269	2.678
MFSD4A	major facilitator superfamily domain containing 4A	0.00321	-2.215
MFSD4A	major facilitator superfamily domain containing 4A	0.00321	-2.215
MAFB	MAF bZIP transcription factor B	0.00417	1.438
TYMP	thymidine phosphorylase	0.00957	2.181
IL4I1	interleukin 4 induced 1	0.00957	1.833
CD47	CD47 molecule	0.01249	1.706
TMEM86A	transmembrane protein 86A	0.01249	1.367
GGA2	golgi associated, gamma adaptin ear containing, ARF binding protein 2	0.01311	1.552
BUB1B	BUB1 mitotic checkpoint serine/threonine kinase B	0.01397	2.136
TSPAN13	tetraspanin 13	0.01397	1.907
APBB3	amyloid beta precursor protein binding family B member 3	0.01397	1.643
ME1	malic enzyme 1	0.01397	1.624
ARHGEF10L	Rho guanine nucleotide exchange factor 10 like	0.01397	1.611
ARRDC2	arrestin domain containing 2	0.01397	1.318
NFKBIA	NFKB inhibitor alpha	0.01469	2.481
TAGAP	T cell activation RhoGTPase activating protein	0.01469	1.596
NLN	neurolysin	0.01678	1.579
VSIG4	V-set and immunoglobulin domain containing 4	0.01678	1.478
KDM6B	lysine demethylase 6B	0.01749	-2.067
KDM6B	lysine demethylase 6B	0.01749	-2.067
PATL2	PAT1 homolog 2	0.01816	-2.323
PATL2	PAT1 homolog 2	0.01816	-2.323
CRTAP	cartilage associated protein	0.01923	2.173
RAB42	RAB42, member RAS oncogene family	0.01998	2.556
PPIF	peptidylprolyl isomerase F	0.02118	1.859
PTGER2	prostaglandin E receptor 2	0.02289	1.291
TCF4	transcription factor 4	0.02289	1.249
CMTM7	CKLF like MARVEL transmembrane domain containing 7	0.02368	1.761
OTULINL	OTU deubiquitinase with linear linkage specificity like	0.02368	1.511
CCL7	C-C motif chemokine ligand 7	0.02416	2.243
C1QB	complement C1q B chain	0.02548	3.516
SLC2A3	solute carrier family 2 member 3	0.02602	1.002
TNFSF13B	TNF superfamily member 13b	0.02639	1.763

ETV5	ETS variant transcription factor 5	0.02659	1.591
PTGIR	prostaglandin I2 receptor	0.03260	1.764
GPR84	G protein-coupled receptor 84	0.04001	1.360
NUPR1	nuclear protein 1, transcriptional regulator	0.04001	1.178
CAMK1	calcium/calmodulin dependent protein kinase I	0.04087	1.267
RNASE2	ribonuclease A family member 2	0.04349	4.194
CST3	cystatin C	0.04349	1.914
AP1S2	adaptor related protein complex 1 subunit sigma 2	0.04790	1.499
MATR3	matrin 3	0.04805	-2.152

Table B4: DEGs in MDMs that have phagocytosed 3 beads compared to non-phagocytic MDMs at 4 hours post-challenge with latex beads.

Gene symbol	Gene name	padj	Log2FC
TIE1	tyrosine kinase with immunoglobulin like and EGF like domains 1	4.97E-18	-2.755
ADRA2B	adrenoceptor alpha 2B	4.97E-18	-3.853
LAT	linker for activation of T cells	4.12E-14	-2.990
CRABP2	cellular retinoic acid binding protein 2	6.79E-13	-4.072
CYP3A5	cytochrome P450 family 3 subfamily A member 5	3.91E-12	-2.072
MARCO	macrophage receptor with collagenous structure	3.91E-12	3.020
TAGAP	T cell activation RhoGTPase activating protein	8.56E-12	2.946
NUPR1	nuclear protein 1, transcriptional regulator	8.56E-12	2.426
DBN1	drebrin 1	9.15E-12	-2.974
DHRS9	dehydrogenase/reductase 9	3.73E-11	-3.028
CXCL8	C-X-C motif chemokine ligand 8	4.88E-11	3.031
IL4I1	interleukin 4 induced 1	6.18E-11	3.094
TMEM163	transmembrane protein 163	1.23E-10	2.880
ATF3	activating transcription factor 3	2.25E-10	-2.381
SNAI3	snail family transcriptional repressor 3	7.67E-10	-2.094
GPR84	G protein-coupled receptor 84	9.63E-10	2.485
MYH10	myosin heavy chain 10	1.03E-09	-5.314
ADORA2A	adenosine A2a receptor	1.13E-09	7.855
ARHGEF10L	Rho guanine nucleotide exchange factor 10 like	1.23E-09	2.678
VSIG4	V-set and immunoglobulin domain containing 4	2.33E-09	2.493
RHOF	ras homolog family member F, filopodia associated	3.12E-09	-2.191
TNFSF13B	TNF superfamily member 13b	5.51E-09	3.061
CSRP2	cysteine and glycine rich protein 2	9.33E-09	-3.784
CCND1	cyclin D1	1.24E-08	-2.056
NCAPH	non-SMC condensin I complex subunit H	2.24E-08	-2.688
MDK	midkine	2.39E-08	-2.176
TBC1D2B	TBC1 domain family member 2B	2.89E-08	-2.152
GPD1	glycerol-3-phosphate dehydrogenase 1	2.90E-08	-2.624
TM4SF19	transmembrane 4 L six family member 19	2.95E-08	-2.147
GPR183	G protein-coupled receptor 183	2.95E-08	2.701
TRIM54	tripartite motif containing 54	3.33E-08	-4.900
CARMIL1	capping protein regulator and myosin 1 linker 1	4.59E-08	-2.791
ANKRD36B	ankyrin repeat domain 36B	4.65E-08	-2.300
KCNJ1	potassium inwardly rectifying channel subfamily J member 1	5.91E-08	-3.525
G0S2	G0/G1 switch 2	6.57E-08	3.778
DUSP7	dual specificity phosphatase 7	7.40E-08	-2.344
PLAU	plasminogen activator, urokinase	9.40E-08	3.897
SLC39A8	solute carrier family 39 member 8	9.40E-08	2.391
SUCNR1	succinate receptor 1	1.06E-07	-2.701
ECE1	endothelin converting enzyme 1	1.06E-07	-2.799

OCSTAMP	osteoclast stimulatory transmembrane protein	1.28E-07	-4.138
COL6A1	collagen type VI alpha 1 chain	1.38E-07	2.290
KIAA1210	KIAA1210	1.87E-07	-2.794
MAP7	microtubule associated protein 7	1.94E-07	-2.921
SEC14L2	SEC14 like lipid binding 2	2.71E-07	-2.241
DEPP1	DEPP1 autophagy regulator	3.32E-07	-2.593
RHOC	ras homolog family member C	3.91E-07	-2.258
MAP1A	microtubule associated protein 1A	4.87E-07	-2.129
DSP	desmoplakin	4.87E-07	-4.170
THBD	thrombomodulin	6.10E-07	2.211
IL18BP	interleukin 18 binding protein	6.84E-07	2.979
CCL22	C-C motif chemokine ligand 22	7.35E-07	-4.557
SYNGR1	synaptogyrin 1	8.08E-07	-2.580
ACAT2	acetyl-CoA acetyltransferase 2	1.48E-06	-2.097
RAB32	RAB32, member RAS oncogene family	1.95E-06	2.163
OTULINL	OTU deubiquitinase with linear linkage specificity like	2.19E-06	2.143
HOPX	HOP homeobox	2.29E-06	-2.620
GNG12	G protein subunit gamma 12	4.25E-06	2.960
LAMB3	laminin subunit beta 3	5.44E-06	2.210
CCL7	C-C motif chemokine ligand 7	6.18E-06	3.075
CXCL1	C-X-C motif chemokine ligand 1	6.67E-06	5.245
AOC1	amine oxidase copper containing 1	7.21E-06	-2.216
FXYD6	FXYD domain containing ion transport regulator 6	8.34E-06	2.345
PMP22	peripheral myelin protein 22	8.39E-06	2.493
SLC30A3	solute carrier family 30 member 3	9.17E-06	-2.837
PERP	p53 apoptosis effector related to PMP22	9.25E-06	-3.395
C3AR1	complement C3a receptor 1	9.53E-06	2.771
NES	nestin	1.07E-05	-4.413
AIF1	allograft inflammatory factor 1	1.16E-05	2.992
MYCL	MYCL proto-oncogene, bHLH transcription factor	1.20E-05	-2.384
CD79A	CD79a molecule	1.21E-05	-3.524
SLC1A2	solute carrier family 1 member 2	1.28E-05	-2.519
MPEG1	macrophage expressed 1	1.28E-05	2.805
RGS20	regulator of G protein signaling 20	1.29E-05	-2.177
MMP2	matrix metallopeptidase 2	1.35E-05	3.400
ENC1	ectodermal-neural cortex 1	1.42E-05	-3.216
ADM	adrenomedullin	1.72E-05	2.475
ALPK3	alpha kinase 3	1.74E-05	-3.557
CRIP1	cysteine rich protein 1	2.21E-05	-2.110
NIPAL4	NIPA like domain containing 4	2.34E-05	2.012
ETV5	ETS variant transcription factor 5	2.79E-05	2.071
PTGFRN	prostaglandin F2 receptor inhibitor	3.27E-05	2.425
HPSE	heparanase	3.28E-05	3.332
CSPG4	chondroitin sulfate proteoglycan 4	3.41E-05	-2.598
TMEM273	transmembrane protein 273	3.52E-05	2.388
PI4KAP2	phosphatidylinositol 4-kinase alpha pseudogene 2	3.82E-05	-2.020

NPR1	natriuretic peptide receptor 1	3.97E-05	-4.356
TSPAN17	tetraspanin 17	4.54E-05	-2.320
BUB1B	BUB1 mitotic checkpoint serine/threonine kinase B	4.54E-05	2.400
HAMP	hepcidin antimicrobial peptide	5.36E-05	2.610
DYRK3	dual specificity tyrosine phosphorylation regulated kinase 3	5.63E-05	2.671
IGFBP6	insulin like growth factor binding protein 6	9.00E-05	-2.907
LAYN	layilin	9.46E-05	-2.159
PTGIR	prostaglandin I2 receptor	0.00010	2.191
OSM	oncostatin M	0.00011	3.421
HIC2	HIC ZBTB transcriptional repressor 2	0.00013	-2.352
CLEC4A	C-type lectin domain family 4 member A	0.00015	2.141
TYMP	thymidine phosphorylase	0.00020	2.282
MCUB	mitochondrial calcium uniporter dominant negative subunit beta	0.00022	2.151
MGAT4A	alpha-1,3-mannosyl-glycoprotein 4-beta-N-acetylglucosaminyltransferase A	0.00025	2.569
PLTP	phospholipid transfer protein	0.00025	2.129
NCKAP1	NCK associated protein 1	0.00026	-2.765
GPAT2	glycerol-3-phosphate acyltransferase 2, mitochondrial	0.00028	-2.629
MNDA	myeloid cell nuclear differentiation antigen	0.00028	2.369
PLS1	plastin 1	0.00028	-2.726
C1QB	complement C1q B chain	0.00030	4.093
GPER1	G protein-coupled estrogen receptor 1	0.00031	-2.071
RGL1	ral guanine nucleotide dissociation stimulator like 1	0.00031	2.161
FPR3	formyl peptide receptor 3	0.00032	2.581
FANCE	FA complementation group E	0.00035	-2.926
PTGDS	prostaglandin D2 synthase	0.00036	-2.185
MRC2	mannose receptor C type 2	0.00037	2.050
CLU	clusterin	0.00038	-2.316
RETREG1	reticulophagy regulator 1	0.00047	-2.930
CXCL3	C-X-C motif chemokine ligand 3	0.00049	5.423
TSPAN4	tetraspanin 4	0.00051	2.038
SLC38A1	solute carrier family 38 member 1	0.00059	-2.335
SLC22A23	solute carrier family 22 member 23	0.00063	2.723
SERPINA1	serpin family A member 1	0.00080	2.290
DTX1	deltex E3 ubiquitin ligase 1	0.00080	4.231
CCNA1	cyclin A1	0.00081	-2.129
HPD	4-hydroxyphenylpyruvate dioxygenase	0.00086	-4.095
TEAD3	TEA domain transcription factor 3	0.00087	-3.834
GALNT12	polypeptide N-acetylgalactosaminyltransferase 12	0.00129	-2.055
MRGPRF	MAS related GPR family member F	0.00129	-2.393
MMP7	matrix metallopeptidase 7	0.00135	-3.443
TIFAB	TIFA inhibitor	0.00138	2.878
COL6A2	collagen type VI alpha 2 chain	0.00138	2.070
DUSP2	dual specificity phosphatase 2	0.00156	-2.393
AHRR	aryl-hydrocarbon receptor repressor	0.00165	2.597

CEP131	centrosomal protein 131	0.00165	2.512
WLS	Wnt ligand secretion mediator	0.00168	2.713
RNASE2	ribonuclease A family member 2	0.00183	4.523
MYLK	myosin light chain kinase	0.00191	-2.037
KCNA10	potassium voltage-gated channel subfamily A member 10	0.00206	-2.184
DPYSL3	dihydropyrimidinase like 3	0.00249	-2.267
FER1L6	fer-1 like family member 6	0.00253	-5.227
MARCKSL1	MARCKS like 1	0.00263	2.872
C11orf45	chromosome 11 open reading frame 45	0.00267	-2.113
EPS8L2	EPS8 like 2	0.00288	-4.731
CLEC5A	C-type lectin domain containing 5A	0.00293	2.878
ARFGEF3	ARFGEF family member 3	0.00313	-2.425
CPNE6	copine 6	0.00319	-3.858
S1PR4	sphingosine-1-phosphate receptor 4	0.00334	-2.662
NOS1	nitric oxide synthase 1	0.00347	-3.972
DUSP13	dual specificity phosphatase 13	0.00354	-2.562
TRIM9	tripartite motif containing 9	0.00355	-3.301
SYT1	synaptotagmin 1	0.00364	4.963
SYNC	syncoilin, intermediate filament protein	0.00384	-3.710
TLN2	talin 2	0.00386	-2.185
S100A8	S100 calcium binding protein A8	0.00406	2.050
SHISA2	shisa family member 2	0.00450	-2.681
GPC3	glypican 3	0.00450	-4.264
GPLD1	glycosylphosphatidylinositol specific phospholipase D1	0.00450	-4.651
H2BC5	H2B clustered histone 5	0.00461	-2.722
CYP4X1	cytochrome P450 family 4 subfamily X member 1	0.00464	-3.115
RND3	Rho family GTPase 3	0.00484	2.265
CCL15	C-C motif chemokine ligand 15	0.00493	3.925
UGT3A1	UDP glycosyltransferase family 3 member A1	0.00528	-3.639
TMIGD3	transmembrane and immunoglobulin domain containing 3	0.00534	2.622
LIN7A	lin-7 homolog A, crumbs cell polarity complex component	0.00592	4.413
TRPV4	transient receptor potential cation channel subfamily V member 4	0.00624	3.154
CD80	CD80 molecule	0.00649	2.703
PRG2	proteoglycan 2, pro eosinophil major basic protein	0.00697	-5.906
HS3ST2	heparan sulfate-glucosamine 3-sulfotransferase 2	0.00708	3.405
PNMA8B	PNMA family member 8B	0.00790	-3.785
PHACTR1	phosphatase and actin regulator 1	0.00799	2.161
CCR7	C-C motif chemokine receptor 7	0.00799	3.528
NFKBIA	NFKB inhibitor alpha	0.00811	2.134
CPEB1	cytoplasmic polyadenylation element binding protein 1	0.00833	-2.392
OTOAP1	OTOA pseudogene 1	0.00833	2.034
VCAM1	vascular cell adhesion molecule 1	0.00969	3.580
BIRC7	baculoviral IAP repeat containing 7	0.00973	3.351
SLC25A48	solute carrier family 25 member 48	0.01000	-2.962
CD163	CD163 molecule	0.01008	2.754

TMEM114	transmembrane protein 114	0.01022	-2.337
IGFLR1	IGF like family receptor 1	0.01039	2.057
COL23A1	collagen type XXIII alpha 1 chain	0.01039	2.042
CCDC169	coiled-coil domain containing 169	0.01061	-2.723
CCL4	C-C motif chemokine ligand 4	0.01070	2.167
TAFA4	TAFA chemokine like family member 4	0.01101	3.999
GJA5	gap junction protein alpha 5	0.01114	-3.296
RAP1GAP	RAP1 GTPase activating protein	0.01147	-2.637
PCDHGC3	protocadherin gamma subfamily C, 3	0.01161	-2.430
CDK6	cyclin dependent kinase 6	0.01188	2.049
RNASE1	ribonuclease A family member 1, pancreatic	0.01208	3.180
PLK1	polo like kinase 1	0.01274	2.088
CPT1B	carnitine palmitoyltransferase 1B	0.01381	-2.497
SH3RF2	SH3 domain containing ring finger 2	0.01382	-2.676
PMEPA1	prostate transmembrane protein, androgen induced 1	0.01409	2.131
MTUS1	microtubule associated scaffold protein 1	0.01443	-2.061
TMEM37	transmembrane protein 37	0.01445	2.269
SOCS3	suppressor of cytokine signaling 3	0.01466	2.602
GPC4	glypican 4	0.01478	-2.583
PPP1R13B	protein phosphatase 1 regulatory subunit 13B	0.01478	-2.494
TREM1	triggering receptor expressed on myeloid cells 1	0.01560	3.149
CX3CL1	C-X3-C motif chemokine ligand 1	0.01618	-2.187
KLK4	kallikrein related peptidase 4	0.01698	-4.483
MYBPH	myosin binding protein H	0.01707	-2.109
KANK3	KN motif and ankyrin repeat domains 3	0.01785	-3.270
ST6GALNAC6	ST6 N-acetylgalactosaminide alpha-2,6-sialyltransferase 6	0.01797	-2.382
TPSAB1	tryptase alpha/beta 1	0.01817	4.974
AKR1C3	aldo-keto reductase family 1 member C3	0.01817	2.884
ITGB3	integrin subunit beta 3	0.01895	-2.107
ALDH8A1	aldehyde dehydrogenase 8 family member A1	0.01946	-3.497
CHRNA1	cholinergic receptor nicotinic alpha 1 subunit	0.01946	3.088
CD14	CD14 molecule	0.01966	2.849
SDCBP2	syndecan binding protein 2	0.01995	-2.797
KCTD15	potassium channel tetramerization domain containing 15	0.02055	-4.435
PRSS30P	serine protease 30, pseudogene	0.02180	-4.072
SMIM11A	small integral membrane protein 11A	0.02222	-4.320
SPP2	secreted phosphoprotein 2	0.02223	-2.166
PDCD6-AHRR	PDCD6-AHRR readthrough (NMD candidate)	0.02289	3.783
TBX21	T-box transcription factor 21	0.02315	-2.633
TGFBI	transforming growth factor beta induced	0.02315	2.889
DUSP4	dual specificity phosphatase 4	0.02353	2.353
KIAA1755	KIAA1755	0.02433	-2.025
RAB42	RAB42, member RAS oncogene family	0.02524	2.017
DEPDC1	DEP domain containing 1	0.02569	2.833
APBA1	amyloid beta precursor protein binding family A member 1	0.02612	2.140
RBP1	retinol binding protein 1	0.02614	-2.135

TJP3	tight junction protein 3	0.02617	-3.013
CCDC171	coiled-coil domain containing 171	0.02891	-2.281
VIT	vitrin	0.02945	-3.741
ASB18	ankyrin repeat and SOCS box containing 18	0.03299	-3.018
PLEKHG4	pleckstrin homology and RhoGEF domain containing G4	0.03305	-2.253
PPM1E	protein phosphatase, Mg2+/Mn2+ dependent 1E	0.03342	-2.114
ENPP2	ectonucleotide pyrophosphatase/phosphodiesterase 2	0.03562	2.295
CCL18	C-C motif chemokine ligand 18	0.03573	5.776
CCNE2	cyclin E2	0.03668	2.415
E2F8	E2F transcription factor 8	0.03671	3.064
SRPX	sushi repeat containing protein X-linked	0.03733	4.516
TRIM2	tripartite motif containing 2	0.03735	-2.923
IL1RN	interleukin 1 receptor antagonist	0.03789	-2.237
CENPS-CORT	CENPS-CORT readthrough	0.03815	-4.005
AP1M2	adaptor related protein complex 1 subunit mu 2	0.03819	-2.642
NBL1	NBL1, DAN family BMP antagonist	0.03880	-2.193
B3GALNT1	beta-1,3-N-acetylgalactosaminyltransferase 1 (globoside blood group)	0.04190	2.263
LAMA2	laminin subunit alpha 2	0.04272	-3.494
TMCC2	transmembrane and coiled-coil domain family 2	0.04320	-3.279
SH3PXD2B	SH3 and PX domains 2B	0.04342	2.659
NEURL3	neuralized E3 ubiquitin protein ligase 3	0.04388	2.534
CFP	complement factor properdin	0.04418	2.825
SPON2	spondin 2	0.04439	-3.345
CCL2	C-C motif chemokine ligand 2	0.04669	3.634
COLQ	collagen like tail subunit of asymmetric acetylcholinesterase	0.04727	-2.533
NDRG4	NDRG family member 4	0.04737	-2.795
C1QA	complement C1q A chain	0.04778	2.945
NID1	nidogen 1	0.04922	2.268

10 Appendix C: Drug and siRNA screen analysis code

Below is the analysis code for two channel analysis in R used to determine the number of GFP or pHrodo positive bacteria per cell (adapted from (Boutros, Hahne and Huber, 2013)). Highlighted in blue is the code that can be removed for single channel analysis, such as DAPI counts for quality control. Highlighted in green are data paths or data files requiring modification to suit the files or channels being analysed.

```
```{r}
if (!requireNamespace("BiocManager", quietly = TRUE))
    install.packages("BiocManager")
BiocManager::install("cellHTS2")
```
```{r}
library(cellHTS2)
```
```{r}
dataPath = "/Users/UOS/Documents/siRNA
screen/Analysis_2022/TO_data/"
expName = "TO 2022 analysis"
outPath = paste(dataPath, "TO_Results_GFP/")
confFile = file.path(dataPath, "TOplateconfiguration.txt")
logFile = file.path(dataPath, "TOlog.txt")
desFile = file.path(dataPath, "TOdescription.txt")
geneIDs = file.path(dataPath, "TOannotation.txt")
posControls = "pos"
negControls = "neg"
filename <- "TOfilelistGFP.txt"
```
```{r}
x <- readPlateList(filename, path=dataPath, name=expName,
verbose = TRUE)
```
```{r}
x<-configure(x,confFile = confFile, logFile = logFile,
descripFile = desFile, path = dataPath)
```
```{r}
xn <-summarizeChannels(x,fun = function (r1,r2) r2/r1)
xnp <- normalizePlates(xn, scale = "multiplicative", log =
TRUE, method = "median", varianceAdjust = "none")
```
```

```
xsc <- scoreReplicates(xnp, sign = "-", method = "zscore")
```
```{r}
xf <- summarizeReplicates(xsc, summary = "mean")
xfw <- annotate(xf, geneIDFile = "siRNAannotation.txt", path =
dataPath)
scores<- Data(xsc)
boxplot(scores~wellAnno(x), col=rainbow(10))
```
```{r}
GFPtable<-Data(xsc)
write.table(GFPtable, "GFP.txt", sep="\t", quote=F,
col.names=F)
out <- writeReport(raw=x, normalized=xnp, scored=xf, force =
TRUE, plotPlateArgs = TRUE, imageScreenArgs = list(zrange=c(-
4,8),ar=1), map=TRUE, outdir = outPath)
```

11 Appendix D: siRNA screen data

Significant increases and decreases in GFP and pHrodo positive *S.* pneumoniae are transfection with siRNA are shown here in table D1. A positive z-score indicates a significant decrease in signal whilst a negative z-score represents a significant increase in signal.

Table D1: siRNA targets that had a significant effect on GFP and pHrodo positive *S. pneumoniae* with their associated z-score and plate positions.

Gene ID	GFP z-score	Plate	Well	Gene ID	pHrodo z-score	Plate	Well
GNG10	3.83	3	P22	DAZ2	3.45	5	H22
DIRC1	3.79	13	A23	FOXA3	3.19	5	F20
FOXA3	3.53	5	F20	REXO1	2.67	5	J20
DAZ2	3.28	5	H22	DHX8	2.63	5	P20
CDA	3.22	2	L14	TMEM45A	2.61	3	P03
KLHL30	3.06	13	P21	GNG10	2.61	3	P22
MRPL10	2.98	13	A21	DACH1	2.47	3	P20
CYP2C8	2.73	2	B22	COX5B	2.4	10	P14
REXO1	2.64	5	J20	MYB	2.39	8	P22
C20orf195	2.61	10	D21	SCGF	2.33	3	L20
MYB	2.55	8	P22	SUPT6H	2.32	1	J22
AKR1B1	2.51	8	F22	ASNA1	2.32	3	L22
HPS4	2.49	3	G19	MGC24975	2.31	13	O19
PLEKHE1	2.47	8	D20	ASAH3L	2.22	4	O03
PPIAL4A	2.46	3	N19	NDUFS5	2.19	5	J22
ASAH3L	2.44	4	O03	C12orf36	2.19	5	N21
KIAA0319L	2.4	11	M23	PPIAL4A	2.17	3	N19
RBPMS2	2.39	10	O22	RHOXF1	2.15	8	I23
CA5B	2.38	2	L18	TM7SF3	2.14	2	A21
ZIM2	2.38	4	I08	C4orf36	2.1	3	P19
TMEM219	2.38	4	I16	TMEM146	2.08	3	P13
ZNF140	2.37	8	C23	PARD3B	2.08	5	L19
CHN1	2.35	13	E22	KRT5	2.06	3	O04
NALP12	2.33	3	B04	CSEN	2.04	6	P22
SHF	2.32	2	D09	OR5AS1	2.03	2	K20
C20ORF85	2.32	13	O23	ZNF672	2.01	2	N19
WDR34	2.31	1	O23	SPRYD3	2.01	5	J21
Scrambled	2.31	13	P23	DNAJC21	1.96	3	E23
MGC24975	2.3	13	O19	RBPMS2	1.96	10	O22
HOXA3	2.29	5	I18	RPL14	-1.96	5	E02
WARS	2.22	3	N16	ZCCHC17	-1.96	8	F05
OGFOD2	2.21	2	J09	RSRC2	-1.99	1	H13
CEP164	2.21	5	D19	RPL30	-1.99	4	K14
ZNF93	2.18	2	H21	CCDC77	-2.01	12	N11

CT47.8	2.18	5	I23
C14ORF48	2.17	5	K12
HS2ST1	2.17	13	P08
PAN3	2.16	2	C10
TRO	2.15	12	E12
MRAP2	2.14	12	A12
RFX7	2.13	4	B07
ZNF816A	2.13	4	J09
WIT1	2.13	5	H09
YJEFN3	2.12	8	I21
WDR40A	2.08	1	I04
SPEC2	2.08	3	F22
TMEM45A	2.08	3	P03
FMO5	2.07	5	D20
SCUBE1	2.07	5	I20
TNFAIP6	2.06	3	K20
TMEM167B	2.06	13	F21
GOSR2	2.05	1	B18
KRT5	2.04	3	O04
Scrambled	2.03	11	P23
LSG1	2.02	2	B21
PTS	2.01	3	F18
XPO1	2	2	D22
ARL6IP6	2	8	L21
COQ7	1.98	4	K21
HIST2H4B	1.97	4	B19
PDRG1	1.96	5	B19
CT45-4	1.96	5	I19
RPL30	-1.96	4	K14
ANGPTL4	-1.96	8	E16
C17orf82	-1.98	8	F09
CCDC105	-1.99	8	F17
RPP25	-1.99	10	K11
ZNF415	-2	8	E05
ALOX15	-2	12	L18
FAM48A	-2.01	13	L19
LRRC57	-2.01	13	N07
RFC2	-2.02	8	F18
ATG9B	-2.02	11	A03
ARL4A	-2.03	8	H16
PCDHB12	-2.05	8	I14
ZBTB5	-2.05	10	E13
LOC643418	-2.06	8	F14
TMEM87B	-2.07	12	N13
C20orf201	-2.08	1	O02
MOSPD1	-2.08	13	I02
SMG7	-2.04	1	F11
PBEF1	-2.08	3	F12
PAXIP1	-2.11	12	H05
UBC	-2.12	2	G11
KTELC1	-2.13	8	H13
CRB3	-2.14	8	E07
ZMYM3	-2.14	10	C03
B3GALTL	-2.15	8	J15
MOSPD1	-2.15	13	I02
KRT13	-2.16	8	E14
KLHDC2	-2.17	3	I12
ANGPTL4	-2.17	8	E16
ARL4A	-2.17	8	H16
BCAS3	-2.19	13	A13
MAP7D2	-2.2	12	F03
ATG9A	-2.21	2	I13
C16orf61	-2.21	8	F11
CCDC105	-2.21	8	F17
S100A14	-2.22	2	E07
LOC643418	-2.23	8	F14
REV3L	-2.23	8	L16
C3orf54	-2.24	8	F13
ATE1	-2.25	8	F10
TMEM64	-2.27	1	J13
NIN	-2.27	12	I23
PPP1R3B	-2.3	3	K02
FAM133A	-2.31	2	J11
ARL11	-2.32	5	G11
RPUSD4	-2.32	12	E15
ANKMY2	-2.33	13	G15
RFC2	-2.36	8	F18
RPL23	-2.37	4	G13
NY-SAR-48	-2.39	1	D07
PCDHB12	-2.39	8	I14
BBX	-2.45	11	K21
TSPAN4	-2.48	8	F15
ZNF550	-2.49	2	I11
ZNF670	-2.49	8	D05
UBAC1	-2.5	8	H15
CCDC91	-2.56	13	F03
APOBEC3B	-2.62	8	D12
TUBA1B	-2.68	12	L07
ZCCHC14	-2.73	12	L09
KRT80	-2.89	8	J13
TMEM164	-2.94	2	F13
COL25A1	-3.7	1	E02

PPP1R3B	-2.09	3	K02
CRB3	-2.11	8	E07
ACTR5	-2.18	11	E07
UTP14A	-2.2	5	A04
SYT7	-2.21	13	M04
RABEP1	-2.23	11	C12
BBX	-2.25	11	K21
SPAG16	-2.26	12	P11
Clemastine	-2.26	13	G17
Clemastine	-2.27	10	O17
MICAL1	-2.28	12	H03
NIN	-2.29	12	I23
Clemastine	-2.3	12	G17
SLC6A16	-2.3	13	D04
KRT80	-2.31	8	J13
PIK3IP1	-2.31	12	D17
SEPSECS	-2.32	5	N05
C15orf43	-2.33	12	L11
MAFG	-2.36	8	F06
Clemastine	-2.37	6	O17
ZNF670	-2.38	8	D05
UBAC1	-2.38	8	H15
WNT7B	-2.4	13	I12
BCAS3	-2.41	13	A13
ATE1	-2.45	8	F10
Clemastine	-2.47	10	G09
PPIA	-2.55	13	J12
C16orf61	-2.57	8	F11
MFSD11	-2.6	12	D03
CCDC91	-2.64	13	F03
CCDC77	-2.72	12	N11
ANKMY2	-2.77	13	G15
PAXIP1	-2.82	12	H05
ZMYM3	-2.85	10	C03
ZCCHC14	-2.88	12	L09
APOBEC3B	-2.95	8	D12
MIER3	-3.09	12	J11
MAP7D2	-3.19	12	F03
TUBA1B	-3.67	12	L07
GUCY1A2	-4.13	5	B04
PTCRA	-4.99	10	O15
GUCY1A2	-6.28	5	B04